



University
of Glasgow

Proto, William Richard (2010) *Characterisation of autophagy and a metacaspase in Trypanosoma brucei*. PhD thesis.

<http://theses.gla.ac.uk/2308/>

Copyright and moral rights for this thesis are retained by the author

A copy can be downloaded for personal non-commercial research or study, without prior permission or charge

This thesis cannot be reproduced or quoted extensively from without first obtaining permission in writing from the Author

The content must not be changed in any way or sold commercially in any format or medium without the formal permission of the Author

When referring to this work, full bibliographic details including the author, title, awarding institution and date of the thesis must be given

**Characterisation of autophagy and a
metacaspase in *Trypanosoma brucei***

**William Richard Proto
BSc**

**Submitted in fulfilment of the requirements
for the Degree of PhD**

**Institute of Infection, Immunity and Inflammation
College of Medical, Veterinary and Life Sciences
University of Glasgow**

September 2010

Abstract

This project focuses on the characterisation of two separate aspects of *Trypanosoma brucei* cell biology; the degradative process of autophagy and a specific cysteine peptidase from the metacaspase family.

Autophagy is a widely conserved intracellular mechanism for the degradation of long lived proteins and organelles, that requires the formation of an autophagosome (double membrane bound vesicle) around cargo destined for the lysosome. The molecular machinery involved in autophagy has been well characterised in yeast and bioinformatic screens have identified many of the core components in *T. brucei*. However, beyond bioinformatics there is limited experimental evidence to support the presence of functional autophagy in *T. brucei*.

A key component of the autophagic pathway is ATG8, a ubiquitin-like protein that is incorporated into the autophagosome membrane. To investigate autophagy in *T. brucei* the three candidate ATG8 genes (ATG8.1 Tb927.7.5900, ATG8.2 Tb927.7.5910 and ATG8.3 Tb927.7.3320) were fused with yellow fluorescent protein (YFP) and expressed in bloodstream form and procyclic form *T. brucei* cultured parasites. Fluorescent microscopy was used to monitor the formation of YFP-labelled autophagosomes, which enabled the evaluation of the autophagic response towards a variety of different stimuli. We provide the first direct experimental evidence confirming a functional autophagy pathway in *T. brucei* and show that it is induced in response to nutrient starvation in the procyclic form and neuropeptide treatment in the bloodstream form and can be blocked by the classical autophagy inhibitor wortmannin. Characterisation of the *T. brucei* ATG8 family revealed that ATG8.1 and ATG8.2 appear to operate as 'ATG8-like' proteins, whereas ATG8.3 behaves atypically, possibly functioning as an ATG12 protein. Furthermore, targeted RNAi downregulation of the predicted *T. brucei* ATG3 (Tb927.2.1890) caused a reduction in cell growth. The vital role of ATG3 in the autophagy pathway suggested that the process was required for normal procyclic form growth.

The second focus of the project was metacaspase 4 (Tb927.10.2440) which belongs to the metacaspases (MCAs), cysteine peptidases of the caspase family found in plants, fungi and protozoa, but absent from mammals. Of the five MCAs possessed by *T. brucei*, only MCA2, MCA3 and MCA5 contain the conserved histidine cysteine catalytic dyad. MCA1 and MCA4 are predicted to contain key substitutions within their active sites, raising interesting questions regarding potential peptidase activity and functions. The exact role of the *T. brucei* metacaspases remains largely unknown, with MCA2, MCA3 and MCA5 appearing to function in association with RAB11 positive endosomes, although independently of the known recycling functions of these endosomes (Helms *et al.* 2006).

To develop our understanding of the MCA family in *T. brucei* a study into the function of MCA4 was undertaken. An antibody was raised against MCA4 and western blotting of cell lysate revealed that MCA4 expression occurred only in bloodstream form *T. brucei*. Interestingly MCA4 localised to the flagellar membrane, appearing in a linear array of punctate structures. Dual acylation is known to mediate flagellar membrane association in *T. brucei* and was implicated in MCA4 targeting following bioinformatic predictions and subsequent experimental confirmation of MCA4 palmitoylation using an acyl-biotin exchange reaction.

MCA4 contains a non-canonical active site residue (serine-219) in the position of the predicted conserved active site cysteine. Activity assays using purified recombinant protein revealed that full length MCA4 was unable to autoprocess and was inactive. However, MCA4 peptidase activity could be detected following proteolytic activation with MCA2. Interestingly, removal of the MCA4 active site serine by mutagenesis (MCA4^{S219G}) did not abolish activity of the processed enzyme, revealing an alternative nucleophile was capable of contributing to activity. Furthermore, mutation of the active site serine to cysteine, produced a constitutively active peptidase capable of autolytic processing in a calcium dependent manner.

Following these key findings the role of MCA4 in the *T. brucei* lifecycle was investigated by RNAi and genetic knockout. Rapid depletion of MCA4 by RNAi caused a block in cytokinesis followed by cell death, nevertheless the generation

of MCA4 null mutant parasites ($\Delta mca4$) was possible. A role for MCA4 in mammalian infection was revealed by monitoring infection progression in mice. Deletion of MCA4 increased host survival and parasite virulence could be restored by the ectopic re-expression of MCA4 in $\Delta mca4$ parasites. However, re-expression of MCA4 lacking both serine-219 and cysteine-218 (potential alternative nucleophile provider) failed to restore $\Delta mca4$ parasite virulence, which confirmed the necessity of enzymatic activity for MCA4 function.

Table of Contents

1	General introduction	15
1.1	Human African Trypanosomiasis	15
1.2	<i>T. brucei</i> cell cycle	17
1.3	Trypanosome cell biology	18
1.4	<i>T. brucei</i> life cycle	23
1.4.1	<i>T. brucei</i> development in the mammalian host	23
1.4.2	<i>T. brucei</i> development in the tsetse fly host	24
2	Methods	28
2.1	Bacteria: strains and culture	28
2.1.1	Bacteria strains	28
2.1.2	Bacterial transformations	28
2.1.3	Bacterial culture and storage	29
2.1.4	Production of competent <i>E. coli</i> cells	29
2.2	Molecular biology techniques	29
2.2.1	Polymerase chain reaction	29
2.2.2	DNA gel electrophoresis	32
2.2.3	Cloning PCR products	33
2.2.4	Restriction endonuclease digestion	33
2.2.5	Ligation	34
2.2.6	Sequencing	34
2.3	Plasmid generation	34
2.3.1	In situ fluorescent tagging of <i>T. brucei</i> ATG8.1	35
2.3.2	Recombinant protein expression plasmids	36
2.3.3	RNAi constructs	36
2.3.4	MCA4 knockout constructs	37
2.3.5	MCA4 re-expression construct	37
2.3.6	Tagging of genes expressed from ectopic locus	37
2.4	Site directed mutagenesis	38
2.5	Preparing DNA for transfection	38
2.6	Southern blotting	38
2.7	Protein biochemistry	39
2.7.1	Recombinant protein: expression and purification	39
2.7.2	MCA4 antibody production and purification	40
2.7.3	ATG8.1 antibody production	41
2.7.4	Antibody affinity purification	41
2.7.5	Protein electrophoresis (SDS-PAGE)	42
2.7.6	Coomassie staining of SDS-PAGE	42
2.7.7	Western blotting	42
2.7.8	Co-immunoprecipitation experiments	43
2.8	Acyl-biotin exchange	44
2.9	MCA4 processing reactions	46
2.9.1	Autocatalytic processing	46
2.9.2	MCA2 processing of MCA4	46
2.9.3	N-terminal Edman degradation	46
2.10	Activity assays	47
2.11	Microscopy	47
2.11.1	Direct cell fluorescence	48
2.11.2	Immunofluorescence analysis	48

2.11.3	Immuno-electron microscopy.....	49
2.12	<i>T. brucei</i> cell culture	50
2.12.1	General culturing techniques.....	50
2.12.2	<i>T. brucei</i> genomic DNA isolation	51
2.12.3	BSF transfection	51
2.12.4	PCF transfection.....	51
2.13	RNAi induction and analyses	52
2.13.1	RNA isolation and reverse transcriptase (RT) PCR.....	52
2.13.2	Quantitative real time PCR	52
2.13.3	Fluorescence activated cell sorting (FACS).....	53
2.13.4	Monitoring autophagy in <i>T. brucei</i>	53
2.13.5	<i>T. brucei</i> animal infection	54
2.13.6	Motility analysis	54
2.13.7	Cell fractionation	54
2.13.8	Statistical analysis of data.....	55
3	Autophagy	56
3.1	Introduction	56
3.1.1	General introduction to Autophagy.....	56
3.1.2	Molecular dissection of autophagy pathway.....	57
3.1.3	Induction of autophagy.....	58
3.1.4	Autophagosome formation	59
3.1.5	Atg12-Atg5 conjugation	60
3.1.6	Atg8 conjugation	61
3.1.7	Autophagosome fusion with the lysosome	63
3.1.8	Physiological functions of autophagy.....	64
3.1.9	Autophagy in Trypanosomatidae Protozoa	64
3.2	Project aims	73
3.3	Results.....	74
3.3.1	Tagging of ATG8.1 in its native locus	74
3.3.2	ATG8 expressed by BSF and PCF <i>T. brucei</i>	76
3.3.3	Localisation of YFP-ATG8.1 and YFP-ATG8.2.....	78
3.3.4	Investigating TbATG8.3.....	91
3.3.5	Selective ATG8 lipid conjugation	94
3.3.6	Essentiality of autophagy pathway in PCF <i>T. brucei</i>	96
3.4	Discussion	99
4	Metacaspases	107
4.1	Introduction	107
4.1.1	General introduction to peptidases	107
4.1.2	Cysteine peptidase mechanism	107
4.1.3	Peptidase classification	109
4.1.4	Clan CD	109
4.1.5	Family C14A: Caspases	110
4.1.6	Family C14B: Metacaspases.....	111
4.1.7	Substrate specificity of MCAs.....	113
4.1.8	Autolytic processing of MCAs	115
4.1.9	Yeast MCAs	116
4.1.10	Plant MCAs	117
4.1.11	Leishmania MCAs	119
4.1.12	Trypanosoma <i>cruzi</i> MCAs	121
4.1.13	Trypanosoma <i>brucei</i> MCAs	122

4.1.14	What is in a name? Are metacaspases caspases?	125
4.2	Project Aims	126
4.3	Results.....	127
4.3.1	Metacaspase expression profile.	127
4.3.2	MCA4 associates with the flagellar membrane.....	128
4.3.3	MCA4 interactions	135
4.3.4	MCA4 activity	137
4.3.5	MCA4 function in BSF analysed by RNAi.....	148
4.3.6	MCA4 null mutants show reduced virulence in vivo	150
4.3.7	Confirming null mutant and re-expression cell lines.....	152
4.3.8	In vivo analysis of Δ mca4 parasites	156
4.4	Discussion	159
4.4.1	MCA4 expression and localisation.....	159
4.4.2	MCA4 activity	163
4.4.3	MCA4 reverse genetics.....	169
4.4.4	Is MCA4 part of a signalling cascade?.....	172
4.4.5	Is MCA4 involved in <i>T. brucei</i> flagellar metabolism?	174
4.4.6	Does MCA4 interact with the host following secretion?	175
5	General discussion	179
5.1.1	Autophagy in <i>T. brucei</i> - future perspective	179
5.1.2	MCA4 - proposed model of activation	180
5.1.3	Interplay between autophagy and MCAs	183
6	References	185

List of Tables

Table 2-1 Oligonucleotides used in this study.....	31
Table 2-2 Oligonucleotides used in this study (continued).....	32
Table 2-3 Plasmids used in this study.	35
Table 4 Core Autophagy Machinery and corresponding putative <i>T. brucei</i> orthologues.....	69
Table 5 Percentage identity of <i>S. cerevisiae</i> and <i>T. brucei</i> ATG8 proteins.	71

List of Figures

Figure 1-1 Hosts cycles of <i>T. brucei</i>	16
Figure 1-2 Cell cycle of <i>T. brucei</i>	18
Figure 1-3 Diagram depicting <i>T. brucei</i>	19
Figure 1-4 Lifecycle of <i>T. brucei</i>	23
Figure 1-5 Development of <i>T. brucei</i> in the tsetse fly.	26
Figure 3-1 Autophagic degradation by the lysosome.	57
Figure 3-2 Atg12 and Atg8 conjugation pathways in <i>S. cerevisiae</i>	63
Figure 3-3 Alignments and features of the three TbATG8s.....	71
Figure 3-4 GFP tagging of native TbATG8.1 locus.	75
Figure 3-5 Monitoring ATG8 expression in BSF and PCF <i>T. brucei</i>	77
Figure 3-6 Constructs for ectopically expressed YFP-ATG8s.	78
Figure 3-7 Tetracycline induced YFP-ATG8.1 and YFP-ATG8.2 expression.....	79
Figure 3-8 Analysis of YFP-ATG8.1 and YFP-ATG8.2 localisation in BSF <i>T. brucei</i>	82
Figure 3-9 Analysis of YFP-ATG8.1 and YFP-ATG8.2 localisation in PCF <i>T. brucei</i>	83
Figure 3-10 Detailed analysis of autophagosome formation in PCF <i>T. brucei</i>	85
Figure 3-11 Localisation of YFP-ATG8.1 and YFP-ATG8.2 in BSF <i>T. brucei</i> following vasoactive intestinal peptide treatment.	87
Figure 3-12 VIP rapidly stimulates autophagosome formation in BSF <i>T. brucei</i> . .	88
Figure 3-13 Rapamycin does not stimulate autophagosome formation in <i>T.</i> <i>brucei</i>	90
Figure 3-14 TbATG8.3 contains an insertion typical of ATG12 proteins.	92
Figure 3-15 Tetracycline induced YFP-ATG8.3 expression.	93
Figure 3-16 YFP-ATG8.3 puncta formation in PCF cells.....	94
Figure 3-17 YFP-ATG8.1 conjugates to a phospholipid.....	96
Figure 3-18 RNAi downregulation of ATG3 reduces PCF growth rate.	98
Figure 4-1 Cysteine peptidase catalytic mechanism.	108
Figure 4-2 Domain structure of metacaspases and caspases.....	113
Figure 4-3 Alignments of select domains of metacaspase proteins.	123
Figure 4-4 Expression profile of MCAs.	127
Figure 4-5 MCA4 is a membrane associated protein.....	129
Figure 4-6 Immunofluorescence analysis of MCA4 in BSF <i>T. brucei</i>	133

Figure 4-7 MCA4 immunogold transmission electron microscopy.....	134
Figure 4-8 Immunoprecipitation of MCA4 from BSF <i>T. brucei</i>	136
Figure 4-9 Calcium chloride induces cleavage and activation of MCA4 ^{S219C} but not MCA4.	139
Figure 4-10 MCA4 ^{S219C} activity against fixed position peptide library.....	140
Figure 4-11 Processed MCA4 is an active peptidase.	142
Figure 4-12 Distinguishing processed MCA4 activity from residual MCA2 activity.	143
Figure 4-13 Investigating MCA4 active site using mutagenesis and peptidase inhibitors.....	145
Figure 4-14 MCA4 ^{S219C} activity and autoprocessing is not inhibited by mutation of lysine-64.	147
Figure 4-15 RNAi of MCA4 in BSF <i>T. brucei</i>	149
Figure 4-16 Metacaspase 4 RNAi alters BSF <i>T. brucei</i> cell cycle progression. ...	150
Figure 4-17 Generating MCA44 null mutants.	153
Figure 4-18 In vitro analysis of MCA4 null mutant parasites.	155
Figure 4-19 MCA 4 deficient parasites show reduced virulence in mice.....	157
Figure 4-20 <i>T. brucei</i> 427 wild type, $\Delta mca4$ and $\Delta mca4:MCA4$ mouse infection profile.	158
Figure 4-21 Alignments of select metacaspase proteins.....	178
Figure 4-22 Model for MCA4 activation.	182

Acknowledgements

Firstly, I would like to thank Jeremy Mottram and Graham Coombs for giving me the opportunity to study in Glasgow. Working in the 'Mottram lab' has been a brilliant experience and I feel particularly indebted to Jeremy for the all the support, encouragement and advice provided over the past few years.

There are a huge number of people in and around the lab, who need endless thanks for their contributions to all aspects of my PhD, ranging from invaluable practical and theoretical help, to equally important friendship and entertainment! It has been great fun working with everyone but unfortunately to list you all would be an impossible task, so I will just offer a collective and sincere thanks to you all! Although, I would like to single out my fellow benchmates Cathy and Elaine for particular thanks, in recognition of your continuing advice and assistance despite years of relentless bad jokes.

This also seems an ideal opportunity to send a small message to my long suffering parents - you will be relieved to hear that it seems my time as a student is finally coming to end and hopefully one day soon I might even have a 'proper' job! Thank you both so much for your constant support, interest and enthusiasm.

Last but by no means least, I would like to thank my wonderful girlfriend Piley C (aka Eileen) for unfailing support, patience and encouragement. You have been legendary.

Author's Declaration

The research reported in this thesis is the result of my own original work, except where stated otherwise, and has not been submitted for any other degree.

William Proto, September 2010

Definitions and abbreviations

aa	amino acid
bp	base pair
ATG	autophagy related gene
Biotin-HPDP	(N-(6-(Biotinamido)hexyl)-3'-(2'-pyridyldithio)-propionamide
BLEO	bleomycin / phleomycin
BSD	blasticidin
BSA	bovine serum albumin
BSF	bloodstream form <i>T. brucei</i>
CMA	chaperone mediated autophagy
CPA / B	cysteine peptidase A / B
CHAPS	3-(3-Cholamidopropyl)dimethylammonio-1-propanesulfonate
DABCO	4-diazabicyclo[2.2.2]octane
DAPI	4,6-diamidino-2-phenylindole (nucleic acid stain)
DMSO	dimethyl sulfoxide
DNA	deoxyribonucleic acid
DTT	dithiothreitol
EDTA	ethylene diamine tetra acetic acid
ER	endoplasmic reticulum
EF-1 α	elongation factor 1 α
FACS	fluorescence activated cell sorting
FCS	fetal calf serum
FT	flow through
GABARAP	γ -aminobutyric-acid-type-A (GABA _A)-receptor associated protein
GATE-16	Golgi-associated ATPase enhancer of 16kDa
GFP	green fluorescent protein
GPI	glycosylphosphatidylinositol
HA	human influenza hemagglutinin
HIS	histamine
HYG	hygromycin B
HRP	horseradish peroxidase
IPTG	isopropyl- β -D-thiogalactopyranoside
IFT	intraflagellar transport
K	kinetoplast
Kb	kilo base
kDa	kilo Dalton
LC MS/MS	liquid chromatograph tandem mass spectrometry
LB	Luria bertani medium
λ (λ_{Ex} / λ_{Em})	wavelength (excitation λ / emission λ)
μ	micro
m	milli / metre
M	molar
MCA	metacaspase
mRNA	messenger ribonucleic acid
n	nano
N	nucleus
NEM	n-ethylmaleimide
NEO	neomycin
nt	nucleotide
NP40	octylphenyl-polyethylene glycol

OD	optical density
PCD	programmed cell death
PCR	polymerase chain reaction
PBS	phosphate buffered saline
PE	phosphatidylethanolamine
PLD	phospholipase D
RNA	ribonucleic acid
RNAi	ribonucleic acid interference
rRNA	ribosomal ribonucleic acid
SEM	scanning electron microscopy
SERA	serine repeat antigen
SDS-PAGE	sodium dodecyl sulphate polyacrylamide gel electrophoresis
TEM	transmission electron microscopy
UV	ultra violet
UTR	untranslated region
V	volts
VIP	vasoactive intestinal peptide
v/v	volume to volume
w/v	weight to volume
WHO	world health organisation
YFP	yellow fluorescent protein
Z-RR-AMC	benzyloxycarbonyl-arginine-arginine-7-amino-4-methylcoumarin

Amino acid abbreviations

A	alanine (Ala)
C	cysteine (Cys)
D	aspartic acid (Asp)
E	glutamic acid (Glu)
F	phenylalanine (Phe)
G	glycine (Gly)
H	histidine (His)
I	isoleucine (Ile)
K	lysine (Lys)
L	leucine (Leu)
M	methionine (Met)
N	asparagine (Asn)
P	proline (Pro)
Q	glutamine (Gln)
R	arginine (Arg)
S	serine (Ser)
T	threonine (Thr)
V	valine (V)
W	tryptophan (Trp)
X	any amino acid
Y	tyrosine (Tyr)

1 General introduction

The work presented in this PhD thesis covers several aspects of biology relating to the protozoan parasite *Trypanosoma brucei*. The general introduction is intended to provide background information about the parasite that will be of direct relevance to the research discussed in sections 3, 4 and 5.

1.1 Human African Trypanosomiasis

Human African trypanosomiasis (also known as sleeping sickness) is a potentially fatal disease caused by the protozoan parasite *T. brucei*. The causative agents of this disease (African trypanosomes) are classified into two subspecies that are located in distinct geographical regions of Africa. *T. brucei gambiense* is responsible for endemic chronic infections occurring in central and western regions of sub-Saharan Africa and *T. brucei rhodesiense* causes an acute form of the disease in east and southern Africa. A third subspecies *T. brucei brucei* only infects domestic and wild animals but not humans (Brun *et al.* 2010).

The impact of these parasites is widespread across sub-Saharan Africa with the World Health Organisation (WHO) estimating millions of people are at risk in 36 countries (<http://www.who.int/>). Due to the inherent difficulties associated with maintaining thorough surveillance programmes over large areas covering multiple developing countries, it is impossible to know the true human cost. However, the WHO estimate that there are currently between 50,000 and 70,000 new cases per year (<http://www.who.int/mediacentre/factsheets/fs259/en/>). The devastating impact on human life combined with an unquantified toll on domestic livestock mean the African trypanosomes cause a stifling burden on the socio-economic development of effected communities represent a significant challenge for the international community.

T. brucei is an extracellular parasite transmitted between mammalian hosts by the blood feeding tsetse fly (genus *Glossina*) (Figure 1-1). Accordingly, the geographical distribution of the disease is intrinsically linked to the range of the vector and thus restricted to regions of sub-Saharan Africa. Following infection from either *T. brucei gambiense* or *T. brucei rhodesiense* the clinical symptoms

of human African trypanosomiasis present in two main phases. During the initial phase of the disease parasites proliferate and colonise the haemolymphatic system. The second phase (meningo-encephalitic stage) is characterised by invasion of the central nervous system and is associated with the more severe disease symptoms.

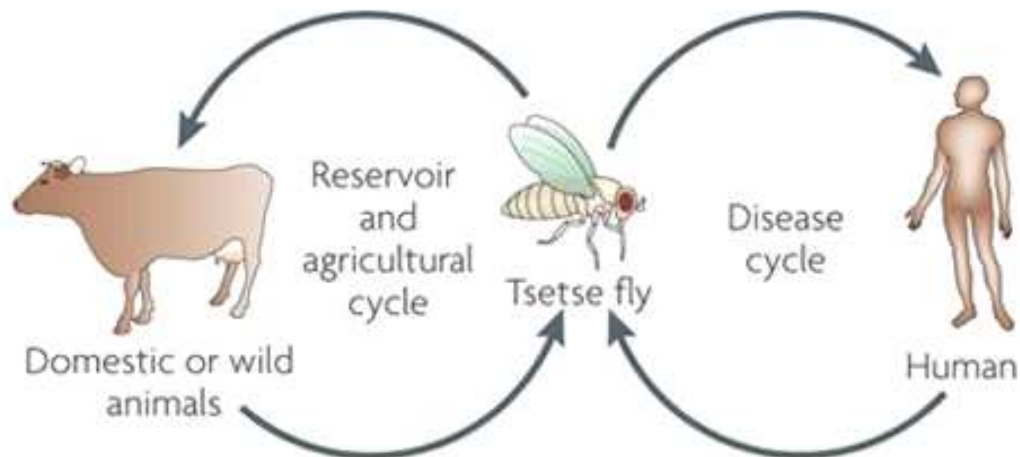


Figure 1-1 Hosts cycles of *T. brucei*.

From Field *et al.* 2009. Diagram depicting the *T. brucei* lifecycle showing tsetse fly vector transmitting parasites between different hosts.

In the absence of treatment infections from both of the human infective subspecies are fatal. *T. brucei gambiense* parasites cause a chronic infection persisting in a patient for an average period of three years (Checchi *et al.* 2008), where as *T. brucei rhodesiense* infections are acute, with patient death typically occurring within months (Odiit *et al.* 1997). The symptoms associated with the initial phase of the disease include general fever and headaches, these are often associated with a flu-like illness which delays formal diagnosis. The latter phase of the disease can be accompanied with bipolar behavioural changes, dysregulation of the circadian rhythm leading to fragmentation of sleeping patterns, coma and ultimately death (Brun *et al.* 2010).

The current therapeutics used to treat human African trypanosomiasis have many limitations: they require lengthy and complex dosing regimens with concurrent high levels of patient care due to frequent adverse reactions. Furthermore, the drugs used to treat the second stage of the disease are linked

to particularly severe complications that can often be lethal (Barrett *et al.* 2007). The limitations of the current therapeutics combined with emerging incidence of drug resistance, highlights the urgent need for the development of new prevention and treatment options.

In the context of this devastating disease a large volume of research has been developed focusing on the characterisation of the fascinating biology of the African trypanosomes. The use of powerful genetic manipulation techniques combined with the wealth of information provided by the sequenced genomes of several trypanosome species (<http://tritrypdb.org>) could eventually help to develop new strategies to combat this disease.

1.2 *T. brucei* cell cycle

At different points during the *T. brucei* lifecycle the parasites are required to colonise the host environment which relies on the rapid proliferation of individual cells. The replication of *T. brucei* parasites broadly follows the same scheme as the mammalian cell cycle. However, an important aspect of *T. brucei* cell division is the coordinated replication and segregation of numerous single copy organelles (e.g. nucleus, mitochondrion, kinetoplast, Golgi, basal body/flagellum complex) with added complexity provided by the independent replication of nuclear and mitochondrial (kinetoplast) DNA (Hammarton 2007; McKean 2003; Sherwin *et al.* 1989). To ensure successful cell division, the organelles are replicated and separated in a precise and ordered manner that occurs during specific phases of the cell cycle (Figure 1-2).

Following the commitment to divide, cells first produce a new basal body which is capable of nucleating the daughter flagellum (Sherwin *et al.* 1989). Shortly afterwards, the Golgi is replicated and localises next to the new basal body and the new endoplasmic reticulum exit site (He *et al.* 2004). Kinetoplast DNA replication commences slightly ahead of the nucleus and takes a shorter amount of time, consequently the kinetoplast DNA is segregated before nuclear replication and segregation are complete (Sherwin *et al.* 1989). In procyclic form cells one nucleus (N) is positioned between both kinetoplasts (K) (giving the formation KNKN), whereas in bloodstream form the two nuclei remain close to

each other (leading to KKNN formation). Cytokinesis occurs after mitosis and follows a unidirectional cleavage furrow moving from the anterior of the cell to the posterior (Hammarton *et al.* 2007; McKean 2003). Due to the highly ordered pattern of cell division, the labelling of cells with appropriate stains, such as DAPI, allows for the accurate determination of the cell cycle stage.

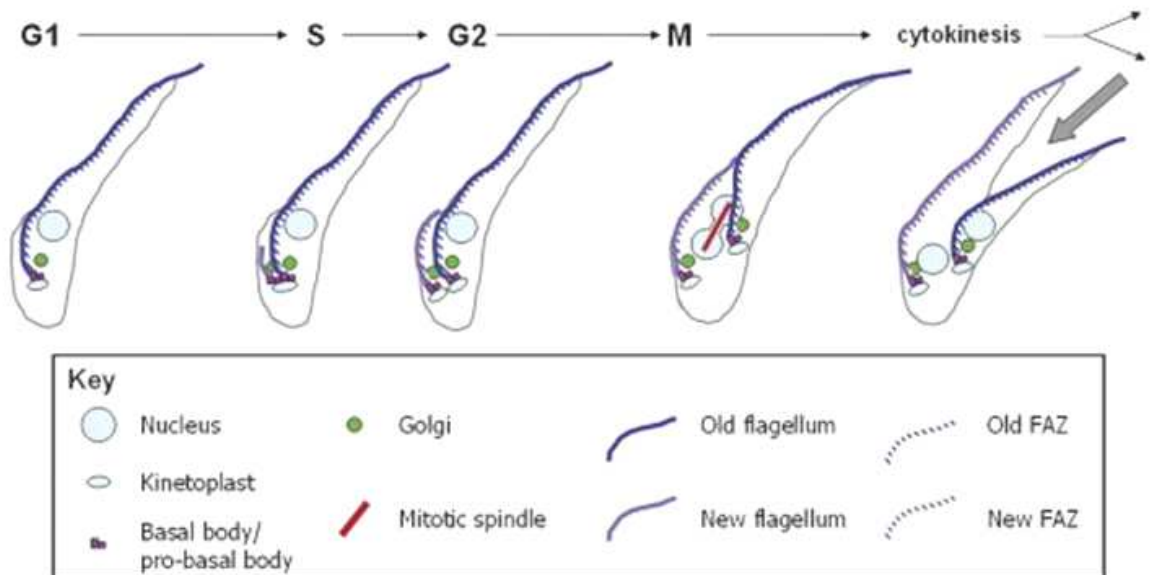


Figure 1-2 Cell cycle of *T. brucei*.

Adapted from McKean 2003. The major events of the cell cycle are illustrated for PCF *T. brucei*. The highly ordered duplication and segregation of single copy organelles is depicted along with the stages of the cell cycle.

1.3 Trypanosome cell biology

T. brucei exist as extracellular parasites that are adapted to survive in two very different host environments (Figure 1-1). A complex lifecycle involving numerous developmental forms ensures that the parasites are optimally adjusted for survival within each host (summarised in Figure 1-4 and discussed in more detail in section 1.4). The parasites replicating in the tsetse fly exist as multiple lifecycle forms (detailed in section 1.4.2) which are broadly referred to as procyclic form (PCF) due to the possession of a surface glycoprotein coat comprised of procyclins (Acosta-Serrano *et al.* 1999). The *T. brucei* lifecycle stage found in mammals are known as bloodstream form (BSF) parasites and are

covered in a dense protein coat comprised of variant surface glycoprotein (VSG) (Johnson *et al.* 1977). In both lifecycle stages the morphology of the parasites is broadly similar characterised by a vermiform shape tapering at both ends. This distinct shape is directed by a spiralled network of over 100 subpellicular microtubules, that run along the axis of the cell beneath the plasma membrane (Sherwin *et al.* 1989).

The trypanosomatids have many characteristic features typical of eukaryotic cells. However, their long independent evolution (Dacks *et al.* 2008) has been accompanied by the development of several unusual organelles and features of cell biology.

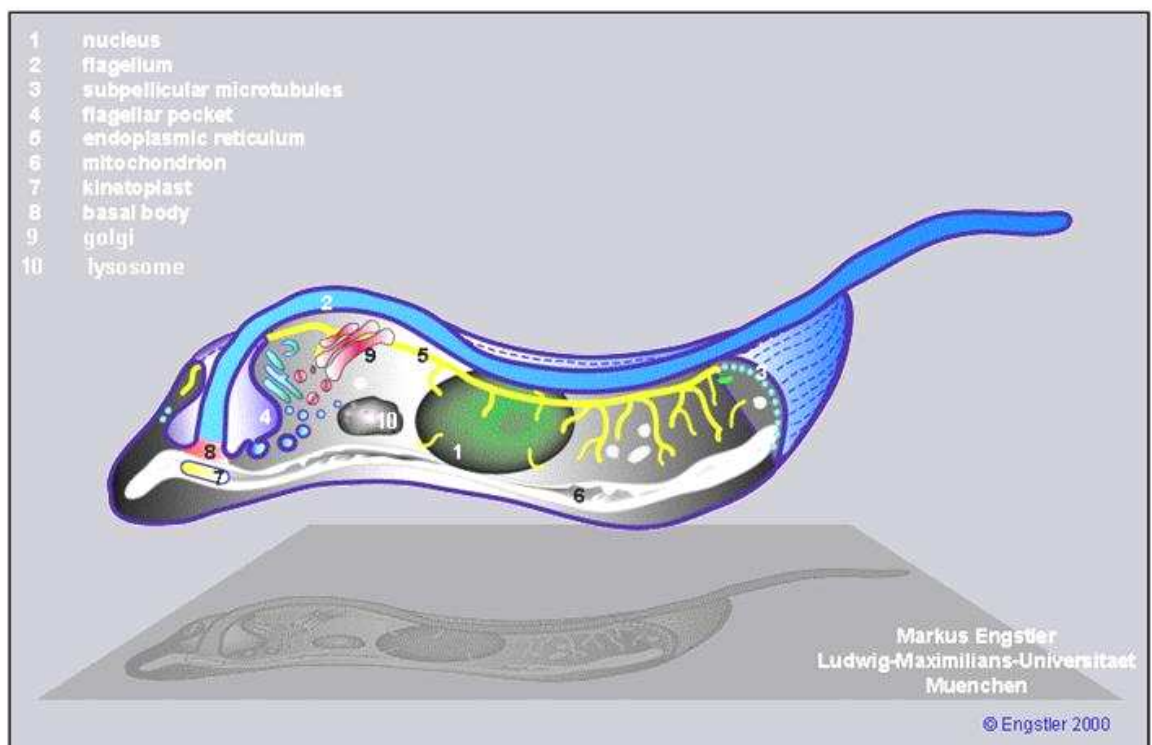


Figure 1-3 Diagram depicting *T. brucei*.

(Diagram adapted from http://www.sanger.ac.uk/Projects/T_brucei/Tryp.cartoon.shtml). Illustration depicting general organisation of bloodstream form *T. brucei* cell. Major cellular structures are indicated.

Perhaps the most apparent feature of the *T. brucei* cell is the highly motile flagellum. This organelle originates from the basal body at the posterior end of the parasite, emerging from the cell body through a specialised invagination in

the plasma membrane called the flagellar pocket (Figure 1-3) (Field *et al.* 2009; Ralston *et al.* 2009). The flagellum is comprised of several prominent structures including the axoneme and the paraflagellar rod (PFR). In common with most other eukaryotes the *T. brucei* axoneme consists of nine outer microtubule doublets encircling a single pair of central microtubule filaments (Ralston *et al.* 2009). The PFR is an unusual flagella structure that is formed from a large paracrystalline filament that runs alongside the axoneme (Ralston *et al.* 2009). The precise role of the PFR is unknown, although it appears essential for flagellar function as PFR disruption causes defects in cell motility (Bastin *et al.* 1998) and cytokinesis in BSF cells (Broadhead *et al.* 2006), which culminates in a loss of infectivity in mouse models (Griffiths *et al.* 2007).

The flagellum is surrounded by its own membrane and is attached to the exterior of the cell body via a series of transmembrane junctions known as the flagellar attachment zone (Kohl *et al.* 1998). The flagellum follows a helical path around the outside of the cell body with a portion freely extending away from the extreme anterior end of the cell. *T. brucei* motility is generated by the propagation of bihelical waves of rotation (left-handed and right-handed helical motion) travelling along the flagellum, separated by a region known as a kink (Rodriguez *et al.* 2009). The flagellum is central to maintaining correct cellular function and pathogenicity, with many critical roles directly linked to motility (Broadhead *et al.* 2006; Griffiths *et al.* 2007; Ralston *et al.* 2006b; Ralston *et al.* 2006a).

Several fundamental aspects of *T. brucei* biology are centred on the flagellar pocket. The plasma membrane surrounding this site is free from the subpellicular microtubule network and consequently represents the only cellular site capable of endocytosis and exocytosis (Field *et al.* 2009). This leads to a highly polarized endomembrane system, with the secretory and endocytic organelles predominantly located between the nucleus and kinetoplast. The endoplasmic reticulum exists as an elongated structure that runs along the length of the cell body from the flagellar pocket to the anterior tip. Excluding the unusual polarization, the endomembrane system of *T. brucei* is broadly similar to other eukaryotes. Indeed representative genes for many protein families known to be involved in vesicle transport have been identified in the *T. brucei* genome (Ackers *et al.* 2005; Berriman *et al.* 2005).

To mediate against the effects of the mammalian host immune system *T. brucei* use two mechanisms that are both heavily reliant on the flagellar pocket and endosomal system. Mammalian anti-VSG antibodies bind to the surface of *T. brucei* and can effectively kill the parasites by complement. One survival method employed by *T. brucei* involves the periodic switching of the VSG surface molecule type to continually evade the host immune response (see section 1.4.1) (Vickerman 1978). A second survival mechanism involves the clearance of surface bound anti-VSG antibodies. This is thought to be mediated by hydrodynamic forces exerted on the swimming parasites that force the anti-VSG antibodies bound to VSG towards to the posterior end of the cell and into the flagellar pocket (Engstler *et al.* 2007). The high endocytic rate in BSF cells ensures that anti-VSG antibody/VSG complexes are rapidly endocytosed by RAB5A containing vesicles from the early endosomal system (Pal *et al.* 2003; Pal *et al.* 2002). The anti-VSG antibody/VSG complexes are separated and anti-VSG is degraded while intact VSG is trafficked back to the surface via RAB11 positive recycling endosomes (Grunfelder *et al.* 2003; Pal *et al.* 2003). Interestingly the enzymes used to selectively degrade anti-VSG antibody are unknown. RAB11 recycling endosomes were found to colocalise with the metacaspase cysteine peptidases MCA2, MCA3 and MCA5, however simultaneous deletion of these MCAs failed to impact on the ability of the null mutant parasites to degrade anti-VSG or recycle VSG (Helms *et al.* 2006).

Given that the flagellar pocket represents only 5 % of the cell surface of *T. brucei*, it does not appear to significantly impede upon rates of trafficking. Indeed BSF *T. brucei* are capable of turning over (endocytosis and recycling back to the surface) their entire pool of cell surface VSG in 12.5 minutes (Engstler *et al.* 2004b). Interestingly endocytosis rates are approximately 10 fold higher in BSF than PCFs, which might reflect the inherent requirement of BSF cells for increased internalisation and degradation in response to the mammalian immune system (Natesan *et al.* 2007).

Unlike many eukaryotes that contain hundreds of individual mitochondria *T. brucei* contains one single elongated mitochondrion that extends the length of the cell body (Figure 1-3). Contained within the mitochondrion is the kinetoplast, a disc-like organelle made of the mitochondrial DNA. The kinetoplast is a complex structure uniquely comprised of a large network of

interlocked circular DNA molecules; thousands of minicircles are interlocked with 20 to 30 maxicircles (Chen *et al.* 1995). The maxicircles all have identical genetic sequences and predominantly encode for the mitochondrial proteins. Minicircles are heterogenous in sequence and encode for guide RNAs which serve as templates for editing maxicircle transcripts (Stuart *et al.* 2005). The kinetoplast is physically connected to the flagellar basal body complex through a series of filaments and the outer mitochondrial membrane (Ogbadoyi *et al.* 2003).

Another interesting feature of *T. brucei* is the compartmentalisation of select metabolic systems into small vesicular structures called glycosomes (Michels *et al.* 2006). The containment of distinct repertoires of metabolic enzymes allows for their rapid turnover which facilitates parasite adaptation in response to changing host environments (Herman *et al.* 2008). In BSF *T. brucei* the mitochondrion is suppressed and the glycosomes are filled with glycolytic enzymes (90% of glycosome protein content) (Michels *et al.* 2006). Oxidative phosphorylation of glucose yields more ATP than glycolysis, however the abundant and constant supply of glucose in mammalian blood, means that the parasites can effectively rely on a simplified metabolism and thus use glycolysis alone to generate ATP (Michels *et al.* 2006). In the tsetse fly sugar availability is changeable and predominantly very low, however amino acids (proline and threonine) are abundant and serve as a more reliable substrate for energy generation. Consequently PCF parasites have a more complex metabolism, involving a functional mitochondrion and more extensive glycosomal metabolic networks (Michels *et al.* 2006).

T. brucei parasites also contain acidocalcisomes, which are distinct organelles involved in the sequestration and storage of polyphosphates, calcium and other cations (Moreno *et al.* 2003). In *T. brucei* the exact role of these small vesicles is not clear, although their surface membrane contains calcium and proton pumps, which has led to the suggestion they are involved in calcium signalling and could facilitate survival during periods of stress (Docampo *et al.* 2005; Moreno *et al.* 2003).

Depending on the developmental form of the parasite the morphological arrangement of several key cellular features is changed. Trypomastigote

parasites are characterised by a kinetoplast and flagellar pocket positioned at the posterior end of the cell with a centrally located nucleus (Field *et al.* 2009). In epimastigotes cells the kinetoplast and flagellar pocket are located to the anterior side of the centrally located nucleus (Field *et al.* 2009).

1.4 *T. brucei* life cycle

1.4.1 *T. brucei* development in the mammalian host

During the *T. brucei* lifecycle the parasite must inhabit the contrasting and challenging environments of the mammalian and insect host (Figure 1-1). The parasite is ingested/transmitted by the tsetse fly (genus *Glossina*) while taking a blood meal during feeding. In mammals the transmitted parasites initially form a lesion (chancre) at the site of the bite, where they multiply before gaining access to the host blood stream. Here parasites exist as rapidly dividing long slender trypanomastigotes that differentiate via an intermediate stage into non proliferative short stumpy trypanomastigotes (Figure 1-4)(Newton 1968). The long slender form is perfectly adapted to exploit the glucose rich environment of the mammalian blood and rapidly divides increasing parasitemia to aid colonisation of the host.

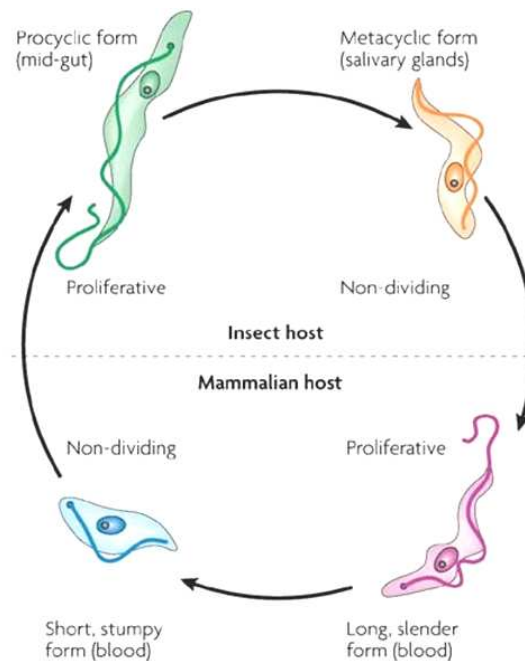


Figure 1-4 Lifecycle of *T. brucei*

Diagram from (Lee *et al.* 2007b). Schematic representing simplified lifecycle of *T. brucei* showing best studied forms from the insect and mammalian host stage.

Following adequate proliferation the long slender trypomastigotes are replaced by the short stumpy form. This differentiation event is suspected to be induced by an as yet unknown parasite signal, referred to as the stumpy induction factor (Vassella *et al.* 1997). The accumulation of non proliferative short stumpy forms at peak parasitemia, prolongs survival within the mammalian host and maximises the chance of successful transmission. The prospects of short stumpy survival in the tsetse fly are further increased by the reactivation of the mitochondrial respiratory chain, which ensures pre-adaptation to the glucose limited environment of the tsetse fly (Michels *et al.* 2006; Priest *et al.* 1994). Thus, stumpy form *T. brucei* are a prerequisite for the efficient transmission from the mammalian to the insect host.

To protect BSF cells from the antagonistic host environment they are coated with a densely packed monolayer of variant surface glycoprotein (VSG), which is comprised of more than 10^7 variable VSG molecules per cell (Cross 1975). Following infection the VSG coat on the surface of the parasite is quickly recognised by the host immune system and a specific antibody response is raised to neutralise and clear the parasites by complement, thus decreasing parasitemia. However in the mammalian host, a subpopulation of trypanosomes arise by changing their surface coat through the expression of different VSG molecules, in a process known as antigenic variation (Vickerman 1978). Through the periodic switching of the surface VSG coat the parasite can evade successive immune responses and persist within the host. The cyclical waves of *T. brucei* parasitemia that are typically observed in chronic *T. brucei* infections, therefore arise from an interplay between the host immune system and parasite derived factors (Lythgoe *et al.* 2007).

1.4.2 *T. brucei* development in the tsetse fly host

Parasites that are fully transformed and adapted to live in the tsetse fly vector are called procyclic form (PCF) cells. When the tsetse fly feeds on an infected mammal the resulting blood meal can contain both long slender and short stumpy parasites. Rapid differentiation of the BSF parasites must take place to ensure PCF cells can prevail in the tsetse mid gut. The transformation to PCF parasites is believed to be triggered by the reduced temperature of the tsetse

fly mid gut, decreasing from 37°C of the mammalian blood to 20°C, the average ambient temperature during peak tsetse fly feeding (Engstler *et al.* 2004a). Additionally, experiments have shown that BSF to PCF differentiation occurs from those cells in the G0 or G1 phase of the cell cycle (Matthews *et al.* 1994; Ziegelbauer *et al.* 1990). Short stumpy cells are arrested in the G0/G1 position of the cell cycle and possess a pre-adapted metabolism; this therefore makes them ideal candidates to rapidly start the differentiation process and attempt colonisation of the tsetse fly mid-gut.

Once in the tsetse fly parasites must undergo a complex development cycle involving several different lifecycle stages and considerable parasite movement between distinct internal compartments of the tsetse fly (Figure 1-5)(Van den Abbeele *et al.* 1999). Despite all the efforts of *T. brucei* to (pre-) adapt to their new environment, two to three days post feeding approximately 99% of the ingested parasites are eliminated by the tsetse fly, with the remaining surviving population fully differentiated into PCF cells (Van den Abbeele *et al.* 1999). Differentiation to PCF cells occurs rapidly and is accompanied by the shedding of the VSG coat and its subsequent replacement with a new surface protein coat comprised of procyclin (Ziegelbauer *et al.* 1990).

In a short space of time the reduced population of PCF cells undergoes vigorous growth and establishes a robust stable population in the midgut. As midgut colonisation progresses (posterior to the anterior direction) there is a concurrent physical elongation of parasites, with long trypomastigote forms (also known as mesocyclic trypomastigotes, displayed in Figure 1-5) found near the proventriculus at 6 days post infection (Van den Abbeele *et al.* 1999). These cells enter the proventriculus and migrate into the tsetse foregut and proboscis, where they undergo further complex differentiation (Figure 1-5). The long trypomastigotes cells replicate their DNA and reposition the kinetoplast and basal body to a location anterior of nucleus (thus becoming long epimastigote forms) and subsequently finish mitosis and divide asymmetrically producing long and short daughter cells (Van den Abbeele *et al.* 1999). The flagella of the short daughter epimastigotes prohibits efficient movement, thus it is proposed that attached asymmetrically dividing cells are propelled to the salivary gland using the flagellar of the long epimastigote. Once in the salivary gland, cell separation occurs and the short epimastigote attaches to the salivary gland wall

and further develops into metacyclic forms ready for retransmission into a mammalian host (Van den Abbeele *et al.* 1999).

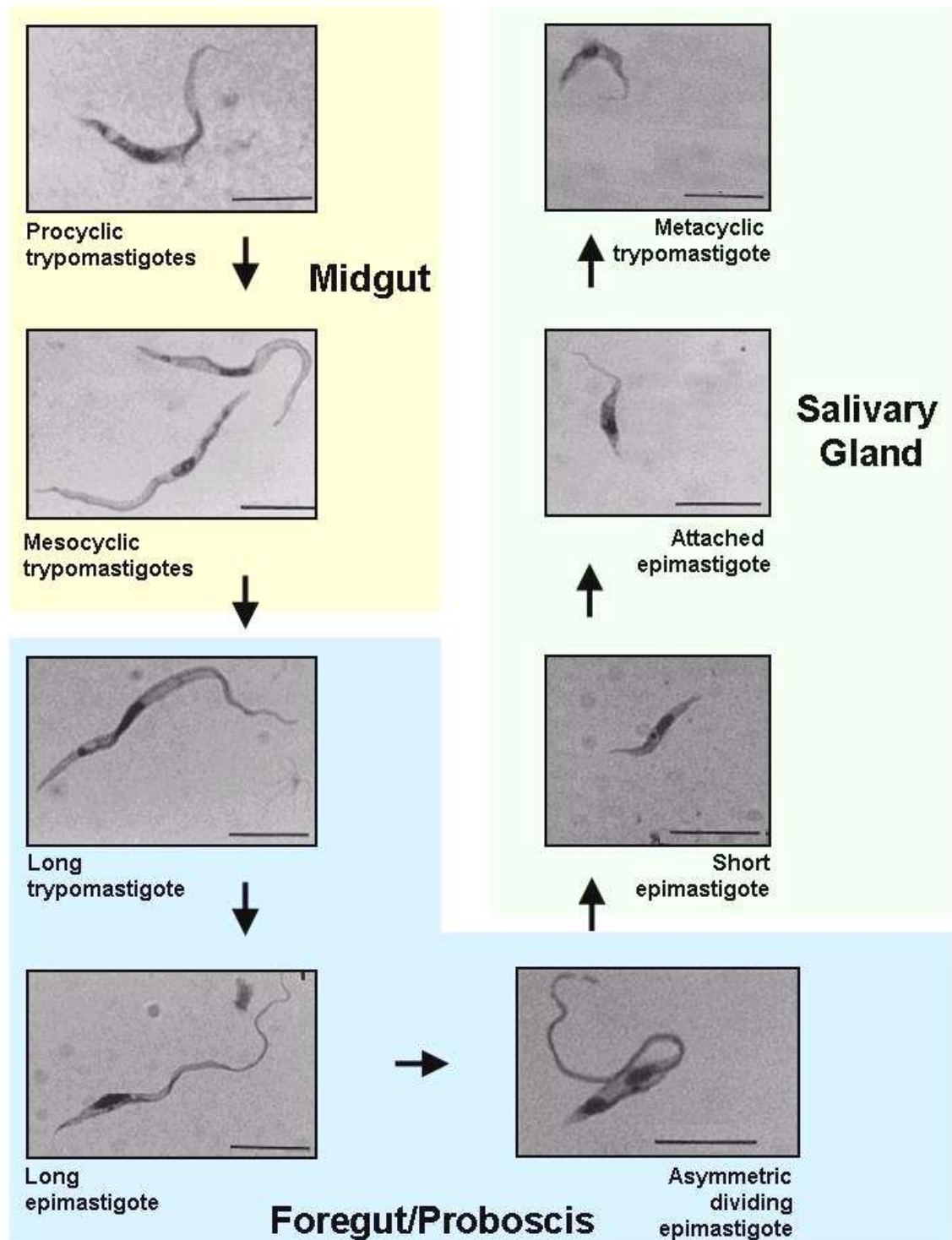


Figure 1-5 Development of *T. brucei* in the tsetse fly.

Adapted from Van den Abbeele *et al.*, 1999. Light microscopy images of the different morphological stages of *T. brucei* isolated from the tsetse fly vector. Scale bar represents 10 μm .

As illustrated in this introduction *T. brucei* is subject to numerous challenges arising from the pressures exerted by hostile host environments. Consequently the parasite has evolved a complex lifecycle that encompasses drastic and varied alterations to help ensure survival. Given the widespread burden inflicted by the disease causing forms of *T. brucei* it is evident that the parasite is extremely successful and increased efforts are needed to gain a more detailed understanding of the complex biology of this parasite. The research presented in this PhD focuses on two different topics:

Autophagy is a degradative process used by eukaryotic cells to break down and recycle their own components in the lysosome. In light of the complex cellular remodelling that occurs during the *T. brucei* lifecycle and the contrasting host environments occupied, we speculate that autophagy could be exploited by the parasites to enable efficient adaptation and survival. In section 3 autophagy is introduced in detail and results generated depicting the characterisation of this process in *T. brucei* are presented and discussed.

In section 4 the focus is turned to *T. brucei* MCA4. The MCAs are cysteine peptidases that are only found in plants, fungi and protozoa but are absent from mammals (detailed introduction in section 4). To provide a more complete understanding of the *T. brucei* MCAs, a detailed investigation into MCA4 was performed focusing on *in vivo* characterisation combined with *in vitro* analysis of the recombinant enzyme.

2 Methods

2.1 Bacteria: strains and culture

2.1.1 Bacteria strains

For standard plasmid transformation and preparation, competent host strains with low endonuclease activity were used to ensure high quality DNA. The strain typically used was *E. coli* XL1-Blue (genotype *recA1 endA1 gyrA96 thi-1 hsdR17 supE44 relA1 lac*, tetracycline resistant) (Stratagene).

When working with restriction endonucleases sensitive to DNA methylation (e.g. *BclI*) a methyltransferase free host strain was used; *E. coli dam-1 dcm- 2925* (New England Biosciences). Due to the low transformation efficiency of these cells they were not used as primary hosts for the transformation of ligation reactions.

For the expression of recombinant proteins different *E. coli* strains were used, each selected following optimisation specific to the individual protein expressed. The strains used were: *E. coli* BL21 (DE3) (Novagen) and *E. coli* BL21 (DE3) Rosetta (Novagen). DE3 strains contain an IPTG-inducible T7 RNA polymerase gene and are specifically designed for high level expression of proteins using compatible vectors such as the pET system (Novagen). *E. coli* (DE3) Rosetta harbour a plasmid encoding for rare *E. coli* tRNAs and consequently are optimised for bacterial expression of proteins containing unusual codons.

2.1.2 Bacterial transformations

Heat shock transformation was used to introduce plasmids into competent *E. coli* cells. Aliquots of competent *E. coli* (strain XL1-Blue) were thawed on ice and mixed with 1 µl purified plasmid or 5 µl ligation reaction mix and incubated on ice for 30 minutes. Cells were heat shocked in a 42°C water bath and returned to ice for 5 minutes, before plating onto Luria Bertani (LB) agar plates supplemented with appropriate antibiotics.

2.1.3 Bacterial culture and storage

Following plasmid transformation into an *E. coli* host strain, the cells were spread onto LB-agar plates supplemented with the appropriate antibiotics (ampicillin 100 $\mu\text{g ml}^{-1}$, kanamycin 50 $\mu\text{g ml}^{-1}$, or chloramphenicol 40 $\mu\text{g ml}^{-1}$) and incubated overnight at 37°C. Individual colonies were used to inoculate liquid cultures as necessary. For long term storage of bacteria 0.5 ml of an overnight culture was mixed with an equal volume of 2 % (w/v) peptone and 40 % (v/v) glycerol and stored at -80°C.

2.1.4 Production of competent *E. coli* cells

Competent *E. coli* cells were prepared using rubidium chloride treatment. Briefly, a single colony of the required *E. coli* strain was inoculated into 5 ml LB broth and grown overnight at 37°C. The following day the culture was diluted 1:1000 into 50 ml of fresh LB broth and grown at 37°C until the optical density reached 0.6 (at 600 nm). The culture was cooled on ice for 10 minutes and centrifuged at 2000 g for 15 minutes at 4°C. The cell pellet was gently resuspended in 16 ml chilled RF1 buffer (100 mM rubidium chloride, 50 mM $\text{MnCl}_2 \cdot 4\text{H}_2\text{O}$, 30 mM potassium acetate, 10 mM CaCl_2 , 15 % glycerol, adjusted to pH 5.8 using acetic acid) and incubated on ice for 15 minutes before repeat centrifugation. The cell pellet was resuspended in 4 ml of ice cold RF2 buffer (10mM MOPS pH 6.8, 10 mM rubidium chloride, 75 mM CaCl_2 , 15 % glycerol adjusted to pH 6.8 with NaOH) and maintained on ice for 1 hour, before snap freezing aliquots in an ethanol-dry ice bath. Competent cell aliquots were stored at -80°C.

2.2 Molecular biology techniques

2.2.1 Polymerase chain reaction

Polymerase chain reactions (PCR) were performed in a PCR Express machine (Hybaid). Standard PCRs were performed with *Taq* polymerase (New England Biolabs), however for cloning work high-fidelity proof-reading enzymes were

used: *Pfx50* (Invitrogen), *PfuTurbo* (Stratagene) and Phusion (Finnzymes). All polymerases were used according to manufacturers' guidelines.

In general PCR reactions were composed of the following constituents: template DNA (100 ng genomic DNA or 100pg plasmid DNA), 2.5 μ l of appropriate 10 x PCR mix (1.13 mg ml⁻¹ BSA, 450 mM Tris pH 8.8, 110 mM ammonium sulphate, 45 mM MgCl₂, 68.3 mM β -mercaptoethanol, 44 μ M EDTA pH 8.0, 10 mM dCTP, 10 mM dATP, 10 mM dGTP, 10 mM dTTP), 5 pmol of each primer, 1 unit of *Taq* polymerase and autoclaved distilled water to a final volume of 25 μ l. Typically the PCR machine was programmed for an initial denaturation step of 95°C for 5 minutes, followed by 30 cycles of: denaturation 95°C for 30 seconds; annealing at [T_m of primers] -2°C for 30 seconds; extension at 72°C for *Taq* polymerase, 30 seconds per 0.5 kb of sequence. The PCR conditions were optimised for each reaction adjusting primer annealing temperature, elongation time and extension temperature as required.

All oligonucleotide primers were designed using Vector NTI software package (Invitrogen) and produced by Eurofins MWG Operon (Ebersberg, Germany). Details of oligonucleotide primers listed in Table 2-1 and Table 2-2.

Description & Gene	Oligo Number	Sequence	Rest. Site
<i>In situ</i> N-terminal GFP tagging			
<i>Tb</i> ATG8.1 (Tb927.7.5900)	OL2304	CAGATATTACGCTAGGGTAGGGAGAAGAAGGGAAAGCTGTG GTAAGTCAAAGGAGAGCAAGGGGGGACAGGGACAAAATTAT GGCCAAGCCTTTGTCTCAAG	
	OL2305	GAAAATGGTTGGGGTACTCTTGCGCACCTTTGCGGATTCA TTCAATCGCTTACCAGAGAATGTGAATCCTTGAAGTTATACT TCTGTACAGCTCGTCCATGCCGAG	
Sequencing primer for <i>in situ</i> GFP-ATG8.1	OL2506	TCTCGATCTGCATCCTGGGATC	
	OL2507	GGGTCAGCTTGCCGTAGGTGGC	
Recombinant protein expression (desination vector pET28a+)			
<i>Tb</i> MCA4 (Tb927.10.2440)	OL2329	<u>CCGCTCGAG</u> CTACAGGAGCGTCCGTTCTCTGC	<i>XhoI</i>
	OL2330	GGAATTC <u>CATATG</u> ATGGAGGCTGCGTCAGTAC	<i>NdeI</i>
Site directed mutagenesis MCA4 S219C	OL2605	GCTGTGTTGACTGCTGCCACTCCGGTTCTATGC	
	OL2606	GCATAGAACCGGAGTGGCAGCAGTCGAACACAGC	
Site directed mutagenesis MCA4 H164A	OL2972	CACTACTCGGGTGCTGGTACGCGTGCTAAC	
	OL2973	GTTAGCACGCGTACCAGCACCCGAGTAGTG	
Site directed mutagenesis MCA4 K64G	OL3650	CGGAAGCTAAGGAATCTGGAGGTTTTTCAGCCCGTGG	
	OL3651	CCACGGCTGAAAACCTCCAGATTCCTTAGCTTCGG	
Site directed mutagenesis MCA4 S219G	OL3652	GCTGTGTTGACTGCGGTCACTCCGGTTCTATGC	
	OL3653	GCATAGAACCGGAGTGACCGCAGTCGAACACAGC	
Site directed mutagenesis MCA4 C218G	OL3654	CACAGCTGTGTTGACGGTTCGCACTCCGGTTC	
	OL3655	GAACCGGAGTGCGAACCGTTCGAACACAGCTGTG	
Site directed mutagenesis MCA4 C218G,S219G	OL3685	CAGCTGTGTTGACGGTGGTCACTCCGGTTCTATGC	
	OL3686	GCATAGAACCGGAGTGACCACCGTTCGAACACAGCTG	
<i>Tb</i> ATG8.1 (Tb927.7.5900)	OL2775	<u>AGCTAGCATGAAGTATAACTTCAAGGATTC</u>	<i>NheI</i>
	OL2776	<u>GCTCGAGTTATCCAAATGCCGCTCACCTG</u>	<i>XhoI</i>
RNAi Constructs (pT27^{ti})			
<i>Tb</i> MCA4 (Tb927.10.2440)	OL2312	TCGGGATCCATTTTGCGGTATTTGGCTTG	<i>Bam</i> HI
	OL2313	TGCCACCTTCTGTCTCACTGAAGCTTTCG	<i>Hind</i> III
<i>Tb</i> ATG3 (Tb927.2.1890)	OL3668	GCAAGCTTGGAGATGAACTGCTGCAC	<i>Hind</i> III
	OL3669	GCGGATCCGACACGGATGAATGCTGATGC	<i>Bam</i> HI
RT-PCR <i>Tb</i> ATG3 (Tb927.2.1890)	OL3734	AACAGTGTTGTTGGTGTAAACCGA	
	OL3735	GCAGTTCATCTCCAGCTTGAATAA	

Table 2-1 Oligonucleotides used in this study.

Targeted gene (tritypDB identifiers in brackets) or description is indication with the appropriate sequence information and where used endonuclease restriction enzyme sites (underlined).

N-terminal YFP Inducible Expression Constructs			
TbATG8.1 (Tb927.7.5900)	OL2621	<u>CCCAAGCTT</u> CCGCCACCATGAAGTATAACTTCAAG	<i>HindIII</i>
	OL2622	CGGGATCCAGAACCTTATCCAAATGCCGCCTCAC	<i>BamHI</i>
TbATG8.2 (Tb927.7.5910)	OL2623	<u>CCCAAGCTT</u> CCGCCACCATGAGTAAAAAAGATAGC	<i>HindIII</i>
	OL2624	CGGGATCCAGAACCTTAGCATCCAAATGTCGC	<i>BamHI</i>
TbATG8.3 (Tb927.7.3320)	OL2625	<u>CCCAAGCTT</u> CCGCCACCATGCCTTCACTACC	<i>HindIII</i>
	OL2626	CGGGATCCAGAACCTCAACCAAATGTATTTTC	<i>BamHI</i>
N-terminal HA Inducible Expression Construct			
TbMCA4 (Tb927.10.2440)	OL3397	<u>CAAGCTT</u> CCGCCACCATGGGAGGCTGCGTC	<i>HindIII</i>
	OL3398	<u>CTGATCAGGATCC</u> AGAACCCAGGAGCGTCCGTTCTG	<i>BamHI BclI</i>
MCA4 knock-out constructs			
TbMCA4 (Tb927.10.2440) 5' knockout flank	OL3245	GCGCGGCCGCTTTCGATAAAAAATGTAAATAAGGGGC	<i>NotI</i>
	OL3246	<u>GCTCTAGAAAAGAAAGCAAAGAGACGTACACTTGGC</u>	<i>XbaI</i>
TbMCA4 (Tb927.10.2440) 3' knockout flank	OL3247	CCGGGCCATTCTTTTTATTCTGTTACAACCTCG	<i>ApaI</i>
	OL3248	GCGGGCCC <u>CTCGAG</u> CGGAAAATAACACGAAACGTGTTTC	<i>ApaI XhoI</i>
MCA4 re-expression construct			
TbMCA4 (Tb927.10.2440)	OL3403	<u>CCTCGAGCCGCCACCATGGGAGGCTGCGTCAGTAC</u>	<i>XhoI</i>
	OL3404	CGGATCCAGAACCCCTACAGGAGCGTCCGTTCTG	<i>BamHI</i>
Site directed mutagenesis pGL1742 -	OL3046	GTCCGAGGGCAAAGGAATGATCACCTCGGAGATC	
	OL3055	GATCTCCGAGGTGATCATTCTTTGCCCTCGGAC	
Site directed mutagenesis pGL1742 -	OL3047	GGTGAGTTCAGGCTTTTTCATATGCACTAGTAGC	
	OL3048	GCTACTAGTGCATATGAAAAAGCCTGAACTCACC	
BSD gene from pGL1466	OL3049	<u>GCCATATGGCCAAGCCTTTGTCTCAAGAAG</u>	<i>NdeI</i>
	OL3050	<u>GCTGATCAGCCCTCCACACATAACCAGAG</u>	<i>BclI</i>

Table 2-2 Oligonucleotides used in this study (continued).

Targeted gene (tritypDB identifiers in brackets) or description is indication with the appropriate sequence information and where used endonuclease restriction enzyme sites (underlined), second restriction site coloured red.

2.2.2 DNA gel electrophoresis

DNA gel electrophoresis was typically carried out in a 1 % gel (w/v) made from agarose (UltraPure, Invitrogen) in 0.5 x TRIS borate buffer (TBE) (20 mM Tris, 20 mM boric acid, 0.5 mM EDTA, pH 7.2). The agarose solution was solubilised in TBE buffer by briefly boiling in a microwave. Once cool 1 $\mu\text{g ml}^{-1}$ of SYBR Safe DNA stain (Invitrogen) was added and the gel was cast. DNA samples were prepared with 6 x DNA loading dye (0.25 % (w/v) bromophenol blue, 0.25 % (w/v) xylene cyanol FF, 30 % (v/v) glycerol) and electrophoresed in Life Technologies Horizon gel tanks at 100 V. For reference, a 1 kb DNA ladder (Invitrogen) was used at 0.5 μg per lane. To visualise nucleic acids gels were exposed to U.V. light, using a BioRad Gel-Doc imager and Quantity One software. When the DNA was destined for use in cloning or transfection it was visualised using a

DarkReader blue light transilluminator and extracted from the agarose gel using a Gel Extraction kit (Qiagen) according to the manufacturer's instructions.

2.2.3 Cloning PCR products

The subcloning vectors pGEM-T-Easy (Promega) and TOPO (Invitrogen) were used to establish stable vectors containing PCR products. Typically, after high fidelity proof reading PCR, the product was incubated at 72 °C for 15 minutes with 0.5 units of *Taq* polymerase (A-tailing step). A 2 µl aliquot of the PCR product was ligated into the pGEM-T-Easy or TOPO vector according to manufacturers' instructions. Ligated plasmids were transformed into heat-shock competent *E. coli* XL1-Blue cells. Successful transformants were selected on LB agar plates containing 50 µg ml⁻¹ of ampicillin and insertion of a PCR product was assessed by a concurrent blue/white colony screen stemming from 0.5 mM IPTG and 80 µg ml⁻¹ X-gal previously applied to surface of LB plates. Integration of the PCR product was confirmed by PCR screen of 10 white colonies, picked using a sterile tooth pick and inoculated into 5 µl of distilled water. PCR was run as standard except the DNA was replaced with 5 µl colony/water mix and the denaturation step increased to 10 minutes. Vector specific primers (pGEM-T-Easy T7 and SP6; TOPO M13 Forward and Reverse) spanning the cloning site were used to verify the presence of an appropriate sized insert. Where necessary the PCR product was sequenced.

2.2.4 Restriction endonuclease digestion

Nucleic acids (plasmid and genomic DNA) were digested using restriction endonucleases from New England Biolabs. Digestion reactions were performed as recommended by the manufacturer, with restriction endonuclease(s) used with the optimum reaction buffer (New England Biolabs), supplemented with BSA where appropriate. Digested DNA was visualised by agarose gel electrophoresis and if required, purified using a Gel Extraction kit (Qiagen) according to the manufacturer's instructions.

2.2.5 Ligation

Ligation of DNA was performed using T4 DNA ligase and T4 ligase buffer (New England Biolabs) in reactions as per the manufacturer's instructions. Typically digested plasmid and DNA insert were purified using a Gel Extraction kit (Qiagen) and added to 10 µl ligation reaction in different ratios (insert:vector, 1:3, 3:1, 1:1) and incubated overnight at 16°C. For blunt-ended ligations digested vectors were treated with CIP (calf intestinal alkaline phosphatase, New England Biolabs) to prevent self religation. Following ligation 2 µl of the reaction was transformed into competent *E. coli* cells and selected using the appropriate antibiotic. Correct ligation was verified by colony PCR (using insert and vector specific primer pairs) or by plasmid purification and restriction digest analysis.

2.2.6 Sequencing

All DNA sequencing was performed by the Sequencing Service of the University of Dundee (www.dnaseq.co.uk). The sequence data were analysed using the Vector NTI applications ContigExpress and AlignX (Invitrogen).

2.3 Plasmid generation

All plasmids described in this study are detailed in Table 2-3, and specific details regarding their construction listed below. All oligonucleotide primers were designed using sequence information provided by tritrypDB or geneDB (<http://tritrypdb.org> or <http://www.genedb.org>). Plasmids generated are listed in Table 2-3.

Plasmid number	Plasmid backbone	Description
pGL1810	ToPO/pGL1466	GFP-ATG8.1 (Tb927.7.5900) <i>in situ</i> fusion. Amp/Bsd
pGL1897	pET28a+	MCA4 (Tb927.10.2440) protein expression. Kan
pGL1811	pET28a+	MCA4 S219C (Tb927.10.2440) protein expression. Kan
pGL2115	pET28a+	ATG8.1 (Tb927.7.5900) protein expression. Kan
pGL1895	p2T7ti	MCA4 (Tb927.10.2440) RNAi. Amp/Bleo
pGL2065	p2T7ti	ATG3 (Tb927.2.1890) RNAi. Amp/Bleo
pGL1843	pGL1731	ATG8.1 (Tb927.7.5900) tetracycline inducible expression of N-terminal YFP fusion. Amp/Bleo
pGL1835	pGL1731	ATG8.2 (Tb927.7.5910) tetracycline inducible expression of N-terminal YFP fusion. Amp/Bleo
pGL1836	pGL1731	ATG8.3 (Tb927.7.3320) tetracycline inducible expression of N-terminal YFP fusion. Amp/Bleo
pGL2010	pGL1728	MCA4 (Tb927.10.2440) tetracycline inducible expression of N-terminal HA fusion. Amp/Bleo
pGL1985	pGL1689	MCA4 (Tb927.10.2440) knockout. Amp/Hyg
pGL1986	pGL1689	MCA4 (Tb927.10.2440) knockout. Amp/Neo
pGL2067	pGL1742	MCA4 (Tb927.10.2440) re-expression. Non- tagged with switched resistance marker in pGL1742. Amp/Bsd
pGL2070	pGL1742	MCA4 C218G, S219G (Tb927.10.2440) re-expression. Non- tagged with switched resistance marker in pGL1742. Amp/Bsd
pGL2071	pGL1742	MCA4 S219C (Tb927.10.2440) re-expression. Non- tagged with switched resistance marker in pGL1742. Amp/Bsd

Table 2-3 Plasmids used in this study.

Plasmids generated for use in this study, including target gene (with tritrypDB identifier in bracket), plasmid backbone and brief description. Drug resistance listed, stating bacterial then trypanosome resistance markers. Plasmid generation described in section 2.3.

2.3.1 *In situ* fluorescent tagging of *T. brucei* ATG8.1

The native *T. brucei* ATG8.1 (Tb927.7.5900) locus was modified to include N-terminal human influenza hemagglutinin (HA) and green fluorescent protein (GFP) epitope tags, using a PCR-based strategy as described by Shen *et al* 2001. Briefly, OL2304 and OL2305 were designed to amplify an HA:GFP cassette (including blasticidin drug resistance) from pGL1466. The oligos also introduced 80 base-pairs (bp) additions to each flank, corresponding to the genomic sequence immediately up- and downstream of the *T. brucei* ATG8 start codon and were used to target the epitope tag and drug resistance marker to the

correct locus. The 1899 bp PCR product was amplified using high fidelity *Pfx50* and cloned into the TOPO vector generating pGL1810. The construct was verified by sequencing and for transfection pGL1810 was digested with *EcoRV*.

2.3.2 Recombinant protein expression plasmids

T. brucei MCA4 was amplified from genomic DNA (strain 427) using *Pfx50* (Invitrogen) with OL2329 (*NdeI*) and OL2330 (*XhoI*), with the added restriction sites indicated in brackets. The resulting product was cloned into TOPO and sequenced before excision using *NdeI* and *XhoI* (New England Biolabs) and ligated into the pET-28a(+) *E. coli* protein expression vector (pGL655), pre-digested with *NdeI* and *XhoI*. The resulting plasmid was named pGL1697.

The same procedure was repeated with ATG8.1 (Tb927.7.5900) amplified from *T. brucei* genomic DNA (strain 427), using primers OL2775 (*NheI*) and OL2776 (*XhoI*). The generated RNAi plasmid was named pGL2115.

2.3.3 RNAi constructs

The MCA4 RNAi target fragment was identified using the TrypanoFAN: RNAi target selection script (<http://trypanofan.path.cam.ac.uk/software/RNAit>). The identified 469 bp fragment of *T. brucei* MCA4 was amplified from genomic DNA (strain 427) by PCR using *Pfx50* (Invitrogen) with primers OL2312 (*BamHI*) and OL2313 (*HindIII*), with the added restriction sites in brackets. The resulting product was cloned into TOPO and sequenced before excision and ligation into pGL571, pre-digested with *BamHI* and *HindIII*. The resulting plasmid was named pGL1695.

The same procedure was repeated with a 500 bp fragment of *T. brucei* ATG3 (Tb927.2.1890) amplified from *T. brucei* genomic DNA (strain 427), using primers OL3668 (*HindIII*) and OL3669 (*BamHI*). The generated RNAi plasmid was named pGL2065.

To prepare the RNAi plasmids for transfection they were digested with *NotI*.

2.3.4 MCA4 knockout constructs

The 5' and 3' flanks of MCA4 (Tb927.10.2440) were amplified by PCR from genomic DNA (strain 427) with Phusion (Finnzymes) and the primer pairs OL3245 (*NotI*) / OL3246 (*XbaI*) and OL3247 (*ApaI*) / OL3248 (*ApaI* and *XhoI*), respectively. The restriction sites added by each oligonucleotide are indicated in brackets. The resulting fragments were cloned separately into pGEM-T-Easy and confirmed by sequencing. The 5' and 3' flanks were excised using *NotI/XbaI* and *ApaI/XhoI* and sequentially ligated into pGL1689, first pre-digested with *NotI/XbaI* and secondly with *ApaI/XhoI*. The resulting construct was named pGL1986, the NEO MCA4 knockout construct. Exchange of resistance genes was achieved by excising the HYG gene from pGL1688 using *BmgBI* and *BglII* and cloning this into pGL1986 pre-digested with *BmgBI* and *BglII*, generating pGL1985 the HYG MCA4 knockout construct. For transfection into *T. brucei* pGL1986 and pGL1985 were digested with *NotI* and *XhoI*.

2.3.5 MCA4 re-expression construct

To switch the HYG resistance gene of pGL1742 site directed mutagenesis was used to introduce specific restriction sites (*NdeI* and *BclI*) flanking the HYG gene, which was subsequently excised using *NdeI* and *BclI* (New England Biosciences) and replaced with the BSD gene. The resulting construct was digested with *XhoI* and *BamHI* (removing YFP tag) and the MCA4 gene was cloned in using the same restriction sites, producing pGL2067.

2.3.6 Tagging of genes expressed from ectopic locus

The plasmids used to for the ectopic expression of epitope tagged genes are described in detailed by Kelly *et al.*, 2007.

ATG8.1 (Tb927.7.5900) was amplified from genomic DNA (strain 427) by PCR with *Pfx50* (Invitrogen) using primers OL2621 (*HindIII*) and OL2622 (*BamHI*), the added restriction sites are in brackets. The resulting fragment was cloned into TOPO and sequenced before ligation into pGL1731, pre-digested with *BamHI* and *HindIII*. This created an N-terminal yellow fluorescent protein (YFP) tagged ATG8.1 expression construct, named pGL1843.

Additional N-terminally tagged YFP expression constructs were prepared by following the same procedure for *T. brucei* ATG8.2 (Tb927.7.5910), using primers OL2623 (*Hind*III) and OL2624 (*Bam*HI), producing pGL1835 and *T. brucei* ATG8.3 (Tb927.7.3320), using primers OL2625 (*Hind*III) and OL2626 (*Bam*HI), producing pGL1836.

A construct to express MCA4 with 6 HA epitope tags fused to the C-terminus was generated as above using primers OL3397 (*Hind*III) and OL3398 (*Bam*HI and *Bcl*I) and the plasmid backbone pGL1728. The resulting construct was named pGL2010.

2.4 Site directed mutagenesis

To change specific amino acids of proteins expressed from plasmids, targeted alterations were made to the nucleotide sequence using the Quick Change Mutagenesis Kit (Stratagene), according to manufacturer's instructions. All mutations were confirmed by DNA sequencing.

2.5 Preparing DNA for transfection

DNA used in trypanosome transfections was linearised by digestion with the appropriate restriction endonucleases and purified by ethanol precipitation. The digestion reaction volume was estimated and 0.1 volumes of sterile 3 M sodium acetate solution pH 5.2, was added and vortex mixed. A further 2.5 volumes of 100 % ethanol was added and vortex mixed before incubation at -80°C overnight. The solution was centrifuged at 14, 000 g for 20 minutes at 4°C. The DNA pellet was then washed twice in 70 % ethanol and re-suspended in 10 µl sterile autoclaved water and stored at -20°C until needed.

2.6 Southern blotting

Southern blotting was used to confirm the presence of specific DNA sequences in genomic DNA isolated from *T. brucei*. Extracted genomic DNA was digested overnight using the appropriate enzymes and efficient digestion was verified by visualisation of 1 µl of digestion mix run on an agarose gel. Digested DNA (5 µg)

from the different cell lines analysed was electrophoresed at a low voltage in a large 0.8 % agarose gel (200 ml) stained with SYBR-Safe DNA stain (Invitrogen). To enable subsequent estimation of DNA fragment size, a photograph of the gel (exposed to U.V. light) was taken with a ruler alongside to allow correlation of the 1 kb DNA ladder bands with the migration distance. Purines were removed from the gel by gentle washing in 0.25 M HCl for 10 minutes, before washing in distilled water. The gel was then immersed in denaturation buffer (1.5 M NaCl, 0.5 M Tris-HCl, pH 7.0) for 30 minutes and gently agitated before rinsing in distilled water. Finally the gel was incubated in neutralisation buffer (3 M NaCl, 0.5 M Tris-HCl, pH 7.0) for 30 minutes and rinsed in distilled water.

To transfer the DNA onto a nylon membrane (Hybond-N, GE Healthcare) the gel was placed onto a blotting paper wick, the ends of which were immersed in 20 x SCC buffer (3 M NaCl, 0.3 M sodium citrate pH 7.0). The membrane was layered on top of the gel, with two sheets of blotting paper and excess weighted paper towels added to draw the 20 X SCC buffer up the wick. The transfer was left to occur overnight and then the membrane was washed in 2 x SCC buffer before the DNA was crosslinked to the membrane in a U.V. Stratalinker 2400 crosslinker (Statagene) set at 1200 mJoules.

The blot was prehybridized and probed overnight with DNA digested out of a plasmid (corresponding to either the 5' flanking region used for MCA4 replacement, pGL1985 or the MCA4 open reading frame, pGL1697) labelled with the Alk-Phos Direct labelling kit (Amersham) as per the manufacturer's instructions. Signal was detected using CDP-Star detection reagent (Amersham) and exposed using a Kodak film imager. The blot was stripped by incubation in 0.5 % SDS and re-probed following the same protocol detailed above.

2.7 Protein biochemistry

2.7.1 Recombinant protein: expression and purification

The MCA4 protein expression vector (pGL1697) was transformed into *E. coli* BL21 Rosetta cells (Stratagene) and an individual colony used to inoculate a 10 ml starter culture of Overnight Express TB Medium (Novagen). After 10 hours

growth the starter culture was used to inoculate 300 ml of pre-warmed Overnight Express TB Medium which was incubated overnight at 37°C with shaking at 220 rpm. The following morning the cells were harvested by centrifugation at 4500 g for 20 minutes and the pellet frozen at -20°C until required.

The cell pellet was thawed on ice and lysed in 40 ml of Bacterial Protein Extraction Reagent (B-PER) (Pierce) supplemented with 10 µg ml⁻¹ DNase 1 (Sigma) and incubated on a rotary shaker at 4°C for 30 minutes. The solution was fractionated by high-speed centrifugation at 16,000 g for 20 minutes and the soluble fraction was filtered through a 0.2 µm filter (Ministart) and stored on ice. The recombinant HIS tagged protein was then purified from the soluble fraction by immobilised metal ion affinity chromatography on a column packed with Metal Chelate-20 (Poros) operated by the BioLogic DuoFlow purification system (Bio-Rad). All buffers used were stored on ice before and during purification. The column was equilibrated with equilibration buffer (50 mM NaH₂PO₄, 300 mM NaCl and 0.5mM imidazole, pH 8.0) before loading of the soluble fraction at 5 ml/minute. Contaminating proteins were removed from the column with wash buffer (50 mM NaH₂PO₄, 300 mM NaCl, 20 mM imidazole) and the bound proteins were released and eluted in 1 ml fractions using elution buffer (50 mM NaH₂PO₄, 300 mM NaCl, 0.5 M imidazole pH 8.0). Peak fractions were pooled and buffer exchanged into 50 mM Tris pH 8 using a PD10 column (GE Healthcare) and for long term storage 150 mM NaCl was added. The protein purity was assessed by SDS-PAGE and quantified using the BCA Protein Assay (Pierce) as per manufacturer's guidelines.

The same protocol was followed for the expression of *T. brucei* ATG8.1 (pGL2115) except the using a modified wash buffer (50 mM NaH₂PO₄, 300 mM NaCl, 40 mM imidazole, pH 8.0) and changing the storage buffer to 50 mM Tris, 150 mM NaCl pH 5.5.

2.7.2 MCA4 antibody production and purification

Recombinant MCA4 was purified as described above and used as an antigen to produce a specific polyclonal antibody. Two chickens were immunised with recombinant MCA4 (four 250 µl inoculations of 1 mg ml⁻¹ protein over the course

of four months) at the Scottish National Blood Transfusion Service (Penicuik, Midlothian) and all eggs laid after the third injection were collected (approximately 50 per chicken) along with pre-immune egg yolks. The egg yolks were separated and stored at -20°C before purification of total IgY using the Eggcellent IgY Purification kit (Pierce).

2.7.3 ATG8.1 antibody production

Recombinant ATG8.1 was purified as described above and used as an antigen to produce a specific polyclonal antiserum. One rabbit was immunised with recombinant ATG8.1 (four 250 μl inoculations of 1 mg ml^{-1} protein over the course of three months) at the Scottish National Blood Transfusion Service (Penicuik, Midlothian) and the pre-immune serum along with three bleeds were collected and stored at -20°C .

2.7.4 Antibody affinity purification

In a 5 ml polypropylene column (Pierce), approximately 2.5 mg of purified recombinant MCA4 or ATG8 protein was covalently linked to 1 ml of AminoLink Coupling Gel (Pierce) according to the manufacturer's protocol and equilibrated with 10 ml of PBS. 4 ml of anti-ATG8 rabbit antiserum (3rd bleed) was diluted 1:1 with PBS, whereas purified anti-MCA4 IgY was already resuspended in PBS. The protein/AminoLink resin was incubated overnight at 4°C in a 50 ml conical tube with the antiserum/total IgY. The resin was transferred back to the 5 ml polypropylene column and washed in 12 ml of PBS before eluting bound antibodies with in multiple 1 ml fractions of Immunopure IgG elution buffer (Pierce). The pH of eluted samples was immediately neutralised by the addition of 50 μl of 1M Tris pH 9. The various elution fractions were then quantified by measurement of their OD at $\lambda = 280\text{ nm}$. The peak fractions were pooled and concentrated using a Vivaspin 2 ultrafiltration unit (10,000 MWCO, Vivascience), at 4000 g. The concentrate was then washed 3 times with 2.5 ml of PBS, and finally time with 2.5 ml of PBS + 0.05 % (w/v) sodium azide, before concentrating to final volume of 1 ml. The aliquots were stored at 4°C .

2.7.5 Protein electrophoresis (SDS-PAGE)

Whole cell extracts and purified recombinant protein were separated by SDS-PAGE (sodium dodecyl phosphate polyacrylamide gel electrophoresis). Typically 12 % or 15 % (w/v) polyacrylamide gels were used, with a layer of 5 % stacking gel cast on top to help load and focus samples before full separation in the resolving gel. Samples were mixed in 2 x SDS-PAGE loading buffer (20 % (v/v) glycerol, 2.5 % (w/v) SDS, 0.05 % (w/v) bromophenol blue, 0.2 M Tris-HCl pH 6.8, 20 mM DTT) and denatured by boiling at 100°C for 4 minutes. Electrophoresis was performed in XCell SureLock Mini Cell chambers (Invitrogen) with SDS-PAGE running buffer (2.5 mM Tris, 19.2 mM glycine and 0.01 % (w/v) SDS). The voltage was set at 100 V while samples were in the stacking gel, then increased to 180 V as samples progressed through the resolving gel. With each gel, 2 µg of protein marker (Pre-stained Protein Marker Broad Range, New England Biolabs) was run as a reference to estimated molecular weight of protein samples.

Where stated polyacrylamide gels were prepared containing 6 M urea by dissolving appropriate weight of urea powder in the Tris and acrylamide solution aided by gentle heating. The remaining components of the gel were added before casting as standard.

2.7.6 Coomassie staining of SDS-PAGE

Protein gels were simultaneously fixed and stained by immersion in Coomassie stain solution (2.5 % (w/v) Coomassie Brilliant Blue R-250, 45 % (v/v) methanol, 10 % acetic acid) for 1 hour at room temperature. Gels were destained with several changes of destain solution (10 % (v/v) methanol, 10% (v/v) acetic acid) until optimum staining/background resolution was observed, following which they were washed in several changes of distilled water and photographed on the Gel-Doc 2000 (Biorad).

2.7.7 Western blotting

To analyse by western blot, samples were separated by SDS-PAGE and transferred by 'wet' transfer to nitrocellulose membrane (Hybond-C, Amersham Biosciences) in an X-Cell II Blot Module (Invitrogen). The inner chamber was

filled with transfer buffer (20 % (v/v) methanol, 20 mM Tris, 15 mM glycine) and efficient protein transfer was ensured by using adequate support pads and filter paper pre-soaked in transfer buffer. Transfer was performed at 30 volts for 1 hour with the outer chamber filled with water to maintain a cool temperature. After transfer the membrane was saturated with a blocking solution of 5 % powdered milk (Marvel) in TBST buffer (25 mM Tris-HCl pH 8, 120 mM NaCl, 0.1 % Tween-20) for at least 1 hour followed by incubation with the appropriate antibodies diluted in blocking solution. Following primary and secondary antibody application the membrane was washed three times for 5 minutes in blocking solution. All secondary antibodies used were conjugated to horse radish peroxidase (HRP) and labelled proteins were revealed by applying an ECL (enhanced chemiluminescence) substrate (SuperSignal West Pico Chemiluminescent Substrate or West Femto Maximum Sensitivity Substrate, Pierce) to the membrane according to manufacturers' instructions. Chemiluminescence was visualised by exposing the western blot on photographic film processed in a Kodak film processor.

2.7.8 Co-immunoprecipitation experiments

To immunoprecipitated MCA4 and any associated proteins pre-immune IgY and affinity purified anti-MCA4 were coupled to Carbolink resin (Pierce) according to manufacturer's instructions.

4.5×10^9 wild type *T. brucei* (strain 427) cells were purified from rat blood using DE52 cellulose (Whatman) and lysed in 4.5 ml of ice cold lysis buffer (50 mM Tris-HCl pH 7.4, 150 mM NaCl, 0.2% (v/v) NP40, 0.5 % (w/v) CHAPS, 1.5 x Roche Protease Inhibitor Cocktail) before centrifugation at 100,000 g for 45 minutes at 4°C. Supernatant was transferred to a fresh tube and pre-cleared with 200 µl pre-immune IgY Carbolink resin, incubated on rotary shaker at 4°C for 2 hours. The pre-clear step was repeated after centrifugation recovery of pre-immune IgY Carbolink. The supernatant was divided and 100 µl of anti-MCA4 Carbolink resin was added to the experimental sample and 100 µl of pre-immune IgY Carbolink added to control sample, before overnight incubation at 4°C on a rotary shaker. The following day the resin was separated from the supernatant using microcentrifuge spin cups (Pierce) and washed with lysis buffer (repeated x3)

and PBS (repeated x3). Precipitated material was released in 8 separate 100 μ l fractions of elution buffer (100 mM glycine pH 2.6) and immediately neutralised with 10 μ l Tris pH 9.0. Where indicated samples (excised band from SDS-PAGE) were analysed by mass spectrometry at the Sir Henry Wellcome Functional Genomics Facility (SHWFGF). Samples were digested with trypsin and analysed by electrospray ionisation mass spectrometry on a Q-STAR Pulsar I hybrid MS/MS system. Resulting data was analysed by SHWFGF using Applied Biosystems Analyst QS (v1.1) software and the automated Matrix Science Mascot Daemon server (v2.2.06) and all identifications were assigned by the Mascot search engine.

2.8 Acyl-biotin exchange

To detect MCA4 palmitoylation an acyl biotin exchange assay was used as previously described by Emmer and co-workers (Emmer *et al.* 2009). Two samples each comprised of 1.2×10^9 BSF *T. brucei* cells were pelleted and washed twice in PBS before suspension in 2.5 ml of lysis buffer 1 (50 mM Tris-HCl pH7.4, 150 mM NaCl, 5 mM EDTA, 1.5 x Roche Protease Inhibitor Mix*, 10 mM NEM *(n-ethylmaleimide, Sigma), * always added just prior to use). Cells were lysed by adding 0.5 ml of 10 % Triton X-100 and incubated for 1 hour at 4°C on a rotary shaker. Intact cells and nuclei were pelleted by low speed centrifugation for five minutes at 800 g at 4°C.

Supernatants were transferred to fresh 50 ml tubes for methanol-chloroform precipitation. To each 3 ml lysate fraction 12 ml methanol, 4.5 ml chloroform, 9 ml distilled water were added sequentially before vortex mixing and centrifugation at 6000 g for 20 minutes at 4°C. The upper phase was aspirated and 9 ml methanol was added before further vortex mixing and centrifugation at 6000 g for 10 minutes at 4°C. Supernatant was aspirated and the protein pellets air-dried for 5 minutes.

The pellets were resuspended in 600 μ l solubilisation buffer 1 (50 mM Tris-HCl pH7.4, 5 mM EDTA, 4 % SDS, 10 mM NEM) and incubated at 37°C for 10 minutes with occasional vortex mixing. Samples were diluted with 2.4 ml lysis buffer 2 (50 mM Tris-HCl pH7.4, 150 mM NaCl, 5 mM EDTA, 1.5 x Roche Protease Inhibitor

Mix, 10 mM NEM, 0.2 % Triton X-100) and incubated overnight at 4°C on a rotary shaker.

NEM was removed by three rounds of methanol chloroform precipitation, as described above but with the protein pellet from round 1 and 2 suspended in 750 µl solubilisation buffer 2 (50 mM Tris-HCl pH7.4, 5 mM EDTA, 4 % SDS) and diluted with 2.25 ml lysis buffer 3 (50 mM Tris-HCl pH7.4, 150 mM NaCl, 5 mM EDTA, 1.5 x Roche Protease Inhibitor Mix, 0.2 % Triton X-100). Following the third and final methanol precipitation the protein pellets were resuspended in 600 µl solubilisation buffer 2.

To the experimental sample 2.4 ml of hydroxylamine-label reagent (200 µM biotin-HPDP (Pierce), 700 mM hydroxylamine (Sigma) pH 7.4, 5 mM EDTA, 0.2 % Triton X-100 and 1.5 x Roche Protease Inhibitor Mix) was added and an equivalent volume of Tris-label reagent (200 µM biotin-HPDP, 50 mM Tris pH 7.4, 5 mM EDTA, 0.2 % Triton X-100 and 1.5 x Roche Protease Inhibitor Mix) was added to the control sample. Both samples were incubated for 1 hour at room temperature on a rotary shaker. The excess labelling reagent was removed by three rounds of methanol chloroform precipitation, as for the NEM removal step but the final pellets were resuspended in 150 µl 2 % SDS buffer (50 mM Tris-HCl pH7.4, 5 mM EDTA, 2 % SDS), with 30 µl collected to represent input samples.

Biotinylated proteins were then precipitated using streptavidin agarose. Excess SDS was diluted out of the remaining samples by adding 2.28 ml lysis buffer 3 and incubating for 30 minutes on a rotary shaker. Particulates were removed by pulse centrifugation at 14, 000 g for 30 seconds and supernatant transferred to fresh tubes containing streptavidin agarose prewashed in precipitation wash buffer (50 mM Tris-HCl pH7.4, 150 mM NaCl, 5 mM EDTA, 1.5 x Roche Protease Inhibitor Mix, 0.2 % Triton X-100, 0.1 % SDS) and incubated for 90 minutes at room temperature. The streptavidin beads were washed 5 times in precipitation wash buffer and bound proteins were eluted by incubation with elution buffer (50 mM Tris-HCl pH7.4, 150 mM NaCl, 5 mM EDTA, 1.5 x Roche Protease Inhibitor Mix, 0.2 % Triton X-100, 0.1 % SDS, 1 % β-mercaptoethanol).

2.9 MCA4 processing reactions

2.9.1 Autocatalytic processing

10 µg of purified recombinant MCA4 or MCA4^{S219C} was incubated in a reaction buffer (50mM Tris-HCl, pH 8, 150 mM NaCl, 5 mM DTT) with and without 10 mM CaCl₂ for 1 hour at 37°C. The extent of autocatalytic processing was monitored by SDS-PAGE.

2.9.2 MCA2 processing of MCA4

10 µg of purified MCA4 was incubated with increasing amounts of purified recombinant MCA2 (0, 1, 10 and 100 ng) in reaction buffer (50mM Tris-HCl, pH 8, 150 mM NaCl, 5 mM DTT, 10 mM CaCl₂) for 1 hour at 37°C. The extent of processing was monitored by SDS-PAGE.

2.9.3 N-terminal Edman degradation

To sequence the N-terminus of processing products reactions were set up as described in section 2.9.1 and 2.9.2 and separated on NuPAGE Novex 10 % Bis-Tris gels (Invitrogen) with MOPS running buffer (Invitrogen). A PVDF membrane (Hybond-P, Amersham Biosciences) was prepared by briefly soaking in 100 % methanol before washing in distilled water for 10 minutes followed by equilibration in transfer buffer (20 % (v/v) methanol, 20 mM Tris, 15 mM glycine) for 10 minutes. Prior to transfer the Bis-Tris gel was also soaked in transfer buffer for 20 minutes. The protein was transferred to PVDF membrane by 'wet' transfer in an X-Cell II Blot Module (Invitrogen) at 30 V for 1 hour. The inner chamber was filled with transfer buffer and the outer filled with water. The membrane was stained (0.1 % (w/v) Coomassie Brilliant Blue R-250, 50 % (v/v) methanol, 1 % (v/v) acetic acid) for 1 minute and destained (40 % (v/v) methanol, 10 % (v/v) acetic acid), followed by extensive washing in distilled water. The blot was air dried and the appropriate bands were excised using a sterile scalpel blade and sent to the University of Dundee, MRC Protein Phosphorylation Unit, to carry out the N-terminal Edman degradation reaction.

2.10 Activity assays

Proteolytic activity of purified recombinant MCA4 was assessed by measuring the hydrolysis of synthetic fluorogenic substrates. All assays were run in clear bottom 96 well plates and typically contained the following components (unless stated otherwise): 2 μg purified enzyme, reaction buffer (50mM Tris-HCl, pH 8, 150 mM NaCl, 5 mM DTT and 10 mM CaCl_2), 10 μM substrate (e.g. Z-RR-AMC) and distilled water to 200 μl . All assays were run in triplicate and included 'no-enzyme' controls.

Fluorescence was read every 2 minutes for maximum of 3 hours in an EnVision Multilabel Reader (Perkin Elmer, Beaconfield, UK) at excitation wavelength (λ_{Ex}) of 355 nm and emission wavelength (λ_{Em}) of 460 nm using the general mirror. The fluorescence readings were analysed using Microsoft Excel. Where indicated peptidase inhibitors were added to the reaction at the concentration in brackets: leupeptin (100 μM), antipain (100 μM), E64 (10 μM), PMSF (0.5 mM) and Pefabloc (2.5 mM).

For activity assays of processed MCA4, purified recombinant MCA2 was added to MCA4 at ratio of 1:100 (e.g. 0.1 μg MCA2 : 10 μg MCA4) and incubated with reaction buffer (50mM Tris-HCl, pH 8, 150 mM NaCl, 5 mM DTT and 10 mM CaCl_2) for 1 hour at 37°C. Aliquots containing 0.02 μg MCA2 and 2 μg MCA4 were removed and added to activity assays as described above and assessed by SDS-PAGE to check for MCA4 processing.

2.11 Microscopy

Fluorescent microscopy images were obtained using an Applied Precision DeltaVision Deconvolution microscope system fitted with a CoolSnap HQ camera. Image capture and microscope operation was performed using the software package SoftWoRx. Fluorescence was viewed using the FITC filter (λ_{Ex} 490 nm / λ_{Em} 528 nm), RD-TR-PE filter (λ_{Ex} 555 nm / λ_{Em} 617 nm), DAPI filter (λ_{Ex} 360 nm / λ_{Em} 457 nm) and reference images were obtained using the differential interference contrast (DIC) filter. Exposure time was set to 1 second with the transmission level of the neutral filter optimised for each sample and 60 x or 100

x oil immersion objectives were used. Typically 15 Z-stacks were obtained and individually deconvolved using the automatic conservative ratio setting before projection into one representative image. To merge images containing multiple fluorescent signals Adobe photoshop was used.

Cell counting for the RNAi induction experiment was performed using a Zeiss Axioplan microscope, with images captured by a Hamamatsu ORCA-ER digital camera and processed using Openlab version 3.5 software.

2.11.1 Direct cell fluorescence

For each slide approximately 1×10^5 *T. brucei* cells were washed twice in trypanosome dilution buffer (TDB) (20 mM Na₂HPO₄, 2 mM NaH₂PO₄, 80 mM NaCl, 5 mM KCl, 1 mM MgSO₄, 20 mM glucose, pH 7.4) before fixation in 1 % (w/v) paraformaldehyde (Sigma) with concurrent incubation on ice for 15 minutes (BSF) or 30 minutes (PCF). After two further washes in TDB the cell pellet was resuspended in 20 µl TDB and evenly spread onto twin frosted end 76 x 26 mm microscope slide (BDH) coated in 0.1 % poly-l-lysine (Sigma) and the cells allowed to sediment.

Excess liquid was removed and the cells on each slide were stained with 10 µl of $1 \mu\text{g ml}^{-1}$ 4,6-Diamindino-2-phenylindole (DAPI) in mounting solution (PBS, 50 % (v/v) glycerol, 2.5 % (w/v) DABCO). All slides were fitted with a coverslip sealed with nail varnish.

2.11.2 Immunofluorescence analysis

The protocol used for immunofluorescence analysis was adapted from the method published by Field and co-workers (Field *et al.* 2004). Briefly, mid-log BSF parasites were washed in vPBS (137 mM NaCl, 3 mM KCl, 16 mM Na₂HPO₄, 3 mM KH₂PO₄, 46 mM sucrose, 10 mM glucose, pH 7.6) before fixation on ice in 3 % paraformaldehyde for 10 minutes. The fix solution was diluted out with excess vPBS and two further cell washes were performed. Fixed cells were applied to a 2 cm² area outlined in nail varnish, on 0.01 % poly-l-lysine treated microscope slides and allowed to sediment. When required the cells were permeabilised by applying 0.1 % (v/v) Triton X-100 in PBS for 10 minutes before washing with PBS

and blocking for 1 hour using 20 % (v/v) foetal calf serum (Sigma) in PBS. The primary antibody was then applied (diluted in 20 % (v/v) foetal calf serum in PBS) and incubated for 2 hours at room temperature. Slides were washed three times with PBS and the corresponding secondary antibody applied (diluted in 20 % (v/v) foetal calf serum in PBS) and incubated for 1 hour. Slides were washed three times with PBS, stained with 1 $\mu\text{g ml}^{-1}$ DAPI in mounting solution and sealed with a coverslip and nail varnish.

Primary antibodies used : affinity purified anti-MCA4 1/400 (chicken) and monoclonal anti-HA (Roche) 1/1000 (mouse). Secondary antibodies used: Alexa Fluor 488 (green)-conjugated anti-chicken (Molecular Probes) and Alexa Fluor 594 (red)-conjugated anti-mouse (Molecular Probes).

2.11.3 Immuno-electron microscopy

Immuno-electron microscopy services were provided by the Integrated Microscopy Facility at the University of Glasgow, with procedures overseen by Dr Laurence Tetley and Ms Margaret Mullin.

Wild type BSF *T. brucei* cell pellet was chemically fixed in suspension and maintained in 0.2 % (v/v) gluteraldehyde, 2 % (w/v) paraformaldehyde in PBS (pH 7.2) on ice for 1 hour. After fixation the cells were rinsed in PBS and embedded in Lowicryl resin using the progressive lowering of the temperature method. Cells were cut into blocks and mounted on metal pins and frozen in liquid nitrogen before sectioning with a Leica Ultracut UCT/FCS. The cryosections were blocked with 0.1 M glycine followed by 5 % (w/v) BSA and then labelled with affinity purified anti-MCA4 (1:10) and 1.4 nm gold (rabbit) anti-chicken (1:20) (Aurion). Cells were contrast stained and the immuno-labelling was enhanced by 15 minutes treatment with R-gent (Aurion). Sections were viewed with a LEO 912 transmission electron microscope.

2.12 *T. brucei* cell culture

2.12.1 General culturing techniques

T. brucei (strain 427) were grown in culture as bloodstream form (BSF) and procyclic form (PCF) parasites. BSF were grown to a maximum cell density of $1 \times 10^6 \text{ ml}^{-1}$ at 37°C in 5 % carbon dioxide in HMI-9 media supplemented with 10 % heat-inactivated foetal calf serum (FCS), 10 % serum plus and $0.5 \mu\text{g ml}^{-1}$ penicillin-streptomycin solution (Sigma). PCF *T. brucei* were grown to a maximum cell density of $1 \times 10^7 \text{ ml}^{-1}$ at 27°C in 5 % carbon dioxide in SDM-79 media supplemented with 10 % FCS and $0.5 \mu\text{g ml}^{-1}$ penicillin-streptomycin solution (Sigma). The genetic knockout of MCA4 was performed in BSF *T. brucei* 427. RNAi analysis and the tetracycline induced expression of tagged transgenes was performed in BSF 427 13-90 and PCF 427 29-13 cell lines (Wirtz *et al.* 1999). To induce RNAi or transgene expression $1 \mu\text{g ml}^{-1}$ tetracycline was added to the culture media.

For all parasite growth analysis, the cell densities of cultures was determined by counting the number of cells in 10 μl of culture using an Improved Neubauer haemocytometer counting chamber (Weber Scientific). When monitoring BSF parasite growth, cultures were seeded at $1 \times 10^5 \text{ cells ml}^{-1}$ and the culture density was determined at regular intervals, with cultures passaged back to $1 \times 10^5 \text{ cells ml}^{-1}$ every 24 hours. PCF cultures were seeded at 5×10^5 and passaged every 72 hours.

Stabilates of *T. brucei* were prepared for long term cryopreservation. Cultured cells (mid-log) were pelleted and resuspended in HM19 with 10 % (v/v) glycerol (BSF) or SDM79 with 10 % (v/v) glycerol (PCF). 1 ml aliquots were transferred to cryovials and stored at -80°C for 24 hours, before transfer to liquid nitrogen tanks for long term storage.

2.12.2 T. brucei genomic DNA isolation

Genomic DNA was prepared from cultured *T. brucei* using the DNeasy Blood and Tissue kit (Qiagen), following the Cultured Animal Cell protocol outlined in the manufacturer's instructions.

2.12.3 BSF transfection

BSF (strain 427) parasites were cultured as previously described. For each transfection 1×10^7 mid-log cells were harvested by centrifugation at 1500 g for 10 minutes at 37°C. The cell pellet was resuspended in 100 µl Human T Cell Nucleofector Solution (Lonza), transferred to an electroporation cuvette (Lonza) and mixed with 10 µg of linearised DNA. A control transfection was performed following the same method but omitting DNA. The cuvettes were then pulsed once on programme X-001 using the Human T Cell Nucleofector machine (Amaxa) and the parasites were immediately transferred to 30 ml of prewarmed complete HM19 containing with no selective drugs. Dilutions of the parasites (1:100 and 1:1000) were then plated out into 24 well plates and incubated at 37°C. The following day selective drugs were added and clones generally, detected after 6 to 8 days. Drug concentrations used for transgenic BSF *T. brucei* 427: $5 \mu\text{g ml}^{-1}$ hygromycin B (Calbiochem), $2.5 \mu\text{g ml}^{-1}$ G418 (Calbiochem), $2.5 \mu\text{g ml}^{-1}$ phleomycin (InvivoGen) and $10 \mu\text{g ml}^{-1}$ blasticidin (Calbiochem).

2.12.4 PCF transfection

PCF (strain 427) parasites were cultured as previously described. For each transfection 3×10^7 mid-log cells were harvested by centrifugation at 600 g for 10 minutes at 27°C. The cell pellet was resuspended in 100 µl Human T Cell Nucleofector Solution (Lonza) and transferred to an electroporation cuvette (Lonza) and mixed with 10 µg of linearised DNA. A control transfection was performed following the same method but omitting DNA. The cuvettes were then pulsed once on programme X-001 using the Human T Cell Nucleofector machine (Amaxa). The parasites were immediately transferred to 10 ml of prewarmed SDM79 (15 % (v/v) FCS) without selective drugs and incubated overnight at 27°C. Following recovery the culture was split into three pools and

selective drugs added. Dilutions (1:100 and 1:1000) were prepared using SDM79 (15 % FCS and appropriate selection drugs), before plating into 96 well plates with clones were detected after 14 to 21 days. Drug concentrations used for transgenic PCF *T. brucei* 427: 50 $\mu\text{g ml}^{-1}$ hygromycin B (Calbiochem), 10 $\mu\text{g ml}^{-1}$ G418 (Calbiochem), 10 $\mu\text{g ml}^{-1}$ zeocin (Calbiochem) and 20 $\mu\text{g ml}^{-1}$ blasticidin (Calbiochem).

2.13 RNAi induction and analyses

RNAi was induced by adding 1 $\mu\text{g ml}^{-1}$ tetracycline to cells passaged to 1 x10⁵ ml⁻¹ (BSF) or 5 x 10⁵ ml⁻¹ (PCF) and the growth rate was compared to identical non-induced control lines. Cells were passaged every 24 hours (BSF) or 72 hours (PCF) and tetracycline added to induced cells. At select time points samples were removed from the cultures for further analysis by western blot, quantitative real time PCR (RT-PCR), FACS analysis and microscopy of DAPI stained cells (<200 cells counted for three replicate cultures).

2.13.1 RNA isolation and reverse transcriptase (RT) PCR

For each sample, RNA was isolated from 1.5 x 10⁷ cells using the RNeasy kit (Qiagen) processed in the automated QIAcube (Qiagen) according to manufacturer's instructions, with an added on column DNase -1 (Sigma) digestion step. The integrity of isolated RNA was inspected on a 1 % agarose gel made with 1 x UltraPure TAE buffer (Invitrogen) stained with ethidium bromide. cDNA was produced from 1 μg of isolated RNA using random hexamer primers (Invitrogen) and SuperScript Reverse Transcriptase III (Invitrogen) according to manufacturers' instructions. To monitor genomic DNA contamination the procedure was performed without reverse transcriptase (-RT).

2.13.2 Quantitative real time PCR

Real time PCR analysis was performed on both +RT and -RT cDNA samples in reactions comprised of following: 1 μl of cDNA, 12.5 μl Power SYBR Green PCR Master Mix (Applied Biosystems), 3 μM primer 1, 3 μM primer 2 and 6.5 μl of water. PCR reactions were carried out in triplicate in sealed 96 well plates,

using an Applied Biosystems 7500 Real Time PCR machine, with resulting data analysed on Applied Biosystems 7500 System Software. Primers used for real time PCR were designed using the Applied Biosystems Primer Express 3.0 programme and designed to amplify a 50 bp product specific to each target ORF.

2.13.3 Fluorescence activated cell sorting (FACS)

To analyse the DNA content of *T. brucei*, 1.5×10^6 cells were centrifuged at 800 g for 10 minutes, then washed with TDB, centrifuged once more and resuspended in 1 ml of 70% (v/v) methanol in PBS. Fixed cells were stored at 4°C. Prior to FACS analysis, the cells were centrifuged at 800 g at 4°C for 10 minutes and washed with 10 ml PBS, centrifuged once more and resuspended in 1ml of PBS supplemented with $10 \mu\text{g ml}^{-1}$ propidium iodide (Sigma) and $10 \mu\text{g ml}^{-1}$ RNase A (Sigma), and incubated at 37°C for 45 minutes, in the dark. FACS analysis was performed on a Becton Dickinson FACSCalibur using the FL2-A Forward Scatter (FSC, relative cell size) and the Side Scatter detectors (SSC, cell granulometry or internal complexity). Introduction of the prepared samples into the cytometer was automated with a FACS Loader (Worklist manager and Loader manager softwares). For each sample, 10 000 events (cells) were analysed. Data interpretation was performed using the CellQuestPro software (BD Bioscience).

2.13.4 Monitoring autophagy in *T. brucei*

Autophagy was monitored by counting the number of autophagosomes labelled with YFP-ATG8 in *T. brucei* cell lines expressing YFP-tagged ATG8 proteins under the control of a tetracycline operator. Autophagosome formation was monitored in response to different conditions, with fluorescence microscopy used to count the number of autophagosomes per cell for more than 200 cells (repeated for three replicate experiments) fixed with 1 % paraformaldehyde. Transgene expression was induced by adding $1 \mu\text{g ml}^{-1}$ tetracycline to cultures before overnight incubation under standard conditions.

The basal rate of autophagosome formation was determined in induced PCF cells following standard growth in nutrient rich SDM79 supplemented with tetracycline. Starvation induced autophagosome formation was monitored by thorough washing and re-suspension of induced PCFs for 2 hours in pre-warmed

PBS supplemented with $1 \mu\text{g ml}^{-1}$ tetracycline (and wortmannin (Sigma) or rapamycin (Sigma) where indicated). Similarly the basal rate of autophagosome formation was determined in induced BSF cells following standard growth in nutrient rich HM19 supplemented with tetracycline. Autophagy induction was investigated using rapamycin and vasoactive intestinal peptide (VIP) (American Peptide Company).

2.13.5 *T. brucei* animal infection

1×10^5 cultured BSF *T. brucei* (strain 427) were inoculated into ICR mice by intra peritoneal injection and the parasitemia monitored daily by haemocytometer cell count of mouse blood taken from a tail vein diluted in 0.83 % ammonium chloride. For infection experiments, groups of four mice were infected with trypanosomes taken directly from the same donor mouse.

For large scale trypanosome purification rats were inoculated with cultured BSF *T. brucei* (strain 427) and culled at peak parasitemia with the maximum blood extracted by cardiac puncture (approximately 12 ml obtained per rat). The blood was mixed heparin and purified by anion exchange on DE52 cellulose (Whatman) columns.

2.13.6 *Motility analysis*

T. brucei resistance to sedimentation was investigated as a function of cell motility. Wild type BSF *T. brucei* and $\Delta mca4$ cells were cultured to the same mid-log densities. 2 ml of culture was divided equally into 2 cuvettes and the OD₆₀₀ was recorded at 0, 3 and 6 hour time points. One cuvette was always left undisturbed and the other mixed and re-suspended before each optical density reading. Three replicate experiments were performed and sedimentation rates determined by subtracting the OD₆₀₀ of the undisturbed control from the OD₆₀₀ of the resuspended culture.

2.13.7 *Cell fractionation*

The cellular fractionation method was adapted from Liu *et al.*, 2010. For detergent lysis 2×10^7 mid-log BSF cells were washed in vPBS and lysed in 500 μl

1% (v/v) Triton X-100, 25mM HEPES, 1mM EDTA pH7.4 for 30 minutes on ice before centrifugation at 14,000 g for 5 minutes. For hypotonic lysis 2×10^7 mid-log BSF cells were washed in vPBS and lysed in 500 μ l 10mM Tris-HCl pH7.4 with 4 x 15 second blasts in an ice cold sonicating water bath (Fisher Scientific FB15047), before centrifugation at 14,000 g for 5 minutes. For both lysis methods, insoluble material in the pellet was solubilised by boiling with 625 μ l 1 x a SDS-PAGE sample buffer for 5 minutes. The supernatant was prepared for electrophoresis by adding 125 μ l 4 x SDS-PAGE sample buffer and boiling for 5 minutes. 1×10^6 cell equivalents were loaded per lane.

2.13.8 *Statistical analysis of data*

Where indicated data were expressed as means \pm standard deviation from the mean. P-values were calculated using an unpaired, two-tailed Student's T-test on Microsoft Excel. Differences were considered significant at a p-value of <0.05 .

3 Autophagy

3.1 Introduction

3.1.1 General introduction to Autophagy

The word autophagy stems from two Greek terms, meaning to eat ('phagy') and oneself ('auto'). It describes a primary intracellular mechanism for the degradation of long lived proteins and organelles, which results in the release of amino acids back into the cytosol. Degradation of an organisms own proteins is an important part of cellular regulation and development, helping to maintain a crucial balance between anabolic and catabolic processes. Eukaryotic cells use two major mechanisms for intracellular protein degradation, the ubiquitin-proteosomal system and the lysosome (vacuole in yeast). The ubiquitin-proteosomal system is the major method for degradation of short lived, damaged or misfolded proteins (Hershko *et al.* 1998). However, unwanted stable proteins or organelles are targeted to the lysosome where they can be degraded and recycled. Autophagy is one of several methods for transporting cargo to the lysosome and is a widespread biological process thought to be conserved in a diverse range of eukaryotic organisms (Meijer *et al.* 2007; Rigden *et al.* 2009).

The process of autophagy is subdivided into three primary forms that differ in mechanism and function: microautophagy, chaperone-mediated autophagy (CMA) and macroautophagy, all summarised in Figure 3-1. Microautophagy is a degradation process that occurs directly at the lysosomal surface, during which the target cytoplasm or organelle is engulfed by invagination, protrusion, and/or septation of the lysosome membrane (Kunz *et al.* 2004). CMA is distinct from both micro- and macroautophagy pathways because there is no vesicle used to target proteins to the vacuole/lysosome. Instead, chaperone molecules recognise a peptide motif (KFERQ-like) present on select cytosolic proteins and binds them to the Lamp type 2A receptors located on the lysosomal membrane. Thus delivering specific cytosolic proteins to the lysosome on a molecule by molecule basis (Bandyopadhyay *et al.* 2010; Cuervo 2010). Like macroautophagy, CMA can be activated by nutrient starvation. However, while

macroautophagy is activated as an initial response it soon declines, whereas CMA is active during prolonged periods of starvation (Dice 2007).

Macroautophagy is the major form of autophagy and is often referred to simply as ‘autophagy’, as will be the case for this work. The process involves the engulfment of cytoplasm or entire organelles into a double-membrane structure, called the autophagosome. The outer membrane of the autophagosome fuses with the lysosome, introducing the inner membrane and the bound contents into the lysosome. In this compartment hydrolases degrade and recycle the contents into constituent amino acids (Reggiori *et al.* 2005a).

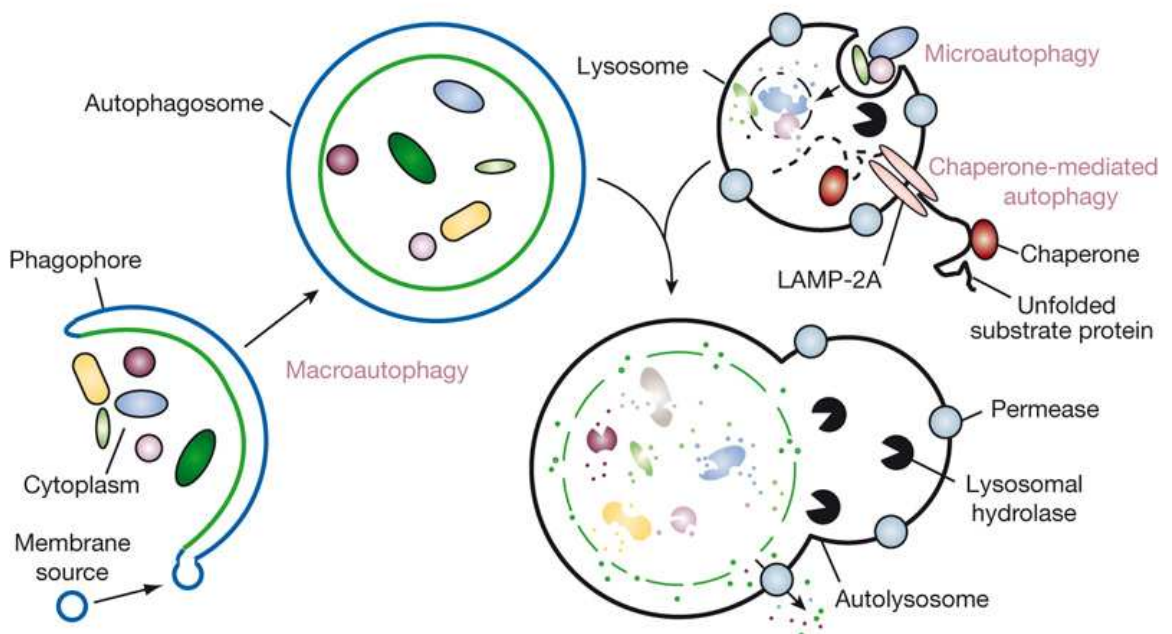


Figure 3-1 Autophagic degradation by the lysosome.

Figure taken from (Mizushima *et al.* 2008). The three types of autophagy are depicted. Macroautophagy cargoes are engulfed in an expanding double membrane structure called the phagophore. The completed vesicle, called the autophagosome, is delivered to the lysosome. Microautophagy describes the engulfment of cytosolic components directly by the lysosome, mediated by the lysosome membrane. Chaperone-mediated autophagy occurs without vesicle formation, unfolded target proteins are translocated into the lysosome via lysosome-associated membrane proteins type 2A (LAMP-2A) and the chaperone hsc70. Once inside the lysosome cargo is degraded by hydrolases and amino acids are released into the cytosol by permeases.

3.1.2 Molecular dissection of autophagy pathway

The scientific principle of autophagy was originally described over 40 years ago (for early review see (de Duve *et al.* 1966). Early work was focused on defining morphological features, however significant developments in the field of

molecular biology have led to a great understanding of the molecular mechanisms behind autophagy. Due to the complex and sometimes overlapping nature of work being carried out in different research labs a universal nomenclature was proposed; the genes are named ATG, which stands for autophagy-related (Klionsky *et al.* 2003). To date over 30 ATG genes have been identified, but many more genes and their products are involved in the wider field of lysosomal degradation and not directly in autophagy thus retain their previous names (Herman *et al.* 2006; Nakatogawa *et al.* 2009; Rigden *et al.* 2009). A subset of genes have been identified as essential for all types of autophagy and were designated the core ATG genes (Xie *et al.* 2007), these are shown along with the putative *T. brucei* orthologues in Table 4. Much of the molecular characterisation was performed in *Saccharomyces cerevisiae*, consequently it is an established model for autophagy and the major steps involved in the yeast process will be outlined.

3.1.3 Induction of autophagy

CMA can only degrade specific soluble proteins, but micro and macroautophagy have the ability to engulf large structures through both selective and non-selective mechanisms. To prevent uncontrolled degradation that would damage cells, tight regulatory mechanisms exist to control autophagy. The most basic and fundamental level of control occurs through mediating the activity of protein kinase Atg1.

In yeast autophagy is primarily a response to nutrient starvation. The abundance of nutrients directly controls Tor (target of rapamycin) signalling, a master regulator of cell growth that influences translation initiation and G1 phase transition (Barbet *et al.* 1996). Coupled to its nutrient sensing capabilities Tor also acts as negative regulator of the autophagic response. Addition of rapamycin, a Tor specific inhibitor, to cells in nutrient rich media produced the same autophagic response as starvation (Noda *et al.* 1998). Deciphering the molecular mechanism revealed that Tor controlled the activity of Atg1. During times of high nutrient availability Tor hyperphosphorylates Atg13 which reduces its affinity for Atg1. However, following Tor inactivation by starvation or rapamycin, Atg13 is rapidly dephosphorylated promoting interaction with Atg1

and stimulating kinase activity and promoting autophagosome formation (Kamada *et al.* 2000).

3.1.4 Autophagosome formation

Genetic screens have determined 16 ATG factors that are directly involved in the formation of the autophagosome, suggesting it requires the input of more autophagy proteins than any other stage. The biogenesis of autophagosomes occurs at a distinct foci called the pre-autophagosomal structure (PAS), which serves as a platform to enable the recruitment and accumulation of the core autophagy proteins (Suzuki *et al.* 2001). Following induction (e.g. starvation) a bowl shaped membrane, called the isolation membrane, emerges from the PAS to engulf and eventually surround the cargo in a mature autophagosome (Mizushima *et al.* 2001). Organisation of proteins at the PAS occurs in an ordered and hierarchical manner with the absence of initial early PAS proteins reducing recruitment of subsequent PAS components (Suzuki *et al.* 2007). Atg17 is the most basic protein required for PAS organisation and serves as a scaffold for the recruitment of all others. The initial tier of PAS recruitment (dependent on Atg17) includes Atg1 and Atg13, along with Atg9 and the phosphatidylinositol (PtdIns) 3-kinase complex I. These in turn help to recruit the Atg2-Atg18 complex, as well as those proteins involved in two conjugation systems that are required for membrane expansion and completion (Atg8-PE and Atg12-Atg5, discussed in detail in sections 3.1.5 and 3.1.6 respectively).

Atg9 is an integral membrane protein that localises to the PAS, small puncta in the cytoplasm and to the surface of mitochondria. The exact function of Atg9 remains unknown but it was postulated that it could serve as a membrane carrier, transporting lipids from the mitochondria to the PAS to help generate new autophagosomes (Reggiori *et al.* 2005b).

The activity of phosphatidylinositol (PtdIns) 3-kinases is essential for autophagy (Kihara *et al.* 2001; Petiot *et al.* 2000). They catalyse the phosphorylation of PtdIns to produce phosphatidylinositol 3-phosphate (PtdIns3P) and have been shown to have diverse regulatory functions including a role in membrane trafficking. In yeast there is only one PtdIns 3-kinase, Vps34 that is known to interact with two complexes; complex I is involved in autophagy and complex II

has a role in vacuolar protein sorting (Kihara *et al.* 2001; Petiot *et al.* 2000). Atg14 associates only with complex I and has been shown to coordinate the localisation of the complex to the PAS (Obara *et al.* 2006). It is speculated that the PtdIns3P produced by complex I could function as a site to aid further recruitment of proteins to the PAS. Indeed the Atg2-Atg18 complex, known to be essential for autophagosome formation has been shown to interact with autophagic membranes in a PtdIns3P dependent manner (Obara *et al.* 2008).

The exact mechanism detailing how the PAS develops into the isolation membrane and complete autophagosome has yet to be fully determined, however it is known that two novel ubiquitin-like protein conjugation systems are critical to the process (Ohsumi *et al.* 2004). The two ubiquitin-like proteins are Atg12 and Atg8. Atg12-conjugation is essential for formation of the preautophagosome, whereas Atg8 is essential for autophagosome formation (Tanida *et al.* 2004b).

Furthermore, for many years the source of the autophagosome membrane has proved both illusive and contentious (Juhász *et al.* 2006). In mammalian systems it appears that different sources provide membrane material. By starving rat kidney cells of nutrients it was recently found that, the outer membrane of the mitochondria served as site for autophagosome biogenesis and provided lipids for the autophagosome membrane (Hailey *et al.* 2010). However an additional site has been identified on the endoplasmic reticulum, called the omegasome, that is enriched in PtdIns3P (a key component of autophagosomes) which could serve as a scaffold for recruitment of further autophagosomal proteins (Axe *et al.* 2008). Furthermore, the plasma membrane can also serve as site for autophagosome biogenesis and directly provides membrane for autophagosomes (Ravikumar *et al.* 2010). Despite the variety of membrane sources used to form the autophagosome it has yet to be determined whether this contrives to influence its function.

3.1.5 Atg12-Atg5 conjugation

In yeast, Atg12 conjugation occurs constitutively and is not dependent upon nutrient conditions, such as starvation. Atg12 is a small ubiquitin-like protein (UBL) that covalently links to Atg5, shortly after translation. The C-terminal

glycine of Atg12 conjugates to a specific lysine residue on Atg5 (position 149) by an isopeptide bond (Mizushima *et al.* 1998). Although Atg12 has very limited amino acid sequence identity with ubiquitin, the mode of conjugation with Atg5 does bear similarities to the process of ubiquitination (Mizushima *et al.* 1998; Ohsumi *et al.* 2004). Atg12 is activated by Atg7 (acting as the E1 enzyme), and then forms a conjugate with Atg7 via a thioester bond between the C-terminal glycine of Atg12 and a cysteine (amino acid position 572) in Atg7 (Tanida *et al.* 2001). Atg12 is then transferred to Atg10 (E2 enzyme) and forms a thioester bond between the C-terminal glycine of Atg12 and cysteine (amino acid position 133) of Atg10 (Shintani *et al.* 1999). Atg12 can then bind to the target molecule Atg5. Once conjugation has occurred Atg16, a coiled-coil protein, associates with Atg5. The coiled coil region of Atg16 allows it to form multimers (with itself), which can then crosslink to conjugated Atg5 (Figure 3-2) (Mizushima *et al.* 1999). Whilst Atg16 is not required for the conjugation reaction, association with the Atg12-Atg5 complex is required for autophagy *in vivo*. Interestingly, there appears to be no peptidase activity enabling deconjugation, suggesting this is an irreversible reaction. The Atg12-Atg5 conjugate leaves the membrane just prior to or just after autophagosome formation (Ohsumi *et al.* 2004).

3.1.6 Atg8 conjugation

Ubiquitin and other UBL proteins (e.g. Atg12) interact with other proteins, however uniquely the UBL Atg8 is conjugated to an abundant membrane phospholipid called phosphatidylethanolamine (PE) (Ichimura *et al.* 2000). In the initial step the cysteine peptidase Atg4 removes the C-terminal arginine (position 117) from newly synthesised Atg8. This exposes a glycine residue (position 116), which allows activation of the Atg8-Glycine-116 intermediate by Atg7 (E1 enzyme), which in turn transfers it to Atg3 (E2 enzyme). Finally, Atg8-Glycine-116 conjugates to PE (forming Atg8-PE) via an amide bond between the C-terminal glycine carbonyl group and the amino group of PE (Figure 3-2). The lipid modification of Atg8 changes the protein from a soluble form to a tightly associated membrane protein. Once the mature autophagosome is formed externally located Atg8-PE is released by the deconjugating action of Atg4, however a portion remains trapped inside (Ohsumi *et al.* 2004). The Atg8 system confers a particular benefit to researchers as it offers the chance to monitor

autophagosome formation through green fluorescent protein (GFP) tagging of Atg8-PE. GFP-Atg8-PE has been shown to function as Atg8-PE and due to its association with the preautophagosome and autophagosome it has been used as a useful autophagy marker in numerous organisms including transgenic mice, yeast and *Leishmania* (Besteiro *et al.* 2006; Klionsky *et al.* 2007; Mizushima *et al.* 2004; Williams *et al.* 2006).

As the membrane expands the ATG factors start to concentrate in specific locations. Atg12-Atg5 and Atg16 congregate on the outside of the curve, whereas ATG8-PE seems to favour the internal surface. The curvature is exaggerated and continued by Atg12-Atg5 and Atg16 forming polymers at the phagophore tips. This could act as a protein framework, which allows the incorporation of the ATG8-PE membrane lipid, effectively plugging the gap (Reggiori *et al.* 2005a). Additionally, the cargo selected could help to form the three-dimensional shape of the membrane. This could explain how selective autophagy, dictates the contents of the autophagosome. And the cargo-directed expansion could provide an explanation for the accommodation of cargos of varying size (Reggiori *et al.* 2005a).

Mammals have eight orthologues of the yeast Atg8 protein, that are divided into LC3 and GABARAP/GATE-16 subfamilies, with LC3B being the best studied (He *et al.* 2003; Kabeya *et al.* 2004). However despite the common autophagosomal association of proteins from both subfamilies, they play distinct roles in autophagosome biogenesis. LC3 proteins appear to function in the early stages of phagophore formation and elongation, where as the GABARAP/GATE-16 subfamily are involved in later stages and possibly mediate the sealing of the autophagosome (Weidberg *et al.* 2010).

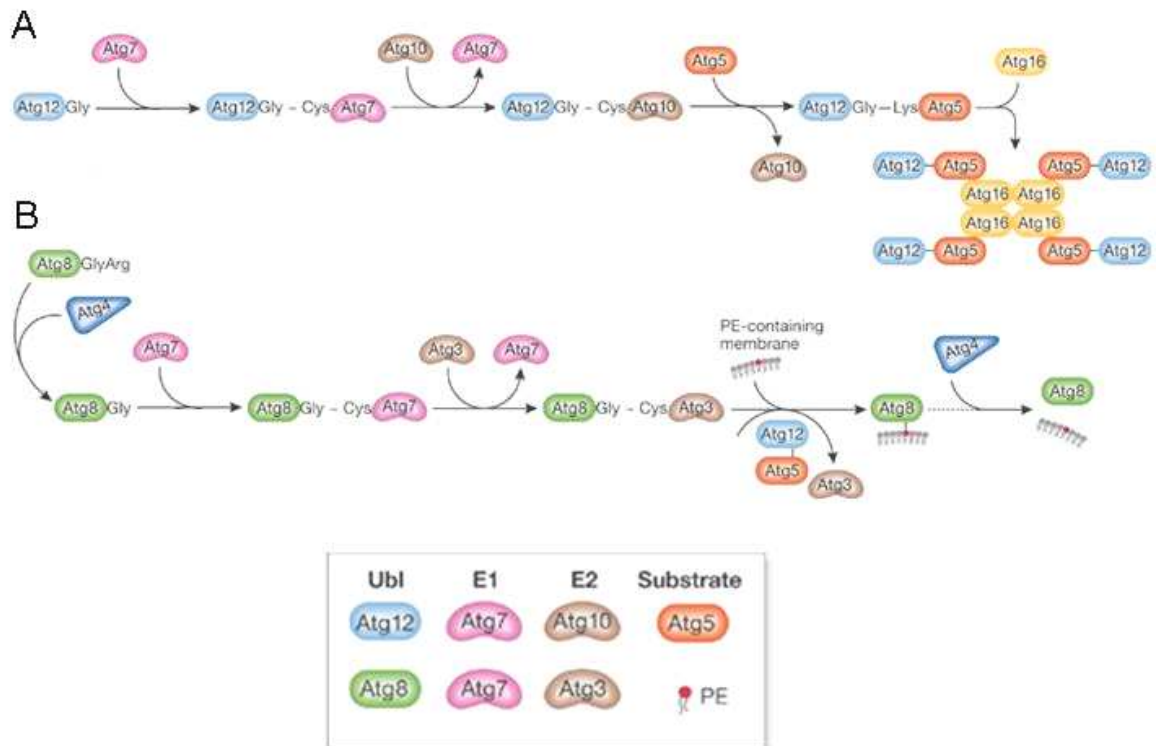


Figure 3-2 Atg12 and Atg8 conjugation pathways in *S. cerevisiae*.

Adapted from (Geng *et al.* 2008) A) Atg12 is conjugated to Atg5 by the action of Atg7 (E1 enzyme) and Atg10 (E2 enzyme). Atg16 associates with the conjugate and helps for multimers. B) Atg8 is cleaved by Atg4 before Atg7 (E1 enzyme) and Atg3 (E2 enzyme) coordinate the conjugation to the membrane lipid phosphatidylethanolamine PE. Atg12-Atg5 complex also facilitates Atg8 conjugation. Ubl, ubiquitin-like proteins. For details of both pathways see section 1-5 and 1-6.

3.1.7 Autophagosome fusion with the lysosome

The external membrane of the autophagosome fuses with the yeast vacuole and releases cargo still bound by the inner membrane into the vacuolar cavity where it can be degraded. To release and reuse the constituent units of the cargo it must be degraded, which requires a low pH, a vacuolar serine peptidase Prb1 and a vacuolar aspartic peptidase PEP4. In yeast degradation of the autophagosome is facilitated by Atg15, a membrane bound lipase (Teter *et al.* 2001). Another important autophagy protein operating in the vacuole is Atg22, a vacuolar membrane protein that functions as an efflux pump to help return regenerated amino acids to the cytosol (Yang *et al.* 2006).

3.1.8 Physiological functions of autophagy

In lower eukaryotic organisms, such as yeast, the primary function of autophagy appears to be ensuring survival during times of starvation. However autophagy also plays a key role in responding to other external stresses like high population densities and temperatures (Levine *et al.* 2004). Unicellular organisms commonly respond to environmental stress by differentiating into alternative life forms that are better adapted for survival. Several studies have highlighted the importance of autophagy in mediating these cellular differentiation and remodelling events. In *S. cerevisiae* starvation induces the differentiation of diploid budding yeast into resistant spore structures (sporulation). Disrupting autophagy by making mutant cell lines blocked sporulation (Talloczy *et al.* 2002). Unicellular *Dictyostelium discoideum* respond to starvation by assembling multicellular fruiting bodies to facilitate the dispersal of spores. Two separate autophagy mutant cell lines were unable to differentiate into productive fruiting bodies (Otto *et al.* 2003).

Perhaps surprisingly mammals also rely on autophagy as a response to nutrient limitation. The upregulation of autophagy in various tissues was seen following the starvation of mice (Mizushima *et al.* 2004) and also in the early neonatal period when the nutrient supply was stopped (Kuma *et al.* 2004). Furthermore, autophagy is increasingly linked to a variety of physiological processes in higher eukaryotes. Critically the deregulation of autophagy has been implicated in a wide spectra of disease pathologies including, cancer, muscular diseases and neurodegenerative disorders (Levine *et al.* 2008; Mizushima *et al.* 2008).

3.1.9 Autophagy in Trypanosomatidae Protozoa

The advantages that autophagy can bring to single celled organisms suggests it is likely to be beneficial to many lower eukaryotes. Bioinformatic analyses only detected half of the *S. cerevisiae* autophagy-associated machinery in *Trypanosomatidae* genomes (Herman *et al.* 2006; Rigden *et al.* 2009; Williams *et al.* 2006). However, many of the missing autophagy proteins were also absent in a wider range of organisms, suggesting that certain proteins are specific to fungi (Rigden *et al.* 2009). The successful bioinformatics screens combined with

accumulating experimental evidence confirm that autophagy is conserved in a wide variety of unicellular eukaryotes (Duszenko *et al.* 2010 in press). Of all the protists that are currently amenable to genetic and experimental investigation much of the research has focused on human and animal pathogens and the current understanding of autophagy in select Trypanosomatidae parasites will be discussed.

3.1.9.1 *Leishmania*

In silico analysis of candidate ATG genes in *L. major*, using *S. cerevisiae* autophagy genes as the queries identified candidates for half of the yeast genes (Williams *et al.* 2006). While strong evidence of an ATG8-PE conjugation system was found, the presence ATG12-ATG5 conjugation pathway was initially disputed (Herman *et al.* 2006; Rigden *et al.* 2009) because weak orthologues were only detected following exhaustive searches using autophagy genes from alternative species. However, extensive alignments revealed the presence of most key residues in the *L. major* orthologues even if their overall sequence similarity was low (Williams *et al.* 2006). Interestingly the genome mining also provided evidence for a unusually large expanded family of ATG8 genes, (discussed in more detail below).

Based on the strong evidence for the presence of an ATG8-PE conjugation system, it was possible to evaluate the use of green fluorescent protein-labelled ATG8 (GFP-ATG8) as an autophagosome marker in *L. mexicana* (Williams *et al.* 2006). Fluorescent microscopy revealed the redistribution of GFP-ATG8 from cytosolic forms to lipid-anchored punctate structures following starvation-induced stress and during differentiation events occurring in the *L. mexicana* lifecycle. The structures were confirmed as autophagosomes by using autophagy inhibitors and ultrastructural analysis (Williams *et al.* 2006). This effective autophagosome marker revealed that autophagy was activated during the differentiation of procyclic promastigotes to the infective metacyclic form and to a higher extent during differentiation of metacyclic promastigotes to amastigotes (Williams *et al.* 2006). Interestingly, *Leishmania* do not have orthologues of the yeast vacuolar peptidases PEP4 and PBR1, but do have an unusually large repertoire of Clan CA, Family C1 cysteine peptidases found in the lysosome. The two major lysosomal peptidase CPA and CPB were shown to be

necessary for effective autophagy in *L. mexicana*. CPA and CPB null mutants showed reduced viability during starvation, impaired differentiation to metacyclic promastigotes and amastigotes forms and an accumulation of GFP-ATG8 autophagosomes in the lysosome (Williams *et al.* 2006). Degradation of the autophagosome by cysteine peptidases instead of aspartic and serine peptidase, represents an interesting difference between *Leishmania* and yeast autophagy.

Additionally, *L. major* dominant negative mutants for VPS4, an ATPase known to be involved in endosomal sorting, were unable to differentiate into metacyclic promastigotes and had defects in the autophagy pathway (Besteiro *et al.* 2006). Increased GFP-ATG8 autophagosome numbers were found in the mutant lines, indicating a possible block of autophagosome with the lysosome. It was also found that mutants lacking the cysteine peptidase ATG4.2, were unable to differentiate into infective metacyclics, supporting the involvement of autophagy in *L. major* differentiation and ultimately virulence (Besteiro *et al.* 2006).

Investigations into the expanded family of *L. major* ATG8s revealed that proteins from the different families were likely to have distinct roles (Williams *et al.* 2009). The 25 ATG8 genes were sub-classified into one ATG8, three ATG8A, eight ATG8B and 13 ATG8C genes. GFP-tagging of representative members of each family revealed different localisations; only GFP-ATG8 formed autophagosomes during both starvation and differentiation indicating it was a 'true' ATG8 (Williams *et al.* 2009). Puncta were also formed by GFP-ATG8A expressing cells, that were strongly induced by starvation but interestingly remained unaffected by differentiation (Williams *et al.* 2009). The proteins selected from the ATG8B and ATG8C families, were found to form punctate structures close to the flagellar pocket in a small number of cells, but appeared unchanged following starvation or differentiation (Williams *et al.* 2009). Despite the differences *in vivo*, all of the proteins were able to fully complement a yeast Atg8 null mutant strain. Additionally, the different *L. major* ATG8 proteins were found to be selectively cleaved by the two ATG4 cysteine peptidases, possibly further indicating regulatory differences. LmATG4.1 was able to cleave ATG8, ATG8B and ATG8C, but LmATG4.2 would only cleave ATG8A (Williams *et al.* 2009).

As referred to earlier the components of the ATG5-ATG12 pathway were tentatively identified and have latterly been characterised and validated. LmATG5, LmATG10, LmATG12 and LmATG16 were shown to complement the respective null mutant *S. cerevisiae* cell lines (Williams *et al.* 2009). Further detailed characterisation showed that GFP-ATG12 and mCherry-ATG5 were always found localised to the same puncta, whereas mCherry-ATG5 only associated with a portion of GFP-ATG8 puncta (Williams *et al.*, 2010 personal communication). This suggests typical ATG5-ATG12-type labelling of the isolation membrane and early autophagosomes but disassociation with the mature autophagosome. Final confirmation of the correct identification of the ATG5-ATG12 pathway proteins was provided by successful *in vitro* reconstitution of the conjugation of ATG5 to ATG12. To achieve this conjugation purified LmATG7, LmATG10 were required along with ATP and a pre-exposed scissile glycine on LmATG5 (Williams *et al.*, 2010 personal communication).

3.1.9.2 *Trypanosoma cruzi*

Ultrastructural changes characteristic of autophagy have been presented in *T. cruzi* following treatment with various compounds. Perhaps the most convincing data was generated when testing the trypanocidal activity of three naphthoimidazoles (Menna-Barreto *et al.* 2009). Electron microscopy revealed an increase in double-membrane bound vesicles following treatment, which corroborated well with an increase in monodansylcadaverine (MDC) staining (Menna-Barreto *et al.* 2009). MDC is commonly used to label autophagosomes, however caution must always be taken when interpreting the results as a direct comparative analysis revealed MDC staining only partially colocalised with GFP-ATG8 labelled autophagosomes (Mizushima 2004). However, increased mRNA levels corresponding to genes involved in the ATG8 conjugation pathway provided additional evidence in support of autophagy upregulation in this particular study (Menna-Barreto *et al.* 2009). Furthermore, pre-treatment of *T. cruzi* with wortmannin and 3-methyladenine (3-MA) inhibited the trypanocidal effects of the three naphthoimidazoles, suggesting that a form of cell death accompanied by autophagy was occurring (Menna-Barreto *et al.* 2009).

Detailed characterisation of part of the *T. cruzi* autophagy pathway revealed potential roles in both the starvation response and differentiation events

occurring during the lifecycle (Alvarez *et al.* 2008). Bioinformatics revealed that *T. cruzi* possesses two orthologues for the *S. cerevisiae* ATG4 and ATG8 genes. TcATG4.1, TcATG4.2 and TcATG8.1 were able to restore autophagy in their corresponding yeast null mutant strains whereas TcATG8.2 was unable to complement ScATG8 (Alvarez *et al.* 2008). Interestingly, only TcATG4.1 was able to process the *T. cruzi* ATG8s, implicating an alternative role for TcATG4.2. Epitope tagging of TcATG8.1 and TcATG8.2 provided insights into the *in vivo* function of these two proteins. Immunofluorescent analysis showed that TcATG8.1 formed punctate structures following starvation. This process could be blocked by mutation of the conserved scissile glycine residue of TcATG8.1, indicating a requirement for PE conjugation in puncta formation (Alvarez *et al.* 2008). The cytoplasmic location of TcATG8.2 was not changed by starvation. Finally, the differentiation of epimastigotes to metacyclic trypomastigotes was also accompanied by an increase in puncta formation.

3.1.9.3 *Trypanosoma brucei*

Bioinformatic screening of the *T. brucei* genome identified half of the yeast autophagy related genes (Herman *et al.* 2006; Williams *et al.* 2006). Orthologues for many of the 'core' autophagy genes were identified (Table 4), including components of both the ATG8 and ATG12 conjugation pathways. In common with the other parasites discussed *T. brucei* has multiple *ATG8* genes, which in the past have been referred to differently. For the purposes of this report the *T. brucei* ATG8 genes will be referred to as ATG8.1, ATG8.2 and ATG8.3 corresponding to the following TritypDB accession numbers Tb927.7.5900, Tb927.7.5910 and Tb927.7.3320 respectively.

<i>S.cerevisiae</i> gene	Description	<i>T. brucei</i> orthologue
Induction of Autophagy		
TOR1	Target Of Rapamycin, PIK-related kinase. Controls growth in response to nutrient availability	Tb927.10.8420
TOR2	Target Of Rapamycin, PIK-related kinase. Regulates cell cycle dependent polarization of actin cytoskeleton	Tb927.4.420
ATG1	Ser/Thr kinase	Too many potential homologues
ATG13	TORC1 substrate regulates Atg1 activity	None identified
Phagophore Initiation		
ATG2	Forms complex with Atg18 and interacts with Atg9 at PAS	None identified
ATG9	Integral membrane protein	Tb11.03.0130
ATG18	PAS localised membrane proteins binds to PtdIns3P	Tb927.3.4150
ATG6	Subunit of phosphatidylinositol 3 kinase complex I required for localisation of ATG8 and ATG5-ATG12 in autophagosome	Tb927.5.3270
Vps34	Class III PtdIns kinase	Tb11.01.0930
Vps15	Ser/Thr kinase required for Vps34 activity	Tb927.8.6210
Autophagosome Completion		
ATG8	Autophagosome membrane protein. Conjugated to PE	ATG8.1 Tb927.7.5900
		ATG8.2 Tb927.7.5910
		ATG8.3 Tb927.7.3320
ATG3	E2-like enzyme in ATG8 conjugation pathway	ATG3 Tb927.2.1890
ATG4	Cysteine peptidase cleaves ATG8 to expose c-terminal glycine	ATG4 Tb11.01.7970
		ATG4.2 Tb927.6.1690
ATG7	E1-like activating enzyme. Mediates conjugation of ATG8 to PE	ATG7 Tb927.10.11180
ATG12	Autophagosome membrane protein. In complex with ATG5 and ATG16	Tb927.7.3320
ATG5	Conjugates to ATG12. Complex required for autophagosome formation	Tb927.6.2430
ATG7	E1-like activating enzyme. Mediates conjugation AT12-ATG5-ATG16 complex.	Tb927.10.11180
ATG10	E2-like enzyme in ATG12-ATG5 conjugation pathway	Tb927.8.7000
ATG16	Forms complex with ATG5-ATG12 conjugates. Required for autophagosome formation	Tb11.02.4790

Table 4 Core Autophagy Machinery and corresponding putative *T. brucei* orthologues.

Genes essential to all types of autophagy were identified and designated 'core autophagy' genes (Xie *et al.* 2007). TritypDB identifiers of *T. brucei* orthologues as identified in Herman *et al.*, 2006 and Williams *et al.*, 2006. Genes grouped by function: autophagy induction (yellow), phagophore initiation (grey), autophagosome completion Atg8 conjugation pathway (blue), autophagosome completion Atg12-Atg5 conjugation pathway (green). Tb927.7.3320 has been designated both as an ATG8 orthologue (Herman *et al.* 2006) and an ATG12 orthologue (Williams *et al.* 2006), and is discussed further in section 3.3.4.

Protein alignment of the three *T. brucei* ATG8s with *S. cerevisiae* shows that there is moderate sequence identity including many of the residues required for

protein interaction (Figure 3-3, Table 5). Indeed the crystal structure of TbATG8.2 has been solved and shows that the overall structure contains a classical ubiquitin fold consisting of central β -sheets (β 1 to β 4) surrounding two α -helices (α 3 and α 4) and displays significant structural homology with ATG8s from higher eukaryotes (Koopmann *et al.* 2009). Detailed mutational studies of the yeast ATG8 identified two sites essential for function; Phe77 and Phe79 form part of the Atg4 recognition site, and Tyr49 and Leu50 that are important for lipidation (*S. cerevisiae* numbering) (Amar *et al.* 2006). The sequence alignment (Figure 3-3) show a high degree of conservation for these key residues. Predictive modelling of TbATG8.2 superimposed over the known structure of rat LC3 in complex with human ATG4, revealed the required orientation of the conserved Phe80 and Tyr82 (*T. brucei* ATG8.2 numbering) to mediate ATG4 interaction (Koopmann *et al.* 2009).

The proteins TbATG8.1 and TbATG8.2 share 82% amino acid identity (Table 5), with only slight divergence in their N-terminal regions. Structurally, therefore, they are likely to be very similar, although interestingly TbATG8.1 terminates in a glycine residue (Figure 3-3). This could mean TbATG8.1 is translated in a mature form that does not require proteolytic activation, hinting at an alternative physiological role. Interestingly TbATG8.3 contains an insertion that is predicted to extend the ubiquitin fold, which modelling suggested would prohibit interaction with TbATG4 (Koopmann *et al.* 2009). However, TbATG8.3 also terminates in a glycine allowing conjugation to PE without the action of ATG4. Furthermore the insertion found in TbATG8.3 is somewhat characteristic of those found in other ATG12 proteins. Indeed, it is predicted to be the orthologue of the LmjF22.1300, which has recently been confirmed to function as an ATG12 protein (Williams *et al.*, 2010 personal communication). Further characterisation of the TbATG8 proteins is required to divulge their true physiological functions and possible roles in the autophagy pathway.

The majority of information on autophagy in *T. brucei* is based on the interpretation of ultrastructural studies depicting characteristic morphological changes attributed to a variety of compounds. One such compound, dihydroxyacetone (DHA) a common substrate for energy in many cells, was found to inhibit BSF *T. brucei* growth (EC₅₀ at 1 mM) by blocking cell cycle progression. Concurrent with this effect DHA treatment was also found to stimulate the formation of autophagic-like bodies (Uzcategui *et al.* 2007). Another class of chemicals reported to induce autophagy in *T. brucei* are neuropeptides. A range of neuropeptides were found to be effective in curing mice of trypanosome infections without any detectable toxicity side effects (Delgado *et al.* 2008). The antimicrobial effect of neuropeptides arises from their ability to punch holes in or destabilise the membrane but unusually *T. brucei* endocytosed the neuropeptides which caused lysosome disruption and cytosolic accumulation of glycolytic enzymes (Delgado *et al.* 2008). This destabilised parasite metabolism and caused cell death. Electron microscopy revealed this was accompanied by the accumulation of autophagic-like vacuoles, which was further verified by immunofluorescence using human anti-LC3, which is a homologue of the yeast ATG8 protein (Delgado *et al.* 2008). Both of these reports show an increased autophagic response accompanying cell death. Whether this is an active process or just an artefact related to aberrant cells in general remains to be determined.

The significance of autophagy to processes such as cellular development and remodelling has been discussed above in the context of numerous different organisms. The lifecycle of *T. brucei* requires significant morphological and metabolic changes (see section 1.4). In BSF *T. brucei* energy is primarily supplied by a simplified cohort of metabolic enzymes sequestered in an organelle called the glycosome (Michels *et al.* 2006). In contrast, PCF parasites have a more complex metabolism including a functional mitochondrion and an elaborated repertoire of glycosomal enzymes. Consequently during the cell cycle there is an obvious requirement for efficient turnover of glycosomes. In yeast, the peroxisome is degraded by an autophagic process called pexophagy (Dunn *et al.* 2005). Indeed in *T. brucei* there was a small tendency for the glycosomes to associate with the lysosome during long slender bloodstream to short stumpy bloodstream differentiation (Herman *et al.* 2008). However this association was

much more pronounced in cells differentiating from short stumpy BSF to PCF and was accompanied by an enlarged lysosome found to contain glycolytic enzymes. No glycosomes were detected within an autophagic membrane suggesting that a process analogous to micropexophagy was occurring (Herman *et al.* 2008).

3.2 Project aims

Evidence is accumulating showing the presence of autophagy in *T. brucei*, however conclusive molecular characterisation of the machinery and process has yet to be carried out. In this project we attempt to provide definitive evidence for autophagy in *T. brucei* by focusing on:

- 1) Autophagy pathway characterisation - using fluorescent reporter systems to investigate and monitor autophagosome formation.
- 2) Investigation of the three predicted *T. brucei* ATG8 genes to determine whether they are all functional Atg8 orthologues.
- 3) Revealing the essentiality of the autophagy pathway to *T. brucei* parasites by using RNAi to downregulate orthologues of key autophagy proteins.

3.3 Results

3.3.1 Tagging of ATG8.1 in its native locus

In mammalian and yeast models the *ATG8* gene encodes a conjugating protein that is incorporated into the membrane of autophagosomes. Labelling of *ATG8* with fluorescent reporter proteins has been shown to be an effective method for the study of autophagy in *Leishmania* and was instrumental in confirming the presence of a functional autophagy pathway in these parasites (Besteiro *et al.* 2006; Williams *et al.* 2006). Consequently, the use of specific protein markers was selected to investigate the roles of the three putative ATG8s of *T. brucei* and their involvement in the autophagy pathway.

The initial strategy was based on a PCR-generated epitope tagging system of *T. brucei* genes (Shen *et al.* 2001). It was anticipated that the fusion of a GFP:HA tag to the N-terminus of the ATG8.1 ORF at the native locus would allow for the visualisation of the transgene under the control of the natural processing signals thus minimising possible artefacts associated with over expression (Benzel *et al.* 2000). To create the native expression construct a reporter cassette containing a GFP:HA tag and drug resistance marker was amplified by PCR with long primers containing flanking sequences specific to ATG8.1. One primer added 80 nucleotides homologous to the 5' UTR immediately upstream of ATG8.1, and the second primer added the first 80 nucleotides of the target ORF (Figure 3-4A). The PCR product was cloned and sequenced before transfection into both BSF and PCF 427 cells. Clones were generated for both lifecycle stages and successful integration and expression was confirmed by western blot using an antibody specific to the HA epitope (Figure 3-4B). Proteins corresponding to the expected size of the GFP:HA ATG8.1 fusion (~43 kDa) were detected in both BSF and PCF, although overnight incubation with the primary antibody was required with only a weak signal detected. This suggested that the expression level of the native protein was very low in the cell lines and conditions tested. The scarcity of GFP-ATG8.1 in both BSF and PCF presented significant problems for microscopic analysis of the cells. High exposure times were needed, which produced substantial background auto-fluorescence and only weak fluorescent signals could be detected.

The analytical challenges of the cells tagged at the native ATG8.1 locus prompted a new approach to enable a more practicable and detailed analysis of autophagy in *T. brucei*. Expression of GFP-ATG8 from an ectopic locus has been shown to be an effective method for monitoring autophagy in Leishmania (Besteiro *et al.* 2006; Williams *et al.* 2006). Accordingly, a system for the ectopic expression of YFP tagged ATG8s in *T. brucei* was developed (see section 3.3.3).

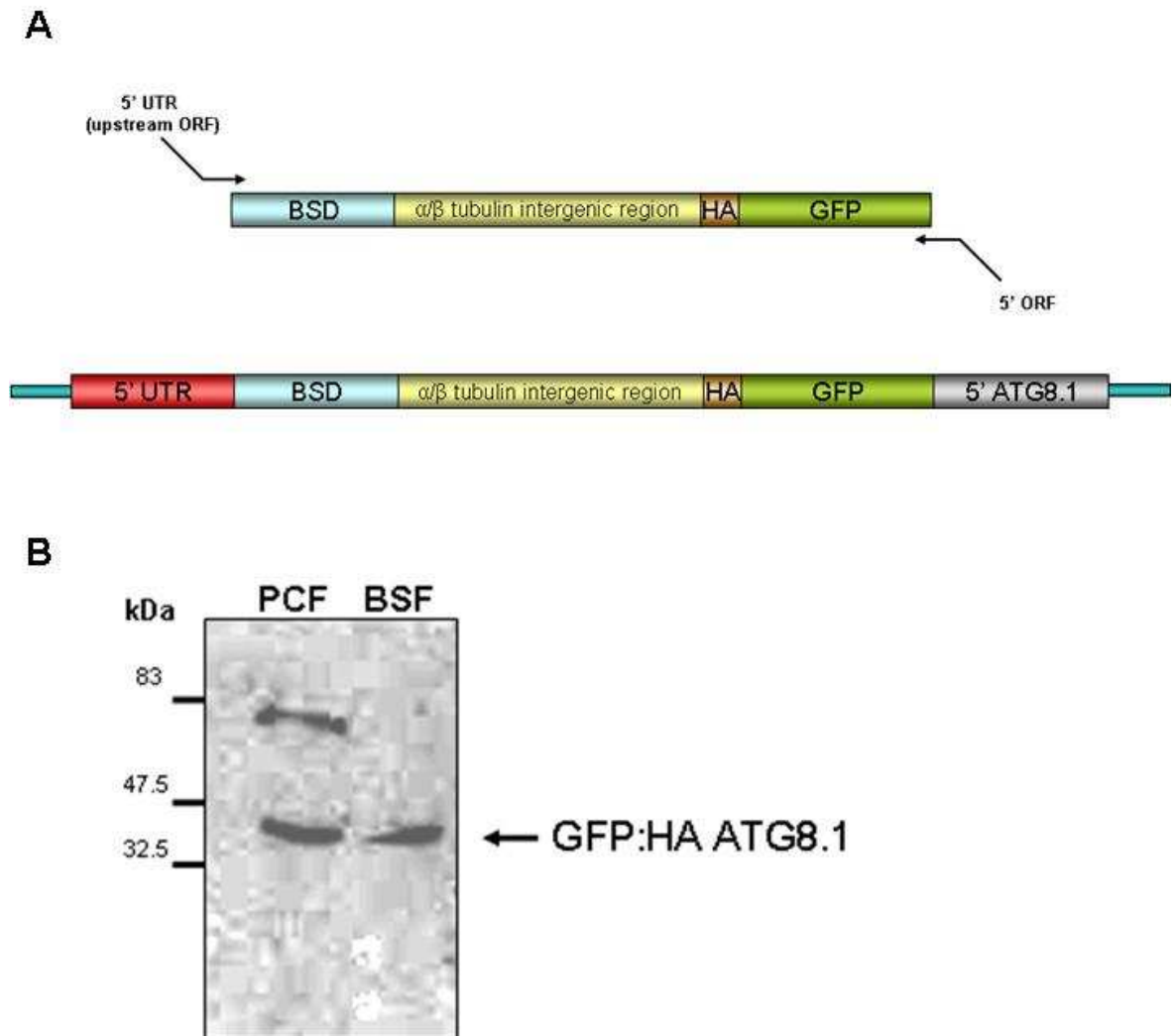


Figure 3-4 GFP tagging of native TbATG8.1 locus.

A) Creating the native expression construct. Reporter cassette was amplified, as indicated, with long primers which added flanking regions containing 80 nucleotides of ATG8.1 5' UTR and 80 nucleotides of 5' end of ATG8.1 ORF. Resulting PCR product was cloned and sequenced. Cloning vector derived EcoRI restriction sites used to digest and prepare linear DNA prior to transfection. B) Western blot analysis of GFP:HA ATG8.1 native tagged PCF and BSF cell lines, using anti-HA. Protein corresponding to expected size of transgene (41.2 kDa) was detected in PCF and BSF. Unknown protein (~70 kDa) detected in PCF cells.

3.3.2 ATG8 expressed by BSF and PCF *T. brucei*

Tagging of the ATG8.1 native locus with GFP suggested that the expression level was low in both lifecycle stages during normal growth. This finding was consistent with those of a subsequent published study on glycosome turnover during *T. brucei* differentiation, in which the expression profile of ATG8 in *T. brucei* was also analysed by western blotting with an antibody raised against TbATG8.2 (Herman *et al.* 2008). To confirm this and to facilitate later studies a polyclonal antibody specific to *T. brucei* ATG8.1 was made. The ORF for ATG8.1 was cloned into protein expression vector pET28a and expressed in BL21 Rosetta *E. coli* overnight at 15°C induced with 0.1mM IPTG. ATG8.1 was purified via the N-terminal HIS tag using immobilised metal ion affinity chromatography (IMAC) (Figure 3-5A). One rabbit was immunised with purified recombinant ATG8.1 and the anti-serum was affinity purified against immobilised ATG8.1 producing anti-ATG8. Due to the high degree of sequence similarity (82%) between ATG8.1 and ATG8.2 proteins it was predicted both proteins would be recognised by anti-ATG8.

Western blotting of whole cell lysate was used to investigate ATG8 expression in wild type BSF and PCF *T. brucei* at different phases of growth in culture. Cells were grown in media and the growth phase determined by haemocytometer counts. Aliquots of cells were removed and prepared for western blot analysis when the culture was classed to be in early, mid and late logarithmic growth phase. It was found that ATG8 expression was maintained at a constant level during logarithmic BSF growth. However, in PCF the protein level increased with culture density (Figure 3-5B). A cross reacting protein detected in the PCF western blot served as an internal control to demonstrate equal loading (Figure 3-5B). The weak bands detected by western blot were attributed to low cellular protein levels and not a low affinity antibody, as the anti-ATG8 antibody has been shown to work effectively with cell lines over expressing ATG8 proteins (Figure 3-7). Additionally, anti-ATG8 recognised both over-expressed ATG8.1 and ATG8.2 (Figure 3-7), which means the exact identity of the protein detected in the wild type cells cannot be discerned and the similarity in predicted protein size (ATG8.1 13.25 kDa, ATG8.2 13.75 kDa) prevented potential separation of the two ATG8s by SDS-PAGE.

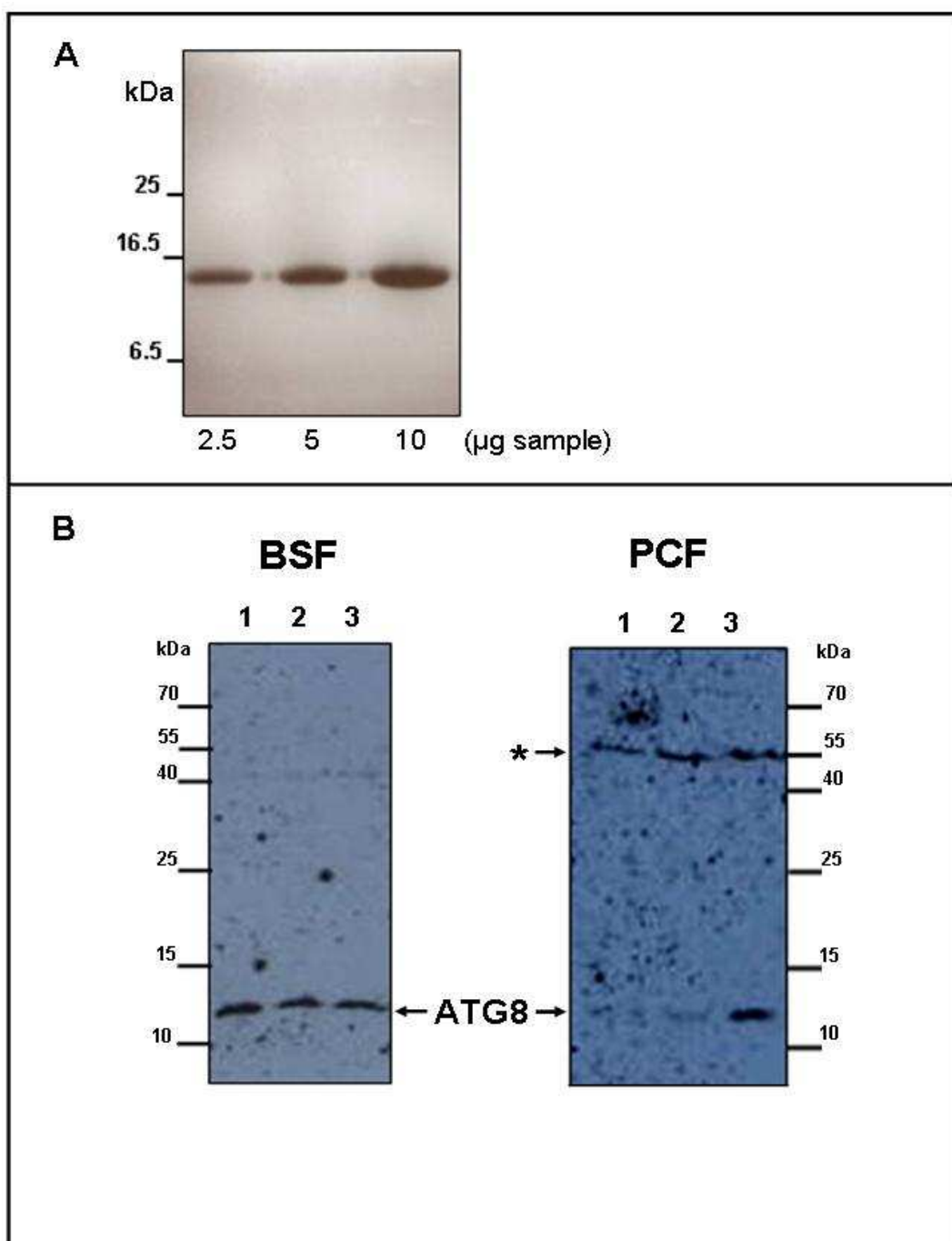


Figure 3-5 Monitoring ATG8 expression in BSF and PCF *T. brucei*.

A) Coomassie stained 15% SDS-PAGE of purified ATG8.1. The ORF of ATG8.1 was cloned into pET28a adding an N-terminal HIS tag. ATG8.1 was expressed in BL21 *E. coli* cells at 15°C induced with 0.1mM IPTG and purified by IMAC on a nickel NTA agarose column. Eluted material was pooled, desalted and analysed for purity by SDS-PAGE before being used to immunise a rabbit. B) Western blot of wild type BSF and PCF cell lines using affinity purified anti-ATG8. The density of cultured BSF and PCF was assessed and 3.5×10^6 cell equivalents were removed and prepared for SDS-PAGE analysis when the cultures were determined to be in early (1), mid (2) and late (3) log growth phases. BSF cell densities: early $2 \times 10^5 \text{ ml}^{-1}$, mid $6 \times 10^5 \text{ ml}^{-1}$, late $2 \times 10^6 \text{ ml}^{-1}$. PCF cell densities: early $1 \times 10^6 \text{ ml}^{-1}$, mid $5 \times 10^6 \text{ ml}^{-1}$, late $2 \times 10^7 \text{ ml}^{-1}$. Asterisk indicates cross reacting band and demonstrates equal PCF loading.

3.3.3 Localisation of YFP-ATG8.1 and YFP-ATG8.2

3.3.3.1 Improved cell lines for the investigation of autophagy

To overcome the difficulties associated with visualising ATG8.1 tagged at the native locus over expression constructs were created for the three ATG8s of *T. brucei* (Figure 3-6). The constructs were based on a plasmid backbone designated p2625 (Kelly *et al.* 2007) also known as pGL1731. It was selected to specifically add an N-terminal YFP tag to the target ATG8 protein to ensure the C-terminal region was free to undergo the processing required for ATG8 modification. The constructs were designed to integrate into a non transcribed spacer region between ribosomal RNA genes with expression of the transgene directed by the EPI procyclin promoter under the control of a tetracycline operator system (Kelly *et al.* 2007). The bleomycin drug resistance marker used for the selection of transfected parasites was expressed by modified T7 RNA polymerase. Consequently cell lines BSF 427 90-13 and PCF 29-13 were used for transfection, as they were engineered to express both T7 RNA polymerase and the tetracycline repressor (Wirtz *et al.* 1999).

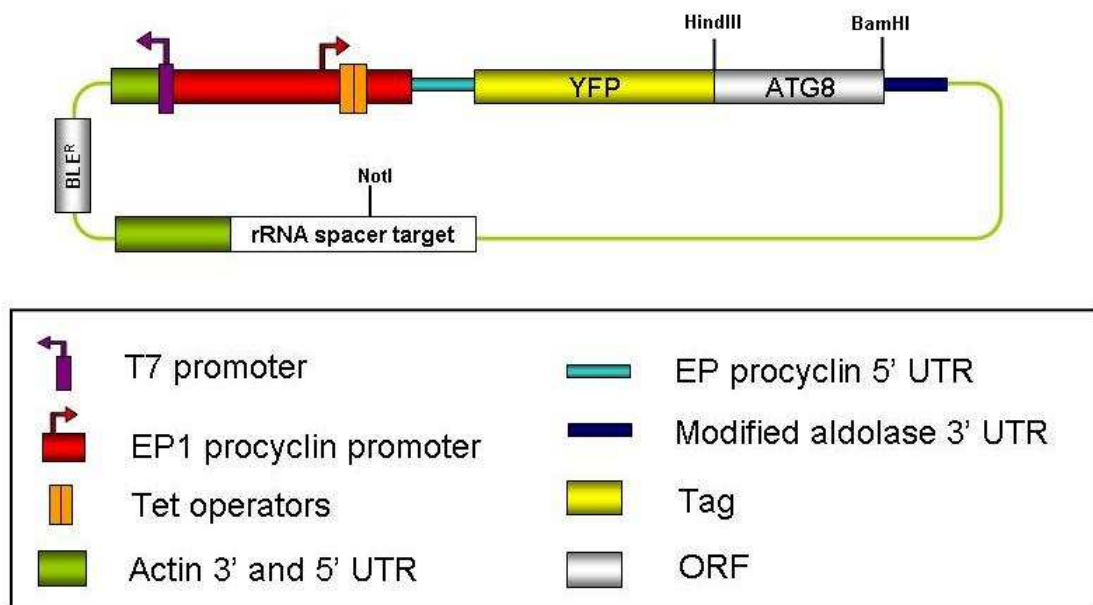


Figure 3-6 Constructs for ectopically expressed YFP-ATG8s.

N-terminal YFP tagging was achieved by cloning the individual ATG8 ORFs using *HindIII* and *BamHI* restriction sites into pGL1731 backbone. Main features of the tetracycline inducible expression vectors are displayed.

Stable cell lines were established for all three ATG8s in both BSF and PCF cells (ATG8.3 is discussed separately in section 3.3.4). Expression of YFP-ATG8.1 and YFP-ATG8.2 transgenes had no negative effects on cell growth (data not shown) and were efficiently induced by the addition of $1 \mu\text{g ml}^{-1}$ tetracycline in both lifecycle stages. Visualising the regulated transgene expression by western blot was easily achieved using anti-ATG8, although the concentration of antibody (1/1000) and incubation time (1 hour), do not enable detection of endogenous ATG8 (Figure 3-7). Subsequent analysis of the fluorescence produced by induced parasites also showed a much stronger signal than the natively tagged proteins and allowed for accurate microscopic analysis and investigation of autophagy in *T. brucei*.

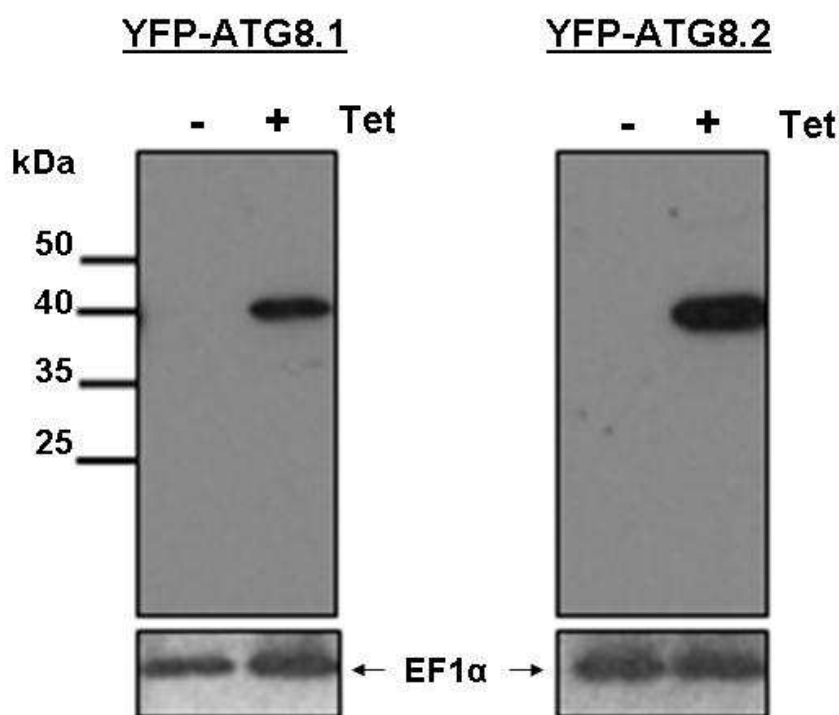


Figure 3-7 Tetracycline induced YFP-ATG8.1 and YFP-ATG8.2 expression.

PCF 29-13 cells transfected with YFP-ATG8.1 and YFP-ATG8.2 expression constructs were grown for 24 hours in SDM79 media supplemented with $1 \mu\text{g ml}^{-1}$ tetracycline (Tet +) or left as uninduced control (Tet -). 1×10^6 cell equivalents were loaded per lane and probed with affinity purified anti-ATG8. YFP-ATG8.1 (40.2 kDa) and YFP-ATG8.2 (40.75 kDa) were only detected in the presence of tetracycline. To demonstrate equal loading the membrane was stripped and reprobed with anti-EF1 α .

3.3.3.2 YFP-ATG8.1 and YFP-ATG8.2 are predominantly located in the cytosol during normal growth

Having established cell lines able to express YFP-ATG8.1 and YFP-ATG8.2, fluorescent microscopy was used to investigate the localisation of the tagged proteins to determine whether any characteristics typical of ATG8 proteins could be detected. For each condition analysed 200 cells were counted for a series of 3 replicate experiments, carried out on three individual clones, with all data presented as means (unless indicated as otherwise).

Early log phase cells were induced with $1 \mu\text{g ml}^{-1}$ tetracycline and maintained in nutrient rich media for 24 hours before fixation in paraformaldehyde and microscopic analysis. For both the BSF and PCF parasites the majority of YFP-ATG8.1 and YFP-ATG8.2 was distributed throughout the cytoplasm, with punctate structures only detected in some cells (BSF Figure 3-8, PCF Figure 3-9). More detailed analysis revealed that the BSF parasites expressing YFP-ATG8.1 had visible punctate structures in 31% of cells, whereas 44% of cells expressing YFP-ATG8.2 contained labelled puncta (Figure 3-8). During normal growth PCF *T. brucei* had fewer cells containing puncta than the BSF cells; only 16% of YFP-ATG8.1 and 11% of YFP-ATG8.2 PCF cells had visible puncta in early log cultures (Figure 3-9). Interestingly under normal cultured growth conditions there was a bias for increased YFP-ATG8.1 puncta formation in PCF cells and YFP-ATG8.2 puncta formation in BSF cells.

To confirm the YFP labelled puncta were autophagosomes, several different methods were used to investigate whether induction or inhibition of puncta occurred in a manner characteristic of autophagy.

3.3.3.3 Nutrient starvation induces puncta formation

Nutrient deprivation is well known to stimulate autophagy, triggering increased autophagosome formation to promote the supply of material to the lysosome. The two lifecycle stages of *T. brucei* are well adapted for survival in vastly different host environments. BSF parasites reside in nutrient rich mammalian blood and rely exclusively on glucose metabolism to produce ATP. The tsetse fly gut inhabited by PCFs is less stable and nutrient availability can fluctuate,

dependent upon potentially infrequent bloodmeals. This is reflected in the PCF metabolism that is adapted to cope with diminishing glucose levels and ensure continued survival during periods of nutrient limitation or starvation. Having established a baseline level of puncta formation during normal growth it was possible to investigate the changes in YFP-ATG8.1 and YFP-ATG8.2 puncta formation caused by nutrient depletion and starvation. Only PCF cell lines were analysed to give an accurate reflection of natural circumstances.

To investigate nutrient depletion a comparison of puncta formation was made by microscopic analysis of cells taken from induced early log cells (nutrient rich) and late log cultures (nutrient depleted). It was found there was a significant increase in the percentage of late log cells with YFP-ATG8.1 puncta compared to early, 21% to 16% respectively (Figure 3-9). However, whilst the percentage of YFP-ATG8.2 puncta containing cells rose from 11% to 16% in late log cultures, this change was not statistically significant (Figure 3-9).

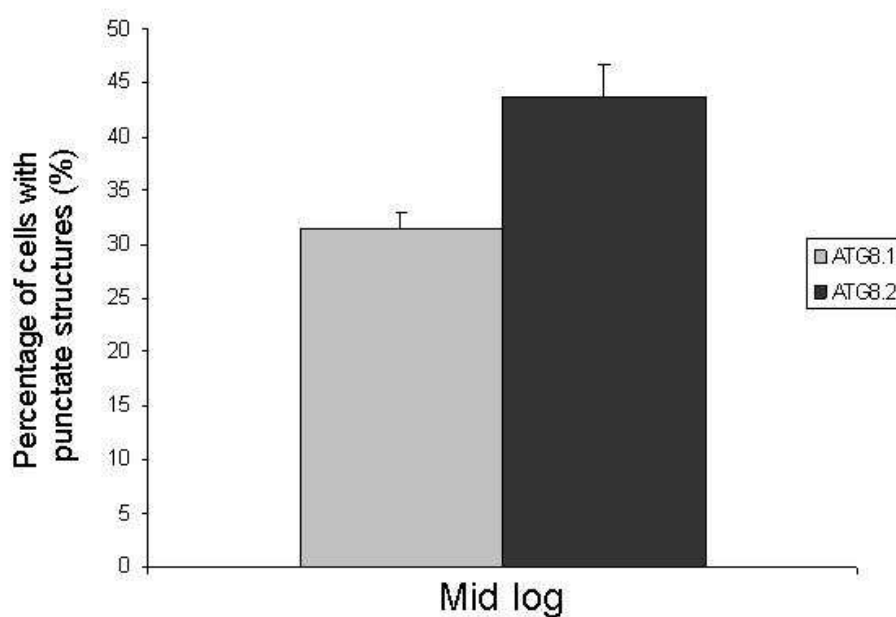
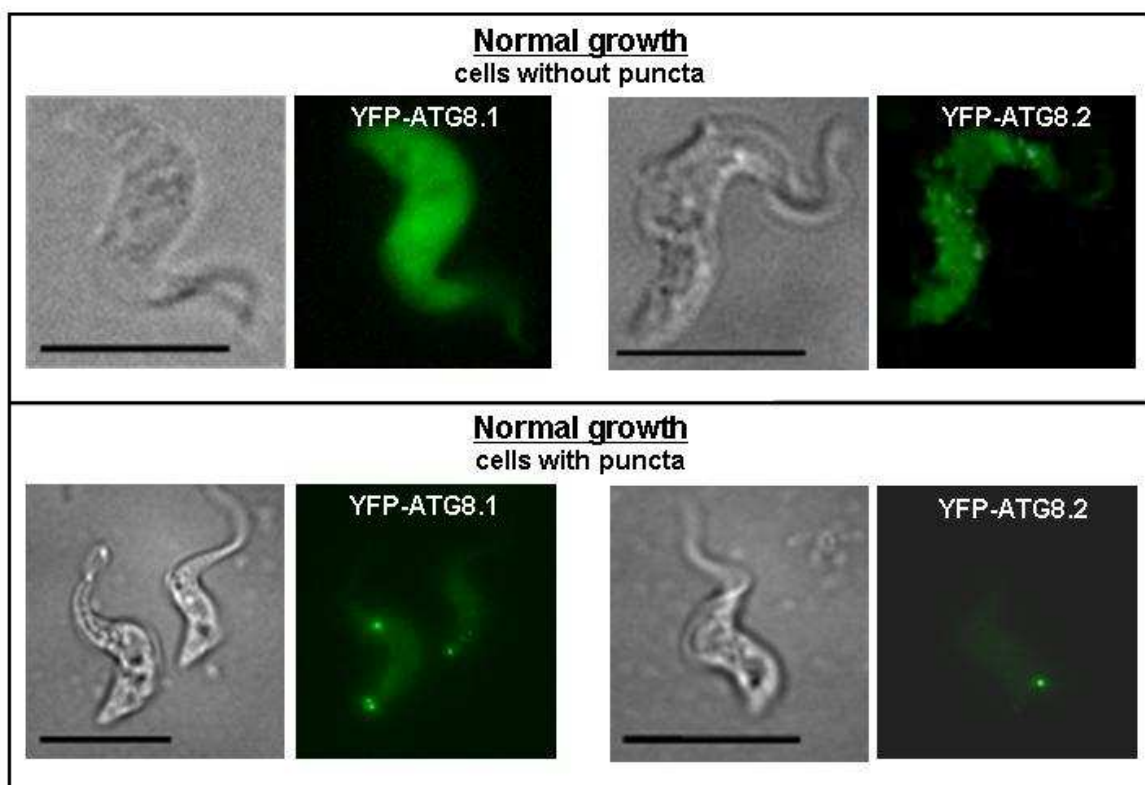


Figure 3-8 Analysis of YFP-ATG8.1 and YFP-ATG8.2 localisation in BSF *T. brucei*.

BSF cells expressing YFP-ATG8.1, YFP-ATG8.2 were induced with $1 \mu\text{g ml}^{-1}$ tetracycline and maintained in nutrient rich HMI9 media for 24 hours (normal growth). Washed cells were fixed in 1% paraformaldehyde before settling onto poly-L-lysine coated slides and analysis on an Applied Precision DeltaVision microscope. Representative images of cells with and without puncta are shown. Left hand images DIC filter, right hand images FITC filter set. Scale bar $5 \mu\text{m}$.

The percentage of cells containing punctate structures was determined by counting >200 cells for each condition, with data displayed as a mean of a series of three replicate experiments for 3 clones, error bars represent standard deviation.

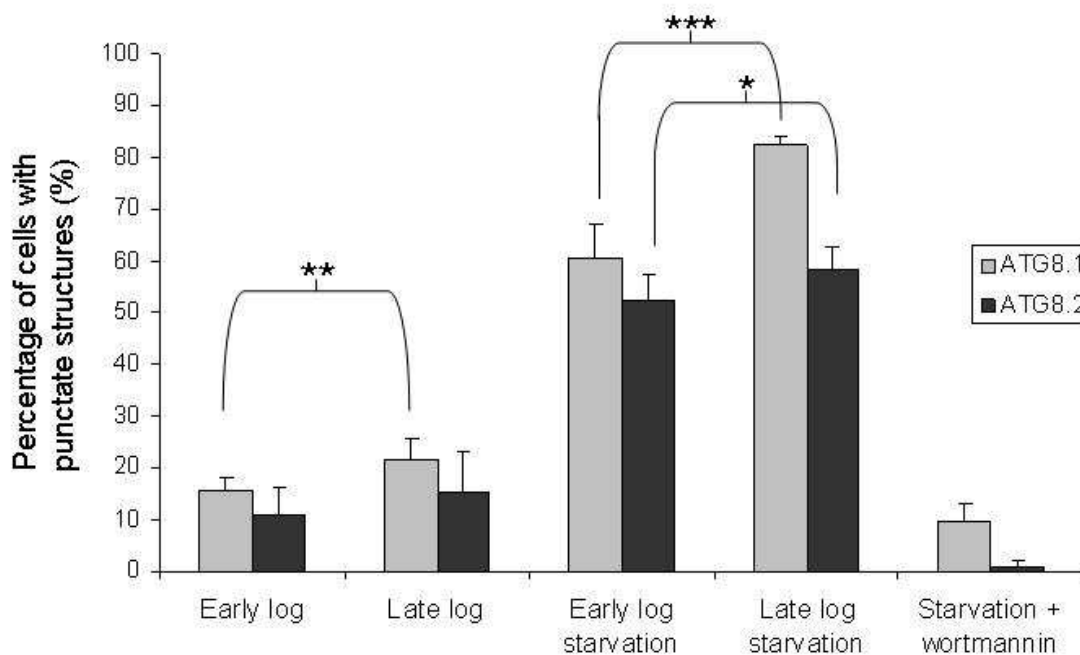
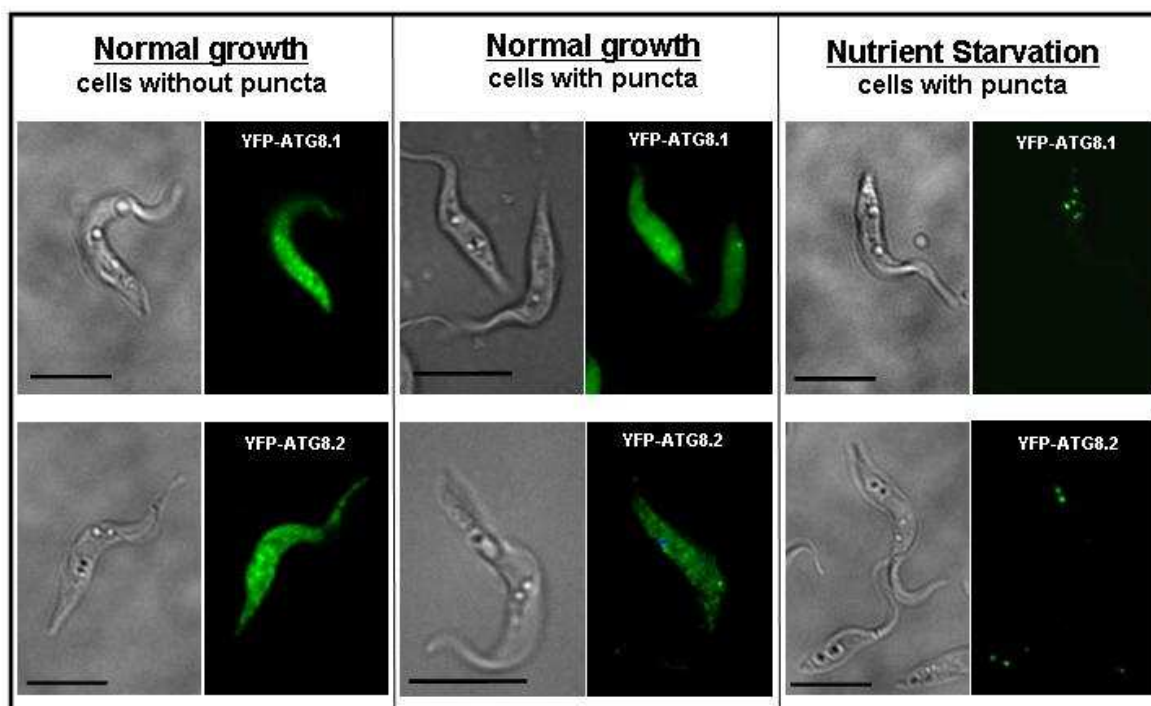


Figure 3-9 Analysis of YFP-ATG8.1 and YFP-ATG8.2 localisation in PCF *T. brucei*.

PCF cells expressing YFP-ATG8.1, YFP-ATG8.2 were induced with $1 \mu\text{g ml}^{-1}$ tetracycline and maintained in nutrient rich SDM79 media for 24 hours (normal growth) or extensively washed and starved of nutrients by incubation in PBS supplemented with $1 \mu\text{g ml}^{-1}$ tetracycline for 2.5 hours (nutrient starvation). Washed cells were fixed in 1% paraformaldehyde and viewed on an Applied Precision DeltaVision microscope. Left hand images DIC filter, right hand images FITC filter set. Scale bar $5 \mu\text{m}$.

Fluorescent microscopy was used to monitor autophagosome formation in PCF cells expressing YFP-ATG8.1 (light grey bars) and YFP-ATG8.2 (dark grey bars) during different stages of cell growth in nutrient rich SDM79 media and following 2.5 hours in nutrient free PBS media (starvation). The effect of $10 \mu\text{M}$ wortmannin on autophagosome formation was also investigated. The percentage of cells containing punctate structures was determined by counting >200 cells for each condition, with data displayed as a mean of three replicate experiments from three independent clones. Error bars represent standard deviation. Asterisk(s) indicate where data from late log cultures differed significantly from early log cultures * $p < 0.05$, ** $p < 0.01$, *** $p < 0.001$.

Cells from early and late log cultures were investigated to determine if there were any growth phase related factors able to influence puncta formation. However, to evaluate the response to complete nutrient starvation, induced PCF cells were washed and incubated in PBS supplemented with tetracycline and analysed for puncta formation by microscopy. Nutrient starvation was found to be a strong inducer of puncta formation for both YFP-ATG8.1 and YFP-ATG8.2 with clear punctate structures detected by microscopy (Figure 3-9). Starved parasites from late-log cultures were more likely to contain puncta, suggesting they were conditioned to respond more rapidly to starvation. After 2.5 hours in nutrient free PBS 60% of starved early log cells contained YFP-ATG8.1 puncta compared to 82% of starved late log cells (Figure 3-9). More detailed analysis revealed an increase in the average number of puncta per positive cell, which rose from 1.4 in non starved to 2.2 and 2.6 in starved early and late respectively (Figure 3-10). For YFP-ATG8.2 the percentage of starved cells with puncta was 52% for early log cultures and 58% of late log cells (Figure 3-10). Again the average number of puncta per positive cell also increased, from 1.2 in non starved to 1.7 and 1.8 in starved early and late respectively (Figure 3-10).

Having successfully established starvation as robust method of inducing puncta formation, we sought to see if this process could be blocked by wortmannin, a classical inhibitor of autophagy. Wortmannin blocks autophagy by inhibition of PI3 kinases and has been shown to be effective in mammalian cells at concentrations of 10 nM (Blommaert *et al.* 1997; Petiot *et al.* 2000). However, the inhibition of autophagosome formation in *Leishmania* required the use of wortmannin at 10 μ M (Besteiro *et al.* 2006; Williams *et al.* 2006), which although much higher than for mammalian cells was selected as the starting concentration for the *T. brucei* experiments. It was found that the addition of 10 μ M wortmannin to the PBS starvation media completely abolished the formation of YFP-ATG8.2 puncta and reduced YFP-ATG8.2 puncta containing cells to only 7% (Figure 3-9). Together the starvation and inhibition data strongly support the hypothesis that TbATG8.1 and TbATG8.2 are true ATG8 proteins and that the punctate structures observed are true autophagosomes.

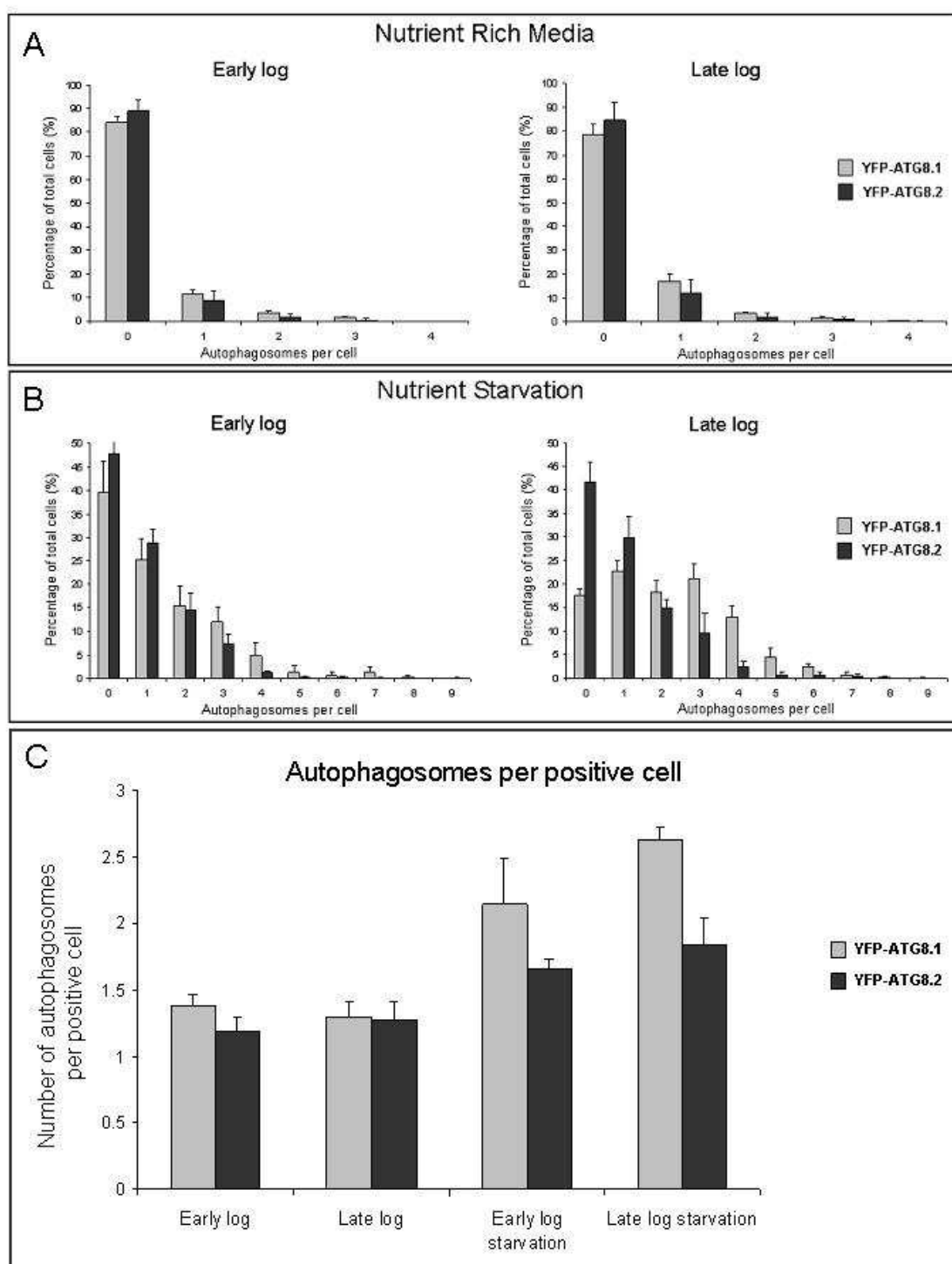


Figure 3-10 Detailed analysis of autophagosome formation in PCF *T. brucei*.

Fixed PCF cells expressing YFP-ATG8.1 (light grey bars) and YFP-ATG8.2 (dark grey bars) were analysed by fluorescent microscopy during different stages of cell growth in nutrient rich SDM79 media and following 2.5 hours in nutrient free PBS media (starvation). A and B show the number of autophagosomes per cell. Determined for >200 cells and the frequency expressed as a percentage of the total number of cells counted. C) The average number of autophagosomes per positive cell was calculated.

All data displayed as means of three replicate experiments from three independent clones. Error bars show standard deviation.

3.3.3.4 Vasoactive Intestinal Peptide rapidly stimulates autophagosome formation in BSF cells.

In an effort to explore novel trypanocidal compounds a selection of endogenous human neuropeptides were found to effectively kill trypanosomes during *in vitro* culture and in *in vivo* mouse models (Delgado *et al.*, 2008). Further detailed characterisation revealed that following neuropeptide uptake an increase in double membrane bound organelles was detected by electron microscopy (Delgado *et al.* 2008). The appearance of autophagosome-like structures in dying cells prompted the suggestion that the cells were dying by autophagic cell death. To investigate the effect of neuropeptides on autophagosome formation, the BSF ATG8 reporter cell lines were treated with a representative neuropeptide, vasoactive intestinal peptide (VIP). Induced cells were incubated with a sub-lethal dose of VIP for 4 and 16 hours and then fixed in paraformaldehyde and analysed by microscopy. Treatment with VIP was found to stimulate redistribution of cytosolic YFP-ATG8.1 and YFP-ATG8.2 into autophagosome-like puncta, which appeared throughout the cell (Figure 3-11). The overall percentage of cells containing both YFP-ATG8.1 and YFP-ATG8.2 labelled autophagosomes increased significantly after the addition of VIP (Figure 3-11), however the increase in the average number of autophagosomes per positive cell was more slight (Figure 3-12). The average number of YFP-ATG8.1 autophagosomes per positive cell increased from 1.6 in the untreated control to 1.9 following 4 hours incubation with VIP. Similarly, the average number of YFP-ATG8.2 autophagosomes per positive cell increased from 1.3 in the untreated control to 1.7 following 4 hours incubation with VIP (Figure 3-12). Induction of autophagosome formation was rapid, however extension of the VIP incubation period to 16 hours did not significantly increase autophagosome formation in comparison to 4 hours treatment.

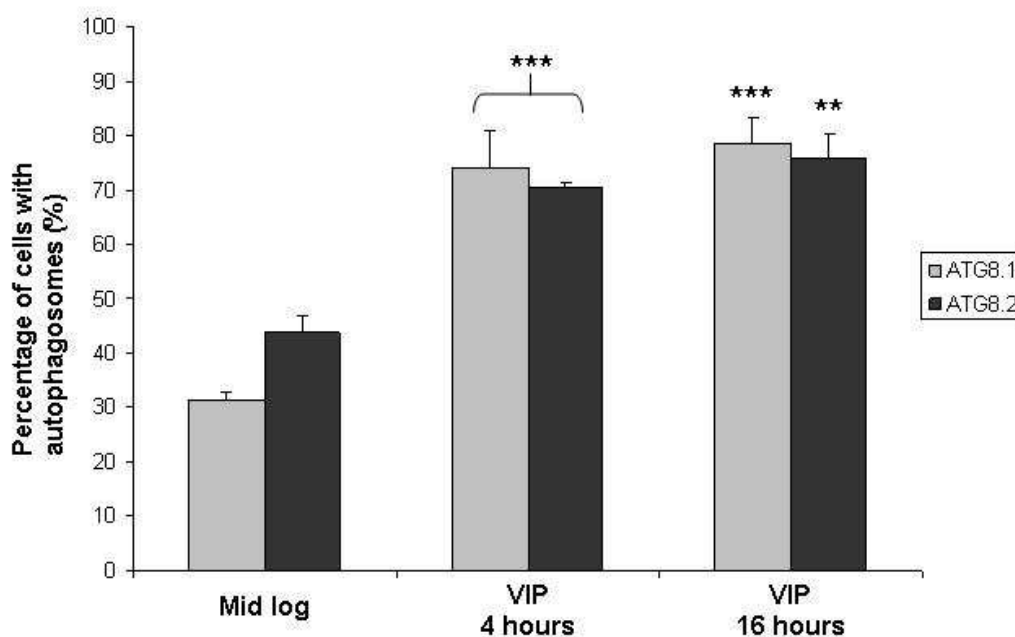
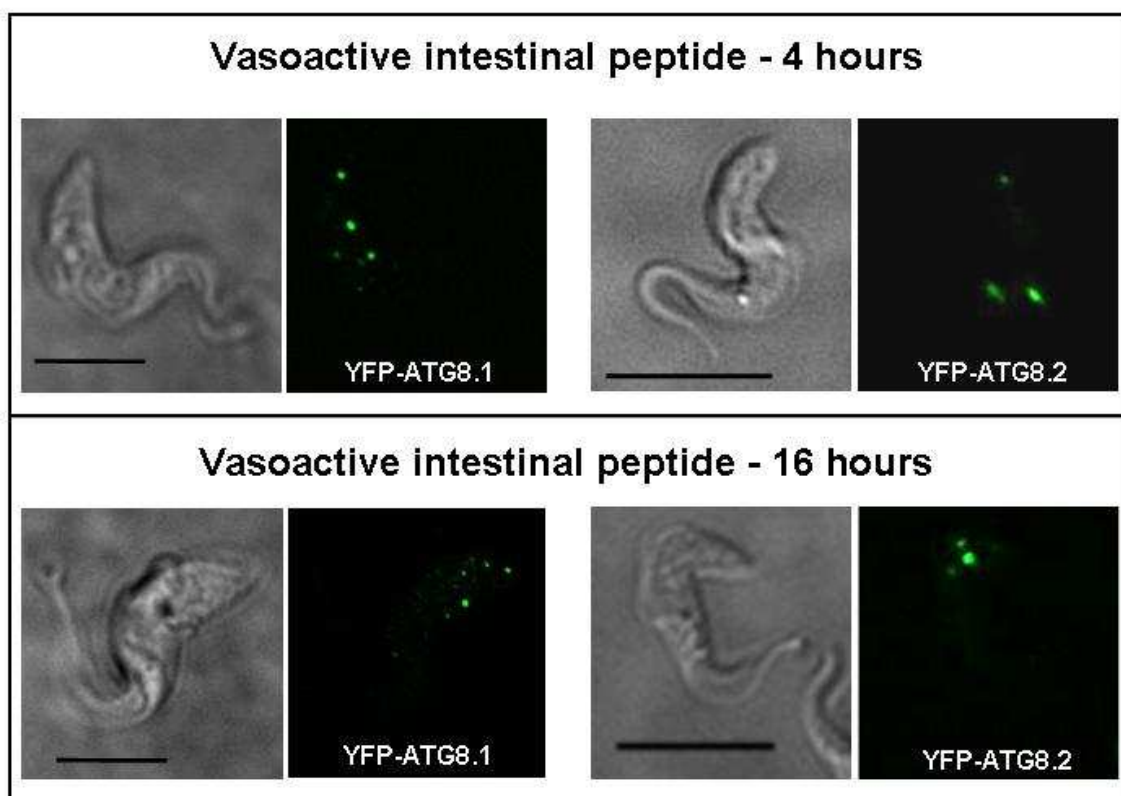


Figure 3-11 Localisation of YFP-ATG8.1 and YFP-ATG8.2 in BSF *T. brucei* following vasoactive intestinal peptide treatment.

BSF cells expressing YFP-ATG8.1, YFP-ATG8.2 were induced with $1 \mu\text{g ml}^{-1}$ tetracycline and maintained in nutrient rich HMI9 media for 24 hours (mid-log) supplemented with $3.75 \mu\text{M}$ vasoactive intestinal peptide for 4 and 16 hours. Washed cells were fixed in 1% paraformaldehyde before settling onto poly-L-lysine coated slides and viewed on an Applied Precision DeltaVision microscope. Left hand images DIC filter, right hand images FITC filter set. Scale bar $5 \mu\text{m}$.

The percentage of cells containing autophagosomes was determined by counting >200 cells for each condition, with data displayed as a mean of three replicate experiments from one clones. Error bars represent standard deviation. Asterisk(s) indicate where data from VIP treated cultures differed significantly from mid log control cultures ** $p < 0.01$, *** $p < 0.001$.

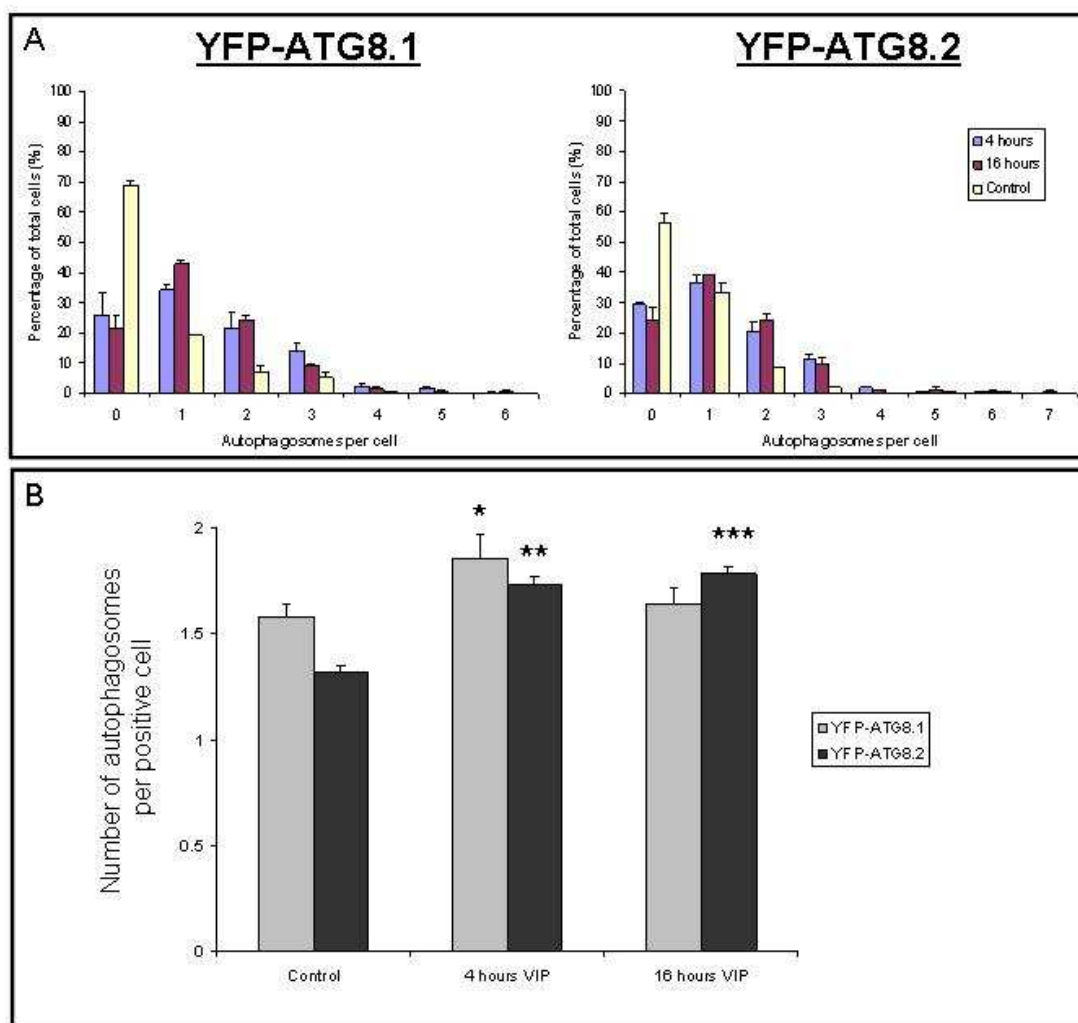


Figure 3-12 VIP rapidly stimulates autophagosome formation in BSF *T. brucei*.

A) The number of autophagosomes per cell was determined by fluorescent microscopy of BSF cells expressing YFP-ATG8.1 and YFP-ATG8.2. Mid log cultures grown in nutrient rich HMI9 media (control) and those supplemented with 3.75 μ M VIP for 4 and 16 hours were analysed. The number of autophagosomes per cell was determined for >200 cells and expressed as a percentage of the total number of cells counted. Data displayed represents means of three replicate experiments for one clone. Error bars show standard deviation.

B) The percentage of cells containing autophagosomes was determined by counting >200 cells for each condition, with data displayed as a mean of three replicate experiments from one clones. Error bars represent standard deviation. Asterisk(s) indicate where data from VIP treated cultures differed significantly from mid log control cultures: * $p < 0.05$, ** $p < 0.01$, *** $p < 0.001$.

3.3.3.5 Rapamycin does not induce autophagy in *T. brucei*

In yeast rapamycin stimulates autophagy through the inhibition of TOR, which is a protein kinase that controls cell growth in response to levels of ATP and amino acids. TOR operates in two separate complexes to exert control upon two distinct aspects of cellular growth. TOR complex 1 (TORC1) regulates temporal cell growth, whereas TOR complex 2 (TORC2) controls spatial cell growth (Wullschleger *et al.* 2006). Rapamycin selectively inhibits TORC1 (Zheng *et al.* 1995), which suggests it is the TOR complex responsible for autophagy regulation (Kamada *et al.* 2000). *T. brucei* possesses two TOR orthologues TbTOR1 and TbTOR2, which through interactions with their respective TOR complexes were shown to regulate temporal aspects of cell growth and cell polarization, respectively (Barquilla *et al.* 2008). Detailed characterisation of the *T. brucei* TOR complexes revealed that only TbTOR2 was specifically inhibited by rapamycin. Unlike TOR kinases in other eukaryotes, TbTOR1 remained insensitive, which suggested rapamycin is unlikely to induce *T. brucei* autophagy in a TOR dependent manner (Barquilla *et al.* 2009).

However, previous to the work of Barquilla and colleagues, rapamycin had been used as a positive control for the induction of autophagy in *T. brucei*, with electron micrographs presented depicting the potential resulting autophagosomes (Uzategui *et al.* 2007). To resolve the disparity and investigate potential TOR independent autophagy stimulation, the effect of rapamycin on YFP-ATG8.1 and YFP-ATG8.2 labelled autophagosomes was investigated. Rapamycin was added to induced cultured cells and the redistribution of YFP-ATG8 into puncta was monitored by microscopy.

Growth of BSF cells with 1 μM and 5 μM rapamycin for 24 hours significantly increased the percentage of cells containing both YFP-ATG8.1 and YFP-ATG8.2 autophagosomes. In PCF only 10 μM rapamycin produced a marginal increase in the percentage of cells with YFP-ATG8.2 autophagosomes (not statistically significant), however no effect on YFP-ATG8.1 was observed (Figure 3-13). Despite statistically significant results of YFP-TG8.1 autophagosome formation in BSF cells, the effects of rapamycin on autophagy induction were very mild, especially when compared to starvation (PCF) and VIP treatment (BSF). The marginally increased autophagosome numbers potentially represented artefacts

relating to unhealthy cells arising from the high concentrations used, as opposed to direct autophagy induction. The small and inconsistent increases in autophagosome formation, in relation to the high concentrations of rapamycin used, suggest the effects observed were unlikely to stem from a direct induction of autophagy but were possibly related to an increase in aberrant cells. Thus it appears rapamycin is unsuitable for use as an inducer of autophagy and does not appear to dramatically stimulate autophagosome formation in a TOR independent manner.

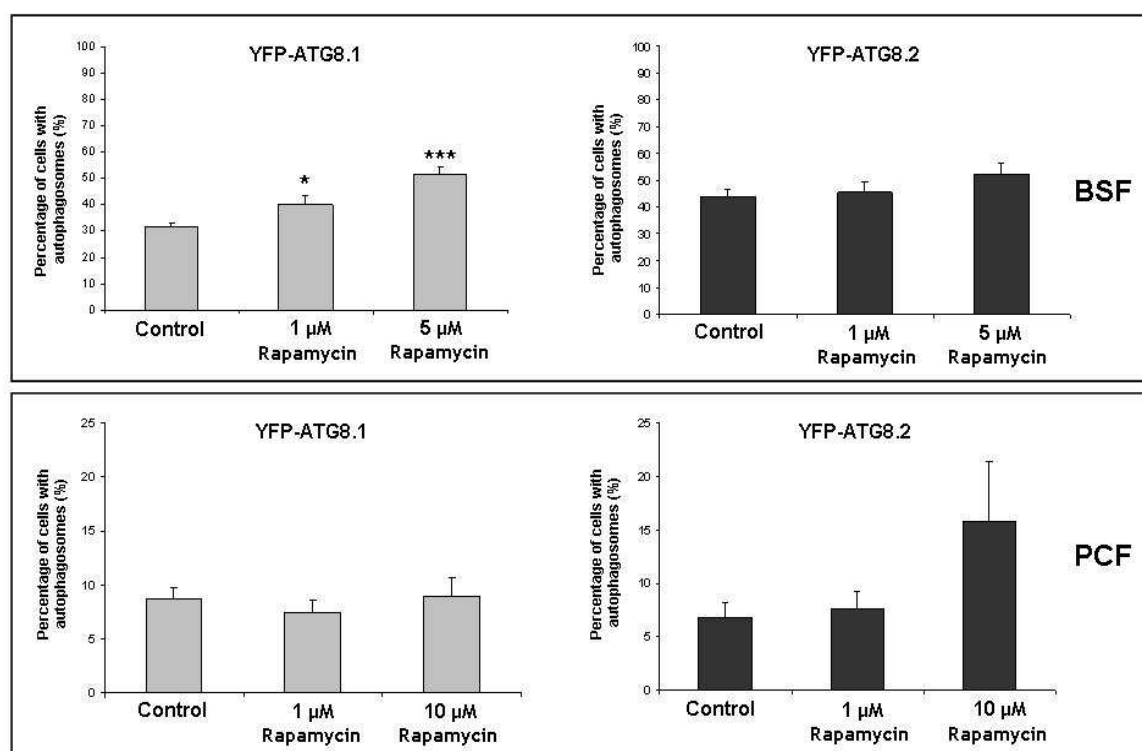


Figure 3-13 Rapamycin does not stimulate autophagosome formation in *T. brucei*.

YFP-ATG8.1 and YFP-ATG8.2 expressing cells were grown in the presence of rapamycin for 24 hours before fluorescent microscopy analysis. The percentage of cells containing punctate structures was determined by counting >200 cells for each condition, with data displayed as a mean of three replicate experiments from an individual clone. Error bars represent standard deviation. Asterisk(s) indicate where data from rapamycin treated cultures differed significantly control cultures: * $p < 0.05$, *** $p < 0.001$.

3.3.4 Investigating TbATG8.3

Multiple copies of ATG8 can be found in mammals and plants; the significance of these expanded ATG8 gene families is not yet fully understood. Yeast has only one ATG8 gene, however humans have eight ATG8 orthologues that are divided into two subfamilies, MAP1LC3 and GABARAP/GATE-16 (He *et al.* 2003). Analysis of the autophagy network identified 67 proteins that interacted with the cohort of human ATG8s, of which only approximately one-third were found to interact with both subfamilies (Behrends *et al.* 2010). This could reflect the distinct roles of the different ATG8 subfamilies (Weidberg *et al.* 2010) but also demonstrates substantial functional overlap of their roles in autophagy.

Leishmania major has an extended repertoire of 25 ATG8-like genes, grouped into ATG8, ATG8A, ATG8B and ATG8C sub-families based on sequence similarity (Williams *et al.* 2006). Characterisation of ATG8 and representative members from each subfamily revealed distinct differences. All of the LmATG8s could complement yeast ATG8 null mutants suggesting a shared ability to function as true 'ATG8 proteins'. Additionally, GFP-labelled puncta were formed by proteins from all four subfamilies, however their distribution and response to starvation and differentiation was markedly different (Williams *et al.* 2009).

In this work the labelling of TbATG8.1 and TbATG8.2 with YFP was used to establish that these proteins were incorporated into autophagosomes and behaved like other yeast and mammal ATG8s. However, as discussed in section 3.1.9.3, bioinformatic searches revealed that a third ATG8 homologue existed in *T. brucei*, ATG8.3 (Tb927.7.3320). The TbATG8.3 protein shares a high degree of sequence similarity to ATG8.1 and ATG8.2, and contains many of the key conserved residues identified in yeast (Figure 3-3). However ATG8.3, contains a large insertion, characteristic of many ATG12 type proteins (Figure 3-14) including LmjF22.1300, an ATG8-like protein that has been shown to function as an ATG12 protein in *L. major* and is able to form punctate structures (Williams *et al.* 2009). In yeast cells the ATG12-ATG5 complex has been shown to be predominantly located in the cytoplasm with only small amounts associated to the isolation membranes and is entirely absent from autophagosomes (Mizushima *et al.* 2001).

For the *in vivo* characterisation of TbATG8.3, the ORF was cloned into the same N-terminal YFP expression vector as used previously. Tightly regulated inducible expression was clearly detectable by western blot using an antibody specific to GFP (recognises the mutant YFP form). Interestingly expression was not detected by the anti-ATG8 antibody (Figure 3-15). This could suggest differences in the protein structure or absent epitopes on ATG8.3. Analysis of the YFP-ATG8.3 cell lines revealed that during normal growth YFP-ATG8.3 was almost entirely dispersed in the cytosol (98.6% of cells) with very few punctate structures detected. Upon starvation there was a slight increase in the percentage of cells containing puncta (Figure 3-16). The localisation of YFP-ATG8.3 conformed to that of an ATG12-like protein, however in the absence of definitive data this finding could not be confirmed.

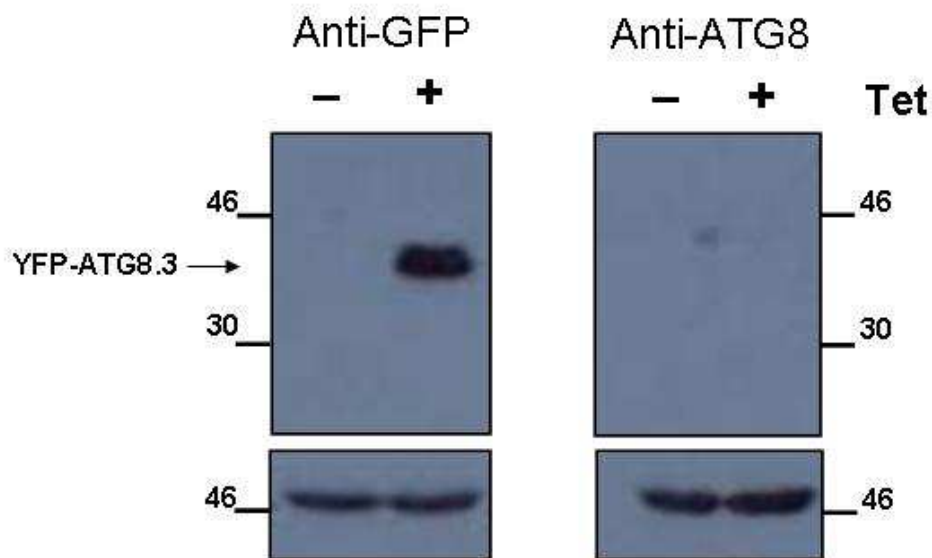


Figure 3-15 Tetracycline induced YFP-ATG8.3 expression.

PCF 29-13 cells transfected with YFP-ATG8.3 expression constructs were grown for 24 hours in SDM79 media supplemented with $1 \mu\text{g ml}^{-1}$ tetracycline (Tet +) or left as uninduced control (Tet -). 1×10^6 cell equivalents were loaded per lane and probed with anti-GFP and affinity purified anti-ATG8. YFP-ATG8.3 (42.2 kDA) were only detected in the presence of tetracycline. To demonstrate equal loading the membrane was stripped and re-probed with anti-EF1 α (bottom boxes).

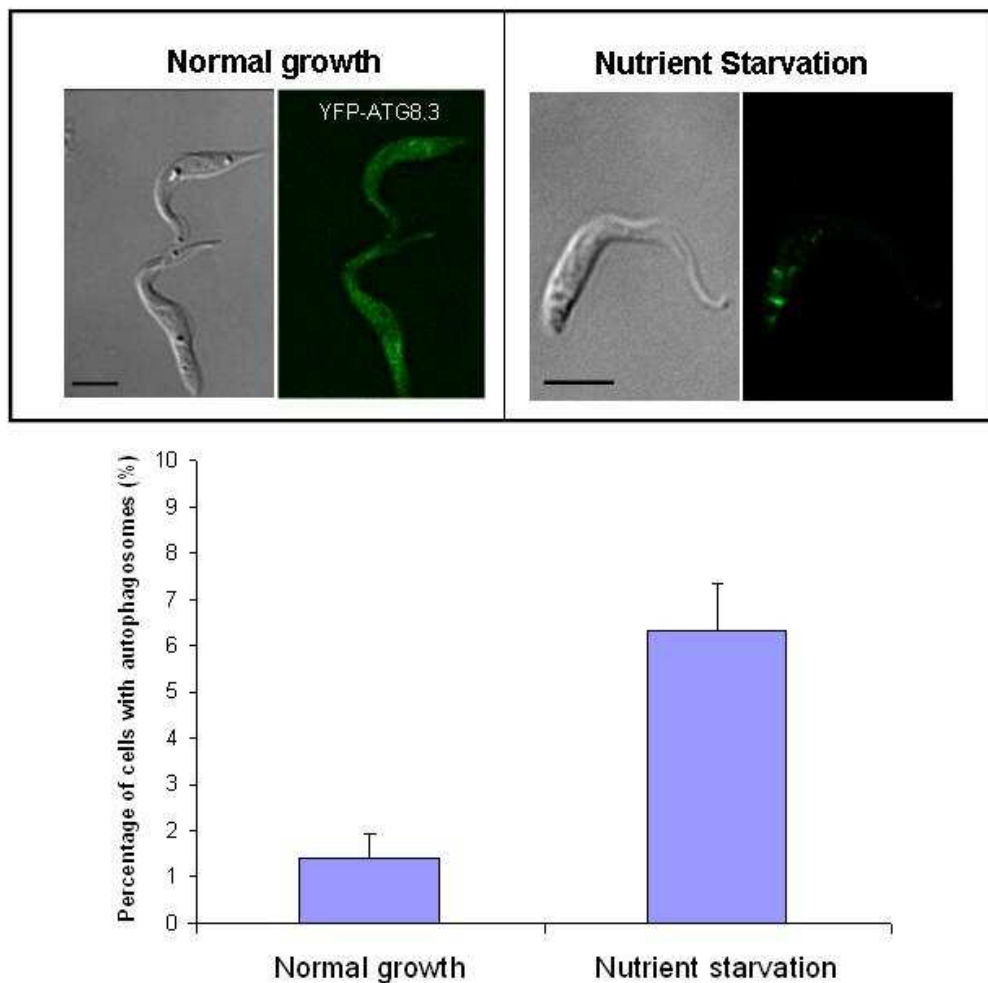


Figure 3-16 YFP-ATG8.3 puncta formation in PCF cells.

Florescent microscopy was used to monitor autophagosome formation in PCF cells expressing YFP-ATG8.3 during cell growth in nutrient rich SDM79 media (normal) and following 2.5 hours in nutrient free PBS media (starvation). Scale bar 5 μ m. The percentage of cells containing punctate structures was determined by counting >200 cells for each condition, with data displayed as a mean of three replicate experiments from three independent clones. Error bars represent standard deviation.

3.3.5 Selective ATG8 lipid conjugation

The formation of autophagosomes requires two ubiquitin-like protein conjugation systems, centred on Atg12 and Atg8. In yeast, Atg8 is conjugated to an abundant membrane phospholipid called phosphatidylethanolamine (PE). The conjugation reaction requires Atg4 (cysteine peptidase) mediated removal of the

C-terminal arginine (amino acid position 117) from newly synthesised Atg8. This exposes a glycine residue (amino acid position 116), which allows activation of the Atg8-Glycine-116 intermediate by Atg7 (E1 enzyme), which in turn transfers it to Atg3 (E2 enzyme). Finally, Atg8-Glycine-116 is conjugated to PE (forming Atg8-PE) via an amide bond between the C-terminal glycine carbonyl group and the amino group of PE. Atg8-conjugation allows incorporation into the autophagosome membrane and is essential for autophagosome formation (Ohsumi *et al.* 2004; Tanida *et al.* 2004a). The possibility that TbATG8.1 and TbATG8.2 undergo posttranslational lipid conjugation reactions was investigated by monitoring their mobility on SDS-PAGE supplemented with urea, combined with analysing their sensitivity to phospholipase D.

Whole cell lysates were made from induced PCF cultures which had either been grown under normal conditions or subject to two hours starvation. The lysates were separated by SDS page in the presence of 6M urea. Under these conditions ATG8 conjugated to a phospholipid will migrate faster and consequently appear as lower molecular weight band on the gel. Western blots using anti-ATG8 revealed that during normal growth there is a low level of lipidated YFP-ATG8.1, however starving the cells increased the amount of lipidated YFP-ATG8.1, which correlated with the increased number of cells containing fluorescent puncta (Figure 3-16). To further verify YFP-ATG8.1 lipidation, starved cell lysates were incubated with phospholipase D, which releases phosphatidic acid from the conjugate corresponding to a decrease in the faster running band. A reduction in the intensity of the lipidated YFP-ATG8.1 was observed, but full delipidation did not occur. Interestingly, lipidated forms of YFP-ATG8.2 were not detected during normal growth or following starvation (Figure 3-16). In other organisms the conjugated phospholipid is PE and it is therefore likely that PE is the phospholipid in this case.

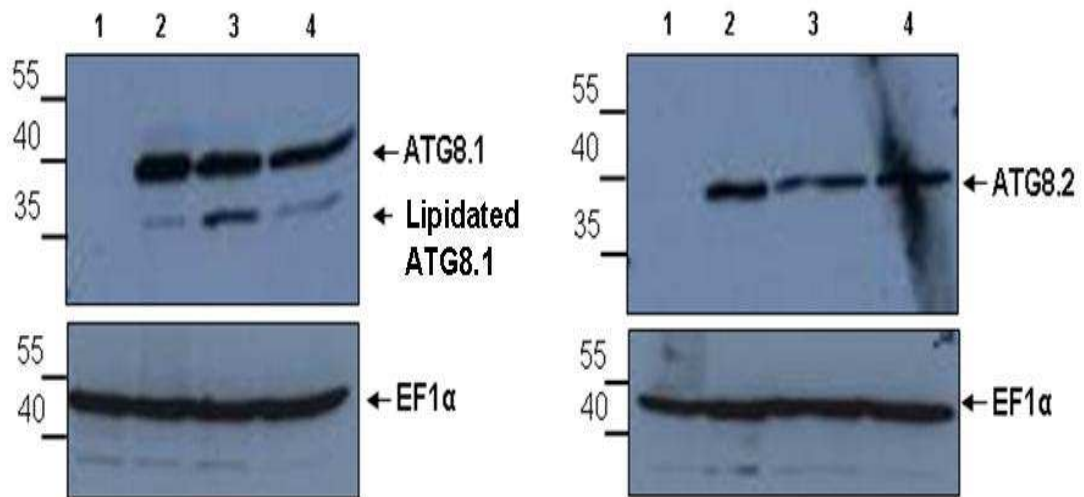


Figure 3-17 YFP-ATG8.1 conjugates to a phospholipid.

6M urea gels were used to separate 30 μ g of PCF cell lysate from YFP-ATG8 overexpressing cell lines and western blotted using affinity purified anti-ATG8.1. Induction was carried out with 1 μ g ml⁻¹ of tetracycline for 24 hours. Starved cells were washed twice before resuspension in PBS for 2 hours. Phospholipase D (PLD) was added to cell lysates and incubated at 37°C for 1 hour. Lane 1, non-induced PCF, lane 2, induced normal growth PCF, lane 3, induced starved PCF, lane 4 induced starved PCF treated with PLD.

3.3.6 Essentiality of autophagy pathway in PCF *T. brucei*

After the discovery of autophagy in yeast it was possible to screen mutants defective in the production of autophagosomes, which originally lead to the identification of 14 autophagy genes (Tsukada *et al.* 1993). This showed that disruption to autophagy was not lethal to yeast maintained in normal culture conditions. For example, analysis of mutant yeast strains lacking either ATG3 or ATG7, not only helped divulged the role of these proteins, but also demonstrated that the absence of a functional autophagy system increased sensitivity to starvation (Kim *et al.* 1999; Schlumpberger *et al.* 1997).

To validate the importance of the autophagy pathway to PCF *T. brucei* a gene fundamental to autophagy was selected for RNAi downregulation. TbATG3 (Tb927.2.1890) was identified as suitable RNAi target due to the detection of only one homologue in the *T. brucei* genome (Herman *et al.* 2006), reducing the possibility of functional complementation from other gene copies. A target region of 500 base pairs was cloned into the 2T7^{ti} RNAi vector pGL571 (LaCount *et al.* 2000) and transfected into the PCF 29-13 cell line (Wirtz *et al.* 1999). Three independent clones were analysed.

RNAi was induced in each clone by the addition of $1\mu\text{g ml}^{-1}$ tetracycline to the culture media and the growth rate of induced (Tet +) was compared to non induced control (Tet -) over a 9 day period to evaluate whether the down regulation of target gene was detrimental to cell growth. Every three days the cells were reseeded in fresh media (supplemented with tetracycline) to maintain cells in exponential growth. All three clones for ATG3 followed the same pattern following induction of RNAi; a strong reduction in the growth rate visible from 4 days post induction continuing for the remainder of the time course (Figure 3-18). No visible defects were detected in appearance of the cells until day 7 when the appearance of elongated cells became more common. To confirm that RNAi induction was targeting and reducing ATG3 mRNA, quantitative RT-PCR was used and revealed an average ATG3 transcript depletion of 78% (average of 3 clones) from 5 days post induction (Figure 3-18).

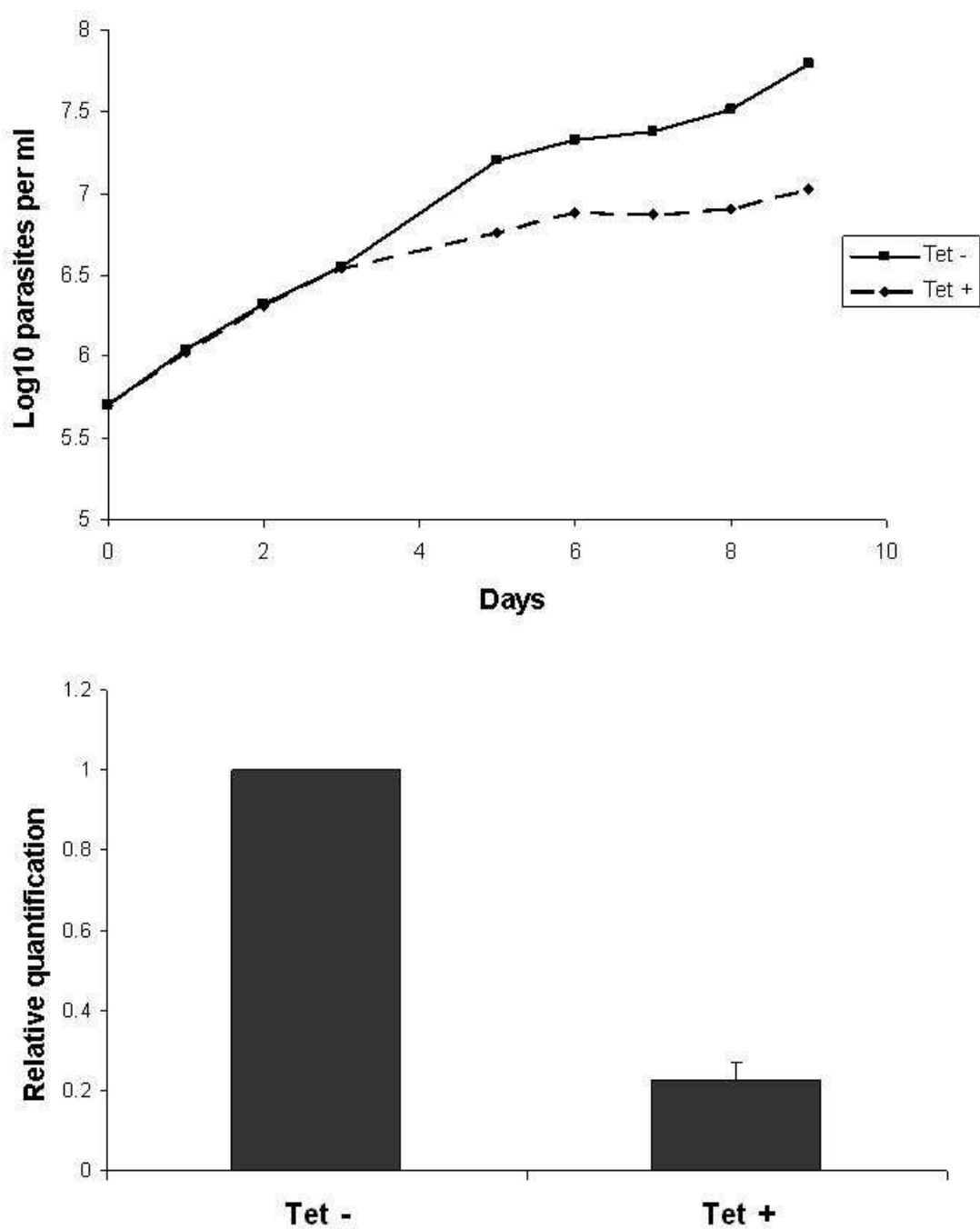


Figure 3-18 RNAi downregulation of ATG3 reduces PCF growth rate.

Top panel, cumulative growth curve for representative PCF ATG3 RNAi clone in the presence (Tet +) and absence (Tet -) of $1\mu\text{g ml}^{-1}$ tetracycline. Bottom panel, relative quantification of ATG3 mRNA in induced and noninduced RNAi cell as determined by real time PCR at day 5. Data mean of average down regulation in three independent clones, error bar shows standard error.

3.4 Discussion

Autophagy has been well characterised in yeast with over 30 individual proteins known to participate in the pathway. The yeast protein sequences were used for bioinformatic screens and identified *T. brucei* orthologues for half of the yeast autophagy machinery (Herman *et al.* 2006; Williams *et al.* 2006).

The presence of many key autophagy genes implied that a functional system was likely to exist. However the absence of certain orthologues raised interesting questions about the conservation of the overall pathway in *T. brucei*. The reduced repertoire of genes could reflect a streamlined version of the autophagy machinery that is fully functional without orthologues specific only to yeast. Alternatively, proteins with limited or no homology to their yeast counterparts could be functioning in the same pathways but remain undetected by BLAST searches. One important finding was the detection of all components of the yeast Atg8 conjugation pathway including three candidate ATG8 genes (Herman *et al.* 2006; Williams *et al.* 2006), one of which (ATG8.3) could encode for an ATG12 (Williams *et al.* 2006). The crystal structure for *T. brucei* ATG8.2 has been solved and shows the presence of many key functional residues in the correct spatial orientation as well as a high degree of structural homology with other ATG8 proteins (Koopmann *et al.* 2009).

To confirm the presence of a functional autophagy system in *T. brucei* the three candidate ATG8 orthologues were N-terminally tagged with YFP and ectopically expressed in both BSF and PCF. Thorough characterisation of YFP-ATG8.1 and YFP-ATG8.2 localisation following a variety of external stimuli revealed that they behaved with hallmarks of other characterised ATG8 proteins. Crucially following nutrient starvation of PCF cells, fluorescent microscopy revealed a dramatic redistribution of cytosolic YFP-ATG8.1 and YFP-ATG8.2 into distinct punctate structures, a process that was blocked by the classical autophagy inhibitor wortmannin. Furthermore, urea gel separation and western blot analysis revealed increased YFP-ATG8.1 lipidation following starvation, although YFP-ATG8.2 appeared not to be conjugated to a lipid. Taken together these key findings suggested that TbATG8.1 and TbATG8.2 are true 'ATG8' proteins that participate in a functional autophagy system in *T. brucei*.

Interestingly the cell densities of PCF cultures influenced the percentage of cells containing YFP-tagged autophagosomes. For both YFP-AG8.1 and YFP-ATG8.2 small but significant increases in the number cells containing autophagosomes were seen in starved cultures taken from late log densities in comparison to early log cultures. Higher culture density also increased the percentage of cells with autophagosomes during growth in normal media, potentially in response to stresses related to high population densities. The increased basal rate of autophagy in late log cells could ensure more of the required molecular components were already present allowing for more rapid adaptation to starvation leading to the observed increase in autophagosome numbers.

BSF parasites were also shown to produce YFP-ATG8.1 and YFP-ATG8.2 labelled autophagosomes during normal growth. However, BSF parasites cannot be maintained at high densities or deprived of nutrients, so alternative methods for the induction of autophagosome formation were investigated. Initially it was hoped that rapamycin would be a suitable candidate but it failed to stimulate high levels of YFP-labelled autophagosome formation, most likely due to the insensitivity of TbTOR1 to rapamycin (Barquilla *et al.* 2008). However, treating BSF cells with the neuropeptide VIP proved to be an effective method of stimulating autophagosome formation; significantly increasing the number of YFP-ATG8.1 and YFP-ATG8.2 autophagosomes per cell. Delgado *et al.*, reported that VIP caused BSF cell death accompanied by autophagy, with increased autophagosome formation revealed by ultrastructural studies using transmission electron microscopy and immunofluorescence analysis using human anti-LC3 (Delgado *et al.* 2008). The demonstration of VIP induced autophagy using confirmed markers for *T. brucei* autophagy (YFP-ATG8.1 and YFP-ATG8.2) provided strong support for the findings reported by Delgado *et al.*

Bioinformatics analysis revealed a third *T. brucei* ATG8, designated TbATG8.3. YFP-tagging of TbATG8.3 revealed a predominant cytosolic distribution with limited puncta formation occurring at much lower frequencies than TbATG8.1 and TbATG8.2. Nutrient starvation induced the formation of puncta, although overall the percentage of cells with puncta remained very low. The different localisation pattern of the *T. brucei* ATG8.3 could be due to a number of factors:

I) ATG8.3 could localise to autophagosomes but is not induced by starvation. Process specific involvement of ATG8-like proteins was found in the expanded *L. major* family of proteins, LmATG8A labelled autophagosomes were only induced by starvation not differentiation (Williams *et al.* 2009).

II) ATG8.3 functions as an ATG12 protein. Despite moderate sequence identity to other ATG8 proteins it contains a 16 amino acid insertion which is characteristic of ATG12 proteins and is predicted to interfere with its ability to interact with ATG4 (Koopmann *et al.* 2009). In *L. major* the gene LmjF22.1300 encodes a protein that has been experimentally verified to function as an ATG12 (Williams *et al.* 2009). However, sequence analysis suggests the protein has a closer resemblance to yeast Atg8 rather than Atg12 (Rigden *et al.* 2009). It is possible that in *L. major* a protein divergent from the yeast Atg12 has evolved to fulfil similar functions within the autophagy pathway. Furthermore interrogation of the *T. brucei* genome using the *L. major* ATG12 protein sequence in a BLAST searches, identified *T. brucei* ATG8.3 as a potential orthologue (Williams *et al.* 2006). Thus it is possible *T. brucei* ATG8.3 plays an equivalent role in the autophagic pathway; resembling an ATG8-like protein while functioning like an ATG12 protein.

The low number of YFP-ATG8.3 puncta observed further supports a possible role as an ATG12 protein. In yeast and mammals the Atg12-Atg5 complex is largely distributed in the cytosol and only localises to the isolation membrane and developing phagophore not to the mature autophagosomes (Mizushima *et al.* 2003; Suzuki *et al.* 2001). The reduced number of YFP-ATG8.3 structures could be attributed to the selective labelling of the developing autophagosomes only, whereas ATG8.1 and ATG8.2 are also present on mature autophagosomes. Indeed the number of PAS structures per cell varies according to species, yeast have only one whereas mammals have multiple sites of autophagosome biogenesis (Mizushima *et al.* 2003).

III) ATG8.3 is not involved in autophagy but functions in another distinct cellular process. ATG8-like proteins have a diverse range of functions, for example in *L. major*, two proteins from the ATG8B and ATG8C families appeared to be involved in autophagy-independent processes (Williams *et al.* 2009).

The affinity purified polyclonal antibody raised against ATG8.1 was able to recognise both ATG8.1 and ATG8.2 proteins, demonstrated by western blots of the individual over expression cell lines. Interestingly the antibody failed to recognise ATG8.3 indicating significant differences between the proteins caused by low amino acid sequence identity.

Endogenous TbATG8 protein was detected in both BSF and PCF monomorphic parasites, although a high antibody concentration and extended overnight incubation period were required which suggested low expression levels. The similarity in the predicted size of ATG8.1 and ATG8.2 proteins means it is impossible to discern which isoform is detected by western blot. Analysis of transcript abundance by microarray confirmed that both genes are expressed, although ATG8.1 is more abundant than ATG8.2 in all the lifecycle stages investigated (Jensen *et al.* 2009).

This investigation revealed in BSF parasites the expression level of ATG8 was constant, whereas in PCFs higher culture densities stimulated an increase in ATG8 expression. These findings correlate well with the microarray analysis of transcript abundance in logarithmically dividing and stationary phase PCF cultures. The general pattern (all genes) revealed a tendency for reduced mRNA levels in stationary cultures compared to the actively replicating log PCF cells (Jensen *et al.* 2009). However, interestingly the abundance of many core autophagy genes was found to peak in PCF stationary phase cultures (ATG6, Vps15, ATG8.2, ATG8.3, ATG3, ATG4.1, ATG10). Indeed, ATG8.1 and ATG8.2 transcript levels were 2.16 and 2.71 times higher respectively in stationary cultures compared to log dividing PCF cultures (Jensen *et al.* 2009). The authors add a note of caution as higher transcript levels may not necessarily indicate active expression but could reflect reduced decay rate. However, it is tempting to speculate that the high transcript abundance for autophagy associated genes in stationary culture conditions helps mitigate against the more stressful conditions. If the higher transcript abundance corresponds to protein level (as it appears to be for ATG8) it could be a contributing factor for the increased puncta formation found in the late log cells.

The increased ATG8 protein expression in stationary phase cultures provides a compelling reason to revisit the natively tagged ATG8.1 cell lines. Initial

investigations were focused on mid log PCF cultures, however increased GFP-ATG8.1 expression in stationary phase PCF cells might yield stronger fluorescent signals. Furthermore a recent report showed that *in situ* YFP-tagging of TbATG8.2 only produced visible punctate structures following prolonged stress to the endoplasmic reticulum not during normal growth conditions (Goldshmidt *et al.* 2010). My work has identified suitable stresses (e.g. starvation, VIP) that could be used to induce autophagosome formation in the natively tagged cell lines to facilitate further investigations.

As discussed ATG8.1 and ATG8.2 are both functional components of the *T. brucei* autophagic pathway. However, one interesting difference between these two proteins is the availability of the conserved glycine residue required for PE conjugation. Unusually ATG8.1 terminates at the site of the conserved glycine (commonly proteolytic cleavage by ATG4 is required for exposure and subsequent conjugation) whereas ATG8.2 has one more cysteine residue. It has been postulated that ATG8.1 is produced as mature protein and is involved in basal autophagic processes. The requirement for ATG8.2 processing (presumably by ATG4.1 or ATG4.2) suggests a regulated function allowing for specific activation during certain conditions such as starvation or differentiation (Koopmann *et al.* 2009).

The selective lipidation of *T. brucei* ATG8.1 and ATG8.2 was an unexpected and interesting finding. In *S. cerevisiae* Atg8 lipidation is a multi step reaction that culminates in the conjugation of Atg8 to PE allowing incorporation into the autophagosome membrane. Western blot analysis was only able to detect *T. brucei* YFP-ATG8.1 phospholipid conjugation. However, further investigation is required as fluorescent microscopy of cells expressing YFP-ATG8.2 revealed that autophagosomes were actively formed.

The high degree of conservation between the two proteins means even subtle differences in sequence and structure could contribute to the regulatory mechanisms that influence ATG8.1 and ATG8.2 interactions. The ubiquitin-cores of *T. brucei* ATG8.1 and ATG8.2 differ by only one amino acid and the proteins only diverge towards the N-terminal region, which corresponds to the $\alpha 1$ and $\alpha 2$ helices. As both ATG8s contain the conserved glycine residue required for PE conjugation it is tempting to speculate that the N-termini are critical in

mediating *T. brucei* ATG8 targeting and interactions. Indeed the N-terminal region of the human Atg8 homologues have been suggested to influence their interactions with other molecules. Structural analysis of LC3, GATE-16 and GABARAP revealed a high degree of conservation in the residues required for attachment of the $\alpha 1$ and $\alpha 2$ helices to the ubiquitin core (Sugawara *et al.* 2004). However despite this critical conservation, the $\alpha 1$ and $\alpha 2$ moieties of the human Atg8 homologues exhibited different electrostatic potentials which was thought to coordinate their interactions with different target proteins (Sugawara *et al.* 2004).

To investigate the essentiality of autophagy in *T. brucei* a gene essential to the pathway was downregulated by RNAi. The ATG3 orthologue was selected as a suitable target due to its fundamental role in autophagy pathway where it functions as the E2-like enzyme in the ATG8 conjugation pathway. Induction of RNAi produced a strong down regulation of ATG3 transcript and a reduction in the growth rate visible from four days post induction. At the end of the 9 day RNAi induction period the cells were still viable but appeared 'unhealthy' and were replicating at much lower level than the control cells. The consistent results from all clones analysed confirms that ATG3 is important and required for normal PCF cell growth. However, from the analysis carried out so far it cannot be discerned whether depletion of ATG3 successfully inhibited autophagy leading to the reduced growth rate or if ATG3 plays other roles in cellular proliferation.

The diversity of the physiological roles of autophagy in *T. brucei* remains unknown. The initial characterisation carried out in this study revealed a robust autophagic response in cultured PCF parasites following nutrient deprivation but whether this translates into the natural environment awaits confirmation. However, as discussed below there is a strong rationale to suggest autophagy is likely to be involved in many aspects of biology of wild *T. brucei* parasites.

The short stumpy BSFs that are ingested during the tsetse fly bloodmeal must undergo a complex differentiation cycle within the fly. A crucial aspect of PCF development is their migration to the tsetse fly salivary glands where they differentiate into mature metacyclics, which are perfectly adapted to ensure survival in a new mammalian host. It can take up to 24 days to establish a mature metacyclic salivary gland infection and many parasites fail to leave the

fly midgut (Van den Abbeele *et al.* 1999). Indeed in nature the tsetse fly infection rate is very low, with approximately only 10% of flies from disease endemic areas carrying trypanosomes (Aksoy *et al.* 2003).

The potential for lengthy PCF maturation means the parasites must be able to successfully persist for extended periods in the turbulent environment of the fly host. Unlike the relatively stable mammalian blood, tsetse flies are at the mercy of their environment and dramatic changes in temperature and rainfall that frequently occur during the cycle of wet and dry seasons can have profound impacts. For example the fluctuating external environment has been shown to alter fly size as well the fat content of *Glossina moristans moristans*, with higher fat levels detected during the cool season and lower levels during hot periods before the rainy season (Van den Bossche *et al.* 1999). Ultimately however all nutrients are obtained from bloodmeals and the feeding frequency of tsetse flies can be variable and subject to external influences such as prey availability. Accurate determination of natural feeding frequencies is difficult although it is generally accepted to occur approximately every 42 hours (Aksoy *et al.* 2003; Van den Bossche *et al.* 1999). Difficulties in securing a blood meal present potential nutrient limitation for both host and parasite.

The tsetse flies fat body functions as an energy reserve and provides proline for the flight muscles (Aksoy *et al.* 2003). The consequent abundance of proline in tsetse flies combined with unreliable and diminishing glucose availability, means proline is used by PCF parasites as an energy source. Therefore any factors resulting in variations to proline abundance, whether seasonal artefacts or bloodmeal frequency could result in host parasite competition for proline. Little is known about the possible compartmentalisation of proline within the tsetse fly and whether access is restricted for PCF parasites (Attardo *et al.* 2006). However complete depletion of tsetse fly proline would create an obvious cost to parasite fitness by blocking transmission. Accordingly autophagy could help to ensure the viability of PCF *T. brucei* in the tsetse fly by recycling internal nutrients during times of stress and proline limitation. Interestingly laboratory experiments have revealed that extended periods of starvation appear to increase the ability of *T. brucei* to establish mature salivary gland infections, possibly due to an impaired immune response in malnourished tsetse flies (Akoda *et al.* 2009; Kubi *et al.* 2006). This raises the interesting possibility that

autophagy allows PCFs to successfully endure periods of starvation and ultimately facilitates parasite transmission.

Autophagy is known to be essential for cellular remodelling in *S. cerevisiae* and *D. discoideum* as well as species more closely related to *T. brucei* such as *L. major* and *L. mexicana* (Besteiro *et al.* 2006; Otto *et al.* 2003; Talloczy *et al.* 2002; Williams *et al.* 2006). The developmental cycle of PCF parasites is very complex and involves multiple developmental steps consisting of morphologically distinct lifecycle stages (see section 1.4.2) and is presumed to require the considerable turnover of redundant proteins and organelles. Indeed variations in metabolism and enzymatic contents of glycosomes are known to exist in parasites from different lifecycle stages. In differentiating *T. brucei* cells microautophagy has been implicated in the efficient and rapid degradation of unwanted glycosomes containing enzymes suited to a previous lifecycle stage (Herman *et al.* 2008). This represents one example of autophagy facilitating *T. brucei* cellular remodelling, however given the complexity and importance of efficient transition between lifecycle stages we speculate that autophagy may have further critical roles to play.

4 Metacaspases

4.1 Introduction

4.1.1 *General introduction to peptidases*

Peptidases (also known as proteases or proteinases and peptide hydrolases) are proteins capable of cleaving peptide bonds. They have a well established role as mediators of non-specific degradation, yet it is becoming apparent that peptidases participate in a wide variety of roles and are emerging as key regulators of many biological processes (Lopez-Otin *et al.* 2010). Controlled proteolytic cleavage is a wide spread post-translational modification known to have far reaching effects on target proteins. Significantly, abnormal peptidase activity is emerging as a major contributor to human disease (Lopez-Otin *et al.* 2008; Lopez-Otin *et al.* 2010).

4.1.2 *Cysteine peptidase mechanism*

Peptidases that cleave within a peptide chain are called endopeptidases, whereas those cleaving at the end of a polypeptide chain are referred to as exopeptidases. A broad requirement for catalytic activity and a key property of all peptidases is their ability to force the formation of a tetrahedral intermediate at a specific site in the substrate peptide chain. This is achieved through specific interaction with the substrate in the highly ordered active site of the enzyme. For successful hydrolysis the substrate must fit in the active site in such a fashion that the scissile bond (amino acid bond cleaved by the peptidase) is positioned in close proximity to the catalytic residues. In cysteine peptidases the catalytic residues are histidine and cysteine but other residues can also participate. The cysteine and histidine work in partnership to cleave the peptide bond; the sulphur atom of the cysteine functions as the nucleophile, capable of attacking the carbonyl carbon of the scissile bond and the histidine is involved in proton shuttling (Stennicke *et al.* 1999).

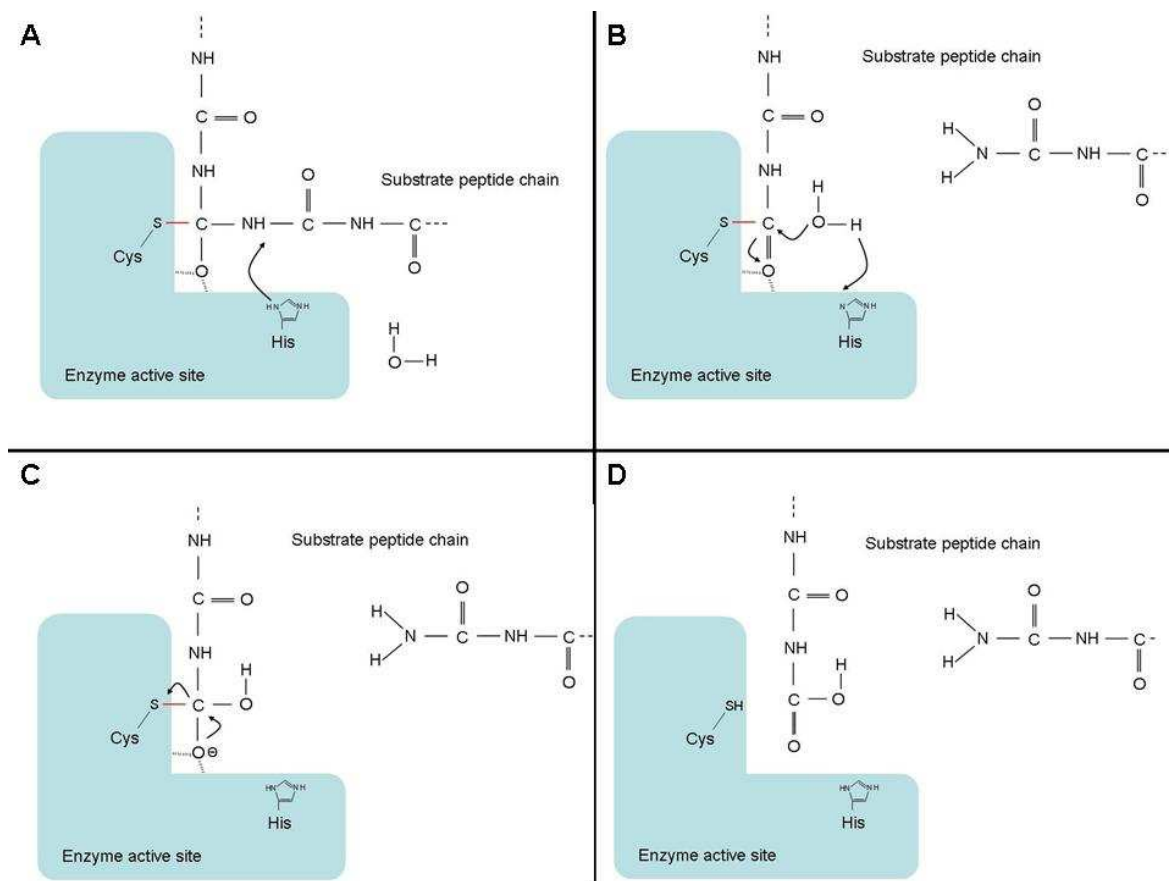


Figure 4-1 Cysteine peptidase catalytic mechanism.

Schematic depicting general mechanism for cysteine peptidase substrate hydrolysis. Enzyme active site depicted in blue, catalytic residues are indicated including nucleophilic sulphur atom of cysteine and imidazole group of histidine. Detailed mechanism outlined in text section 4.1.2.

The basic side chain of the histidine residue (imidazole group) mediates the deprotonation of the thiol belonging to the active site cysteine, promoting nucleophile formation. In some cysteine peptidases (e.g. caspases) nucleophilic attack is facilitated by hydrogen bond donation from the active site cysteine and another residue proximal to the carbonyl oxygen, which serves to polarise the carbon oxygen bond (Fuentes-Prior *et al.* 2004). The electrophilic carbon is attacked by the nucleophilic thiol group of the active site cysteine, creating a tetrahedral intermediate (Figure 4-1A). At this stage the imidazole group of histidine protonates the α amino group of the cleaved peptide chain, ensuring the peptide bond is not reformed (Figure 4-1A/B) (Fuentes-Prior *et al.* 2004). The enzyme-substrate complex is broken by the deprotonated histidine extracting a proton from water, which creates a nucleophile capable of attacking the thioester bond and forming a second tetrahedral intermediate, with a hydroxyl group now attached to the carbonyl carbon (Figure 4-1B/C). The process is ended by rupturing the sulphur-carbon bond, which frees the cleaved

substrate from the enzyme (Figure 4-1D)(Fuentes-Prior *et al.* 2004). In serine peptidases the reactive hydroxyl group of the serine residue functions as the nucleophile.

4.1.3 Peptidase classification

The vast number of identified peptidases and their diverse structures and mechanisms prompted the formation of a central database (called MEROPS), that currently contains sequences for over 140,000 peptidases (Rawlings *et al.* 2010). To facilitate the interpretation and investigation of this data set, the peptidases are ordered according to a classification system which is based on primary and tertiary structural similarities. Peptidases with statistically significant similarities in amino acid sequence are assigned into ‘families’ and structurally homologous families and grouped together in a ‘clan’ (<http://merops.sanger.ac.uk>).

Peptidases are first subdivided by catalytic type. This distinguishes the broad mechanism used for peptide bond hydrolysis, of which the cysteine peptidases represent one of eight classes (aspartic, cysteine, glutamic, metallo, mixed, serine, threonine and unknown). The cysteine peptidases are then further subdivided into 9 clans: CA, CD CE, CF, CH, CL, CM, CN and CO.

Clan CA peptidases are the largest and most thoroughly researched clan of cysteine peptidases. Indeed members of clan CA peptidases represent 84% of the known cysteine peptidases found in parasitic helminths and protozoa, with peptidases from 12 out the 24 families identified (Atkinson *et al.* 2009).

4.1.4 Clan CD

Clan CD peptidases have several characteristics that separate them from the familiar clan CA peptidases. For example they are all endopeptidases and have well defined and strict substrate specificity, directed towards the P1 residue (Mottram *et al.* 2003). Accordingly, E-64, a potent inhibitor of clan CA activity fails to inhibit clan CD peptidases because it lacks a corresponding P1 residue and thus does not bind to the active site (Mottram *et al.* 2003).

4.1.5 Family C14A: Caspases

Since the initial identification of the *ced-3* gene of *Caenorhabditis elegans* as a key requirement for developmental cell death (Yuan *et al.* 1993), vast amounts of work have contributed to the molecular characterisation of a form of programmed cell death (PCD) called apoptosis. At the cellular level apoptosis is characterised by various morphological and biochemical events, including DNA degradation, chromatin condensation, membrane blebbing and cell volume contraction (Danial *et al.* 2004). It has been the focus of intense research because deregulation of apoptosis leads to a variety of human pathologies including cancer, autoimmune diseases and neurodegenerative disorders (Elmore 2007). After the initial discovery in *C. elegans*, it was soon found that apoptosis was conserved in metazoan organisms, where it was regulated by a group of clan CD, family C14A peptidases, called caspases (CED-3-like proteins). Consequently caspases represent an extremely well studied family of enzymes and much is known about their activation and regulation.

The human caspase family is comprised of 15 members (<http://merops.sanger.ac.uk>) which are known to play distinct roles in apoptosis or inflammation (Pop *et al.* 2009). Recent studies however, have extended the boundaries of caspase function, revealing involvement in cell proliferation, differentiation, adhesion and motility (Frisch 2008; Kuranaga *et al.* 2007).

The caspases are not directly associated with non-specific degradation events but instead function in specific signalling pathways. This in part is due to the highly specific nature of caspase proteolysis which is directed to a specific amino acid in the P1 position of the substrate, creating highly defined cleavage events (Fuentes-Prior *et al.* 2004). The name 'caspase' derives from their ability to cleave peptide chains only after an aspartic acid residue (cysteinyl aspartate-specific proteinases). This well defined substrate specificity ensures their proteolytic activities can be exploited to transmit signals through limited cleavage of a variety of molecules.

Caspases play pivotal roles in many cellular processes and to stop uncontrolled activity they are subject to tight regulation. As a principle level of regulation caspases are produced as inactive zymogens, which are comprised of a variable

length prodomain followed by two subunits, a large P20 (~20 kDa) and a small P10 (~10 kDa) (Stennicke *et al.* 1999). Activation of the zymogen occurs either by an intramolecular reaction (autoprocessing) or following proteolytic cleavage performed by upstream peptidases (Pop *et al.* 2009).

Based on their role in the cell death pathway the apoptotic caspases are divided into initiator and effector peptidases. Following cell death signals initiator caspases (caspase-8, -9 and -10) are recruited to specific activation platforms via signalling motifs present in their long N-terminal prodomains; caspase-9 to the apoptosome (Jiang *et al.* 2004) and caspase-8 and -10 to the death-inducing signalling complex (DISC) (Yu *et al.* 2008). The resulting localised increase in caspase concentration facilitates dimerization which induces activation (Boatright *et al.* 2003). Executioner caspases (caspase-3, -6 and -7) have short prodomains and consequently lack protein-protein interaction motifs. However, shortly after synthesis they form inactive homodimers which require proteolytic activation from upstream initiator caspases. Specific cleavage events occurring in the linker regions between the P10 and P20 subunit stimulate the reorganisation of the active site and generate activity (Pop *et al.* 2009).

4.1.6 Family C14B: Metacaspases

In the year 2000 two new caspase-related families were identified in plants, fungi and protozoa (Uren *et al.* 2000). They were identified by Uren *et al.* following iterative database searches using previously identified *Dictyostelium discoideum* and human protein sequences that showed distant yet significant similarities to caspases (Aravind *et al.* 1999). The two families were named paracaspases and metacaspases and separated based on sequence similarity and domain structure. Paracaspases are found in metazoan organisms and slime moulds (*Dictyostelium* species) whereas metacaspases are found in plants, fungi and protozoa (Uren *et al.* 2000). The absence of metacaspases from mammals suggests they could be promising targets for the development of novel therapeutics against protozoa parasites such as *T. brucei*.

The MCAs have been further classified into two categories based on structure and sequence similarity (Uren *et al.* 2000). Type I MCAs have prodomains containing proline rich repeats (plants and fungi) and zinc finger domains (plants

only). The Type II MCAs from plants have no N-terminal prodomain and contain large C-terminal insertions.

The classification of protozoan MCAs is less straight forward. Phylogenetic analysis of select MCAs revealed that the kinetoplastid MCAs clustered together in a separate group, distinct from the fungi and plant type I and type II clusters (Kosec *et al.* 2006). Furthermore the domain architecture of kinetoplast MCAs reveals they do not fully conform to either Type I or Type II classification (Figure 4-2). Several contain extended C-terminal domains rich in proline repeats similar to type II MCAs (*T. brucei* MCA5, *T. cruzi* MAC5, *Leishmania donovani* MC1 and MC2, *Leishmania major* MCA, *Leishmania braziliensis* MCA and *Leishmania infantum* MCA); and *T. brucei* MCA2, MAC3 and MCA5 contain N-terminal proline rich repeats somewhat reminiscent of type I MCAs.

The canonical caspase active site histidine and cysteine catalytic dyad is well conserved, however several MCAs contain substitutions that could effect activity (Figure 4-2) (Mottram *et al.* 2003). For example *Plasmodium* MCA2 and MCA3 and *T. brucei* MCA1 do not contain either a histidine or cysteine in the conserved active site positions, making it unlikely they possess catalytic activity.

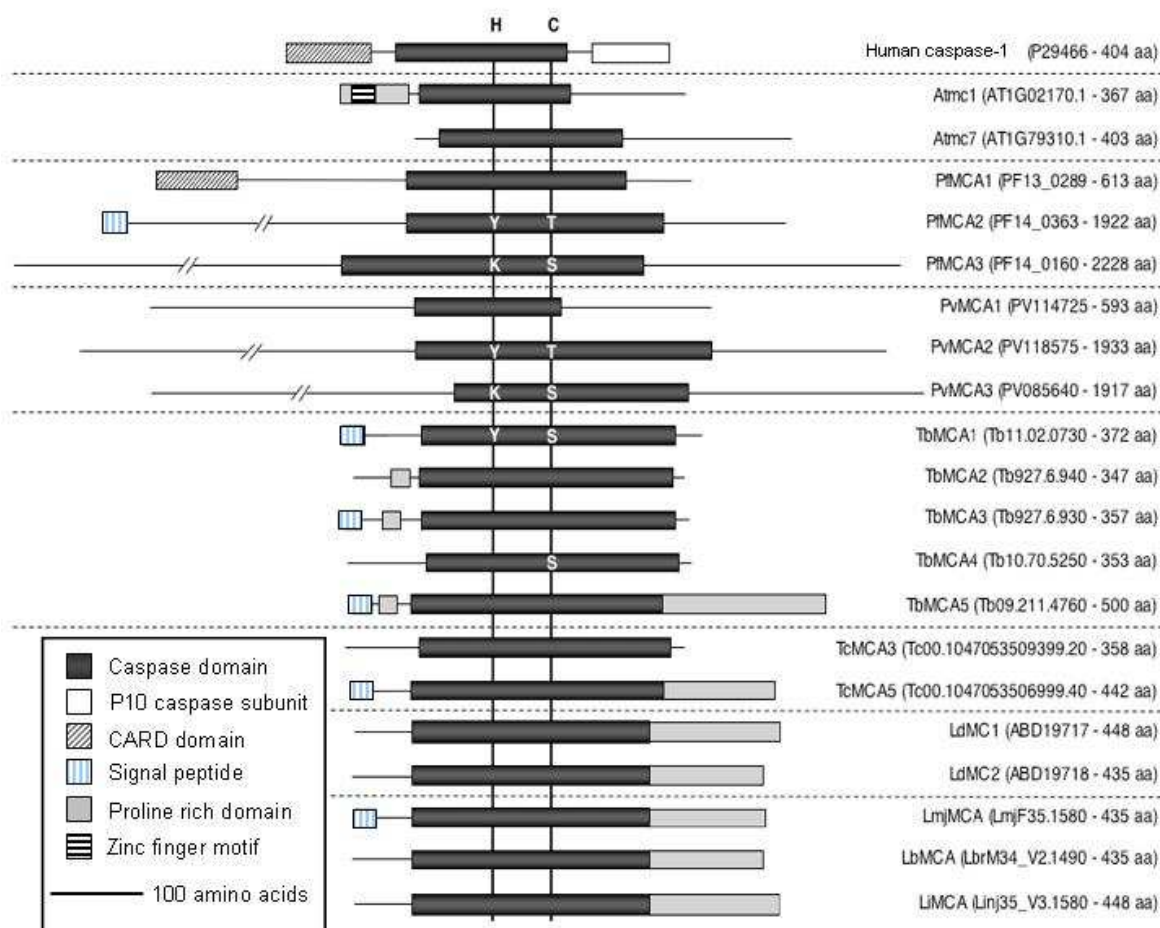


Figure 4-2 Domain structure of metacaspases and caspases.

Adapted from González 2009. Schematic representation of human caspase-1 and MCAs from *Arabidopsis thaliana* (Atmc1 type I, Atmc7 type II), *Plasmodium falciparum*, *P. vivax*, *Trypanosoma brucei*, *T. cruzi*, *Leishmania donovani*, *L. major*, *L. braziliensis* and *L. infantum*. The major domains of each protein are depicted. Where the conserved catalytic dyad differs from the canonical histidine and cysteine, the amino acids are marked in white. Gene identifiers and length of peptide chain displayed in brackets. All proteins are represented as full length zymogens.

4.1.7 Substrate specificity of MCAs

MCAs possess the conserved histidine-cysteine catalytic dyad and the general mechanism of catalysis is likely to be similar to other cysteine peptidases with substrate limitations directed by strict P1 specificity, typical of Clan CD peptidases (Mottram *et al.* 2003). In caspases this selectivity is dictated by conserved residues in the mature enzyme (arginine-179, arginine-341 and glutamine-283, caspase-1 numbering) that form a deep and highly basic S1 pocket. The basic nature of the caspase S1 pocket is perfectly adapted to accommodate the acidic side chain of aspartic acid in the P1 position of substrates (Fuentes-Prior *et al.* 2004). While MCAs contain a caspase-like fold,

alignment with mammalian caspases revealed that glutamine-283 is replaced by an aspartic acid and arginine-341 is replaced by aspartic acid or glutamic acid (Vercammen *et al.* 2007). These highly conserved MCA-specific substitutions are predicted to create an acidic S1 pocket, which is more suited to accepting the basic amino acid side chains of arginine and lysine in the P1 position (Vercammen *et al.* 2007). Indeed experimental evidence from numerous MCAs confirms the arginine/lysine specificity, which reveals a fundamental difference in MCA and caspase activity.

Evidence for MCA arginine and lysine P1 specificity was first demonstrated for the type II *Arabidopsis thaliana* MCAs, Atmc4 and Atmc9 (Vercammen *et al.* 2004). Expression in *E. coli* revealed caspase-like autoprocessing (abolished for active site cysteine mutant) and using N-terminal Edman degradation the Atmc9 processing site was mapped to an arginine residue. Further characterisation of purified recombinant Atmc4 and Atmc9, revealed arginine and lysine dependent activity that was resistant to classical caspase inhibitors and E-64 (Vercammen *et al.* 2004). Similar substrate specificities were also reported for the yeast MCA (Yca1) and two further *A. thaliana* MCAs (Atmc2 type I and Atmc5 type II) following overproduction in *E. coli* and analysis of cell lysate (Watanabe *et al.* 2005).

Analysis of kinetoplastid MCAs further confirmed the Clan CD family C14B peptidase requirement for processing substrates after a basic P1 residue. The *L. major* MCA overexpressed in yeast cells missing Yca1 ($\Delta yca1$) was found to preferentially cleave substrates with arginine in the P1 position (Gonzalez *et al.* 2007). Furthermore detailed biochemical characterisation of purified *T. brucei* recombinant MCA2 revealed it was an active peptidase capable of cleaving after arginine and lysine residues in both short peptides and whole proteins (Moss *et al.* 2007). Interestingly the activity of TbMCA2 was dependent on calcium, which was also found for the plant type II MCAs (Moss *et al.* 2007; Vercammen *et al.* 2004; Watanabe *et al.* 2005).

Shortly after the discovery of the MCAs a report was published detailing the caspase-like processing activity of Yca1 (Madeo *et al.* 2002). Cell lysates from yeast cells overexpressing Yca1, were more active against substrates with aspartic acid in the P1 position (designed for caspases) than control lysates

(Madeo *et al.* 2002). The later studies into MCA specificity, combined with a lack of firm evidence directly showing Yca1 protein specifically produced the caspase-like activity, suggested downstream peptidases could be responsible (Vercammen *et al.* 2007).

4.1.8 Autolytic processing of MCAs

Autolytic processing is a key step in the activation of several caspases (detailed in section 4.1.5). Indeed, the MCAs from yeast and *L. major* undergo autoprocessing in a caspase-typical manner when expressed in yeast (Yca1) (Madeo *et al.* 2002) or heterologously in bacteria (LmjMCA) (Gonzalez *et al.* 2007), producing processing products analogous to the small and large caspase subunits.

In plants only the type II MCAs are known to autoprocess. Recombinant Atmc4 and Atmc9 zymogens autoprocessed producing two major proteins (approximately 25 kDa and 15 kDa) that were proposed to heterodimerize like caspases to form the active peptidase (Vercammen *et al.* 2004). Atmc9 autoprocessing was essential for activity of the recombinant protein (Vercammen *et al.* 2004). Further investigation into AtMCA9 revealed the presence of a second catalytic cysteine residue (position-29, Atmc9 numbering) that is widely conserved in all metacaspases (Belenghi *et al.* 2007). Specific Atmc9 mutants were created in which the canonical active site cysteine-147 (Atmc9^{C147A}) and cysteine-29 (Atmc9^{C29A}) were replaced with alanine. Interestingly mutation of the canonical active site cysteine-147 blocked both autoprocessing and activity. However, Atmc9^{C29A} was able to partially autoprocess, but only displayed 10% of the wild type activity, implicating a key role for cysteine-29 in catalysis (Belenghi *et al.* 2007). To exclude an inhibitory role of an uncleaved N-terminal peptide present in the Atmc9^{C29A} protein, full processing was ensured by adding a minimal amount of Atmc9. Indeed activity of Atmc9^{C29A} increased dramatically when fully processed (as per wild type) an effect not observed in a double cysteine mutant (Belenghi *et al.* 2007).

A proposed explanation for the two Atmc9 catalytic cysteines was developed by analysing a predicted three dimensional structure of Atmc9 modelled on the structure of human procaspase-7. The Atmc9 zymogen model predicted

cysteine-29 would lie in the active site, but too far away from the catalytic histidine, thus inhibiting deprotonation of thiol group from cysteine-29 (Belenghi *et al.* 2007). The processing event (mediated by cysteine-147) would favour a reorganisation and a reduction in the distance between the second cysteine-29 and the histidine, thus allowing two cysteines to participate in catalysis (Belenghi *et al.* 2007).

Interestingly recombinant *T. brucei* MCA2 autoprocesses into three fragments (30 kDa, 6 kDa and 4 kDa) in a calcium dependent manner (Moss *et al.* 2007). Mutation of the TbMCA2 autoprocessing sites generated a recombinant protein resistant to calcium induced autolysis, which still retained full activity towards small peptide substrates (Moss *et al.* 2007). This was somewhat unusual given the autoprocessing dependent activity of caspases and Atmc9. Furthermore no evidence for *in vivo* autoprocessing of TbMCA2 has been detected in BSF *T. brucei* (Helms *et al.* 2006). Although it is possible that autoprocessing only occurs following specific induction conditions such as stress.

4.1.9 Yeast MCAs

Apoptosis, a common form of PCD, is an evolutionary conserved cell suicide mechanism commonly used by metazoan organisms to selectively eliminate dangerous, superfluous or damaged cells. Thus in multicellular organisms the *raison d'être* for apoptosis appears obvious; sacrificing one cell for the overall benefit of the whole organism. However apoptosis in unicellular organisms is a controversial proposition, due to questionable benefits to the individual and concerns over the potential evolutionary advantage provided by cell suicide. To counter this argument it has been proposed that forms of PCD could confer benefits in an altruistic manner to a population rather than individual cells (Buttner *et al.* 2006). Indeed in *Saccharomyces cerevisiae*, cell death accompanied by hallmark characteristics of apoptosis has been detected (Madeo *et al.* 1997) and given the absence of orthologs of classical metazoan apoptotic regulators it was speculated that the single yeast MCA (Yca1) could mediate the apoptotic pathway in yeast (Madeo *et al.* 2002).

Disruption of the *yca1* gene ($\Delta yca1$) increased yeast survival following incubation with two known inducers of apoptosis, hydrogen peroxide (H₂O₂) and acetic acid,

with a concurrent reduction in the physical hallmarks of apoptosis such as DNA fragmentation and chromatin condensation. Additionally $\Delta yca1$ cells were less prone to age related clearance linked to apoptosis (Madeo *et al.* 2002). Furthermore overexpression of Yca1 increased apoptotic markers in cells challenged by H₂O₂ and acetic acid (Madeo *et al.* 2002). Similar studies using $\Delta yca1$ yeast implicated a role for the protein in apoptosis following a variety of stresses including: hyperosmotic stress caused by high concentrations of glucose or sorbitol (Silva *et al.* 2005); viral toxin challenge (Ivanovska *et al.* 2005) and increased mRNA stability caused by disruption to RNA splicing and decapping (Mazzoni *et al.* 2005).

These studies highlight Yca1 involvement in numerous PCD pathways, however non cell death roles for Yca1 have also been described. Detailed characterisation of the DNA content of $\Delta yca1$ and wild type cells revealed no differences during normal growth conditions. However upon growth in fermentative conditions (more representative of natural environment) the $\Delta yca1$ cells exhibited a significant decrease in the proportion of cells in the G1 phase of the cell cycle and a concurrent increase in G2/M phase cells (Lee *et al.* 2008). Additionally Yca1 enzyme activity was shown to be required for correct progression through the cell cycle, with yeast expressing inactive Yca1 showing decreased doubling times and abnormal G1 and S phase progression (Lee *et al.* 2008). Furthermore under fermentative conditions $\Delta yca1$ cells failed to arrest at G2/M checkpoint following addition of nocodazole, a compound known to block the cell cycle. Thus it seems that the accumulation of wild type cells at the G2/M checkpoint depends of Yca1 activity (Lee *et al.* 2008). These studies provide an interesting insight to a multifunctional role for the single yeast MCA.

4.1.10 Plant MCAs

PCD has a well defined and critical role to play in many developmental processes in plants, including embryogenesis, leaf and petal senescence, development of vascular tissues (xlogenesis), sex determination of unisexual plants, seed development and germination (Watanabe *et al.* 2004). Additionally, cell death observed in response to a variety of abiotic stresses, such as heat shock, low temperature, UV irradiation, ozone exposure, as well as pathogen invasion has

also been attributed to apoptosis (Watanabe et al. 2004). Indeed MCA activity has since been directly linked to apoptosis required for embryogenesis in Norway spruce (*Picea abies*) (Bozhkov et al. 2005) and PCD induced by H₂O₂ and ultraviolet (UV) light exposure (He et al. 2008).

A. thaliana contains 9 MCAs (Atmc1-3 type I and Atmc4-9 type II) and given the variation in pH optima and substrate specificity of the Atmcs characterised so far it has been hypothesised that they could play different roles or operate in different cellular compartments (He et al. 2008). Indeed analysis of *Atmc1-9* expression revealed that only the transcript for *Atmc8* is up-regulated in response to oxidative stress (He et al. 2008). Furthermore *Atmc8* could complement PCD phenotypes of $\Delta yca1$ yeast cells and overexpression in *A. thaliana* protoplasts increased apoptosis when stimulated by UV light and H₂O₂ (He et al. 2008). Supporting experimental evidence was provided by knocking out *Atmc8* from *A. thaliana* protoplasts, which resulted in decreased cell death following exposure to UV light and H₂O₂ stress (He et al. 2008). Additionally a tentative link to apoptosis was provided for two different Atmcs (*Atmc2* and *Atmc5*) that were able to successfully complement apoptotic phenotypes of $\Delta yca1$ yeast cells and induce apoptosis in wild type yeast when overexpressed (Watanabe et al. 2005)

Using synthetic caspase substrates, caspase-like activity has been detected in plant tissues undergoing PCD (Bonneau et al. 2008). For example, during *in vitro* *P. abies* embryogenesis cells committed to PCD showed increased activity towards a synthetic caspase substrate (Suarez et al. 2004). Additionally incubation with the corresponding caspase specific inhibitor blocked differentiation and prevented apoptotic cell death events associated with normal embryogenesis. Furthermore a similar phenotype was observed following genetic disruption of the *mcll-Pa* gene. Therefore it was proposed that *mcll-Pa* was the peptidase responsible for the caspase-like activity detected (Suarez et al. 2004). However, recombinant *mcll-Pa* was later shown to have canonical MCA substrate specificity, cleaving only after arginine residues (Bozhkov et al. 2005). Therefore although *mcll-Pa* is not directly responsible for the caspase-like activity accompanying embryogenesis, it seems its proteolytic activity is required for some aspect of the PCD linked to development. In support of this hypothesis immunofluorescent microscopy depicted *mcll-Pa* translocation from

the cytoplasm into the nuclei of cells selected to be eliminated by apoptosis (Bozhkov *et al.* 2005). Furthermore extracellular assays were used to show that mcll-pa enzyme activity caused nuclear envelope disassembly and DNA fragmentation, both classic features of apoptosis (Bozhkov *et al.* 2005).

A significant advance towards understanding MCA function has been provided by the identification of the first known *in vivo* substrate for a MCA (Sundstrom *et al.* 2009). Mcll-Pa was found to cleave the *P. abies* tudor staphylococcal nuclease protein (TSN) at four different sites following either arginine or lysine residues. Expression of inactive mutant mcll-Pa or addition of an inhibitor blocked this cleavage process (Sundstrom *et al.* 2009). PaTSN cleavage was concurrent with PCD events during embryogenesis and following H₂O₂ stress and correlated well with the activity profile of the mcll-Pa in cell lysate. Indeed silencing of mcll-Pa by RNAi reduced both mcll-Pa activity and the cleavage of PaTSN (Sundstrom *et al.* 2009). The cleavage of PaTSN caused an impairment in its ribonuclease activity, a function shown to be essential for both plant viability and reproduction (Sundstrom *et al.* 2009).

These findings were of particular interest as the authors also demonstrated that human caspase-3 was responsible for both *in vitro* and *in vivo* cleavage of human TSN, although occurring after an aspartate residue (Sundstrom *et al.* 2009). Caspase-3 proteolytic control of the intracellular abundance of functional HsTSN was demonstrated using a mutant non-cleavable form of HsTSN. Expression of non-cleavable HsTSN increased cell proliferation and resistance to apoptosis, whereas RNAi depletion of HsTSN directly induced apoptosis (Sundstrom *et al.* 2009). Functional analysis of HsTSN revealed caspase-3 cleavage inhibited ribonuclease activity and reduced its ability to stimulate pre-mRNA splicing. Thus despite the different substrate requirements of mcll-Pa and caspase-3 cleavage (P1 residues must be arginine/lysine or aspartic acid respectively) they appear to inactivate a conserved nuclease that functions in a PCD pathway of human and plants (Sundstrom *et al.* 2009).

4.1.11 Leishmania MCAs

Metacaspases have been detected in a variety of protozoan parasites and most work has so far been restricted to disease causing organisms. In parallel to the

MCAs of other organisms links to PCD have been investigated, however in protozoa they were not always established.

L. major contains one MCA (LmjMCA), which is a syntenic orthologue of TbMCA5 and has a predicted N-terminal signal sequence and a proline, glutamine and tyrosine rich C-terminal extension (Figure 4-2). Expression of LmjMCA was detected in both procyclic promastigote and amastigote stages of the parasite lifecycle (Ambit *et al.* 2007). Expression of LmjMCA in $\Delta yca1$ yeast demonstrated it was able to functionally complement the role of Yca1 in the PCD death pathway (Gonzalez *et al.* 2007). Furthermore the proteolytic activity of LmjMCA was implicated in the yeast PCD response, as expression of catalytically inactive LmjMCA restored H₂O₂ induced cell death rates to the parental $\Delta yca1$ levels (Gonzalez *et al.* 2007). However no functional evidence has been presented to support a role for LmjMCA in *L. major* PCD processes.

In fact the only detailed investigation to date revealed that LmjMCA played an essential role in the progression of the *L. major* cell cycle (Ambit *et al.* 2007). Immunofluorescent analysis of *L. major* promastigote cells using an antibody specific to the TbMCA2 and TbMCA3 active site (generated similar LmjMCA protein recognition to the anti-LmjMCA antibody but with reduced background) revealed an association with different organelles at different stages of the cell cycle (Ambit *et al.* 2007). During interphase LmjMCA appeared as punctate structures dispersed throughout the cytoplasm. However, in cells undergoing mitosis LmjMCA was found to be tightly associated with the nucleus and mitotic spindle. Additionally LmjMCA was also localised to the kinetoplast during division of this organelle. Overexpression of LmjMCA lead to aneuploid cells which grew poorly due to abnormal cell cycle progression (Ambit *et al.* 2007). The LmjMCA locus initially proved refractory to genetic deletion and both alleles could only be removed with simultaneous ectopic expression of LmjMCA at physiological levels; implying an important role for LmjMCA in controlling regulating nuclear and kinetoplast division (Ambit *et al.* 2007). However recently adopting a more sensitive transfection procedure it has been possible to knockout LmjMCA, showing it is not essential for the parasite. The phenotypic characterisation of $\Delta LmjMCA$ parasites is ongoing (E. Castanys-Muñoz personal communication 2010).

Interestingly *L. donovani* contains two highly similar MCA proteins (LdMC1 and LdMC2), which both show considerable sequence homology to LmjMCA and TbMCA5 proteins (Lee *et al.* 2007a). LdMC1 and LdMC2 were detected in procyclic promastigote and amastigote lifecycle stages and immune precipitated protein (combined LdMC1 and LdMC2) was shown to have proteolytic activity (Lee *et al.* 2007a). LdMCs were linked to PCD following the finding that protein precipitated from cells pretreated with H₂O₂ displayed increase in activity (Lee *et al.* 2007a). However the link to PCD based on activity must be treated with caution especially as the proteolytic activity of precipitated LdMC1 did not appear to require the conserved active site histidine and cysteine residues (Lee *et al.* 2007a). Thus whether the activity detected genuinely represented LdMC activity is questionable because proteolysis relying on residues not in the conserved active site seems unlikely.

4.1.12 Trypanosoma cruzi MCAs

In the draft *T. cruzi* genome one group of MCAs homologous to *TbMCA3* and a single MCA homologous to *TbMCA5* were identified. The haploid genome of *T. cruzi* was predicted to contain approximately 16 copies of *TcMCA3*, arranged in two tandem repeat clusters in stark comparison to the single copy of the *TcMCA5* gene (Kosec *et al.* 2006).

TcMCA3 genes were expressed throughout all four of the major developmental life cycle stages (epimastigote, amastigotes, trypomastigotes and metacyclic trypomastigotes). However, *TcMCA5* was only expressed in epimastigotes, a form limited to the insect host stage (Kosec *et al.* 2006). Additionally there was a strong antigenic reaction in response to sera from patients with Chaga's disease to *TcMCA3* but not *TcMCA5* (Kosec *et al.* 2006). Indirect evidence of *TcMCA* involvement in PCD was provided by immunofluorescence analysis of *TcMCA3* cellular localisation following PCD induction using human serum. *TcMCA3* translocated from cytoplasm to the nucleus following serum treatment where it possibly contributed to nuclear degradation (Kosec *et al.* 2006). Furthermore overexpression of *TcMCA5* in epimastigote cells caused increased sensitivity to human serum induced PCD (Kosec *et al.* 2006). Whilst no firm

conclusions can be drawn from these results, they do hint at an involvement of TcMCAs in a PCD process.

4.1.13 Trypanosoma brucei MCAs

Five distinct MCA genes (TbMCA1-TbMCA5) were identified in the *T. brucei* genome (Mottram *et al.* 2003; Szallies *et al.* 2002). Alignments of *T. brucei* MCAs with human caspase-3 identified conservation of the Clan-CD histidine and cysteine catalytic dyad in TbMCA2, TbMCA3 and TbMCA5 (Mottram *et al.* 2003; Szallies *et al.* 2002). However, in TbMCA1 the predicted conserved histidine and cysteine catalytic dyad was replaced with tyrosine and serine respectively. The predicted TbMCA4 active site contains the canonical histidine residue but has a serine in place of the cysteine nucleophile (Figure 4-2 and Figure 4-3). Due to the irregular active site residues it has been speculated that TbMCA1 and TbMCA4 might not be catalytically active enzymes (Mottram *et al.* 2003). This appears most likely for TbMCA1, which is missing both the histidine required for proton shuttling and an active site nucleophile. TbMCA4 however does have the active site histidine and contains a serine residue which is capable of utilising a reactive hydroxyl group as a nucleophile, thus might retain activity and function as mixed type peptidase. Additionally all kinetoplastid MCAs have a second cysteine immediately adjacent to (C-terminal side) the canonical cysteine residue and it has been proposed this residue could function as an alternative catalytic residue (Figure 4-3) (Szallies *et al.* 2002).

Analysis of the *T. brucei* MCA proteins reveals that TbMCA2 and TbMCA3 show 89% sequence identity with divergence at the N-terminus only (Mottram *et al.* 2003). The N-terminal region of TbMCA3 contains a potential transmembrane import domain that is absent of TbMCA2 (Figure 4-2). This could confer different cellular localisation upon these two similar peptidases (Mottram *et al.* 2003). Additionally TbMCA1 and TbMCA5 also have predicted N-terminal signal peptides (Figure 4-2). Interestingly the three MCAs with the conserved catalytic dyad (TbMCA2, TbMCA3 and TbMCA5) have N-terminal proline rich domains and TbMCA5 contains an extended C-terminal proline rich domain that contains repeating sequences of proline, glutamine, alanine and tyrosine (Figure 4-2).

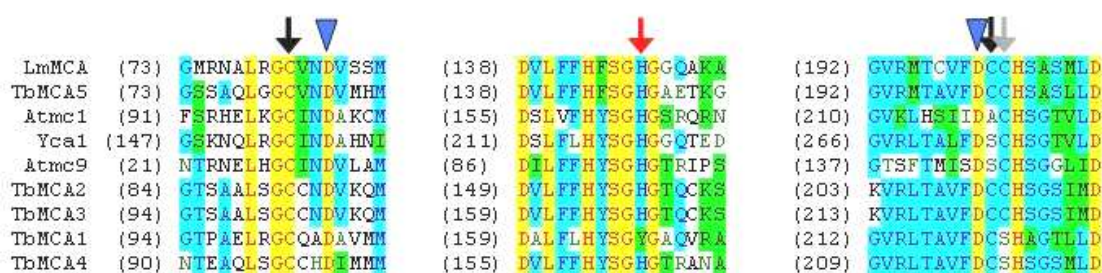


Figure 4-3 Alignments of select domains of metacaspase proteins.

Selected regions of Vector NTI protein sequence alignment of MCA proteins, tritrypDB and accession numbers in brackets: LmMCA (LmjF35.1580), TbMCA5 (Tb09.211.4760), Atmc1 (AAP44514.1), Yca1 (NP_014840.2), Atmc9 (NP_196040.1), TbMCA2 (Tb927.6.940), TbMCA3 (Tb927.6.930), TbMCA1 (Tb11.02.0730) and TbMCA4 (Tb927.10.2440). Sequences aligned using Clustal W algorithm of the Align X program. Identical and conserved amino acids are highlighted yellow and blue respectively. Blocks of similar sequences are highlighted in green and green coloured text indicates weak conservation. Numbers in brackets indicate the position of the first amino acid in the linear polypeptide in the section of each protein analysed. The red and grey arrows indicate the position of the canonical metacaspase active site histidine and cysteine residues, respectively. The back arrows indicate additional cysteine with potential catalytic activity. The blue arrowheads label the aspartic acid residues predicted to comprise the enzyme S1 pocket. Whole alignment shown in (Figure 4-21).

Separate antibodies raised against TbMCA2/TbMCA3 and TbMCA5 revealed a regulated pattern of expression in specific parasite lifecycle stages. TbMCA5 was expressed in both BSF and PCF parasites, whereas TbMCA2 and TbMCA3 proteins were only detected in BSF parasites (Helms *et al.* 2006). A combination of reverse genetic techniques (RNAi and gene knockouts) was used to provide functional insights into the physiological role of these three MCAs. Individual RNAi of TbMCA2/TbMCA3 and TbMCA5 failed to generate detectable phenotypic changes. However, simultaneous triple RNAi demonstrated their collective essentiality to BSF parasites, with multi-nuclei and multi-kinetoplast containing cells rapidly accumulating post induction, indicating a pre-cytokinesis block (Helms *et al.* 2006). Despite this severe phenotype it was possible to generate triple null mutant parasites ($\Delta mca2/3\Delta mca5$) by sequential replacement of both MCA2/3 alleles followed by the MCA5 alleles with drug resistance cassettes. The $\Delta mca2/3\Delta mca5$ parasites exhibited no growth defects *in vitro* in culture or *in vivo* in mice (Helms *et al.* 2006). These data combined suggested that TbMCA2, TbMCA3 and TbMCA5 were essential for BSF parasites but displayed overlapping functions that could be compensated for following gradual elimination (generation of triple knockout lines) (Helms *et al.* 2006).

It was reported that prostaglandin D₂ induced PCD in *T. brucei* that was accompanied by many hallmark features associated with apoptosis (Figarella *et al.* 2005). As prostaglandin D₂ is produced by *T. brucei* it was proposed that this could serve as mechanism to limit parasitemia and prolong infection (Figarella *et al.* 2005). The mediators of this cell death phenotype remain unknown (Figarella *et al.* 2005) and analysis of $\Delta mca2/3\Delta mca5$ parasites revealed they responded as wild type cells following prostaglandin D₂ induced PCD, suggesting they are not the effectors in this cell death pathway (Helms *et al.* 2006).

Immunofluorescence microscopy revealed that TbMCA2, TbMCA3 and TbMCA5 were predominantly associated in the same subcellular compartment located between the nucleus and kinetoplast and significant colocalisation with RAB11 positive endosomes was observed (Helms *et al.* 2006). Interestingly the $\Delta mca2/3\Delta mca5$ showed no defects in the known functions of RAB11 positive endosomes (VSG recycling and degradation of internalised anti-VSG), suggesting an alternative unknown role for MCA containing RAB11 positive endosomes.

Direct evidence of TbMCA2 and TbMCA3 proteolytic activity was provided by detailed characterisation of the recombinant enzymes purified from bacteria, discussed in sections 4.1.7 and 4.1.8 (Moss *et al.* 2007). Having confirmed the essentiality of MCAs to *T. brucei* and developed robust activity assays using recombinant protein the development of specific MCA inhibitors was undertaken. An initial investigation used the substrate specificity of TbMCA2 to inform the design of a range of substrate based inhibitors with arginine or lysine in the P1 position (Berg *et al.* 2010). The most potent inhibitor had IC₅₀ values of 0.6 μ M against recombinant TbMCA2, and 32.9 μ M against cultured *T. brucei* parasites. Encouragingly this inhibitor also showed low cytotoxicity towards human fibroblast cells (Berg *et al.* 2010).

TbMCA1 and TbMCA4 were excluded from initial investigations due to their unusual active site configurations (Helms *et al.* 2006). However an insight into the role of TbMCA4 was provided by the individual heterologous expression of all *T. brucei* MCAs in *S. cerevisiae*. It was demonstrated that only TbMCA4 produced a detectable phenotype when overexpressed in yeast, causing growth inhibition, reduced clonogenicity, loss of respiratory competence and mitochondrial function (Szallies *et al.* 2002).

Interestingly alignments of multiple metacaspases from different species revealed the presence of a well conserved cysteine residue (position-98 TbMCA4 numbering). Furthermore predictive modelling of MCA using the known crystal structures of two clan CD enzymes (gingipain and caspase-1) as templates revealed cysteine-98 was located within the active site (Szallies *et al.* 2002). Heterologous expression of mutant forms of TbMCA4, in which the active site residues (cysteine-98 and -99, histidine-164 and cysteine-218) were replaced with alanines was not detrimental to the yeast cells. Thus it seems that the proteolytic activity of TbMCA4 is required to stimulate mitochondrial dysfunction in yeast (Szallies *et al.* 2002). Any conclusions regarding TbMCA4 function are clearly limited as these experiments involved the expression of non-native protein in yeast. However, the findings do suggest that TbMCA4 has proteolytic activity. The significance of a 'second' MCA active site cysteine (cysteine-98 TbMCA4 numbering) was also investigated in *A. thaliana*, where the equivalent residue in Atmc9 (cysteine-29, Atmc9 numbering) was demonstrated to be required for full proteolytic activity of the recombinant protein, with the Atmc9^{C29A} mutant displaying a 90 % reduction in activity (see section 4.1.8 for details) (Belenghi *et al.* 2007).

4.1.14 What is in a name? Are metacaspases caspases?

The identification of MCAs in plants fungi and protozoa (Uren *et al.* 2000), prompted much speculation and interest that these peptidases could be responsible for initiating and executing apoptosis like their mammalian namesakes the caspases. Indeed several early studies directly connected MCAs to caspase-like activity in yeast and plant cells undergoing apoptosis. However, it subsequently became evident that the strict P1 substrate specificity of MCAs was entirely different to caspases and would prevent caspase-like proteolytic activity. The MCAs only cleave after basic arginine and lysine residues whereas caspases require acidic aspartate residues in the P1 position.

Nevertheless many investigations have revealed a link between MCAs and PCD; with one report even showing mClI-PA and caspase-3 cleave and inactivate an evolutionary conserved component of a human and plant apoptosis pathway (Sundstrom *et al.* 2009). Clearly some evidence exists to show that MCAs and

caspases function in similar cellular pathways which prompted Carmona-Gutierrez *et al.*, to state that MCAs are unequivocally caspases (Carmona-Gutierrez *et al.* 2010).

However, as outlined MCAs do not meet the strict biochemical classification for caspases, so in that sense alone they cannot be classified as caspases (Enoksson *et al.* 2010; Vercammen *et al.* 2007). Furthermore it is now evident that caspases do not only play fundamental roles in apoptosis, but also function in a wide range of other cellular processes including motility, proliferation, adhesion and differentiation (Frisch 2008; Kuranaga *et al.* 2007) . Equally other peptidases are known to play a role cell death processes yet these are not caspases (Enoksson *et al.* 2010). This therefore highlights the dangers and possible pitfalls of classifying peptidases solely by function.

4.2 Project Aims

The five MCAs of *T. brucei* are an interesting family of cysteine peptidases. Significant effort has been put in to investigating their function and activity, however there are clearly many remaining questions to be answered. Discovering the exact physiological function of these peptidases is a priority and will require a thorough knowledge of all members of the *T. brucei* MCA family. Consequently this project aims to characterise *T. brucei* MCA4, by focusing on the following topics:

- 1) MCA4 peptidase activity - does the non-canonical active site serine prohibit peptidase activity?
- 2) MCA4 function - inferred from investigations into expression, localisation, interactions and loss of function phenotypes.

4.3 Results

4.3.1 Metacaspase expression profile.

The expression of MCA2 and MCA3 is tightly regulated with the proteins only detected in BSF and not PCF parasites (Helms *et al.* 2006)(illustrated in Figure 4-4A and Figure 4-4C). Interestingly MCA5 is expressed at approximately the same level in both lifecycle stages (Figure 4-4C) (Helms *et al.* 2006). To see if MCA4 was subject to similar regulation a chicken polyclonal antibody was raised against purified full length MCA4. The purified total IgY extract was able to cleanly detect one protein corresponding to the approximate size of full length MCA4 (38.9 kDa) only in BSF cell lysate, no MCA4 protein was detected in PCF cell lysate (Figure 4-4B). The total IgY extract was highly specific for MCA4 and western blotting of $\Delta mca2/3 \Delta mca5$ cell lysate revealed the presence of the same protein which confirmed the antibody did not cross react with either MCA2, MCA3 and MCA5 proteins. It was also evident that MCA4 expression remained unchanged in the triple null mutant line, confirming it was not upregulated in response to MCA2, MCA3 and MCA5 deletion. For future subsequent procedures the total IgY extract was affinity purified against immobilised recombinant MCA4 (described in Materials and Methods 2.7.2).

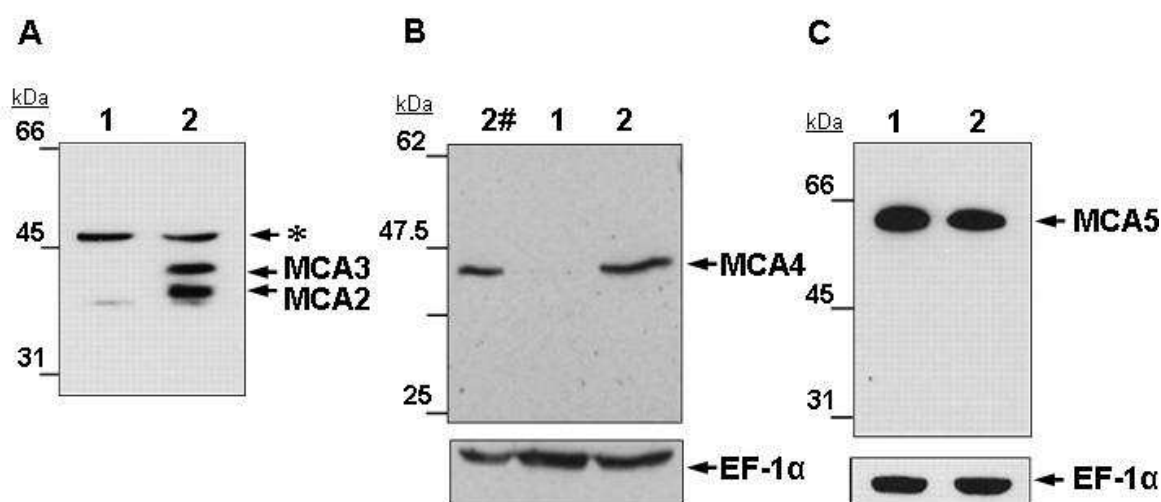


Figure 4-4 Expression profile of MCAs.

Total cell lysates were prepared from *T. brucei* PCF (lane 1) and BSF (lane 2) and BSF $\Delta mca2/3 \Delta mca5$ null mutant (lane 2#) and separated by SDS-PAGE and transferred to Hybond-C membrane before western blotting. A) 5×10^6 cell equivalents probed with rabbit anti-MCA2-MCA3. B) 1×10^6 cell equivalents probed with chicken anti-MCA4. C) 5×10^6 cell equivalents probed with sheep anti-MCA5. MCA2, MCA3, MCA4 and MCA5 proteins are labelled. A cross reacting protein (labelled *) and an antibody specific to EF-1 α demonstrate equal loading. Immunoblots A and C taken from Helms *et al.* 2006.

4.3.2 MCA4 associates with the flagellar membrane

4.3.2.1 Membrane localisation

Having established MCA4 expression was limited to the BSF lifecycle stage the cellular localisation of the protein was investigated. Cellular fractionation techniques can be used to separate cellular compartments and organelles from homogenous cell lysate. For the initial characterisation of MCA4 a simple cellular fractionation strategy was employed to distinguish between soluble, cytoskeletal and membrane associated proteins. Cultured BSF parasites were washed and equally divided into two aliquots and lysed by different methods: a hypotonic lysis buffer combined with sonication and lysis by a buffer containing the non ionic detergent triton X-100. Following centrifugation membrane associated proteins remained restricted to the pellet fraction of hypotonically lysed cells but were solubilised by the detergent. This method also distinguished cytoskeleton associated proteins which showed resistance to the detergent solubilisation and remained in the pellet. Western blotting of the different *T. brucei* lysate fractions revealed that MCA4 was a membrane associated protein, demonstrated by its resistance to hypotonic lysis and sonication but solubility in detergent (Figure 4-5A). To validate the findings and to confirm the quality of the cellular fractionation the different lysis fractions were probed with antibodies specific to β -tubulin and EF-1 α . The double band seen in the MCA4 detergent soluble fraction could represent a non-specific degradation product, phosphorylated and non phosphorylated MCA4 or a proteolytic cleaved form of MCA4 (discussed in sections 4.3.3 and 4.3.4 respectively).

4.3.2.2 MCA4 is palmitoylated

Having established MCA4 was a membrane associated protein we sought to identify the potential mechanism(s) responsible for mediating this interaction. Sequence analysis of MCA4 failed to identify any transmembrane domains, however more detailed bioinformatic screening revealed that the N-terminal region of MCA4 is potentially subject to specific lipid modifications. The covalent attachment of lipid groups to proteins is a common modification

occurring on a wide variety of eukaryotic proteins and is known to regulate many processes including membrane interactions (reviewed in Resh 2006).

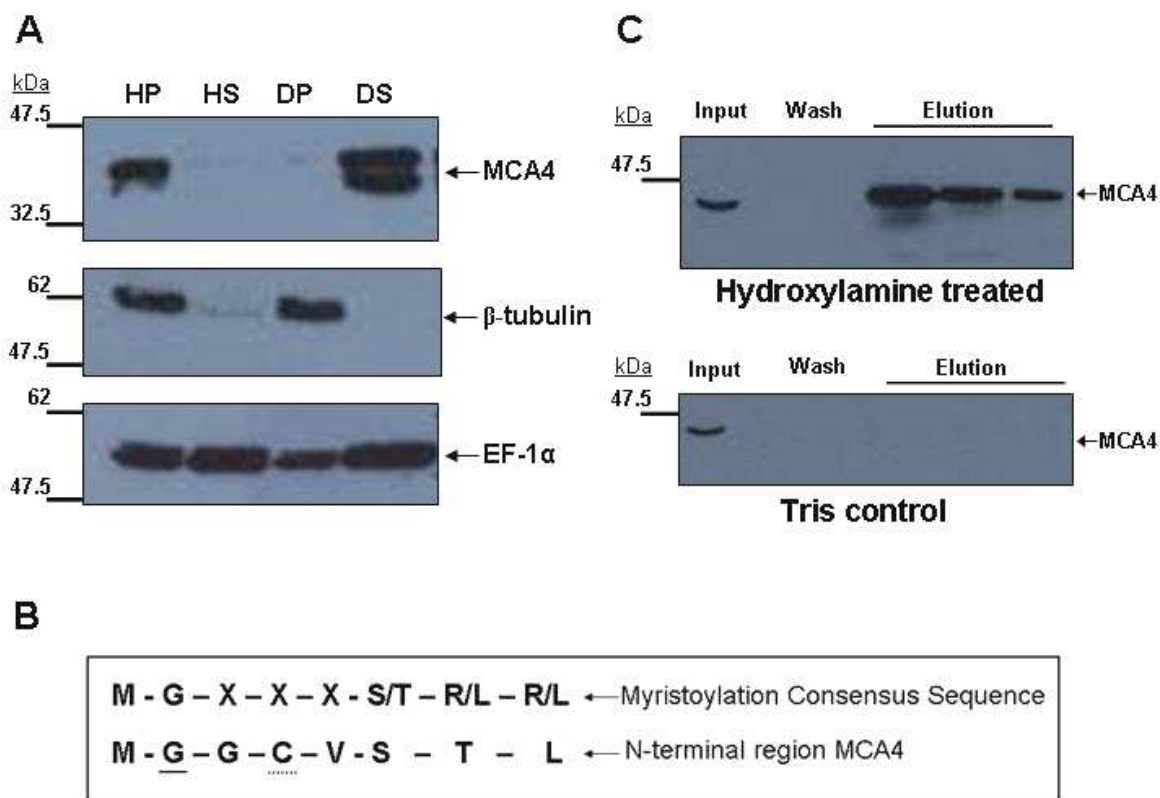


Figure 4-5 MCA4 is a membrane associated protein.

A) Cell fraction of BSF *T. brucei*. 2×10^7 cells lysed in hypotonic buffer followed by sonication before centrifugation and separation into pellet (HP) and soluble (HS) fractions. 2×10^7 cells lysed in buffer containing 1% triton X-100 detergent before centrifugation and separation into pellet (DP) and soluble (DS) fractions. Loaded 1×10^6 cell equivalents per lane and separated by SDS-PAGE before western blotting, with anti-MCA4. The fractionation was validated by probing fractions with antibodies specific to β -tubulin (anti-KMX monoclonal) and EF1 α . B) Substrate consensus sequence recognised by eukaryotic N-myristoyl transferases aligned with N-terminal of MCA4 protein. Predicted acylated residues underlined, N-myristoylation bold line (Mills *et al.* 2007), palmitoylation dashed line (Ren *et al.* 2008). C) Acyl-biotin exchange reaction. Palmitoylated proteins from BSF *T. brucei* were specifically labelled by cleaving palmitate-thioester bonds with hydroxylamine. The free thiol groups created were reacted with biotin-HPDP and purified with streptavidin agarose. Original cell lysate (input), the wash fraction and eluted material from hydroxylamine treated and Tris control samples were immunoblotted with anti-MCA4. MCA4 protein is indicated and is present in both input fractions but is only purified in the presence of hydroxylamine.

The attachment of myristate, a 14-carbon fatty acid (N-myristoylation) is catalysed by the enzyme N-myristoyl transferase (NMT), which recognises the substrate consensus sequence Met-Gly-X-X-X-Ser/Thr, where X represents any amino acid (Resh 1999). Further substantial work on eukaryotic NMTs has identified additional substrate amino acids that influence N-myristoylation and has enabled the development of algorithms that can confidently predict

myristoylated proteins. Comprehensive analysis of *L. major*, *T. brucei* and *T. cruzi* genomes revealed a predicted subset of myristoylated proteins, which included a high confidence prediction for TbMCA4 (Mills *et al.* 2007). Figure 4-5B shows the N-terminus of MCA4 and its comparison with the short NMT N-terminal consensus sequence and highlights the predicted N-myristoylation of glycine-2.

The attachment of hydrophobic myristoyl moieties confers limited affinity for membrane association. However this interaction is often strengthened by a secondary acylation reaction, in which a 16-carbon fatty acid (palmitate) is reversibly attached by a thio-ester linkage to cysteine residues in the protein (S-palmitoylation). This reaction is catalysed by membrane bound palmitoyl acyltransferases (PATs) on proteins already associated with membranes (Greaves *et al.* 2007). The substrate consensus sequence for PATs is not clearly defined which makes predicting palmitoylation sites difficult. However, one on-line algorithm (CSS Palm 2.0, <http://csspalm.biocuckoo.org/>) has been developed based on a data set of published palmitoylation sites in proteins (Ren *et al.* 2008), and was used to predict the potential palmitoylation of MCA4 cysteine-4.

Generally N-myristoylation is a prerequisite for palmitoylation, indeed blocking N-myristoylation of Tb44, a dual acylated *T. brucei* calflagin, inhibited palmitoylation and impeded membrane association (Emmer *et al.* 2009). To experimentally confirm the palmitoylation of MCA4 *in vivo*, an acyl-biotin exchange reaction was performed (Figure 4-5C). The method was recently used to generate the palmitoylproteome of yeast (Roth *et al.* 2006) and has subsequently been adapted for use in *T. brucei* (Emmer *et al.* 2009; Liu *et al.* 2010). The acyl-biotin exchange reaction can be broken down into the following steps. Firstly all the existing free thiols on proteins in the cell lysate were blocked with NEM before the addition of hydroxylamine, which selectively released all palmitoyl moieties. The newly exposed thiols were then labelled with a thiol-reactive biotinylation reagent, which enabled purification using streptavidin agarose. Non specific labelling and interaction with streptavidin were monitored in the control reaction by substituting hydroxylamine with a Tris buffer.

Subsequent western blotting of eluted material from the experimental and control reactions, using anti-MCA4, revealed that MCA4 was purified in a

hydroxylamine dependent manner from BSF *T. brucei* cell lysate (Figure 4-5C). The confirmation of MCA4 palmitoylation combined with the strong bioinformatic prediction for myristoylation suggests that the protein is likely to be dually acylated and is the probable mechanism mediating membrane association.

4.3.2.3 MCA4 localises to the flagellum

Immunofluorescence microscopy had been used to reveal the cellular location of MCA2, MAC3 and MCA5 (Helms *et al.* 2006). These three MCAs showed a high level of colocalisation and predominantly appeared as punctate structures located between the nucleus and kinetoplast. Further analysis revealed significant colocalisation of the MCA labelled structures with RAB11 positive endosomes (Helms *et al.* 2006). To compare and investigate the cellular localisation of MCA4, affinity purified anti-MCA4 was used for immunofluorescence microscopy on BSF *T. brucei*. Mid log cells were fixed in 3% paraformaldehyde and permeabilised with 0.1% triton X-100 before incubation with affinity purified anti-MCA4 (1/400) and anti-chicken Alexa fluor 488 conjugate. Fluorescent microscopy revealed that MCA4 was found to predominantly localise to the flagellum, appearing as a linear array of punctate structures and larger confluent foci along the entire flagellum length (Figure 4-6). The signal detected was confidently attributed to MCA4 specific labelling because no fluorescence was visible following the immuno-staining of $\Delta mca4$ parasites or after secondary antibody only application to wild type cells.

The distinct cellular fractionation and immunofluorescence patterns of MCA4 indicate that it was likely to be associated to the BSF flagellar membrane. To determine whether MCA4 was located on the internal or external surface of the flagellar membrane immunofluorescent analysis was performed in the presence and absence of the detergent triton X-100 (Figure 4-6). Strong flagella staining was only detected in cells treated with triton X-100, suggesting that cell permeabilisation was required to expose the internally facing MCA4 epitopes. Although interestingly the cells analysed without triton X-100, consistently displayed one or two small punctate structures close to the proximal end of the flagellum suggesting a small portion of MCA4 is located on the external surface.

To verify MCA4 localisation BSF 427 *T. brucei* cells were engineered to express MCA4 fused with 6 C-terminal HA tags leaving the N-terminus free for acylation and membrane interaction. The MCA4 ORF was cloned into pGL1728 (designated p2471 in Kelly *et al.*, 2007) and transfected into the BSF 90-13 cell line (Wirtz *et al.* 1999). Clonal populations were isolated and effective tetracycline induction of transgene expression was verified by western blot (data not shown). Immunofluorescent analysis of induced cells using anti-HA, generated flagellar localised fluorescent signals, similar to the anti-MCA4 immunofluorescence (Figure 4-6). The anti-HA recognised a tag fused to the C-terminus of MCA4, because of the presumed importance of N-terminal acylation for flagellar membrane association this suggested full length MCA4 localised to the flagellum. However it does not preclude other forms of the enzyme associating with either the flagellar membrane or different cellular compartments.

To provide further details on the nature of the MCA4 localisation affinity purified anti-MCA4 was used for immunogold transmission electron microscopy studies (Figure 4-7). The analysis provided further evidence supporting the punctate nature of MCA4 along the flagellum. The enhanced immunogold particles clustered at unmarked but distinct foci and consistently appeared to be on the internal surface of the flagellum. The MCA4 signal was clean and very low background staining was observed.

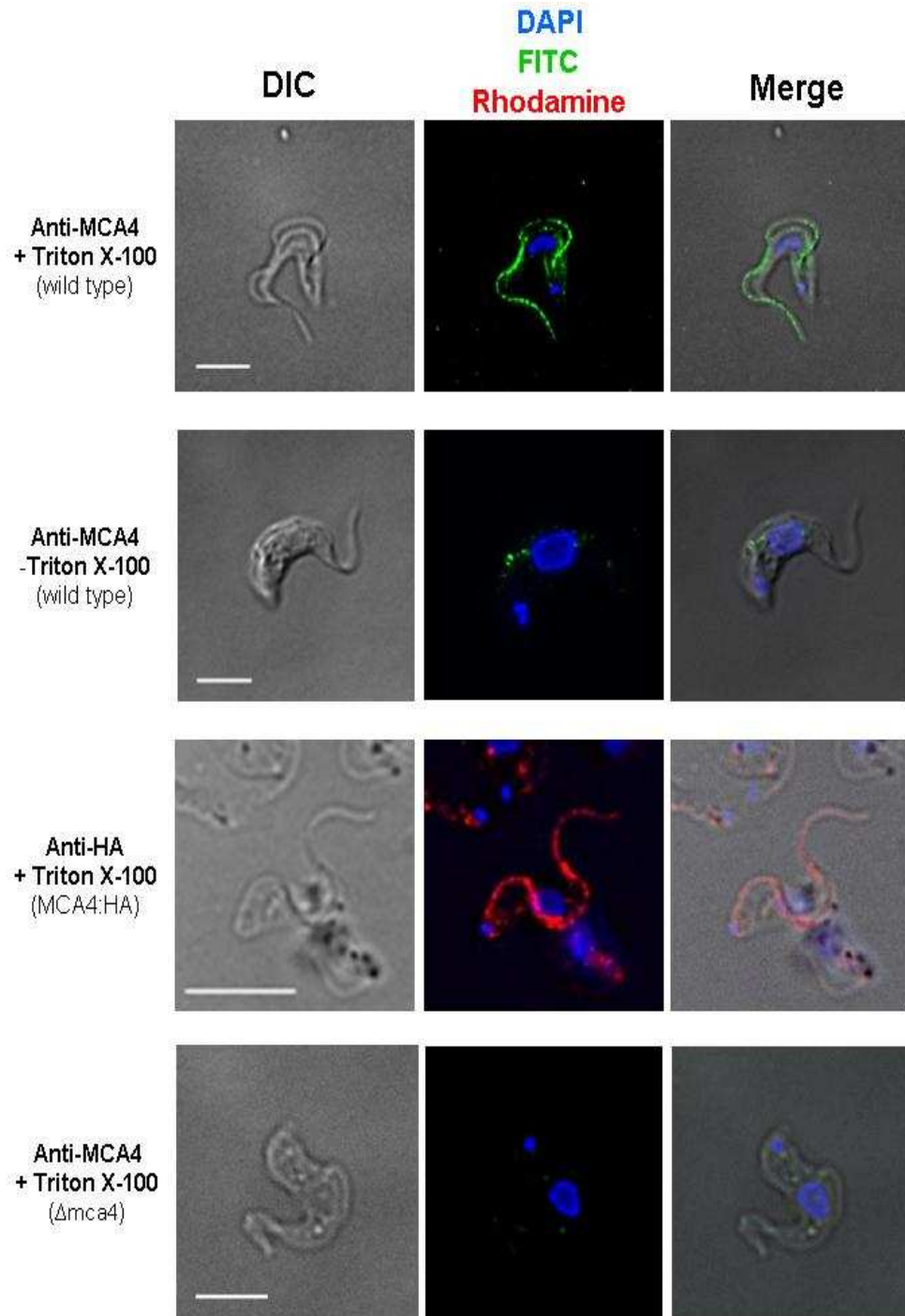


Figure 4-6 Immunofluorescence analysis of MCA4 in BSF *T. brucei*.

Cultured BSF *T. brucei* were washed before 10 minutes fixation in 3% paraformaldehyde and subsequent adherence to poly-L-lysine treated microscope slides. Cells were permeabilized (+ Triton X-100) or left intact (- Triton X-100) and blocked by incubation with 20% foetal calf serum (FCS) in PBS. Wild type BSF and $\Delta mca4$ cells were incubated with affinity purified anti-MCA4 followed by anti-chicken Alexa Fluor 488 conjugate, visualised using FITC filter set (green). BSF cells expressing C-terminally tagged MCA4 (MCA4:HA) were incubated with monoclonal anti-HA followed by anti-mouse Alexa Fluor 594 conjugate, visualised using Rhodamine filter set (red). DNA was stained by DAPI (blue) and reference images were taken by differential interference contrast (DIC) filter settings. Analysis performed on Applied Precision DeltaVision microscope with fluorescent images displayed as deconvolved projection of 20 individual Z-stacks. Scale bar 5 μm .

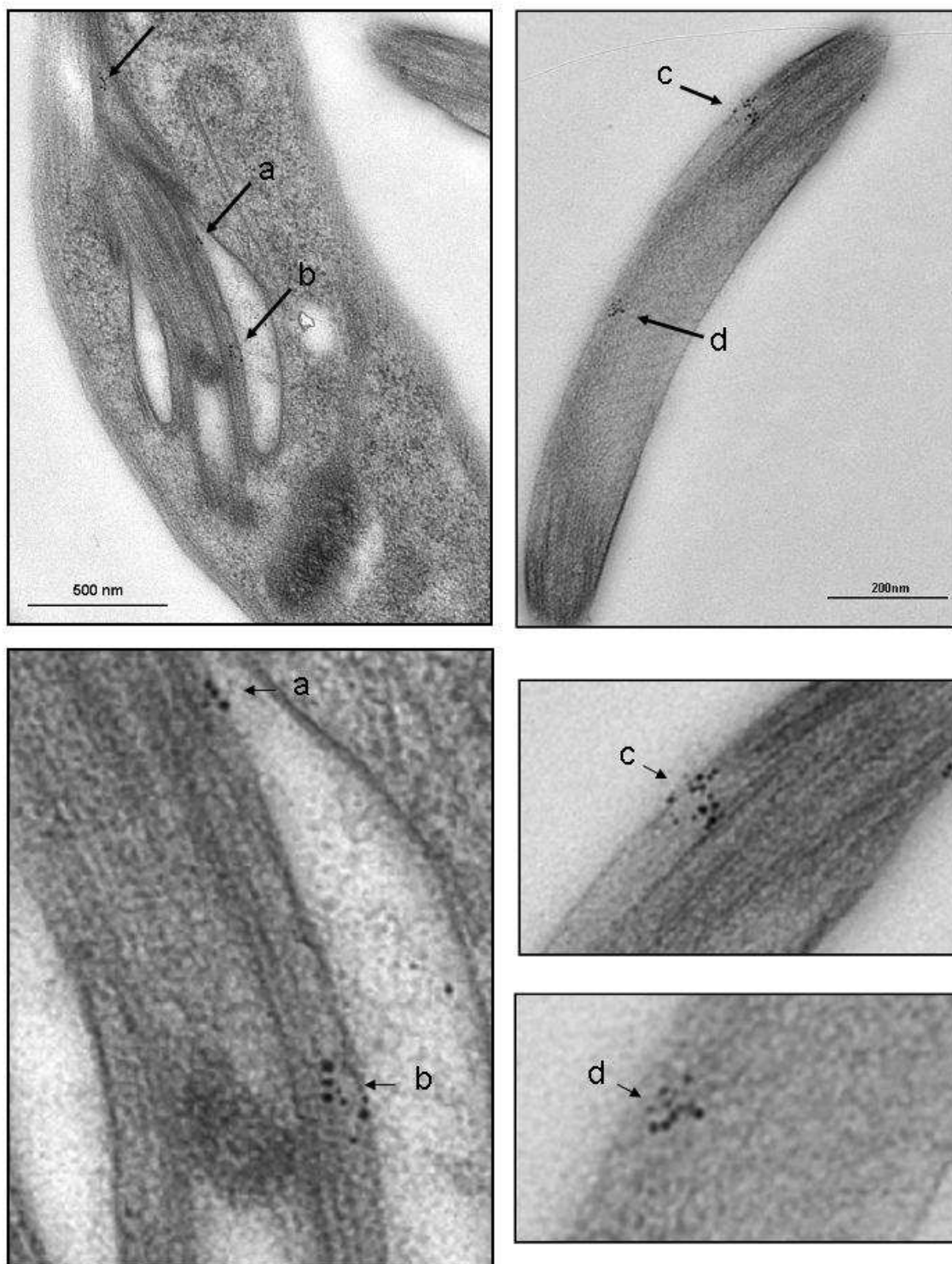


Figure 4-7 MCA4 immunogold transmission electron microscopy.

Fixed wild type BSF *T. brucei* were cryosectioned and labelled with affinity purified anti-MCA4 and 1.4 nm gold (rabbit anti-chicken). Immuno-labelling was enhanced by R-gent (Aurion) and visualised with a LEO 912 transmission electron microscope. Black arrows show enhanced immunogold particles clustering along length of BSF flagellum. The bottom images represent digitally magnified sections of the corresponding images above.

4.3.3 MCA4 interactions

Co-immunoprecipitation is a useful technique for the analysis of protein-protein interactions and can provide vital functional information. To investigate potential interacting partners and substrates of MCA4, affinity purified anti-MCA4 was covalently linked to CarboLink resin (Pierce) and used to directly pull down MCA4 and any interacting proteins from BSF parasite lysate (Figure 4-8). Carbolink was preferred over traditional two step co-immunoprecipitation approaches, which rely on precipitating antibody antigen complexes with protein A or G, because anti-MCA4 was raised in chickens and IgY immunoglobulins have significantly different properties to mammalian IgGs; crucially they do not bind protein A or G (Dias da Silva *et al.* 2010).

Approximately 2.25×10^9 BSF cells were purified from rat blood and lysed in a buffer containing 0.2% NP40 and 0.5% CHAPS. A mild lysis buffer was used to solubilise MCA4 and release it from the plasma membrane, while simultaneously attempting to maintain any protein interactions. Proteins were precipitated from the soluble fraction and separated by 12% SDS-PAGE and analysed by western blotting, silver staining and SYPRO staining. Western blotting confirmed that MCA4 was successfully precipitated and the specificity was validated by a parallel experiment using pre-immune IgY, which failed to precipitate MCA4 (Figure 4-8A). Silver staining of the eluted material revealed the presence of multiple proteins (lanes 7 and 8 Figure 4-8B) which were excised and analysed by liquid chromatography tandem mass spectroscopy (LC-MS/MS). Only band 2 generated a significant protein hit, for which seven peptides were mapped to MCA4. The limited identification rates were possibly caused by formaldehyde and/or silver ions present in the stain and destain solutions, which are known to interfere with the LC-MS/MS (Richert *et al.* 2004). Interestingly for the one protein identified evidence was found indicating the phosphorylation of serine 341, which corroborated the same finding in the phosphoproteome analysis of BSF *T. brucei* (Nett *et al.* 2009).

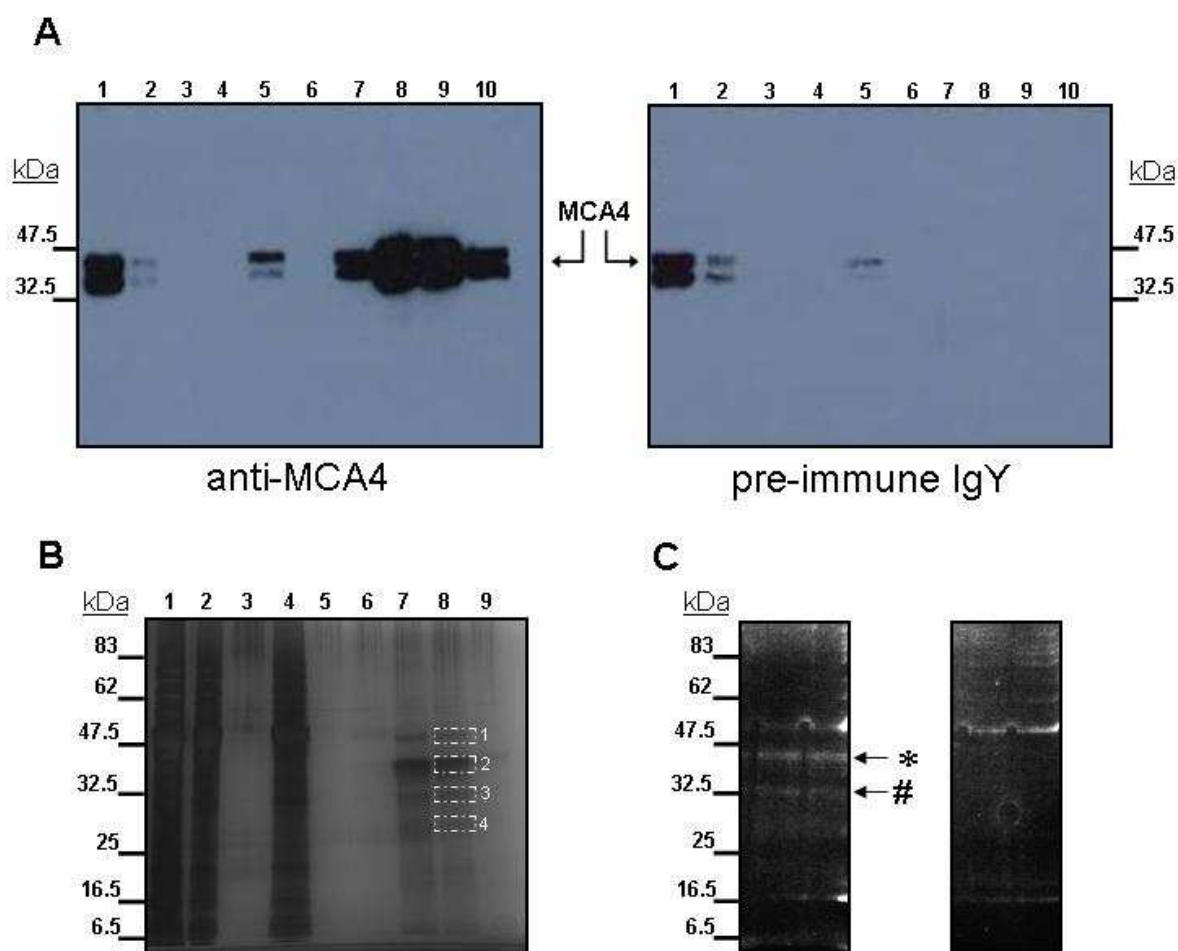


Figure 4-8 Immunoprecipitation of MCA4 from BSF *T. brucei*.

Wild type BSF *T. brucei* 427 were purified from rat blood using DE52 anion exchange. Approximately 4.5×10^9 cells were lysed in buffer containing 0.2% NP40 and 0.5% CHAPS and centrifuged at 100,000 x g for 45 minutes. The soluble fraction was pre-cleared with pre-immune IgY coupled Carbolink resin and divided into two. To one aliquot affinity purified anti-MCA4 Carbolink resin was added and to the other pre-immune IgY Carbolink. Both samples were incubated over night at 4°C. The resin was washed 5 times and bound material eluted using a low pH buffer. A) The efficiency of the precipitation (anti-MCA4) and non-specific binding (pre-immune IgY) was analysed by western blot using affinity purified anti-MCA4. Lane 1, total cell lysate; Lane 2, unbound flow through material; Lane 3, first pre-clear; Lane 4 second pre-clear; Lane 5, first wash; Lane 6, last wash; Lane 7, elution 1; Lane 8 elution 2; Lane 9 elution 3; Lane 10 elution 4. B) Anti-MCA4 precipitation was separated by SDS-PAGE and silver stained. Lane 1, total cell lysate; Lane 2, unbound flow through material; Lane 3, first pre-clear; Lane 4 first wash; Lane 5, last wash; Lane 6, elution 1; Lane 7 elution 2; Lane 8 elution 3; Lane 9 elution 4. The bands indicated were excised and analysed by LC-MS/MS. Band 2 was positively identified as MCA4. C) The elutions for experimental and control precipitations were pooled and separated by SDS-PAGE then stained with colloidal blue. The bands indicated were excised and analysed by LC-MS/MS. Band labelled * was identified as MCA4. Band # generated two protein hits, MCA4 and glycerol-3-phosphate dehydrogenase (Tb927.8.3530).

To improve the sensitivity of the LC-MS/MS the remaining precipitated material was separated and stained with colloidal blue protein stain. This stain was less sensitive and only two predominant bands were visible, both of which generated significant hits for MCA4 following LC-MS/MS analysis. However, interestingly

the lower molecular weight band (Figure 4-8C marked with #) also produced an additional significant hit, with 6 peptides mapped to glycerol-3-phosphate dehydrogenase (Tb927.8.3530). The predicted size of glycerol-3-phosphate is ~37.81 kDa which corresponds to the approximate size of the protein stained by colloidal blue. To determine if this was a genuine interaction will require repeat co-immunoprecipitation experiments and potential verification by yeast two hybrid interaction analysis.

The western blot analysis of immunoprecipitated MCA4 detected two different size proteins corresponding to ~40 and ~35 kDa. It appears unlikely that the two MCA4 bands occurred through nonspecific degradation because not only were they present in the experimental input fraction but high concentrations of protease inhibitors were also used throughout. It is possible that the two proteins represent two cellular states of MCA4; either full length zymogen and proteolytic processed forms or phosphorylated and non-phosphorylated MCA4.

4.3.4 MCA4 activity

4.3.4.1 Processed MCA4 is an active peptidase

Detailed biochemical characterisation of recombinant MCA2 revealed it was an active peptidase with strict specificity for the basic residues of arginine and lysine at the P1 position (Moss *et al.* 2007). To investigate MCA4 peptidase activity it was cloned into an N-terminal HIS tagging protein expression vector and expressed in *E. coli*. The recombinant protein was purified by immobilised metal ion affinity chromatography using a nickel agarose column, yielding approximately 1.4 mg of protein per 100ml of bacterial culture. MCA4 purity was assessed by coomassie stained SDS-PAGE and when necessary further purified by ion exchange chromatography. To facilitate further characterisation of MCA4 the active site serine (position 219) was mutated to a cysteine residue (MCA4^{S219C}) producing an enzyme with the canonical metacaspase conserved histidine-cysteine active site. Purification of MCA4^{S219C} was performed as before but produced reduced yields, typically 250 µg per 100 ml culture. Where indicated MCA2 was produced as previously described (Moss *et al.* 2007).

Recombinant MCA2 was found to undergo autolytic processing in the presence of calcium (Moss *et al.* 2007). To investigate MCA4 autoprocessing purified MCA4 and MCA4^{S219C} were incubated in a reaction buffer supplemented with 10 mM calcium chloride and 5 mM DTT at 37°C and analysed by SDS-PAGE. As displayed in (Figure 4-9A), MCA4 did not undergo autoprocessing in the presence of calcium, however MCA4^{S219C} was capable of autoprocessing, producing three lower molecular weight products in a time dependent manner (Figure 4-9B).

The ability to autoprocess suggested that MCA4^{S219C} was a constitutively active peptidase. Insights into the substrate specificity of this enzyme were revealed using N-terminal Edman degradation to sequence the lowest molecular weight proteolytic processing product (marked with an asterisk in Figure 4-9B). Six amino acids (GFQPWK) were identified, which showed that MCA4^{S219C} cleaved itself after a lysine-64. This finding was consistent with MCA2 specificity, where cleavage occurred only after basic residues (Moss *et al.* 2007).

Peptidase activity was further investigated by monitoring the ability of MCA4 and MCA4^{S219C} to cleave synthetic fluorogenic peptide substrates. The peptides contained the fluorophore 7-amino-4-methylcoumarin (AMC) which fluoresced upon cleavage and subsequent release from the peptide and protecting group, benzyloxycarbonyl (Z). Accordingly enzyme activity was determined by monitoring the fluorescence produced from any given reaction. Unless otherwise stated all activity assays were run in triplicate and included the following components: purified recombinant enzyme, 10 µM Z-RR-AMC substrate and reaction buffer containing 10mM calcium chloride and 5 mM DTT.

Fluorogenic activity assays revealed that full length MCA4 was inactive, whereas MCA4^{S219C} was an active peptidase able to cleave after arginine residues (Figure 4-9C).

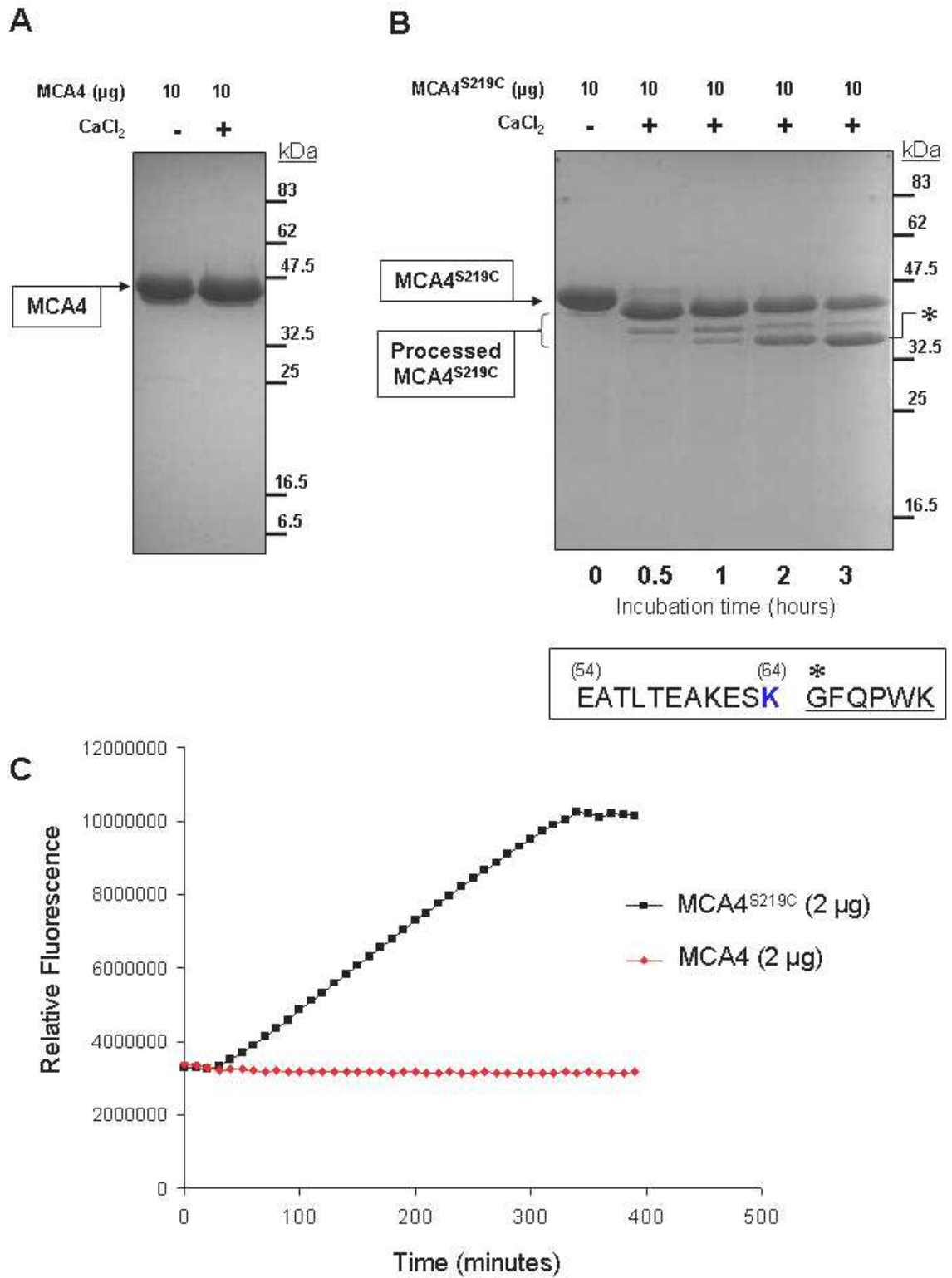


Figure 4-9 Calcium chloride induces cleavage and activation of MCA4^{S219C} but not MCA4.

A) Calcium dependent MCA4 autolysis was analysed by SDS-PAGE. 10 μg MCA4 was incubated with and without 10 mM calcium chloride for 1 hour. Full length MCA4 is indicated. B) MCA4^{S219C} was incubated with 10mM calcium chloride and a Tris buffer (-CaCl₂). 10 μg aliquots were removed at time indicated and autolysis was analysed by SDS-PAGE. Full length protein and products of autolytic processing are indicated. The N-terminal of the major processed product (marked with asterisk) was sequenced by Edman degradation and six amino acids were identified (underlined) which revealed cleavage after lysine-64, highlighted in blue, MCA4 amino acid numbering in brackets. C) Cleavage of Z-RR-AMC by 2 μg MCA4^{S219C} and 2 μg MCA4 was measured in a buffer containing 10 mM calcium chloride. Enzyme activity displayed is representative of three replicate experiments.

This finding suggested that MCA4^{S219C} had similar substrate preferences to MCA2. To confirm this, MCA4^{S219C} activity was screened against a library of 19 fluorogenic substrates comprised of a mixture of 7-residue peptide chains, where one amino acid was fixed and the remaining positions were occupied randomly by any of the 19 amino acids (cysteine omitted to exclude dimerization). The maintenance of one specific amino acid ensures this type is over-represented in each of the 19 sub-libraries and fluorescence generated represents cleavage after this residue. Indeed MCA4^{S219C} was most active against peptides containing arginine and lysine in the fixed position further supporting a preference for basic amino acids in the P1 position (Figure 4-10). However low overall enzyme activity meant the separation from background fluorescence was limited. Additionally MCA4 was screened against the whole peptide library and no proteolytic activity was detected, which further supported the finding that full length MCA4 was inactive.

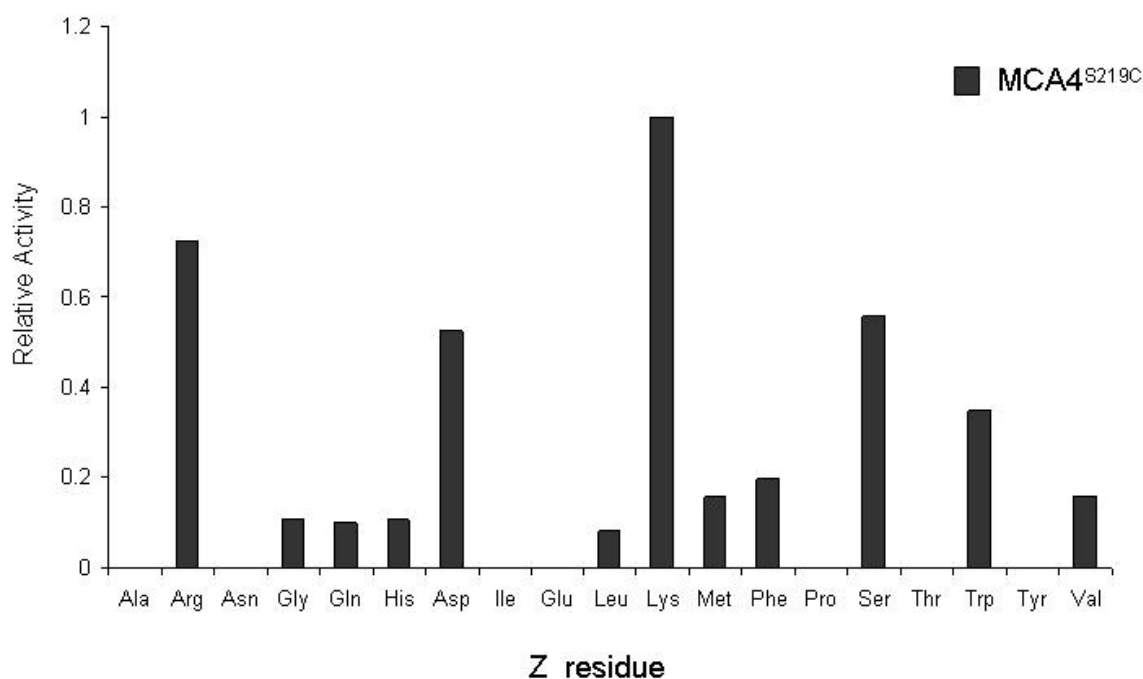


Figure 4-10 MCA4^{S219C} activity against fixed position peptide library.

Purified MCA4^{S219C} (10 µg) was incubated with 10 mM calcium chloride and 10 µM Abz-XXZXXQ-EDDnp substrate, where Abz stands for o-aminobenzoic and EDDnp for ethylenediamine 2,4-dinitrophenyl. X represents any amino acid and Z indicates fixed amino acid (excluding cysteine). Enzyme activity expressed as a relative value and given as means of two replicates.

Many peptidases require proteolytic processing to activate the enzyme, accordingly this was investigated for MCA4. Limited proteolysis reactions

containing 10 µg MCA4 and low ng quantities of MCA2 were incubated with calcium chloride at 37°C. Analysis by SDS-PAGE revealed that MCA2 reproducibly processed MCA4 generating processing products similar to the MCA4^{S219C} autoprocessing pattern (Figure 4-11A). Sequencing of the prominent processing product by N-terminal Edman degradation revealed the same six amino acid sequence (GFQPWK) as previously identified for MCA4^{S219C}. MCA2 cleavage of MCA4 lysine-64, further supports the overlap of substrate specificity for MCA2 and MCA4^{S219C}.

Full length MCA4 showed no activity against a Z-RR-AMC substrate (Figure 4-9A), however MCA4 processed by MCA2 was active (Figure 4-11B). Controls were established to distinguish MCA4 activity from residual MCA2 activity, which was also capable of cleaving Z-RR-AMC (Moss *et al.* 2007). Accordingly the activity of processed MCA4 was found to be higher than control assays containing the equivalent amount of MCA2 used for the limited proteolysis reactions (Figure 4-11A and Figure 4-12A). Furthermore, potential stabilising or enhancing effects of an additional protein in the reaction were shown to be negligible by substituting MCA4 with BSA, with no effect on MCA2 activity (Figure 4-12A).

Additional evidence linking processed MCA4 to the detected activity was provided by altering the progression of the processing reaction. Extension of the limited proteolysis reaction time reduced the abundance of full length MCA4 and created more processing products (Figure 4-12B). Proteolytic activity of these samples was found to be relative to the amount of processed MCA4 present; more processed MCA4 corresponded to an increased cleavage rate of Z-RR-AMC. However, increasing the reaction time did not alter the activity of MCA2, suggesting the change in activity is dependent on MCA4.

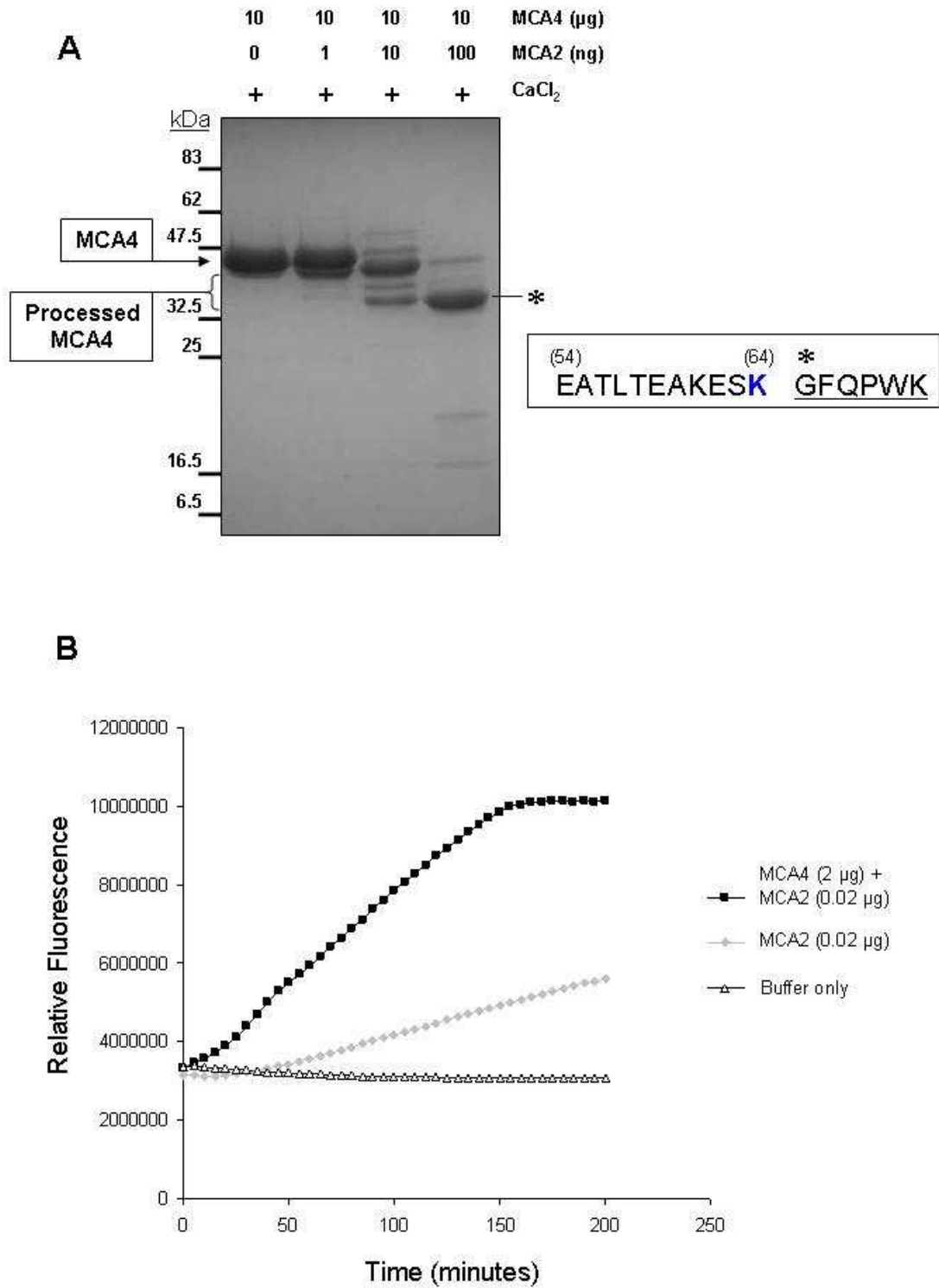


Figure 4-11 Processed MCA4 is an active peptidase.

A) MCA4 processing by MCA2 was analysed by SDS-PAGE. 10 μg MCA4 was incubated with 10 mM calcium chloride and MCA2 as indicated. Full length and processed forms of MCA4 are labelled. The N-terminal of the major processed product (marked with asterisk) was sequenced by Edman degradation and six amino acids were identified (underlined) which revealed cleavage after lysine-64, highlighted in blue, MCA4 amino acid numbering in brackets. B) Cleavage of Z-RR-AMC by: 2 μg MCA4 processed by 0.02 μg MCA2; 0.02 μg MCA2; and buffer only control was measured in a buffer containing 10 mM calcium chloride. Enzyme activity displayed is representative of three replicate experiments.

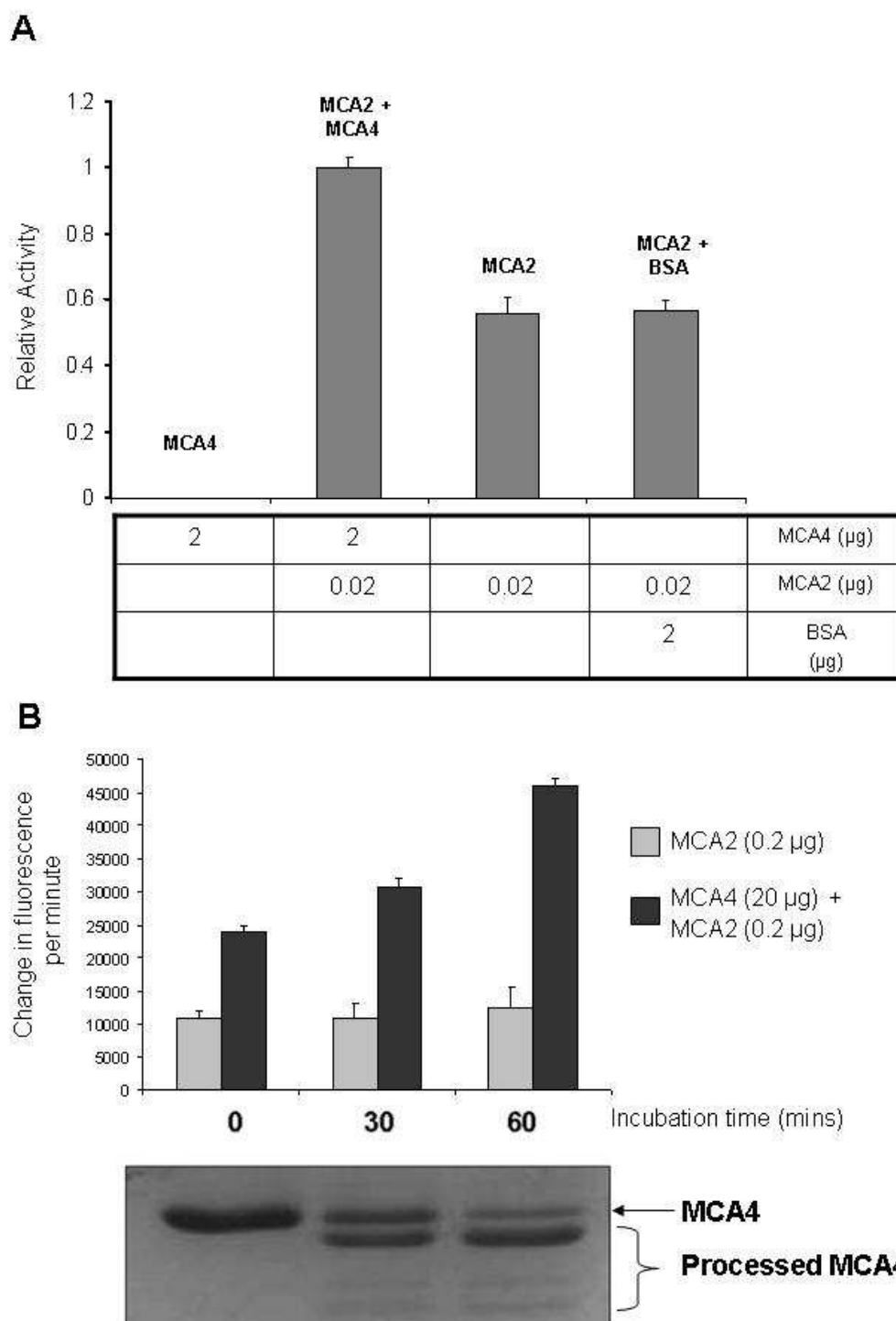


Figure 4-12 Distinguishing processed MCA4 activity from residual MCA2 activity.

A) Cleavage of Z-RR-AMC by MCA4, processed MCA4, and MCA2 controls was measured in buffer containing 10 mM calcium chloride. Recombinant enzymes present in each assay are indicated in the table. Enzyme activity is expressed as a relative value and given as means of three replicates, error bars show standard deviation. B) Processing reactions containing MCA4 and MCA2 (ratio 100:1) were incubated at 37°C for 0, 30 and 60 minutes in buffer containing 10 mM calcium chloride. Aliquots containing 20 μg MCA4 and 0.2 μg MCA2 were removed and assayed for activity (Z-RR-AMC cleavage). Enzyme activity mean of three replicates and error bars show standard deviation. Aliquots containing 5 μg MCA4 and 0.5 μg MCA2 were analysed for processing by SDS-PAGE.

Concerted efforts were made to purify an inactive MCA4 mutant to provide unequivocal verification that the activity detected stems from MCA4. Site directed mutagenesis was used to mutate potential catalytic residues: histidine-164 to alanine, cysteine-218 to glycine, serine-219 to glycine and a double mutant simultaneously changing cysteine-218 and serine-219 to glycines. To obtain soluble protein, expression was attempted at a range of temperatures (15°C, 25°C and 37°C) induced with different IPTG concentrations (0.01 mM and 0.1 mM) and using autoinduction media incubated at two temperatures (25°C and 37°C). However only MCA4^{S219G} could be purified, mutation of histidine-164 or cysteine-218 consistently resulted in insoluble protein (under all conditions tested), which was refractory to standard purification attempts.

Preliminary experiments showed that MCA4^{S219G} was active when processed by MCA2 (Figure 4-13A). Although more thorough analysis is required (specifically SDS-PAGE analysis), the data generated so far suggest cysteine-218 is catalytically active in MCA4. Interestingly the cysteine is conserved in all kinetoplast MCAs and mutation of the equivalent cysteine residue to glycine in MCA2^{C212G} decreased enzyme activity by approximately 70% (Moss *et al.* 2007).

MCA4 activity was further investigated by adding specific peptidase inhibitors to the activity assay (Figure 4-13B). Supplementing processed MCA4 with the broad profile cysteine and serine peptidase inhibitors leupeptin (100 µM) and antipain (100 µM) completely abolished activity. Addition of E64, a specific inhibitor of clan CA cysteine peptidases had limited effect on activity at 10 µM, inhibiting activity by 5%. These results were consistent with the inhibition profile of MCA2, however given the presence of a serine residue in the proposed MCA4 active site (position 219) the effects of specific serine peptidase inhibitors were investigated. PMSF did not inhibit activity at 0.5 mM and Pefabloc only reduced activity by 20% at 2.5 mM. The absence of inhibition of on processed MCA4 activity by two serine peptidase inhibitors does not specifically rule out a catalytic serine residue. It is possible that structural features specific to clan CD cysteine peptidases could restrict the access of these two serine peptidase inhibitors to the MCA4 active site and thus prevent inhibition.

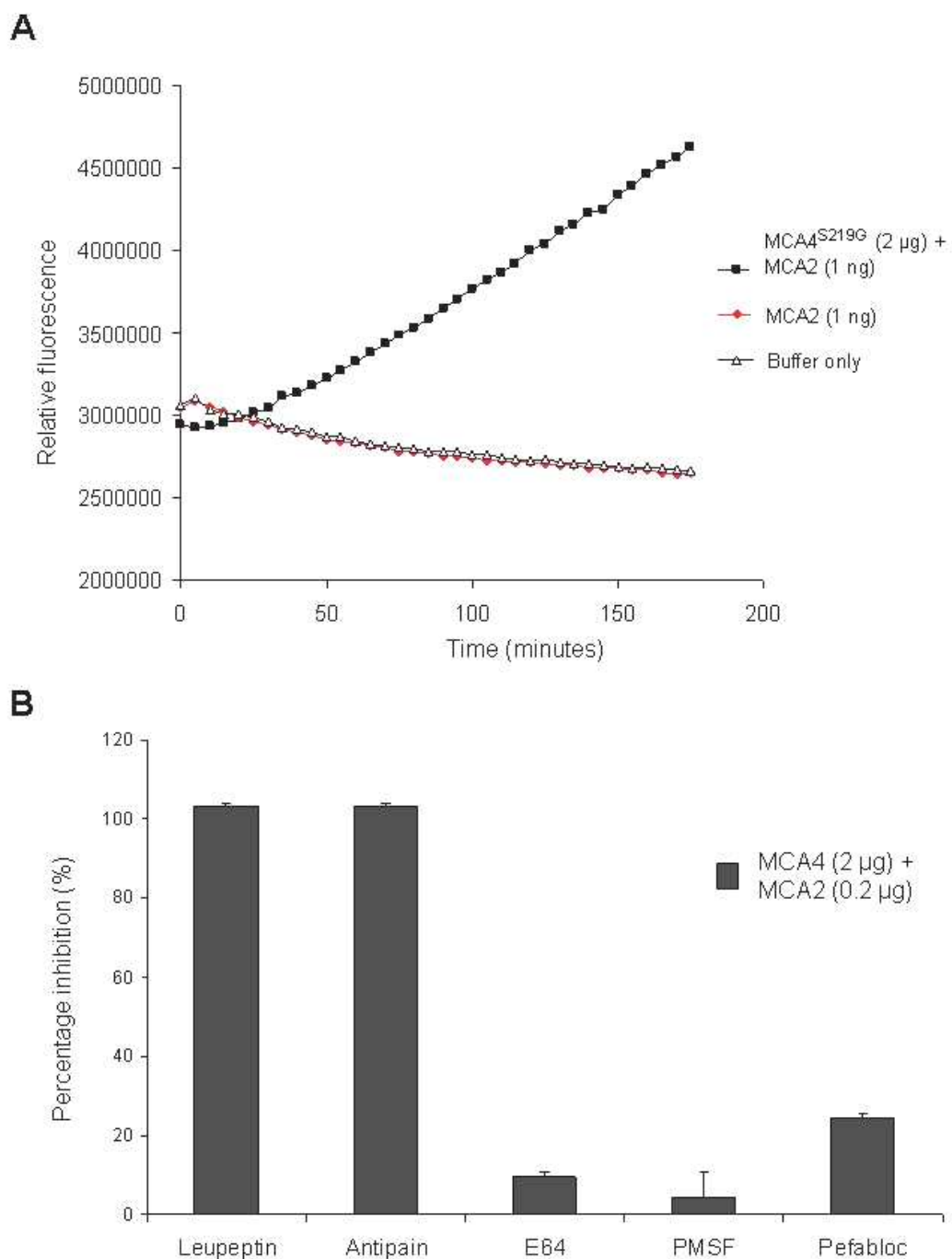


Figure 4-13 Investigating MCA4 active site using mutagenesis and peptidase inhibitors.

A) Cleavage of Z-RR-AMC by 2 µg MCA4^{S219G} processed by 1 ng MCA2 and MCA2 control (1ng), was measured in buffer containing 10 mM calcium chloride. Enzyme activity displayed is representative of three replicate experiments. B) The effect of peptidase inhibitors on the activity of 2 µg processed MCA4 was assed by cleavage of Z-RR-AMC. Standard assays conditions were supplemented with 100 µM leupeptin, 100 µM antipain, 10 µM E64, 0.5 mM PMSF, 2.5 mM Pefabloc. Enzyme activity is representative of three replicate experiments and expressed as percentage of full activity, error bars show standard deviation.

The active site mutant MCA4^{S219C} was also able to cleave Z-RR-AMC without being processed by MCA2 (Figure 4-9C). As previously demonstrated MCA4^{S219C} autoprocesses which could be a requirement of MCA4 activity. The creation of a mutant MCA4^{S219C} that is unable to autoprocess was attempted by mutating the processing site, lysine-64 (the residue identified as the processing site by N-terminal Edman degradation), to a neutral glycine residue. Interestingly MCA4^{S219C,K64G} retained activity and separation by SDS-PAGE revealed evidence of autoprocessing, presumably occurring at an additional available lysine or arginine residue (Figure 4-14).

The data generated so far show that recombinant MCA4 was active only after proteolytic processing. This is consistent with many mammalian caspases, which require cleavage to generate an active enzyme from the inactive zymogen (Fuentes-Prior *et al.* 2004). Evidence has also been presented for similar processing events occurring in the MCA of *L. major* (Ambit *et al.* 2007; Gonzalez *et al.* 2007), Yca1 of yeast (Madeo *et al.* 2002) and several of the *A. thaliana* MCAs (Vercammen *et al.* 2004). Interestingly while recombinant MCA2 was found to autoprocess, it was not required for enzyme activity (Moss *et al.* 2007). Investigation into the MCA4 active site points to cysteine 218 as a catalytic residue although further work is required to provide complete characterisation of MCA4 activity.

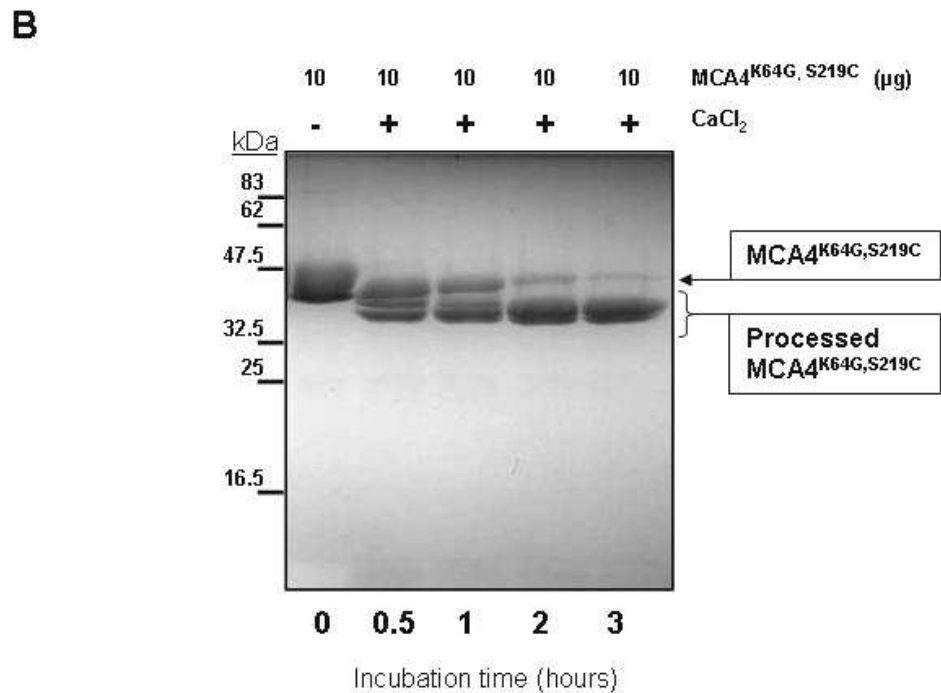
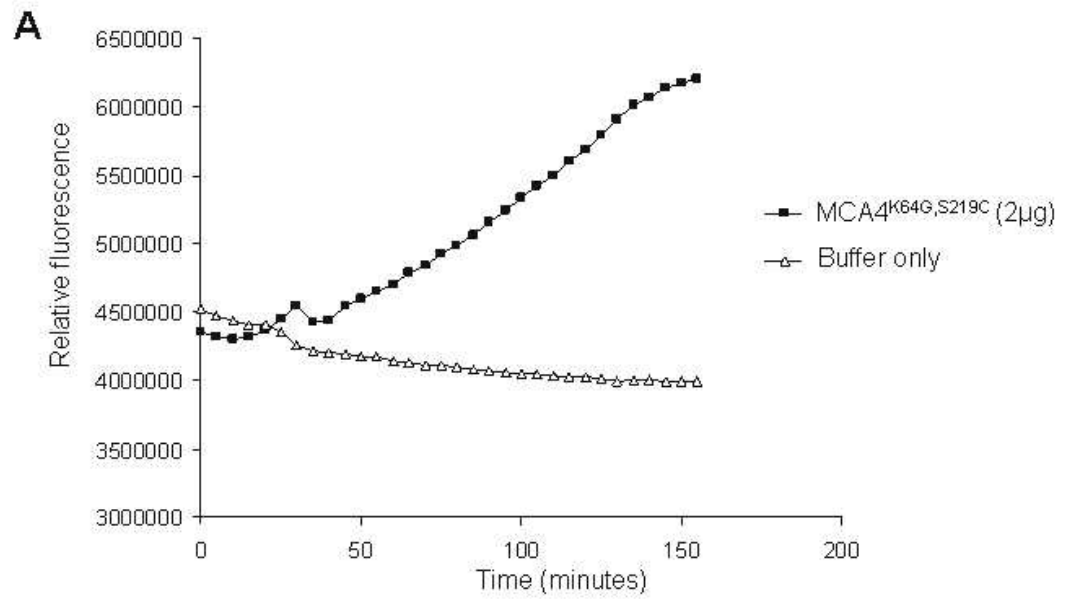


Figure 4-14 MCA4^{S219C} activity and autoprocessing is not inhibited by mutation of lysine-64.

A) Cleavage of Z-RR-AMC by 2 µg MCA4^{K64G,S219C} was measured in a buffer containing 10 mM calcium chloride. Enzyme activity displayed is representative of three replicate experiments. B) MCA4^{K64G,S219C} was produced by site directed mutagenesis and was incubated with 10mM calcium chloride and in Tris storage buffer. Aliquots were removed at the times indicated and analysed by SDS-PAGE. Full length protein and products of autolytic processing are indicated.

4.3.5 MCA4 function in BSF analysed by RNAi

In previous studies the function of *T. brucei* MCA2, MCA3 and MCA5 were investigated by RNAi (Helms *et al.* 2006). Individual downregulation produced no discernable phenotypic defects, however simultaneous triple RNAi caused rapid growth arrest with cells accumulating pre-cytokinesis (Helms *et al.* 2006). Further detailed characterisation of this phenotype provided insights into their physiological roles. To investigate MCA4 function a 500 base pair gene fragment was cloned into the 2T7^{ti} RNAi vector pGL571 (LaCount *et al.* 2000) and transfected into the BSF 90-13 cell line (Wirtz *et al.* 1999). Following RNAi induction a consistent phenotype was observed in three independent clones, hence only data from one representative is presented.

RNAi was induced by the addition of 1 $\mu\text{g ml}^{-1}$ tetracycline to the culture media and the growth rate of induced (Tet +) cultures was compared to non induced controls (Tet -). Following RNAi induction rapid growth arrest occurred. A reduced growth rate was initially detected at 8 hours and cell numbers remained consistently low throughout the RNAi time course (Figure 4-15A). The efficiency and timing of MCA4 downregulation following induction was analysed by western blot. Whole cell extracts were prepared from induced and non-induced cultures at different time points throughout the first 24 hours of induction. Probing the western blot with anti-MCA4 revealed that MCA4 expression remained constant in uninduced control cells. However following MCA4 RNAi induction, depletion of the protein was evident by 16 hours and at 24 hours post induction the MCA4 protein level was severely reduced in comparison to the non-induced control cells (Figure 4-15B).

To analyse the progression of RNAi induced parasites through the cell cycle the configuration of nuclei and kinetoplasts was determined by fluorescent microscopy of DAPI stained cells (Figure 4-16A). Following induction of RNAi the proportion of cells with 1N1K decreased steadily from an initial figure of 76% in non-induced to 31% at 24 hours post induction. This was accompanied by a minor reduction in 1N2K cells and a rapid persistent increase of 2N2K cells; rising from 6% (0 hours) to approximately 18% at 8, 16 and 24 hours post induction. The concomitant decrease of 1N1K cells and increased 2N2K cells and 'others'

suggested that cells were able to replicate their DNA but failed to correctly execute cytokinesis. Defective cytokinesis was the most credible explanation for the dramatic accumulation of aberrant cells containing misconfigured DNA (predominantly cells with increased DNA content and zoids, all classified as 'others'), which were the most abundant cell types at 24 hours post induction (Figure 4-16C). The flow cytometry profiles of the induced cells confirmed the DAPI analysis; showing a reduced 2C peak (1N1K) and increased 4C peak (2N2K) combined with the appearance of abnormal 8C cells (>2N2K) and those with less than 2C at later time points (Figure 4-16B). These data suggest that MCA4 is essential for the multiplication of BSF *T. brucei* and that MCA4 is involved in mediating interactions linked to post-mitotic or cytokinetic events.

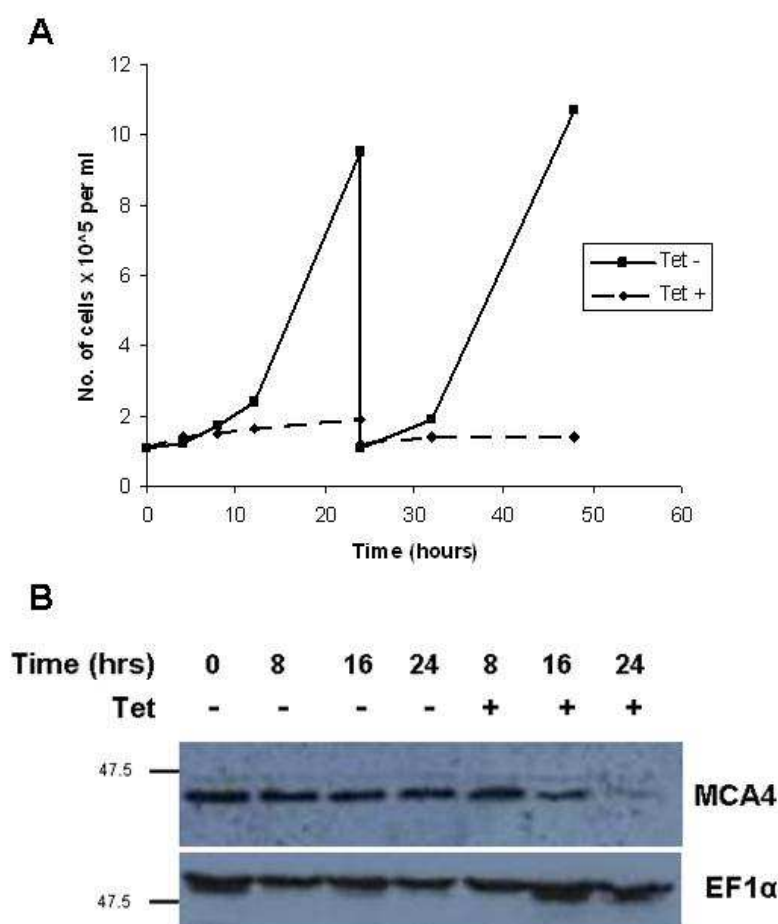


Figure 4-15 RNAi of MCA4 in BSF *T. brucei*.

A) MCA4 RNAi was induced by 1 $\mu\text{g ml}^{-1}$ tetracycline (TET+) and growth rate determined by haemocytometer cell counts and compared to non-induced control (TET-). Cells induced at $1 \times 10^5 \text{ ml}^{-1}$ and reseeded to same density after 24 hours. B) Western blot analysis of MCA4 protein level during MCA4 RNAi time course. Cell lysates taken during first 24 hours from induced (TET+) and non induced (TET-) cultures and probed with anti-MCA4. To demonstrate equal loading the membrane was stripped and re-probed with anti-EF-1 α .

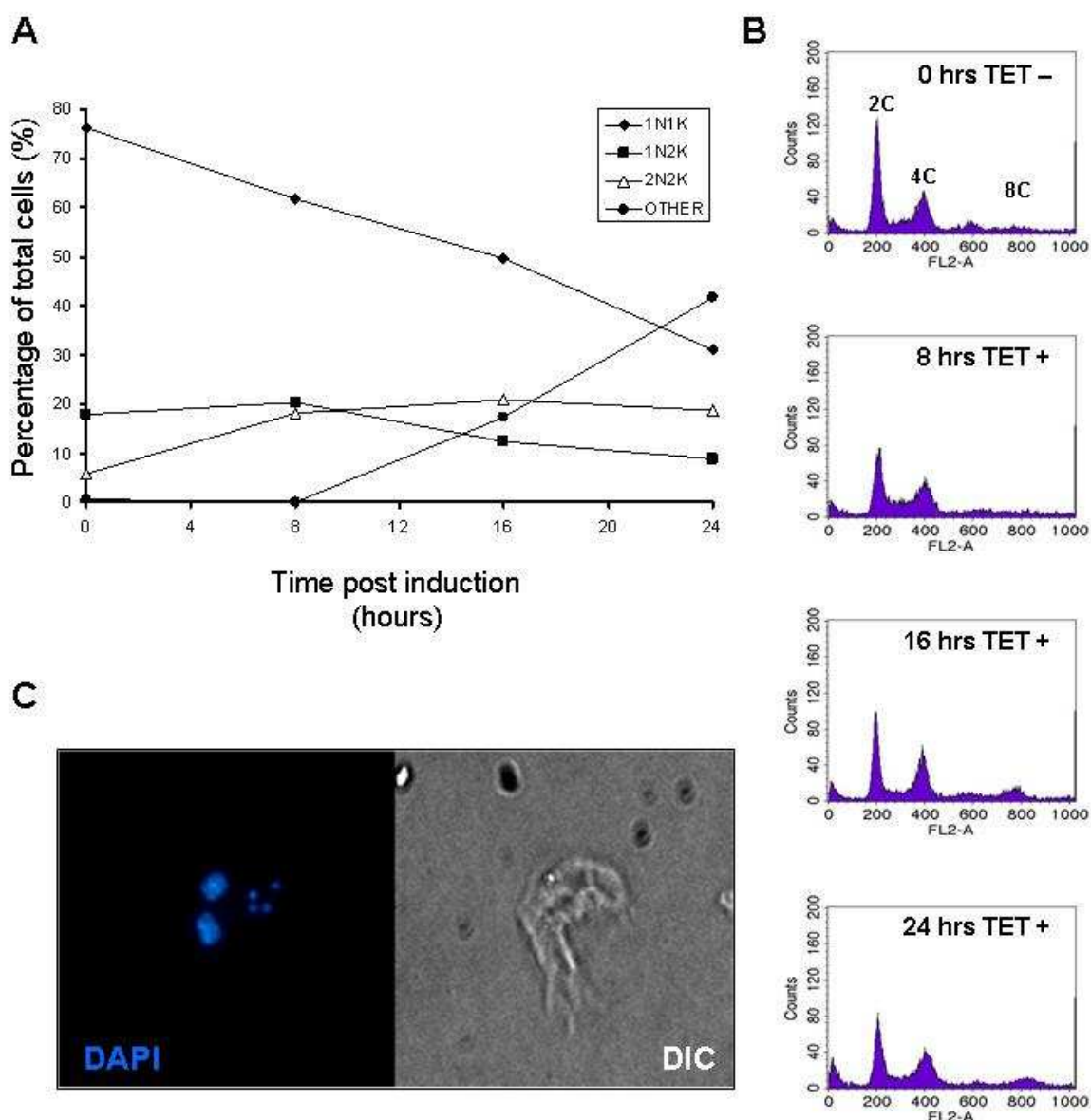


Figure 4-16 Metacaspase 4 RNAi alters BSF *T. brucei* cell cycle progression.

A) The effects of MCA4 RNAi on the DNA configuration of BSF *T. brucei* following induction was measured over time, as revealed by DAPI staining and fluorescence microscopy. Classification was based on number of nuclei (N) and kinetoplasts (K) per cell, with >200 cells counted per time point. Cells with abnormal DNA content classified as 'other'. B) Flow cytometry profiles of propidium-iodide stained cells were determined at time point throughout the course of the RNAi induction. 2C peaks represent 1N1K cells, 4C 2N2K cells and 8C cells with abnormal elevated DNA content C) Image of typical induced cell, classified as 'other', fixed in methanol and stained with DAPI (blue). Reference image taken using differential interference contrast (DIC) filter settings.

4.3.6 MCA4 null mutants show reduced virulence in vivo

4.3.6.1 Generating MCA4 null mutant lines

Simultaneous downregulation suggested that MCA2, MCA3 and MCA5 were essential genes. Yet surprisingly it was possible to create null mutant BSF cell

lines ($\Delta mca2/3 \Delta mca5$) by sequential replacement of the *MCA2/3* locus and latterly the *MCA5* locus with drug resistance cassettes (Helms *et al.* 2006). The $\Delta mca2/3 \Delta mca5$ parasites initially grew poorly in culture but recovered after several weeks and grew at the same rate as wild type. The disparity between the triple RNAi and null mutant phenotypes was attributed to the different speeds of MCA removal. Rapid simultaneous down regulation of *MCA2*, *MCA3* and *MCA5* by RNAi occurred too quickly for the parasites to activate alternative pathways. However the triple knockout strategy involved sequential removal dispersed by long periods of recovery and adjustment.

To investigate whether a similar phenomenon might occur with *MCA4*, genetic knockout was attempted. Two unique regions flanking the *MCA4* ORF were cloned into knockout constructs, which contained a drug resistance marker with the appropriate tubulin intergenic sequences to drive mRNA expression. Constructs containing two different drug resistance cassettes were developed to allow the replacement of both *MCA4* alleles. The constructs were digested out of the plasmid backbone and transfected sequentially into wild type BSF cells. The unique flanking regions targeted the drug resistance cassette to the *MCA4* locus where it integrated into the *T. brucei* genome replacing the *MCA4* ORF. Single allele heterozygote cells (*mca4* +/-) were generated by transfection of the neomycin (NEO) resistant cassette and null mutants ($\Delta mca4$) were created following integration of the hygromycin (HYG) cassette.

When analysing null mutant cell lines it is important that any loss of function phenotype can be directly attributed to the absence of the target protein. Re-expression of the deleted gene from an alternative site returns the protein to the cell, but maintains the previous genetic modifications. This allows for thorough analysis of protein function while controlling against any potential negative effects of disruption to the target genetic locus.

For the ectopic re-expression of *MCA4*, a YFP-tagging construct (pGL1742 originally published as p2628 in Kelly *et al* 2007) was modified for use in the $\Delta mca4$ cell line. The resistance marker was switched from HYG to blasticidin (BSD) and the *MCA4* ORF was cloned into the expression site using *XhoI* and *BamHI* restriction sites, which removed the YFP tag from the plasmid backbone. Following linearization and transfection the construct was designed to integrate

into repetitive DNA sequences (the 177 bp repeat) found in minichromosomes and intermediate sized chromosomes (Kelly *et al.* 2007). Expression of the BSD resistance cassette was mediated by the EPI procyclin promoter and transgene expression was controlled by a rRNA promoter. The isolated clones were designated $\Delta mca4:MCA4$.

4.3.7 Confirming null mutant and re-expression cell lines

Correct integration of the drug resistance cassettes and subsequent deletion of *MCA4* was confirmed by Southern blotting (Figure 4-17). Genomic DNA was digested with *PvuI* and *AvrII* and the Southern blot was probed with the 5' flanking region used to target the knockout constructs and DNA fragments of the predicted sizes were obtained (Figure 4-17B). A 2.3 kb fragment, corresponding to the predicted size of the native locus was detected only in wild type and heterozygote DNA. Fragments corresponding to the predicted size of the NEO (2.56 kb) and HYG (1.44 kb) replacement loci were only detected in the correct heterozygote, null mutant and re-expression cell lines. For further verification the 5' flank probe was stripped from the membrane and the Southern blot was re-probed using the *MCA4* ORF. Positive fragments were only detected in the wild type, heterozygote (2.3 kb) and re-expressor (4.22 kb) DNA. This confirmed the correct integration of the knockout constructs and the successful deletion and subsequent re-expression of *MCA4*.

Using anti-*MCA4* it was possible to verify the successful generation of the $\Delta mca4$ parasites by western blot (Figure 4-17C). Protein corresponding to *MCA4* was detected in the parental wild type cell line (lane 1) but was absent in the $\Delta mca4$ cell line (lane 2). Furthermore, western blotting revealed that the $\Delta mca4:MCA4$ cell line was a functional re-expressor, with *MCA4* protein detected in the cell lysate (lane 3).

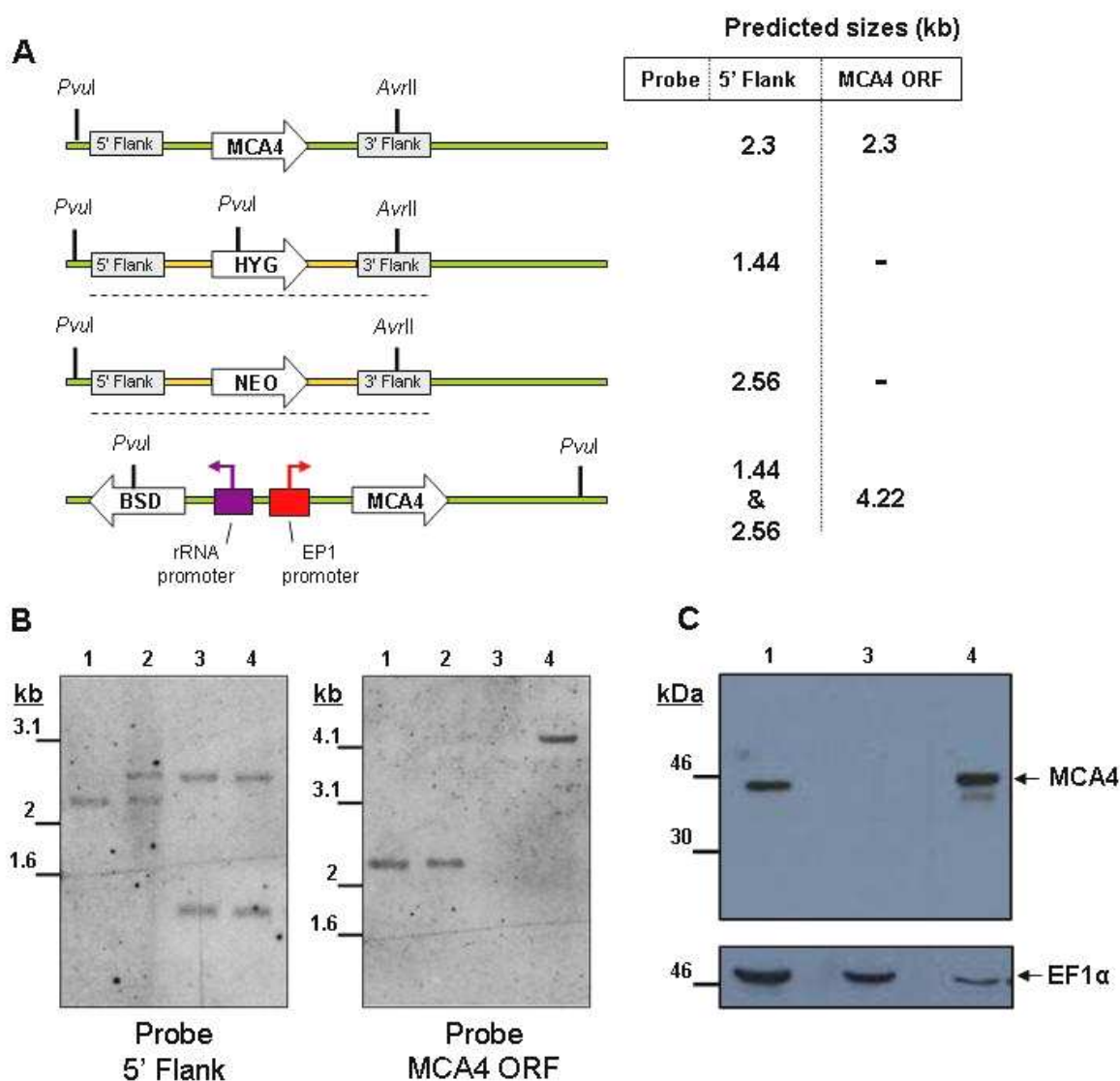


Figure 4-17 Generating MCA44 null mutants.

A) Schematic representation of the *MCA4* locus in *T. brucei* 427 before and after integration of the targeted hygromycin (HYG) and neomycin (NEO) gene replacement constructs, underlined. Yellow indicates α/β tubulin intergenic regions. Lower diagram depicts schematic representation of *MCA4* re-expression from ectopic locus. The predicted sizes DNA fragments of both the native and modified *MCA4* locus are shown following *PvuI* and *AvrII* digest of genomic DNA, with corresponding Southern blot probes. B) Genomic DNA was digested with *PvuI* and *AvrII*, separated on a 0.8% agarose gel and transferred to a Hybond-N nylon membrane before hybridization with a chemiluminescent labelled probe specific to the *MCA4* 5' flank. After detection the Southern blot was stripped and reprobed using second labelled probe, specific to the *MCA4* ORF. C) Cell lysate from 1×10^6 cells was prepared and analysed by western blot to investigate *MCA4* expression. To demonstrate equal loading the blot was stripped and reprobed with anti-EF-1 α . B and C: Lane 1, wild type *T. brucei* BSF 427; Lane 2, NEO-resistant heterozygote; Lane 3 $\Delta mca4$; Lane 4 $\Delta mca4$:*MCA4*. The NEO-resistant heterozygote is absent in C.

4.3.7.1 In vitro analysis of $\Delta mca4$.

Generation of $\Delta mca4$ parasites without any significant difficulties was surprising given the severity of the RNAi phenotype. Several independent clones were

obtained and analysed. No obvious morphological defects were detected however the cultured $\Delta mca4$ cells grew at a reduced rate in comparison to wild type cells (Figure 4-18A).

To see if the reduced growth rate was linked to a defect in the cell cycle, fixed mid-log cells were stained with DAPI and analysed by microscopy. Unlike the MCA4 RNAi phenotype which dramatically altered the cell cycle, $\Delta mca4$ parasites were only subtly affected with a small yet statistically significant decreased percentage of 1N2K cells. This slight defect to cell cycle progression could be responsible for the reduced growth rate witnessed (Figure 4-18B).

As MCA4 has been shown to associate with the flagellar membrane we postulated that null mutant phenotypes could be linked to deficiencies in flagellum function. A prominent role of the *T. brucei* flagella is motility and flagellum motility is known to be essential for BSF trypanosomes (Broadhead *et al.* 2006). Wild type BSF parasites actively swim in the culture media, whereas mutants with motility defects sediment more rapidly (Bastin *et al.* 1999). To investigate $\Delta mca4$ motility, cultured cells ($1 \times 10^6 \text{ ml}^{-1}$) were divided equally into cuvettes and incubated under standard conditions. Sedimentation rates were determined by comparing the optical density (600 nm) of undisturbed cultures with resuspended controls. Both wild type and $\Delta mca4$ cells sedimented at similar rates, thus it appears the mechanical motility of the flagellar is not altered by the absence of MCA4 (Figure 4-18C).

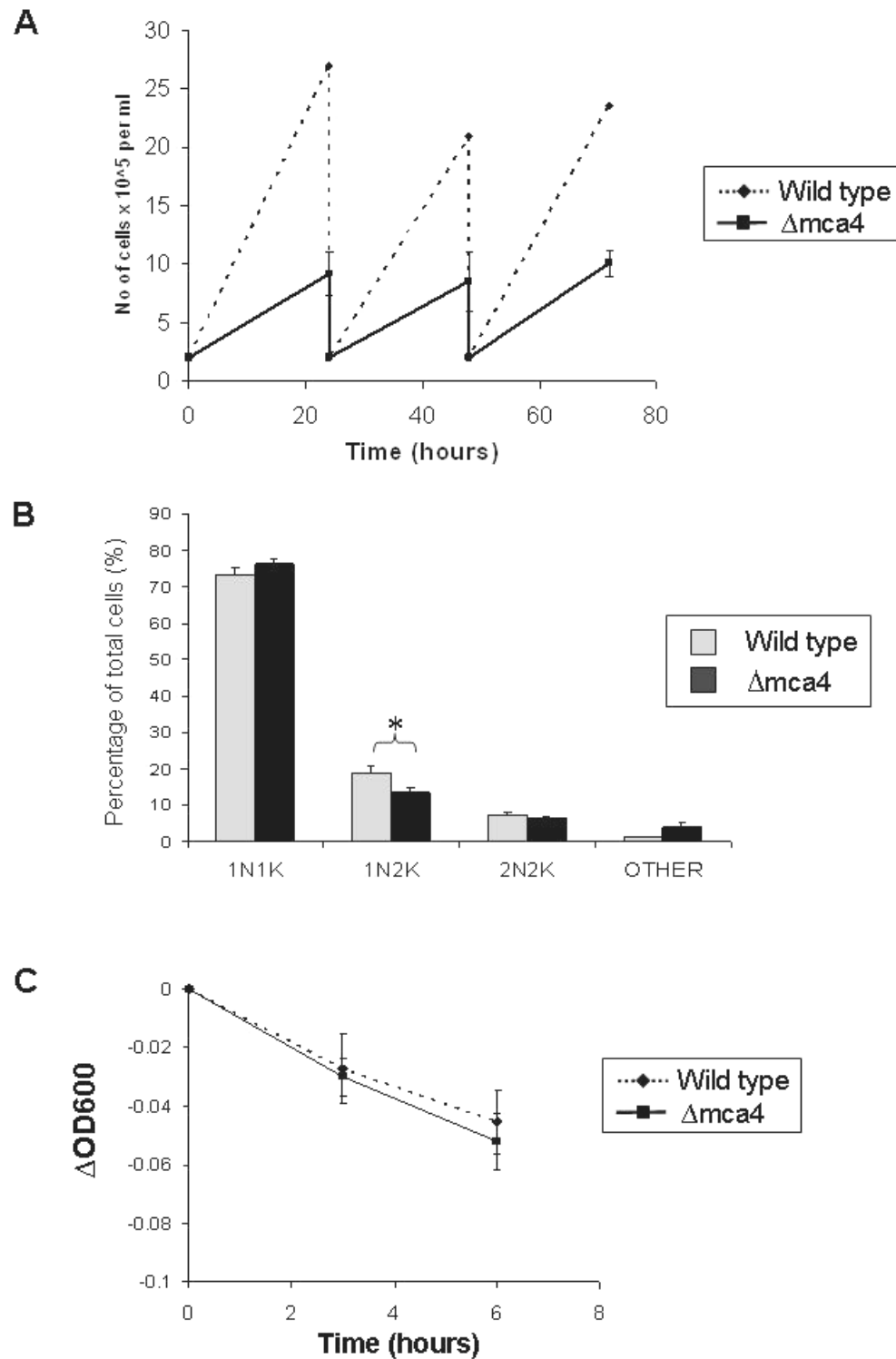


Figure 4-18 In vitro analysis of MCA4 null mutant parasites.

A) The growth rate of BSF wild type 427 and $\Delta mca4$ parasites was determined by daily haemocytometer cell counts. The cultures were seeded every 24 hours at $2 \times 10^5 \text{ ml}^{-1}$ and maintained in HMI9. $\Delta mca4$ growth rate mean of four clones, error bars SD B) The DNA configuration of wild type and $\Delta mca4$ parasites (one representative clone) as revealed by DAPI staining and fluorescent microscopy. Classification was based on number of nuclei (N) and kinetoplast (K) per cell, with >200 cells counted for both cell lines. Data mean of 3 replicates, error bars SD. Asterisk (*) indicates where $\Delta mca4$ data differed significantly from wild type cells, $P < 0.05$. C) The motility of wild type and $\Delta mca4$ parasites was analysed by assessing their ability to resist sedimentation in culture. Cultures were divided into experimental and control cuvettes and the optical density (600 nm) recorded over a 6 hour period. Before each measurement control cells were resuspended. The density of experimental cultures was subtracted from control cells produce ΔOD_{600} value, which shows parasite sedimentation. Data mean of 3 replicates, error bars SD

4.3.8 *In vivo* analysis of $\Delta mca4$ parasites

Given that MCA4 expression was detected only in BSF *T. brucei* a potential role in the mammalian infection process was investigated by comparing wild type and $\Delta mca4$ infection profiles of ICR mice (Figure 4-19A). Groups of 4 mice (2 for wild type control) were infected by intraperitoneal injection with 5×10^3 parasites, provided by a donor mouse. The parasitemia of individual mice was monitored by regular haemocytometer counts of parasites in blood taken from the tail vein. To ensure the animal model experiments conformed to regulations and that high standards of animal welfare were maintained, those mice displaying severe clinical symptoms or with a parasite burden greater than $1 \times 10^8 \text{ ml}^{-1}$ of blood were removed from the study.

Consistent with published data it was found that *T. brucei* 427 wild type are highly virulent in ICR mice (Lanteri *et al.* 2006) and rapidly established parasitemia above the cut off point in 100% of the infected mice by 4 days (Figure 4-19A). Interestingly infection with $\Delta mca4$ parasites drastically altered the course of infection and prolonged mouse survival to 15.25 days (mean of 4 mice). The reduced *in vivo* growth rate of MCA4 deficient parasites was partially restored to wild type levels by the re-expression of MCA4. The mean mouse survival time for $\Delta mca4:MCA4$ parasites was 7.5 days post infection, with 3 out of 4 mice succumbing to infection by day 7.

The discovery of a quantifiable phenotype complemented by re-expression of 'wild type' MCA4, allowed for the *in vivo* investigation of MCA4 activity. Site directed mutagenesis was used to alter predicted key catalytic residues of MCA4 in the re-expression construct. Initially, histidine-164 was mutated to alanine however no clones were isolated following transfection. Accordingly a double mutant was produced, changing the active site serine-219 and the adjacent cysteine-218 (predicted MCA4 catalytic residue) to glycines to ensure all enzymatic activity was abolished. Following transfection of this construct several independent clones were isolated and successful re-expression of $MCA4^{C218G,S219G}$ was confirmed by western blot (Figure 4-19B). Infection of mice with $\Delta mca4:MCA4^{C218G,S219G}$ cells produced an infection profile which most closely resembled the null mutant with the mean mouse survival time (4 mice) greatly

extended to 18.75 days (Figure 4-19A). This strongly suggested that MCA4 peptidase activity was required for optimum parasite viability.

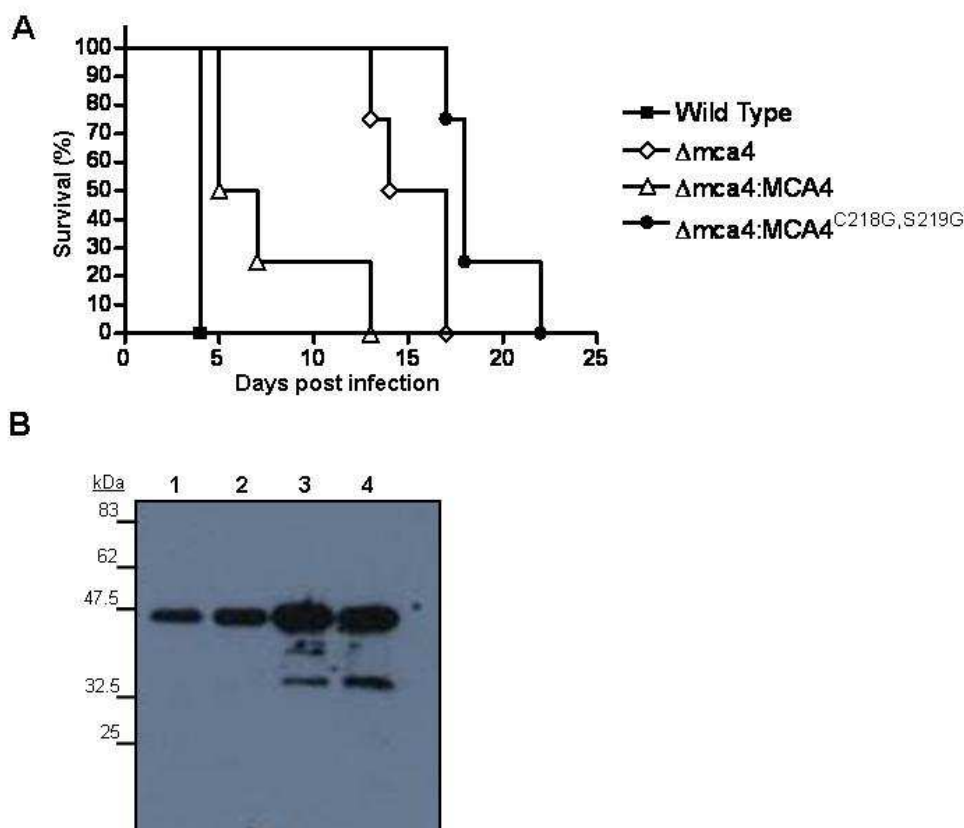


Figure 4-19 MCA 4 deficient parasites show reduced virulence in mice.

A) Groups of 4 ICR mice were infected with 3×10^5 parasites (2 ICR mice for wild type parasites) taken directly from a specific donor mouse. Parasitemia was monitored by tail prick and haemocytometer cell count. Mice were culled when parasitemia reached $>1 \times 10^8$ cells ml^{-1} or upon presentation of severe symptoms. Mouse survival was monitored daily and is shown by a Kaplan-Meier survival curve. B) BSF $\Delta mca4$ parasites were engineered to re-express mutant MCA4^{C218G,S219G} (lanes 1 and 2) and MCA4^{S219C} (lanes 3 and 4). Western blotting was used to confirm that the mutant MCA4 proteins were being expressed, demonstrated in two independent clones for each cell line.

Detailed analysis of the parasitemia patterns of the infected mice revealed several interesting trends. As previously mentioned wild type 427 *T. brucei* are extremely virulent and the parasitemia increased consistently and rapidly. The infection profile of $\Delta mca4$ was drastically different with peaks of parasitemia separated by troughs, periods of time where parasitemia was below the detection threshold of haemocytometer counting (Figure 4-20) The $\Delta mca4$ parasitemia profiles in individual mice broadly followed the same pattern with

peaks generally occurring at four days post infection and recrudescence not detected until 10 days post transfection. The parasitemia in 75% of mice remained high after the second peak and slowly increased over the remainder of the infection, whereas one mouse showed two further troughs in parasitemia. In the $\Delta mca4:MCA4$ re-expression cell line the parasitemia profile was much more reminiscent of wild type cells with consistent parasite growth and only one mouse briefly able to clear the infection. Re-expression of inactive mutant $\Delta mca4:MCA4^{C218G,S219G}$ generated variable growth profiles with multiple peaks of parasitemia, although interestingly the prolonged trough observed early in the $\Delta mca4$ infection was not detected.

Further cell lines re-expressing the constitutively active mutant $MCA4^{S219C}$ were generated. Western blot analysis confirmed successful re-expression and interestingly revealed two MCA4 proteins (Figure 4-19). The lower molecular weight MCA4 indicated that autolytic processing of $MCA4^{S219C}$ occurred in similar a similar manner both in *in vivo* and in *in vitro* settings.

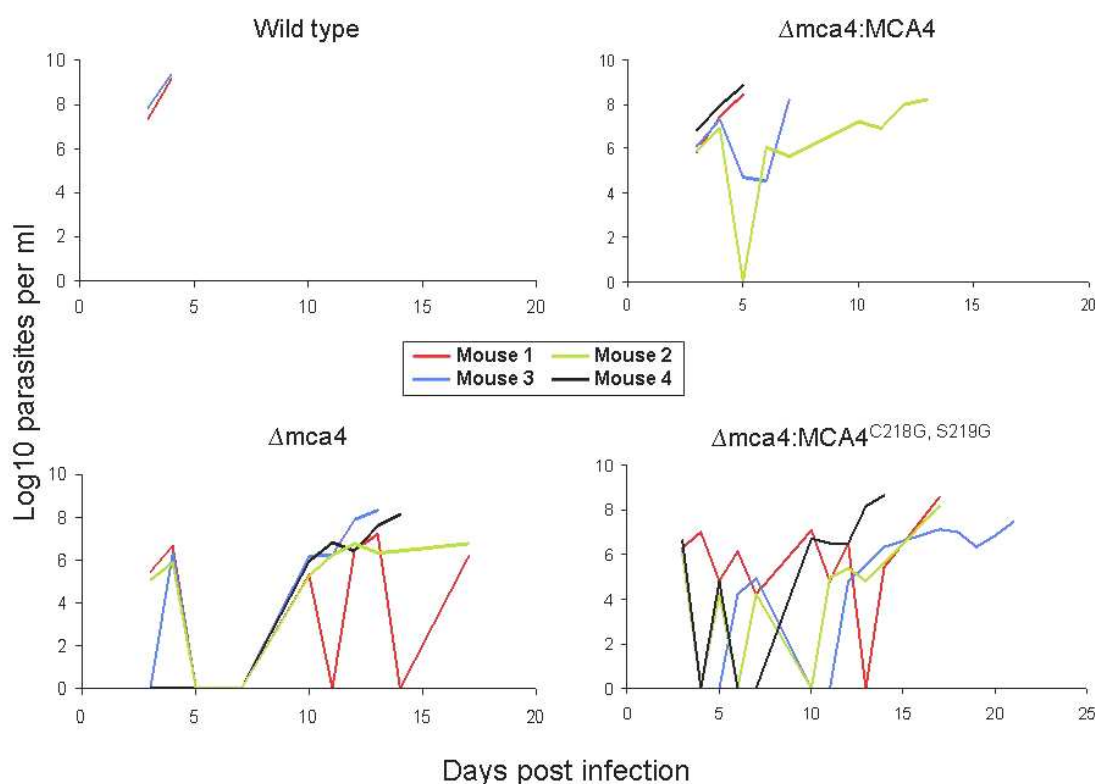


Figure 4-20 *T. brucei* 427 wild type, $\Delta mca4$ and $\Delta mca4:MCA4$ mouse infection profile.

Individual ICR mice (labelled mouse 1-4 in each separate study) were infected with 3×10^5 parasites taken directly from a specific donor mouse. Parasitemia was monitored by tail prick and haemocytometer cell count. Mice were culled when parasitemia reached $>1 \times 10^8$ cells ml^{-1} or upon presentation of severe symptoms.

4.4 Discussion

The MCAs are one of several families of cysteine peptidases found in protozoan parasites (Atkinson *et al.* 2009; Mottram *et al.* 2003). Five MCA genes were identified in the *T. brucei* genome (Szallies *et al.* 2002), although only MCA2, MCA3 and MCA5 contained the conserved histidine-cysteine catalytic dyad predicted to be required for activity, raising questions over the catalytic activity of MCA1 and MCA4. Comprehensive analysis of MCA2, 3 and 5 in BSF *T. brucei* revealed a combined essentiality and provided potential insights into their physiological functions (discussed in detail 4.1.13) (Helms *et al.* 2006). To improve our understanding of *T. brucei* MCAs a comprehensive characterisation of MCA4 was undertaken which revealed many unexpected and unique features of this enzyme.

4.4.1 MCA4 expression and localisation

One prominent observation of the *T. brucei* MCAs was their regulated expression in different lifecycle stages. Indeed in common with MCA2 and MCA3 the expression of MCA4 protein was restricted to the mammalian infective BSF parasites. Whilst expression was not experimentally verified in all lifecycle stages, the absence of these MCAs from procyclic parasites strongly suggested they were likely to be specific to BSF stage parasites. However, the function of MCA4 appears not to overlap with that of MCA2, MCA3 and MCA5. Firstly MCA4 protein level remained unchanged in $\Delta mca2/3 \Delta mca5$ parasites, showing that MCA4 was not upregulated or proteolytically activated by the parasites to compensate for the loss of other MCAs. Secondly the cellular localisation of MCA4 was distinct from the other studied MCA family members in *T. brucei*. Cellular fractionation of BSF cell lysate identified MCA4 as a membrane associated protein. Subsequent immunofluorescence microscopy revealed that MCA4 was specifically localised to the flagellar membrane appearing in a linear array of punctate structures. Further detailed investigation using immunoelectron microscopy identified distinct clusters of MCA4-labelling along the length of the flagellum, confirming the punctate nature of MCA4 localisation.

Whilst drastically different to the punctate appearance of MCA2, MCA3 and MCA5 the localisation pattern detected was consistent with several other *T. brucei* flagellar membrane proteins. One such protein, glycosylphatidylinositol-specific phospholipase C (GPI-PLC), an enzyme that cleaves the GPI-anchor of VSG and other GPI-anchored proteins was found to be located on the external surface of the flagellar membrane (Hanrahan *et al.* 2009). To provide functional insights into MCA4 functions and possible substrates the position of the protein on the flagella membrane was investigated. Removal of triton-X100 from the MCA4 immunofluorescence protocol resulted in a stark change in detection. The prominent flagellar localisation was only visible when the cells were permeabilised by triton-X100 treatment indicating that MCA4 was located on the internal surface of the flagellar membrane.

The plasma membrane that surrounds *T. brucei* is one contiguous structure but it is separated into three distinct regions: the pellicular (cell) body, the flagellar membrane and the flagellar pocket (Fridberg *et al.* 2007; Gull 2003; Landfear *et al.* 2001). The classification of these distinct plasma membrane zones is reinforced by differences in their protein and lipid composition (Tyler *et al.* 2009). As proteins are not synthesized in the flagellum, a process must exist to aid their selective transfer into the flagellum. To date no single flagellar targeting signal has been identified in kinetoplastids (Fridberg *et al.* 2007), however the localisation of several flagellar membrane proteins has been shown to depend on dual acylation. This was originally described for a flagellar calcium binding protein (FCaBP) in *T. cruzi*, where blocking acylation by mutagenesis lead to mislocalisation away from the flagellum (Godsel *et al.* 1999). Similarly the dual acylation of the *L. major* small myristoylated protein 1 (SMP-1) was identified as one mechanism controlling its flagellar membrane localisation (Tull *et al.* 2004).

An indepth study has been carried out on the dually acylated *T. brucei* calflagins (Tb17, Tb24 and Tb44), which are a family of proteins predicted to be involved in calcium binding (Emmer *et al.* 2009). In PCF cells both wild type Tb44 and C-terminally myc tagged Tb44^{myc} localised to the flagellar membrane, however disruption to the acylation status of the N-terminus changed the cellular localisation. Mutation of Tb44^{myc} glycine-2 to an alanine (blocked N-myristoylation and subsequent palmitoylation of cysteine-3) resulted in a

cytoplasmic localisation. Whereas, mutation of cysteine-3 to alanine (allowed N-myristoylation but not palmitoylation) moved Tb44^{myc} to the pellicular membrane. Dual acylation was further implicated in flagellar membrane localisation by screening the 12 candidate palmitoyl acyltransferases genes (*PAT1-12*) by RNAi. The *T. brucei* PATs were highly specific; only downregulation of PAT7 blocked Tb44^{myc} palmitoylation resulting in abnormal localisation to the pellicular membrane (Emmer *et al.* 2009).

Further evidence implicating dual acylation in flagellar membrane association was provided by characterisation of the expanded calpain family of *T. brucei*. Calpains are a large family of calcium dependent cysteine peptidases that are implicated in a wide variety of cellular events including signalling and cellular remodelling (Croall *et al.* 2007). N-terminal acylation was predicted for six of the *T. brucei* calpain-like proteins (Ersfeld *et al.* 2005). Subsequent characterisation of myc-tagged CALP1.3 revealed it was a palmitoylated membrane associated protein. Immunofluorescence microscopy localised CALP1.3^{myc} to the tip of the flagella, which was disrupted by deletion of the acylation sites (Liu *et al.* 2010).

The combined findings of these studies and the *in silico* acylation predictions prompted further experimental investigation of MCA4. N-myristoylation was confidently predicted for MCA4 (Mills *et al.* 2007), thus palmitoylation was investigated by acyl-biotin exchange. This technique confirmed that MCA4 was palmitoylated, implicating dual acylation as a potential mechanism mediating association with the flagellar membrane. To confirm this prediction, mutant MCA4 with blocked predicted acylation sites could be re-expressed and analysed in the $\Delta mca4$ cell line.

Although dual acylation has been shown to mediate the flagellar membrane targeting of several different kinetoplastid proteins, details of the precise mechanism are only beginning to emerge. The modification of proteins with two lipid moieties allows association with lipid rafts, which are specific microdomains found within the plasma membrane. Lipid rafts differ from the surrounding membrane principally in terms their composition; they contain enhanced levels of sphingolipids and sterols, which are densely packed and highly ordered reducing the membrane fluidity (Tyler *et al.* 2009). Recent

characterisation of the *T. brucei* flagellar membrane revealed it was enriched in sphingolipids and sterols, suggesting a high concentration of lipid rafts (Tyler *et al.* 2009). Indeed it was shown that disruption of lipid raft formation caused the mislocalisation of the calflagin Tb24 away from the flagellar membrane. It was postulated that dual acylation serves as a mechanism to anchor and/or retain specific proteins to the flagellar membrane (Tyler *et al.* 2009).

However, acylation only accounts for lipid raft association and does not fully explain the flagellar localisation. A theory for flagellar membrane trafficking has recently been proposed by Emmer and co-workers in which they implicated targeted delivery as a mechanism to ensure the correct proteins and lipids arrive at the flagellum (Emmer *et al.* 2010a; Maric *et al.* 2010). They describe a system where membrane-associated proteins synthesised on the rough endoplasmic reticulum are subject to N-myristoylation (if required) before transfer to the Golgi, where PATs can catalyse their palmitoylation. Different proteins destined for different locations can then be selectively packaged into Golgi derived vesicles composed of different lipids; acylated flagellar membrane proteins associate with lipid rafts and are packaged into sterol and sphingolipid rich vesicles (Emmer *et al.* 2010a). These can then be trafficked to the base of the flagellum where unknown sorting processes, presumably occurring at the flagellar pocket membrane, allow entry of the correct cargo into the flagellum. Thus explaining the enrichment of lipid rafts and associated proteins in the flagellar and outlining how they are separated from other regions of the plasma membrane (Emmer *et al.* 2010a).

It should be noted that although blocking dual acylation stops flagellar localisation it is not the exclusive factor determining localisation. It is likely additional signals exist because several other dually acylated kinetoplastid proteins have been identified that do not localise to the flagellum. The *T. brucei* calpain-like protein CAP5.5 associates with the subpellicular cytoskeleton of the cell body but is absent from the flagellar axonemes (Hertz-Fowler *et al.* 2001) and the hydrophilic acylated surface protein B (HASP B) protein of *L. major* is located extracellularly (Denny *et al.* 2000). In addition, truncation of the C-terminus of CALP1.3 caused mislocalisation raising the possibility this region contained additional flagellar targeting information (Liu *et al.* 2010).

Furthermore, the exact mechanisms involved in transporting proteins and lipids along the length of the flagellum are unknown. It is unlikely to occur solely by passive diffusion due to the potentially restrictive nature of the flagellar pocket membrane and the prohibitive length of the mature flagellum (Emmer *et al.* 2010a). However, one active process known to transport proteins along the length of the flagellum is intraflagellar transport (IFT). This is defined as the bidirectional movement of protein particles within the flagellar matrix, independent of the flagellar beat (Kozminski *et al.* 1993). IFT is driven by two microtubule associated motor complexes, each responsible for transporting particles in a specific direction. IFT particles assemble at the base of the flagellum and travel along the length of the axoneme, unloading their cargo at the distal tip before exchanging the motor protein and transporting cargo down to the base of the flagellum. Analysis of the *T. brucei* genome revealed it contained the full repertoire of genes known to be involved in IFT (Absalon *et al.* 2008). An active IFT system was demonstrated in live *T. brucei* cells using GFP tagged IFT52 (component of IFT complex) which demonstrated the rapid (bi-directional) movement of GFP-IFT52 labelled particles along the flagellum (Absalon *et al.* 2008). Interestingly, IFT was essential for *T. brucei* with RNAi downregulation of IFT proteins interfering with the production of new flagella and causing loss of cell polarity and defective cytokinesis (Absalon *et al.* 2008). Given the punctate distribution of MCA4 along the length of flagellum it is possible this represents an association with IFT particles; explaining how MCA4 is transported through the flagellum and its punctate appearance. Confirmation of this hypothesis would provide the first example of a novel IFT cargo in *T. brucei*.

4.4.2 MCA4 activity

Enzyme active sites are specifically organised to ensure efficient catalytic activity. This is maintained in different family members by conservation of key catalytic residues. Thus the predicted substitution of the canonical active site cysteine to a serine residue within the MCA4 active site (Figure 4-21) prompted speculation regarding the catalytic properties of the enzyme (Moss *et al.* 2007; Mottram *et al.* 2003; Szallies *et al.* 2002). In this respect MCA4 is far from unique, the accumulation of sequenced genomes has revealed that the occurrence of atypical residues in peptidase active sites is surprisingly

widespread in both metazoan and protozoan organisms (Atkinson *et al.* 2009; Pils *et al.* 2004). Indeed a recent analysis of peptidases from medically important parasitic protozoa revealed that 16% of cathepsin-like proteins (clan CA family C1) do not contain the classic cysteine-histidine catalytic dyad (Atkinson *et al.* 2009). Given the variety of substitutions found in active sites it is likely this will translate into a wide spectra of functional consequences and evidence is now emerging to support this assumption.

The mammalian cFLIP_L protein shows significant structural homology to caspase-8 and caspase-10, containing the same N-terminal signalling domains and the C-terminal caspase domain (Inohara *et al.* 1997). However, crucially key substitutions present in the cFLIP active site (histidine and cysteine to arginine and tyrosine respectively) preclude peptidase activity (Inohara *et al.* 1997). Interestingly this inactive caspase homologue still plays an important role in the regulation of apoptosis. Overexpression lead to a dominant negative effect and inhibited the initiation of apoptosis, a process that requires a proteolytic activation cascade initiated by caspase-8 and caspase-10 cleavage (Inohara *et al.* 1997). Interestingly cFLIP can also activate caspase-8 allowing rapid maturation into the to fully active form. Caspase-8 is produced as zymogen and forms heterodimers with cFLIP, which further stimulates activation of mature caspase-8 (Yu *et al.* 2009).

Conversely some mutations do not categorically inhibit catalytic activity. The crystal structures of the 3C peptidases from several *Picornaviridae* virus species (including Hepatitis A, rhinovirus, poliovirus) reveal an active site highly reminiscent of the classical serine peptidase chymotrypsin. The catalytic triad is located on a two-domain β -barrel structure and is unusually comprised of a histidine, cysteine and glutamic acid. The histidine and glutamic acid appear to function as for serine peptidases, however the nucleophile is a cysteine. Thus 3C peptidase appear to be hybrids of serine and cysteine peptidases and despite this unusual configuration they retain proteolytic activity and are instrumental in processing expressed viral proteins. Additionally it was possible to mutate the nucleophile to a serine and maintain proteolytic activity in the 3C peptidases of poliovirus and cowpea mosaic virus (Dessens *et al.* 1991; Sarkany *et al.* 2003). Interestingly substitution of a serine into the poliovirus 3C peptidase active site reduced the specific activity by 430-fold (Sarkany *et al.* 2003), however it

demonstrated that for some peptidases cysteine and serine nucleophiles are interchangeable. Although these substitutions may have functional implications it crucially shows that they are still viable catalytically.

Several active site mutations have been identified in parasite peptidases of which perhaps the best characterised are the serine repeat antigen (SERA) proteins from *Plasmodium*. They belong to clan CA family C1 and possess a central domain which shows strong homology to the papain cysteine peptidases. In a similar fashion to the *T. brucei* MCA family, *Plasmodium falciparum* SERA6-8 maintain the conserved catalytic cysteine whereas SERA1-5 and SERA9 have an active site serine (Hodder *et al.* 2003). A renatured form of the recombinant peptidase domain of SERA5 demonstrated that a cysteine peptidase-like structure could function with a serine in the catalytic site. The renatured SERA5 domain was able to cleave peptide substrates and also displayed autolytic processing that was blocked by serine peptidase inhibitors (Hodder *et al.* 2003). Subsequent structural analysis has revealed several anomalies in the SERA5 active site (impaired substrate binding capacity and limited access to active site) that could potentially limit its proteolytic activity (Hodder *et al.* 2009). Collectively the SERA proteins have been implicated in mediating the egress of daughter merozoites from infected red blood cells and potentially the re-invasion of red blood cells by merozoites (Blackman 2008). However the weak activity detected and the apparent structural limitations of the SERA5 active site raise questions over its *in vivo* activity and the biological significance of these unusual features awaits clarification.

As highlighted the configuration of peptidase active sites is more diverse than widely acknowledged. The broad significance of active site substitutions is not yet fully understood, thus characterisation of MCA4 activity would add valuable knowledge to the field.

Purified recombinant MCA4 was recovered close to the approximate size of the predicted full length protein and was highly stable but inactive. Incubation at 37°C for 1 hour revealed no evidence of calcium dependent autolytic activity (Figure 4-9). Furthermore no proteolytic activity was detected when recombinant MCA4 was analysed in fluorometric activity assays with a range of substrates, including the fixed position peptide library.

Incubation of MCA4 with small amounts of MCA2 resulted in a defined and reproducible processing pattern. Given that many peptidases are produced as inactive zymogens and require activation either by themselves or another enzyme we postulated that the processed form of MCA4 might be active. Indeed activity assays using fluorogenic synthetic peptide substrates revealed that processed MCA4 activity was detected. However, interpretation of the results was complicated by the presence MCA2 in the reaction, a peptidase also capable of cleaving the Z-RR-AMC substrate. The similarity in the active site structure of the two enzymes (excluding the cysteine to serine switch in MCA4) meant it was unlikely a substrate unique to MCA4 would be identified. Therefore additional assays were used to established residual MCA2 activity and any potential enhancement to MCA2 activity related to an exogenous protein in the reaction. Although overall activity was weak (approximately 50 times lower than MCA2) it was relative to the quantity of processed enzyme in the reaction, further suggesting the activity detected was attributed to processed MCA4.

In the absence of a metacaspase structure the key active site residues have been identified based on homology and sequence alignment to known caspase enzymes and subsequently experimentally verified by mutagenesis (Moss *et al.* 2007; Vercammen *et al.* 2004). The active site of MCA4 is particularly interesting because it is predicted to have a serine nucleophile set in a cysteine peptidase structure (Figure 4-21). Having established MCA4 activity we sought to investigate the active site residues. Independent mutation of histidine 164 and cysteine 218 (adjacent to active site serine) produced an insoluble protein preventing any further study of these mutants. However, the active site serine was amenable to mutation and it was possible to purify both MCA4^{S219C} and MCA4^{S219G}. Mutating the active site serine to cysteine, produced an active peptidase capable of autolytic processing, although the overall activity was still much lower than recombinant MCA2. This could reflect additional differences in the MCA4 active site causing reduced activity or suboptimal assay conditions for MCA4^{S219C} (substrate preference or missing cofactors). Interestingly MCA4^{S219G} still exhibited activity once processed by MCA2, implying an additional nucleophile is responsible for or contributes to catalysis. The most likely candidate is cysteine-218, conserved in all *T. brucei* metacaspases (Figure 4-21), however unfortunately the potentially inactive MCA4^{C218G} mutant could not be

purified and used to experimentally verify this hypothesis. Interestingly mutation of the corresponding residue in MCA2 impacted on its peptidase activity (~70% reduction) (Moss *et al.* 2007).

Proteolytic activity was only detected for processed MCA4 or MCA4^{S219C} (that was able to autoprocess) which implicated processing as a requirement for creating a mature active peptidase. SDS-PAGE analysis of MCA4^{S219C} autoprocessing and MCA2 directed MCA4 processing revealed strikingly similar processing patterns. Both proteins were cleaved into three main products of approximately 38, 36 and 34 kDa. To identify the MCA4 processing sites the N-terminal amino acids of the main 36 kDa fragments were sequenced by Edman degradation and identified a common sequence of six amino acids for both proteins. Mapping the six amino acid sequence onto full length MCA4 revealed the fragments were generated following cleavage at lysine-64. The common cleavage site showed a partial overlap of MCA2 and MCA4^{S219C} substrate specificity. Combined with fluorometric activity assay data this confirmed the ability of MCA4^{S219C} to cleave substrates only with basic residues in the P1 position.

MCA2 autolytic processing occurred at lysine-55 and lysine-268 (Moss *et al.* 2007). Interestingly sequence alignment of MCA2 and MCA4 proteins revealed that the MCA2 lysine-55 is conserved in MCA4 (Figure 4-21). However to date MCA4 processing has only been mapped to a lysine three residues upstream, namely lysine-64 (MCA4 numbering) (Figure 4-21). To investigate the significance of autoprocessing on MCA4^{S219C} activity lysine-64 was mutated to a neutral glycine residue. However, the enzyme was still able to autoprocess and retained proteolytic activity. The identification and removal of further processing sites will help to define the importance of processing on MCA4 activity. One prominent candidate residue for future mutation is MCA4 lysine-61, which corresponds to the site of MCA2 autoprocessing. Interestingly mutation of the MCA2 active site cysteine to glycine (C213G) completely blocked activity and autoprocessing, whereas MCA2^{C212G} could still autoprocess.

It is tempting to speculate that the MCA4 active site serine restricts autoprocessing and places the activation of MCA4 under the control of an upstream peptidase(s). Indeed re-expression of the constitutively active MCA4^{S219C} in the $\Delta mca4$ background generated two prominent proteins; full

length MCA4 and a smaller processed protein of about 36 kDA (Figure 4-19B), which corroborates well with the autoprocessing pattern of recombinant protein (Figure 4-9B). Western blot analysis of *T. brucei* whole cell lysate revealed that MCA4 is mostly represented by one protein corresponding to the full length. Occasionally however evidence of processing was detected (see Figure 4-5A, Figure 4-8A, Figure 4-17C Lane 4) although no consistent pattern was detected, thus identifying any stimulus was not possible.

In the recombinant activity assays MCA4 was successfully activated by MCA2, however whether this occurs in *T. brucei* is unknown. The distinct flagellar membrane localisation of MCA4 would seem to place the enzyme out of reach of MCA2, which was localised to RAB11 positive vesicles (Helms *et al.* 2006). However, it is possible that localisation of the proteins could change and coincide following a specific stimulus such as cell stress.

Alternatively another activating peptidase localised to the flagellum could control MCA4 activity. An extensive inventory of flagellar proteins has been compiled (Ralston *et al.* 2009) from several proteomic and genomic studies (Baron *et al.* 2007; Broadhead *et al.* 2006; Hart *et al.* 2009). Searching this list identified several candidate peptidases for MCA4 activation. Numerous calpain-like proteins were identified as flagellar proteins (Liu *et al.* 2010). They are interesting candidates given their signalling roles in other organisms, however all *T. brucei* calpain-like proteins (except one) are predicted to contain active site substitutions and thus may not be proteolytically active (Croall *et al.* 2007; Ersfeld *et al.* 2005). Another interesting candidate is a subtilisin-like serine peptidase (Tb927.3.4230) that was identified as part of a cohort of 50 proteins unique to organisms with motile flagellar or cilia (Baron *et al.* 2007), although no experimental evidence has been presented to confirm its flagellar localisation. Interestingly a subtilisin-like peptidase of *P. falciparum* (PfSUB1) has recently been identified as the protein responsible for the proteolytic processing of SERA5 (Yeoh *et al.* 2007). It must also be considered that the proteomic identifications of flagellar proteins were performed on flagellar isolated from PCF, so it is possible that if a specific MCA4 activator exists it could also be restricted to BSF stage of the lifecycle and therefore absent from these proteomic studies.

4.4.3 MCA4 reverse genetics

A two pronged approach was taken to investigate MCA4 loss of function, firstly downregulation by RNAi and secondly genetic knockout. Unlike the other *T. brucei* MCAs, which showed individual redundancy (Helms *et al.* 2006), MCA4 was essential for BSF cell division and growth. Targeted RNAi down regulation reduced MCA4 protein to almost undetectable levels by 24 hours post induction. This was accompanied by the concurrent block of cell cycle progression, which manifested in the appearance of abnormal cells with elevated DNA content indicating a post mitotic block.

The MCA4 RNAi phenotype was consistent with the findings of other studies that used RNAi to downregulate BSF flagellar proteins (Ralston *et al.* 2008). The most thorough investigation was carried out by Broadhead *et al.* who selected five proteins identified in their flagellar proteome and targeted them individually by RNAi (Broadhead *et al.* 2006). The selected axoneme associated proteins included three newly identified flagellar proteins (TAX-1, PACRGA and DIGIT), a homologue of a known *Chlamydomonas* flagellar protein MBO2 and paraflagellar rod protein 2 (PFR2). Despite the diversity of the selected group, RNAi downregulation resulted in a remarkably consistent phenotype. All five proteins were essential for BSF *T. brucei* and prior to cell death 'monstrous cells' accumulated containing multiple nuclei and kinetoplasts (Broadhead *et al.* 2006). The cells continued to replicate their organelles but failed to carry out cytokinesis; each round of replication produced new organelles but the lack of cellular organisation and division rapidly caused detrimental complications for the parasites.

Several other studies on BSF flagellar proteins have reported similar phenotypes including: the inducible downregulation of trypanin a component of flagellar dynein regulatory complex possibly responsible for axoneme association (Ralston *et al.* 2006a), and the double silencing of two phosphodiesterases TbPDEB1 and TbPDEB2 (Oberholzer *et al.* 2007).

The severity and physical appearance of the RNAi phenotypes described showed compelling similarities to MCA4 downregulation. There are two possible explanations for this. Firstly, the BSF flagellum is particularly sensitive to

functional perturbations and any defect manifests in a terminal block in cytokinesis. This would support the concept of MCA4 playing a key role in maintaining correct BSF flagellar function or a more defined role in cytokinesis. The other flagellar mutants discussed associate with either the PFR or axoneme; thus the MCA4 investigation adds a third flagellar compartment (the membrane) to those already associated with maintenance of optimum flagellar function. The consistent phenotype observed in a variety of flagellar RNAi mutants adds weight to a broad argument supporting complete flagellar function as an absolute requirement for BSF viability (Portman *et al.* 2010). One interesting finding was that RNAi analysis of the flagellar mutants in PCF revealed no evidence for cell cycle defects or reduced viability (Portman *et al.* 2010; Ralston *et al.* 2008).

The second explanation for these common findings could be that this terminal phenotype is common to BSF RNAi mutants in general, where a wide range of cellular defects cause cells to accumulate at a critical cell cycle checkpoint, independent of flagellar function. Either way it points to MCA4 playing a role in maintaining flagellar function as opposed to a direct involvement in cytokinesis.

The severe RNAi phenotype implied MCA4 was an essential gene for BSF *T. brucei* and was likely to be refractory to genetic deletion. However, MCA2, MCA3 and MCA5 displayed collective essentiality when downregulated by RNAi but were open to genetic deletion (Helms *et al.* 2006). Similarly, it was possible to delete the MCA4 ORF by targeted replacement of both alleles with drug resistance cassettes. The severity of the MCA4 phenotype can perhaps be attributed to the rapid depletion of MCA4 occurring before parasite adaptation, whereas the sequential replacement of each MCA4 allele provided sufficient time for adjustment to diminishing MCA4 levels. Whether the contrasting RNAi and knockout phenotypes is specific only for the MCAs is unknown; attempting to knock out other BSF flagellar proteins previously shown to be essential by RNAi (Broadhead *et al.* 2006) could shed light on this interesting finding.

The $\Delta mca4$ cells were verified by Southern and western blotting, which confirmed the correct integration of the knockout constructs and the subsequent deletion of the MCA4 gene and protein from BSF 427 *T. brucei*. Analysis of cell growth *in vitro* revealed a reduced growth rate compared to the parental wild

type line, which could have been caused by a reduction in 1N2K cell types. However, unlike the RNAi phenotype no defects in cytokinesis were detected in $\Delta mca4$ cells, with cells appearing to divide normally. One crucial aspect of flagellum function that was amenable to quantitative analysis was motility. Live $\Delta mca4$ cells appeared morphological similar to wild type cells and sedimentation assays showed no apparent defects in flagellar motility. Although it is possible more sensitive analytical techniques could reveal subtle defects.

As MCA4 expression was only detected in BSF cells we speculated it could be involved in mediating mammalian infectivity. Indeed infection of mice with wild type and $\Delta mca4$ cells revealed strikingly different patterns of infection. The parasitemia of $\Delta mca4$ cells was subject to periods where parasites were undetectable as well as consecutive days with stable reduced parasite burdens. This contributed to prolonged mouse survival and revealed a role for MCA4 in parasite virulence within the mammalian host. Interestingly several other *T. brucei* flagellar proteins have been shown to influence parasitemia in mice. The deletion of the GPI-PLC created a prolonged infection in mice (although extended compared to $\Delta mca4$ parasites), that was accompanied by multiple peaks and troughs of parasitemia (Webb *et al.* 1997). In addition *in vivo* RNAi silencing of the calflagins (Tb17, Tb24 and Tb44) prolonged mouse survival by attenuating parasite growth (Emmer *et al.* 2010b). The infection was characterised by waves of parasitemia associated with the expression of alternative VSGs (Emmer *et al.* 2010b).

It has yet to be determined whether the waves of $\Delta mca4$ parasitemia were accompanied by a VSG switch but it seems likely the reduced virulence allowed the mouse immune system more time to clear the original infection before the re-emergence of a second wave of parasitemia of cells with a different VSG type. Whether prolonged mouse survival was directly linked to the loss of MCA4 reducing parasite virulence or arose from a MCA4 dependent interaction with the host is yet to be determined. Either way the identification of proteins such as MCA4 that influence the mammalian infection process is an important step in identifying new target for future therapeutic development.

The importance of MCA4 to BSF *T. brucei* has been demonstrated by RNAi and genetic knockout. The precise physiological role is still unclear but depends on

the catalytic activity of the protein. This was demonstrated by the re-expression of mutant MCA4 (no nucleophile in active site, MCA4^{C218G,S219G}) in the $\Delta mca4$ background. Successful expression of the protein was confirmed by western blot, however it failed to rescue the growth of phenotype of $\Delta mca4$ parasites in mice, confirming the necessity of enzymatic activity for MCA4 function.

In the absence of a confirmed physiological substrate(s) for MCA4, we can only speculate what roles the protein might play, some of which are discussed below.

4.4.4 Is MCA4 part of a signalling cascade?

One interesting finding that could have functional implications was the identification of two phosphorylation sites in MCA4. The two different sites of phosphorylation were identified as threonine 56 or 58 (Nett *et al.* 2009) and serine 341 (our experiments and Nett *et al.* 2009). The phosphorylation of peptidases is a wide spread phenomenon with diverse roles potentially influencing protein localisation and substrate specificity, as well as controlling catalytic activation and inactivation (Lopez-Otin *et al.* 2010).

One well characterised example of phosphorylation dependent peptidase activity is caspase-9. This heavily phosphorylated peptidase is subject to numerous phosphorylation events, one of which confers crucial regulation to the catalytic activity of this initiator caspase serving to control its role in apoptosis (Allan *et al.* 2009). The phosphorylation of threonine-125 inhibits caspase-9 proteolytic activation and consequently inhibits its ability to activate downstream targets (Allan *et al.* 2003). Threonine-125 is located in the flexible linker region between the caspase recruitment domain (CARD) and the large subunit of the processed enzyme. However, in the absence of structural data for the region surrounding threonine-125, the exact mechanism of inhibition is unknown. However, once phosphorylated at threonine-125, caspase-9 can still associate with apoptotic protease activating factor 1 (Apaf1, a key component of the apoptosome) which suggested that either phosphorylation blocked a conformational change required for activation or created a dominant negative effect inhibiting further activation of other caspase-9 associated with Apaf1 (Allan *et al.* 2009). Furthermore phosphorylation of serine-348, located between

the large and small subunit of murine caspase-9 protected aspartate-358 from caspase-8 mediated cleavage ensuring the protein remained inactive (McDonnell *et al.* 2008).

Further work is required to characterise the consequences of the MCA4 phosphorylation. Although the close proximity of a phosphorylation site (threonine-56 and/or threonine-58) to one of the identified locations of proteolytic processing (lysine-64) (Figure 4-21), raises the interesting possibility of phosphorylation regulating processing and thus activity. Another potential function of MCA4 phosphorylation could involve control of cellular trafficking, acting as a secondary signal facilitating flagellar targeting. The identification of the kinases and phosphatases responsible for controlling the phosphorylation status of MCA4 will no doubt be extremely important in helping to define the role of the protein.

Conversely the MCA4 proteolytic activity could be required to participate in specific signalling cascades. Recent work linking the human kinome (total kinase genes) and degradome (total peptidase genes) revealed that more than 100 of the 518 kinases are specifically regulated by peptidases (Lopez-Otin *et al.* 2010). This could involve kinase activation through the proteolytic cleavage of an inhibitory kinase domain or inactivation by degradation, well demonstrated by the many interactions between caspases and kinases (Kurokawa *et al.* 2009).

The flagellar membrane represents an interface between the parasite and the host environment. Flagellar proteins of other organisms are known to serve an important sensory and signal transduction role. For example the flagellate protozoan *Chlamydomonas reinhardtii* relies on flagellar cAMP signalling to mediate fusion of gametes and zygote formation. In response to nitrogen starvation vegetative cells differentiate into gametes of two opposite mating types (Pan *et al.* 2000). Flagellar adhesion of gametes from opposing mating type stimulates localisation of a flagellar membrane cyclic GMP-dependent protein kinase (PKG) (Wang *et al.* 2006). Calcium mediated activation of PKG stimulates adenylyl cyclase activity and drastically increases flagellar cAMP levels, which then permeate the cell body and facilitates cell fusion (Pan *et al.* 2000).

Interestingly many potential components of calcium and cyclic nucleotide signalling pathways have been identified in the *T. brucei* flagellum: the calflagins (Tb17, Tb24 and Tb44) a family of calcium binding proteins (Emmer *et al.* 2009; Tyler *et al.* 2009); an adenylate cyclase (expression site associated gene 4, ESAG.4) an enzyme that catalyses the conversion of ATP to cAMP in a calcium dependent fashion (Paindavoine *et al.* 1992); and two phosphodiesterases (TbPDEB1 and TbPDEB2) proteins associated with cAMP degradation and homeostasis (Oberholzer *et al.* 2007). This strongly suggests the presence of functional signalling cascades operating within the flagellum and it is possible MCA4 activity is required for some form of flagellar signal transduction.

It would seem unlikely that MCA4 is a primary activator protein because the recombinant enzyme required processing for activity. Therefore it could operate within a signalling cascade, responding to proteolytic activation from a calflagin-like protein or subtilisin -like peptidase, before processing downstream targets.

4.4.5 Is MCA4 involved in *T. brucei* flagellar metabolism?

The maintenance of flagellum function requires high levels of ATP and diffusion alone is unlikely to meet this demand, leading to potential ATP starvation in distal regions of the flagellum. Consequently flagellar specific metabolic networks are proposed to maintain ATP levels (Ginger *et al.* 2008). In *C. reinhardtii* the last three reactions of the glycolytic pathway were identified in the isolated flagellum and proposed to help provide ATP to maintain flagellar function (Mitchell *et al.* 2005). In *T. brucei* two adenyl kinases have been localised to the length of the flagellum and proposed to function in a phosphotransfer relay, delivering ATP and removing ADP as required in the flagellum (Pullen *et al.* 2004). Immunoprecipitation of MCA4 also surprisingly co-precipitated glycerol-3-phosphate dehydrogenase, an enzyme known to function in the in glycosome helping to maintain the redox balance (Michels *et al.* 2006). Given the abundance of many glycolytic enzymes non-specific contamination/interaction cannot yet be ruled out. However, interestingly glycerol-3-phosphate dehydrogenase has also been identified in the PCF flagellar proteome, thus adding tentative support to the co-immunoprecipitation result

(Hart *et al.* 2009). However the significance of such and interaction between MCA4 and glycerol-3-phosphate is not obviously explained.

4.4.6 Does MCA4 interact with the host following secretion?

Recently MCA4 was identified in the secretome (total secreted proteins) of two different *T. brucei gambiense* strains (Geiger *et al.* 2010). Proteins identified in several trypanosomatid secretomes were analysed *in silico* for the presence of classical N-terminal signal peptides. Those proteins predicted to contain eukaryotic signal peptides without any transmembrane domains were deemed to utilise the classic pathway for secretion. Using this bioinformatic approach only 14% of proteins in the *L. donovani* secretome were found to contain an N-terminal classical secretion signal sequence (Silverman *et al.* 2008) and similarly only 7% of the *T. brucei gambiense* secretome were identified accordingly (Geiger *et al.* 2010). Thus it seems likely that trypanosomatids utilise novel mechanisms for protein secretion, with two possible models suggested.

Recent experimental evidence revealed the presence of exosomes (30-100 nm vesicles released by many mammalian cell types) budding off the *Leishmania* cell body membrane and flagellar pocket (Silverman *et al.* 2008; Silverman *et al.* 2010). Proteomic characterisation of purified exosomes revealed they contained 52% of the total secretome suggesting it is prominent mechanism for delivery of proteins to the environment (Silverman *et al.* 2010). Additionally Emmer *et al.* speculate that the flagellar membrane itself could also be involved in vesicle shedding and release (Emmer *et al.* 2010a). This prediction stems in part from the identification of *T. cruzi* flagellar protein FCaBP in vesicles shed from the cell combined with the TEM and SEM evidence depicting vesicle budding and release from the tip of the *C. reinhardtii* flagellar (Bergman *et al.* 1975). However, recent evidence has been presented showing the budding of vesicles from undefined areas of the *T. brucei* cell membrane (Geiger *et al.* 2010). Although this process has only been visualised by TEM so further analysis is required.

Alternatively MCA4 could be actively secreted out of the flagellar pocket. This would presumably require release from the flagellar membrane, occurring either via the reversal of palmitoylation (catalysed by a PAT protein) to diminish

membrane association or by proteolytic cleavage to separate the activated form of MCA4 from the N-terminal portion left in the flagellar membrane.

Irrespective of the secretion mechanism used, MCA4 was detected as part of the secretome (Geiger *et al.* 2010) which raises very interesting questions regarding its potential functions. Initial attempts to detect MCA4 in the serum of *T. brucei* infected mice by western blotting were inconclusive, however further investigation is clearly warranted to enable a more comprehensive definition of MCA4 function.

		1		70
LmMCA	(1)	-----	-----	-----MADLFDIWCTGAVASLIPMIGAN
TbMCA5	(1)	-----	-----	-----MDAALALLFGQVAVLPIVYVWN
Atmc1	(1)	-----	-----	-----MYP P P P S S I Y A P P M L V N C S C C R T P L Q L P S G A R S L R C A L C Q A V T H L A
Ycal	(1)	MYP	GSGRYTYNNA	GCGNCGYQRPMAPPPNQYCGQQYCYQYRQQYCYQQQNDQYQFQQYVAPP
Atmc9	(1)	-----	-----	-----
TbMCA2	(1)	-----	-----	-----MCSLITQLCDAGQLADYVGLGWLNAVSSQPYLVQ
TbMCA3	(1)	-----	-----	-----MAVDPRCLLSLCS TISKASSAGTNDVFKLIGELWQT AQP YLVQ
TbMCA1	(1)	-----	-----	-----MSSEKVAQYVQCVVGIIFGVVTGGASIVVTIDMELLLQVAVPYLVV
TbMCA4	(1)	-----	-----	-----MGGCVSTALRVCARTVAREGHIDLISFALINYPFNAVPYLVK
		71		140
LmMCA	(23)	CLL	LVDFPP	-----KQVDVNA
TbMCA5	(23)	SLG	RVVPP	-----KQVDVRFKAMCEAHQCRPVVPPYR
Atmc1	(47)	DPRT	ADPP	-----QPSAP
Ycal	(71)	NRP	YVPP	PFQFQEQAKAQLSMGYNPNVNASNMYGPPQMSL
Atmc9	(1)	-----	-----	-----MDQQGMVGRRLAVL
TbMCA2	(35)	ALC	IQPP	-----RQVDVDA
TbMCA3	(45)	ALC	IQPP	-----PKVDVDA
TbMCA1	(46)	TLC	IQRP	-----PKCVDK
TbMCA4	(41)	YLG	PQRP	-----KQVDEATL
		141		210
LmMCA	(67)	ICIN	YTSIRNALRGC	VNDVSSMLLQTLQIISFPIS
TbMCA5	(67)	ICIN	YTSIRNALRGC	VNDVSSMLLQTLQIISFPIS
Atmc1	(85)	CCIS	YRFRS	RHELRGCINDARCMRHLLIN-KRFRS
Ycal	(141)	ICIN	YTSIRNALRGC	VNDVSSMLLQTLQIISFPIS
Atmc9	(15)	YCC	NYPT	RNELHGCINDVLANKEIIS-RFC
TbMCA2	(78)	ICIN	YTSIRNALRGC	VNDVSSMLLQTLQIISFPIS
TbMCA3	(88)	ICIN	YTSIRNALRGC	VNDVSSMLLQTLQIISFPIS
TbMCA1	(88)	ICID	YRGT	PARLRGCQADAVMMACTHETIC
TbMCA4	(84)	ICV	YVGT	EAQLS
		211		
LmMCA	(137)	C--	DVLF	FFHYSCHGCAKATR-DSEKRYD
TbMCA5	(137)	C--	DVLF	FFHYSCHGCAKATR-DSEKRYD
Atmc1	(154)	C--	DVLF	FFHYSCHGCAKATR-DSEKRYD
Ycal	(210)	N--	DVLF	FFHYSCHGCAKATR-DSEKRYD
Atmc9	(83)	CSC	NTL	FFHYSCHGCAKATR-DSEKRYD
TbMCA2	(148)	C--	DVLF	FFHYSCHGCAKATR-DSEKRYD
TbMCA3	(158)	C--	DVLF	FFHYSCHGCAKATR-DSEKRYD
TbMCA1	(158)	C--	DVLF	FFHYSCHGCAKATR-DSEKRYD
TbMCA4	(154)	N--	DVLF	FFHYSCHGCAKATR-DSEKRYD
		281		350
LmMCA	(204)	SAS	MLD	-----LPS
TbMCA5	(204)	SAS	MLD	-----LPA
Atmc1	(222)	SCI	VLD	-----LPL
Ycal	(278)	SCI	VLD	-----LPT
Atmc9	(149)	SCG	MLD	-----LPA
TbMCA2	(215)	SCS	MLD	-----LPT
TbMCA3	(225)	SCS	MLD	-----LPT
TbMCA1	(224)	ACT	MLD	-----LPS
TbMCA4	(221)	SCS	MLD	-----LPA
		351		420
LmMCA	(221)	-----	-----	-----GCGACEYH
TbMCA5	(221)	-----	-----	-----SSNQREH
Atmc1	(239)	-----	-----	-----QYVWEDH
Ycal	(318)	NRA	ALIC	LSGIFKTVKCGMNVDR
Atmc9	(219)	-----	-----	-----LKFRLP
TbMCA2	(232)	-----	-----	-----QAS
TbMCA3	(242)	-----	-----	-----QAS
TbMCA1	(240)	-----	-----	-----DCS
TbMCA4	(238)	-----	-----	-----DGS

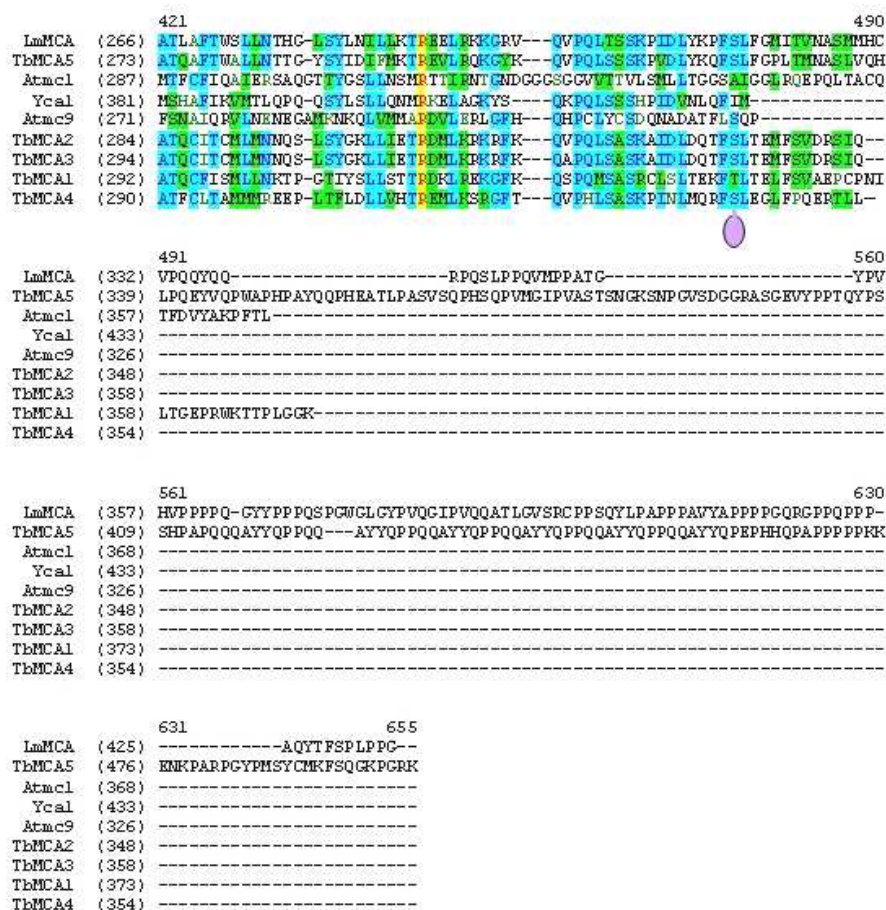


Figure 4-21 Alignments of select metacaspase proteins

Selected regions of Vector NTI protein sequence alignment of MCA proteins, tritrypDB and accession numbers in brackets: LmMCA (LmjF35.1580), TbMCA5 (Tb09.211.4760), Atmc1 (AAP44514.1), Yca1 (NP_014840.2), Atmc9 (NP_196040.1), TbMCA2 (Tb927.6.940), TbMCA3 (Tb927.6.930), TbMCA1 (Tb11.02.0730) and TbMCA4 (Tb927.10.2440). Sequences aligned using Clustal W algorithm of the Align X program. Identical and conserved amino acids are highlighted yellow and blue respectively. Blocks of similar sequences are highlighted in green and green coloured text indicates weak conservation. Numbers in brackets indicate the position of the first amino acid in the linear polypeptide in the section of each protein analysed. The red and grey arrows indicate the position of the canonical metacaspase active site histidine and cysteine residues, respectively. The back arrows indicate additional cysteine with potential catalytic activity. The blue arrowheads label the aspartic acid residues predicted to comprise the enzyme S1 pocket. Red asterisks above alignment indicate MCA2 and MCA4 processing sites, with P1 residue coloured red. MCA4 phosphorylation sites identified in this study and by (Nett *et al.* 2009), marked beneath the alignment with purple ovals.

5 General discussion

5.1.1 Autophagy in *T. brucei* – future perspective

Using fluorescently labelled ATG8 proteins expressed in *T. brucei* it was possible to monitor the formation of autophagosomes and provide direct evidence of a functional autophagy system. As expected autophagy in PCF *T. brucei* is upregulated in response to nutrient starvation and inhibited by the classical autophagy inhibitor wortmannin. Furthermore, an increased autophagic response is induced in BSF cells following treatment with the neuropeptide VIP.

This work has characterised specific components of the *T. brucei* autophagy pathway and revealed that autophagy plays a role in responding to stress. However to provide a more thorough understanding of autophagy in *T. brucei*, future work could be developed pursuing two main themes: physiological functions and molecular machinery.

To characterise the molecular machinery of autophagy RNAi downregulation represents a quick and effective method of targeting and studying select proteins. To facilitate future investigations constructs expressing YFP-ATG8.2 and YFP-ATG8.3 have been created and integrated into PCF (13 -29) RNAi cell lines (Wirtz *et al.* 1999). These parasites cell lines are intended to act as autophagosome reporter lines for use with RNAi based screens. This should serve to validate the action of known autophagy orthologues and crucially help in the discovery of new proteins involved in the pathway.

Having successfully validated the use of YFP-tagging to monitor autophagy in monomorphic *T. brucei*, similar tools could be developed for pleiomorphic fly transmissible strains. This would allow for thorough investigation of autophagy in all forms of the parasite in both the mammalian and insect hosts, providing crucial insights into differentiation processes.

This investigation has begun to expand the known roles of autophagy through the targeted downregulation of a key component of the autophagy pathway (ATG3). This reduced PCF growth, however it is currently unclear whether this stemmed

from inhibition of autophagy or interference with another cellular function of the ATG3 protein. If downregulation of ATG3 does indeed block autophagy then silencing ATG3 by RNAi could be used to identify further physiological processes requiring a functional autophagy system.

5.1.2 MCA4 – proposed model of activation

The research carried out on MCA4 provided some interesting and surprising findings. Drawing all the data generated together and including concepts covered in the discussion of section 4.4, we have developed a proposed model for the regulation and activation of MCA4 (Figure 5-1).

We hypothesise that following synthesis of MCA4, the protein is trafficked to the flagellar membrane where it is anchored in position by N-terminal dual acylation. Full length MCA4 remains associated to the flagellar membrane as an inactive peptidase and the autolytic activation of MCA4 is restricted by serine-219.

To activate MCA4 a proteolytic cleavage event, potentially occurring at lysine-64, is performed by an upstream peptidase. The exact process used to convert the MCA4 zymogen is unknown, however by extrapolating from established systems of peptidase inhibition and activation we can predict potential mechanisms. Effector caspases require proteolytic cleavage to reorganise the active site of the dimerized P10 and P20 subunits (Fuentes-Prior *et al.* 2004). It is possible proteolytic cleavage of the MCA4 zymogen causes a conformational change favouring activity (perhaps similar to the conformational change prediction for Atmc9, as discussed in section 4.1.10), however the release of P10-like and P20-like subunits was not detected for MCA4. An alternative activation hypothesis centres on a possible inhibitory effect of the MCA4 N-terminal region. This is a common mechanism used to control enzyme activity and has been well characterised for the cathepsins (clan CA, family C1), where the N-terminal propeptide occupies the active site preventing substrate access (Groves *et al.* 1998). Accordingly it is possible that proteolytic cleavage at lysine-64 serves to separate the mature MCA4 from the inhibitory properties of the N-terminal region.

In our model a further level of regulation is added by phosphorylation of threonine-56 and threonine-58, a modification that serves to protect the lysine from proteolytic activity of the activating peptidase. Therefore following the appropriate signals MCA4 is dephosphorylated and activated by an unknown flagellar peptidase which releases MCA4 from the flagellar membrane. Alternatively palmitoylation could be reversed by the activity of a flagellar localised palmitoyl acyltransferase and MCA4 released for subsequent activation by proteolytic reorganisation of the active site.

The activated MCA4 is then either able to interact with proteins in the flagellum or is secreted from *T. brucei* for interaction with the host.

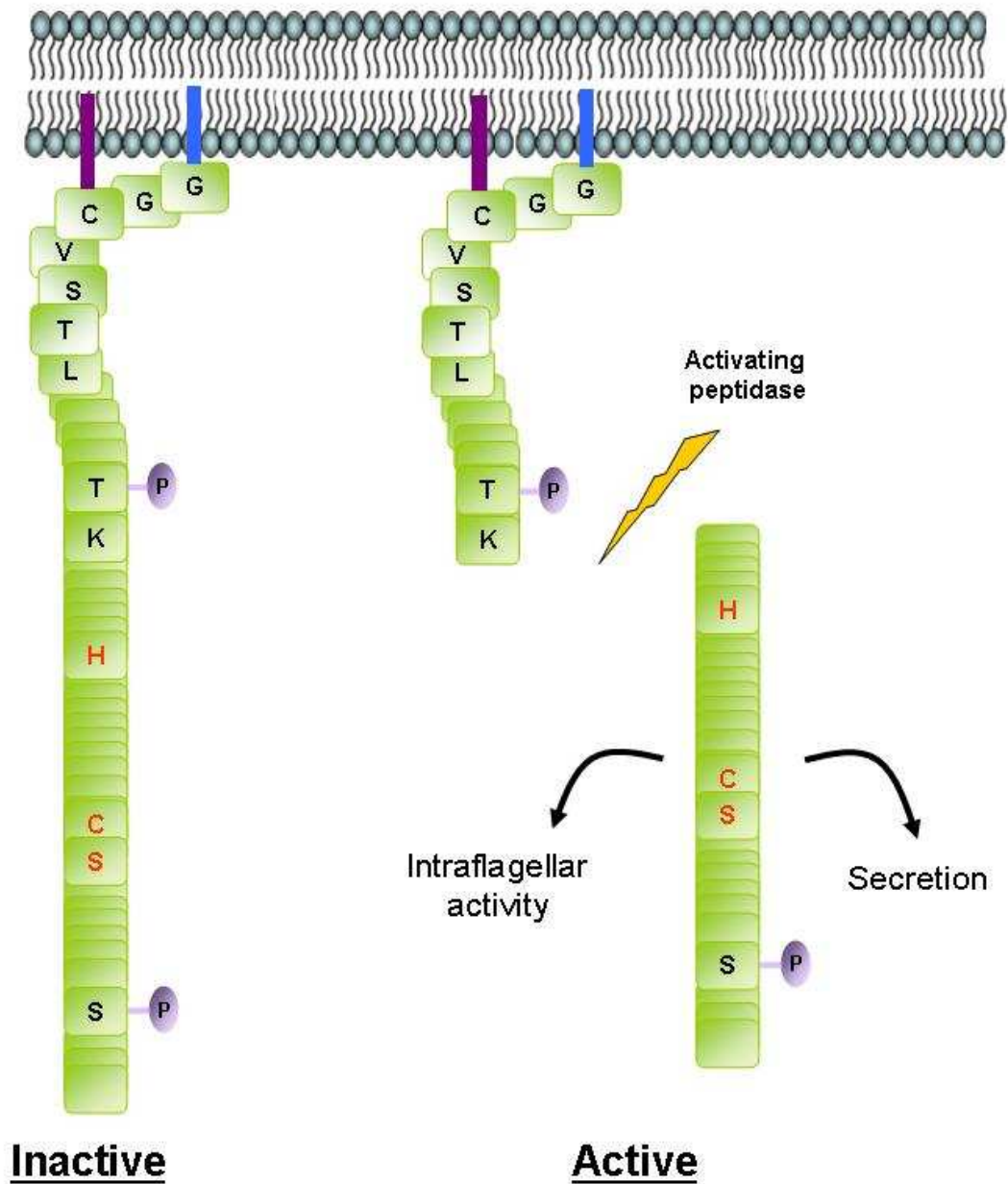


Figure 5-1 Model for MCA4 activation.

Schematic representation of inactive MCA4 attached to the flagellar membrane and subsequent release of active MCA4 following proteolytic cleavage. MCA4 protein depicted in green boxes with select amino acids in black depicting: the N-terminal region; phosphorylated residues threonine-56/58 and serine-341 labelled with purple circles and site of proteolytic cleavage lysine-64. Predicted active site residues coloured in red. N-myristoylation of glycine-2 indicated with blue bar and palmitoylation of cysteine-4 indicated with purple bar.

5.1.3 Interplay between autophagy and MCAs

The two main topics covered in this work appear to represent different and distinct aspects of cell biology. However recent work in yeast has revealed a link between the autophagic degradation of protein aggregates and the yeast MCA (Yca1) (Lee *et al.* 2010). In mammalian cells it is well known that autophagy plays a critical role in mediating the turnover of proteins prone to aggregate formation. In fact the accumulation of such protein aggregates in neuronal cells has been associated with several neurodegenerative diseases, including Alzheimers, Parkinsons and Huntingdons (Levine *et al.* 2008; Mizushima *et al.* 2008).

As part of continuing efforts to characterise potential non cell death functions of Yca1, it was discovered that deletion or inactivation of this protein changed progression of the cell cycle by elongating G1 phase and disrupting a G2/M checkpoint (discussed in section 4.1.9) (Lee *et al.* 2008). Further evidence for a role of Yca1 promoting cell viability was provided by proteomic analysis of Yca1 cells. This revealed an increased level of stress response chaperones and proteins involved in vacuolar degradation, suggesting activation of compensating stress pathways (Lee *et al.* 2010). The specific cellular stress induced by Yca1 deletion was identified as the accumulation of protein aggregates. Indeed following the artificial induction of protein aggregate formation (heat shock at 42°C), fluorescently labelled Yca1 translocated from the cytoplasm and colocalised with aggregate remodelling chaperones and insoluble protein aggregates (Lee *et al.* 2010). Interestingly, both deletion and inactivation of Yca1 lead to an accumulation of protein aggregates in yeast cells, however the effect was partly reduced by proteolytic activation (Lee *et al.* 2010). Importantly the targeting of Yca1 to insoluble aggregates was controlled by the prodomain region (Lee *et al.* 2010). This region of Yca1 is rich in glutamine and asparagine repeats and is predicted to possess prion-like functions (Nemecek *et al.* 2009). Indeed removal of the prodomain region caused mislocalisation and spontaneous autolytic processing of Yca1 (Lee *et al.* 2010).

Based on these findings Lee and co-workers proposed a model where Yca1 targets and facilitates the clearance of protein aggregates, either directly by

proteolytic degradation or through the formation of a Yca1 scaffold that serves to facilitate the enzymatic activity of other aggregate processing enzymes (Lee *et al.* 2010). Thus in the absence of Yca1, the autophagic pathway is up-regulated to help clear aggregated proteins (Lee *et al.* 2010). This shows that MCAs and autophagy both play vital roles in maintaining cellular equilibrium. In *T. brucei* this is perhaps most relevant to MCA2, MCA3 and MCA5. These three MCAs possess N-terminal prodomains (of unknown function) and have all been shown to localise to RAB11 positive recycling endosomes (Helms *et al.* 2006). To date the role of these MCA associated RAB11 endosomes is unknown, but it is tempting to speculate they may be involved in the removal of unwanted protein aggregates.

6 References

- Absalon, S., Blisnick, T., Kohl, L., Toutirais, G., Dore, G., Julkowska, D., Tavenet, A., & Bastin, P. 2008, "Intraflagellar Transport and Functional Analysis of Genes Required for Flagellum Formation in Trypanosomes", *Molecular Biology of the Cell*, vol. 19, no. 3, pp. 929-944.
- Ackers, J. P., Dhir, V., & Field, M. C. 2005, "A bioinformatic analysis of the RAB genes of *Trypanosoma brucei*", *Molecular and Biochemical Parasitology*, vol. 141, no. 1, pp. 89-97.
- Acosta-Serrano, A., Cole, R. N., Mehlert, A., Lee, M. G. S., Ferguson, M. A. J., & Englund, P. T. 1999, "The procyclin repertoire of *Trypanosoma brucei* - Identification and structural characterization of the Glu-Pro-rich polypeptides", *Journal of Biological Chemistry*, vol. 274, no. 42, pp. 29763-29771.
- Akoda, K., Van den Abbeele, J., Marcotty, T., De Deken, R., Sidibe, I., & Van den Bossche, P. 2009, "Nutritional stress of adult female tsetse flies (Diptera: Glossinidae) affects the susceptibility of their offspring to trypanosomal infections", *Acta Tropica*, vol. 111, no. 3, pp. 263-267.
- Aksoy, S., Gibson, W. C., & Lehane, M. J. 2003, "Interactions between tsetse and trypanosomes with implications for the control of trypanosomiasis", *Advances in Parasitology*, Vol 53, vol. 53, pp. 1-83.
- Allan, L. A. & Clarke, P. R. 2009, "Apoptosis and autophagy: Regulation of caspase-9 by phosphorylation", *Febs Journal*, vol. 276, no. 21, pp. 6063-6073.
- Allan, L. A., Morrice, N., Brady, S., Magee, G., Pathak, S., & Clarke, P. R. 2003, "Inhibition of caspase-9 through phosphorylation at Thr 125 by ERK MAPK", *Nature Cell Biology*, vol. 5, no. 7, p. 647-U45.
- Alvarez, V. E., Kosec, G., Anna, C. S., Turk, V., Cazzulo, J. J., & Turk, B. 2008, "Autophagy is involved in nutritional stress response and differentiation in *Trypanosoma cruzi*", *Journal of Biological Chemistry*, vol. 283, no. 6, pp. 3454-3464.
- Amar, N., Lustig, G., Ichimura, Y., Ohsumi, Y., & Elazar, Z. 2006, "Two newly identified sites in the ubiquitin-like protein Atg8 are essential for autophagy", *Embo Reports*, vol. 7, no. 6, pp. 635-642.
- Ambit, A., Fasel, N., Coombs, G. H., & Mottram, J. C. 2007, "An essential role for the *Leishmania major* metacaspase in cell cycle progression", *Cell Death Differ*, vol. 15, no. 1, pp. 113-122.

- Aravind, L., Dixit, V. M., & Koonin, E. V. 1999, "The domains of death: evolution of the apoptosis machinery", *Trends in Biochemical Sciences*, vol. 24, no. 2, pp. 47-53.
- Atkinson, H. J., Babbitt, P. C., & Sajid, M. 2009, "The global cysteine peptidase landscape in parasites", *Trends in Parasitology*, vol. 25, no. 12, pp. 573-581.
- Attardo, G. M., Strickler-Dinglasan, P., Perkin, S. A. H., Caler, E., Bonaldo, M. F., Soares, M. B., El Sayeed, N., & Aksoy, S. 2006, "Analysis of fat body transcriptome from the adult tsetse fly, *Glossina morsitans morsitans*", *Insect Molecular Biology*, vol. 15, no. 4, pp. 411-424.
- Axe, E. L., Walker, S. A., Manifava, M., Chandra, P., Roderick, H. L., Habermann, A., Griffiths, G., & Ktistakis, N. T. 2008, "Autophagosome formation from membrane compartments enriched in phosphatidylinositol 3-phosphate and dynamically connected to the endoplasmic reticulum", *The Journal of Cell Biology*, vol. 182, no. 4, pp. 685-701.
- Bandyopadhyay, U., Sridhar, S., Kaushik, S., Kiffin, R., & Cuervo, A. M. 2010, "Identification of Regulators of Chaperone-Mediated Autophagy", *Molecular Cell*, vol. 39, no. 4, pp. 535-547.
- Barbet, N. C., Schneider, U., Helliwell, S. B., Stansfield, I., Tuite, M. F., & Hall, M. N. 1996, "TOR controls translation initiation and early G1 progression in yeast", *Molecular Biology of the Cell*, vol. 7, no. 1, pp. 25-42.
- Baron, D. M., Ralston, K. S., Kabututu, Z. P., & Hill, K. L. 2007, "Functional genomics in *Trypanosoma brucei* identifies evolutionarily conserved components of motile flagella", *Journal of Cell Science*, vol. 120, no. 3, pp. 478-491.
- Barquilla, A., Crespo, J. L., & Navarro, M. 2008, "Rapamycin inhibits trypanosome cell growth by preventing TOR complex 2 formation", *Proceedings of the National Academy of Sciences of the United States of America*, vol. 105, no. 38, pp. 14579-14584.
- Barquilla, A. & Navarro, M. 2009, "Trypanosome TOR as a major regulator of cell growth and autophagy", *Autophagy*, vol. 5, no. 2, pp. 256-258.
- Barrett, M. P., Boykin, D. W., Brun, R., & Tidwell, R. R. 2007, "Human African trypanosomiasis: pharmacological re-engagement with a neglected disease", *British Journal of Pharmacology*, vol. 152, no. 8, pp. 1155-1171.
- Bastin, P., Pullen, T. J., Sherwin, T., & Gull, K. 1999, "Protein transport and flagellum assembly dynamics revealed by analysis of the paralysed trypanosome mutant *snl-1*", *Journal of Cell Science*, vol. 112, no. 21, pp. 3769-3777.
- Bastin, P., Sherwin, T., & Gull, K. 1998, "Paraflagellar rod is vital for trypanosome motility", *Nature*, vol. 391, no. 6667, p. 548.

- Behrends, C., Sowa, M. E., Gygi, S. P., & Harper, J. W. 2010, "Network organization of the human autophagy system", *Nature*, vol. 466, no. 7302, pp. 68-76.
- Belenghi, B., Romero-Puertas, M. C., Vercammen, D., Brackenier, A., Inz+®, D., Delledonne, M., & Van Breusegem, F. 2007, "Metacaspase Activity of *Arabidopsis thaliana* Is Regulated by S-Nitrosylation of a Critical Cysteine Residue", *Journal of Biological Chemistry*, vol. 282, no. 2, pp. 1352-1358.
- Benzel, I., Weise, F., & Wiese, M. 2000, "Deletion of the gene for the membrane-bound acid phosphatase of *Leishmania mexicana*", *Molecular and Biochemical Parasitology*, vol. 111, no. 1, pp. 77-86.
- Berg, M., Van der Veken, P., Joossens, J., Muthusamy, V., Breugelmans, M., Moss, C. X., Rudolf, J., Cos, P., Coombs, G. H., Maes, L., Haemers, A., Mottram, J. C., & Augustyns, K. 2010, "Design and evaluation of *Trypanosoma brucei* metacaspase inhibitors", *Bioorganic & Medicinal Chemistry Letters*, vol. 20, no. 6, pp. 2001-2006.
- Bergman, K., Goodenough, U. W., Goodenough, D. A., Jawitz, J., & Martin, H. 1975, "Gametic differentiation in *Chlamydomonas reinhardtii*. II. Flagellar membranes and the agglutination reaction", *The Journal of Cell Biology*, vol. 67, no. 3, pp. 606-622.
- Berriman, M., Ghedin, E., Hertz-Fowler, C., Blandin, G., Renauld, H., Bartholomeu, D. C., Lennard, N. J., Caler, E., Hamlin, N. E., Haas, B., Bohme, U., Hannick, L., Aslett, M. A., Shallom, J., Marcello, L., Hou, L., Wickstead, B., Alsmark, U. C., Arrowsmith, C., Atkin, R. J., Barron, A. J., Bringaud, F., Brooks, K., Carrington, M., Cherevach, I., Chillingworth, T. J., Churcher, C., Clark, L. N., Corton, C. H., Cronin, A., Davies, R. M., Doggett, J., Djikeng, A., Feldblyum, T., Field, M. C., Fraser, A., Goodhead, I., Hance, Z., Harper, D., Harris, B. R., Hauser, H., Hostetler, J., Ivens, A., Jagels, K., Johnson, D., Johnson, J., Jones, K., Kerhornou, A. X., Koo, H., Larke, N., Landfear, S., Larkin, C., Leech, V., Line, A., Lord, A., MacLeod, A., Mooney, P. J., Moule, S., Martin, D. M. A., Morgan, G. W., Mungall, K., Norbertczak, H., Ormond, D., Pai, G., Peacock, C. S., Peterson, J., Quail, M. A., Rabinowitsch, E., Rajandream, M. A., Reitter, C., Salzberg, S. L., Sanders, M., Schobel, S., Sharp, S., Simmonds, M., Simpson, A. J., Tallon, L., Turner, C. M., Tait, A., Tivey, A. R., Van Aken, S., Walker, D., Wanless, D., Wang, S., White, B., White, O., Whitehead, S., Woodward, J., Wortman, J., Adams, M. D., Embley, T. M., Gull, K., Ullu, E., Barry, J. D., Fairlamb, A. H., Opperdoes, F., Barrell, B. G., Donelson, J. E., Hall, N., Fraser, C. M., Melville, S. E., & El Sayed, N. M. 2005, "The Genome of the African Trypanosome *Trypanosoma brucei*", *Science*, vol. 309, no. 5733, pp. 416-422.
- Besteiro, S., Williams, R. A. M., Morrison, L. S., Coombs, G. H., & Mottram, J. C. 2006, "Endosome sorting and autophagy are essential for differentiation and virulence of *Leishmania major*", *Journal of Biological Chemistry*, vol. 281, no. 16, pp. 11384-11396.
- Blackman, M. J. 2008, "Malarial proteases and host cell egress: an 'emerging' cascade", *Cellular Microbiology*, vol. 10, no. 10, pp. 1925-1934.

- Blommaart, E. F. C., Krause, U., Schellens, J. P. M., VreelingSindelarova, H., & Meijer, A. J. 1997, "The phosphatidylinositol 3-kinase inhibitors wortmannin and LY294002 inhibit autophagy in isolated rat hepatocytes", *European Journal of Biochemistry*, vol. 243, no. 1-2, pp. 240-246.
- Boatright, K. M., Renatus, M., Scott, F. L., Sperandio, S., Shin, H., Pedersen, I. M., Ricci, J. E., Edris, W. A., Sutherlin, D. P., Green, D. R., & Salvesen, G. S. 2003, "A Unified Model for Apical Caspase Activation", *Molecular Cell*, vol. 11, no. 2, pp. 529-541.
- Bonneau, L., Ge, Y., Drury, G. E., & Gallois, P. 2008, "What happened to plant caspases?", *Journal of Experimental Botany*, vol. 59, no. 3, pp. 491-499.
- Bozhkov, P. V., Suarez, M. F., Filonova, L. H., Daniel, G., Zamyatnin, A. A., Rodriguez-Nieto, S., Zhivotovsky, B., & Smertenko, A. 2005, "Cysteine protease mcll-Pa executes programmed cell death during plant embryogenesis", *Proceedings of the National Academy of Sciences of the United States of America*, vol. 102, no. 40, pp. 14463-14468.
- Broadhead, R., Dawe, H. R., Farr, H., Griffiths, S., Hart, S. R., Portman, N., Shaw, M. K., Ginger, M. L., Gaskell, S. J., Mckean, P. G., & Gull, K. 2006, "Flagellar motility is required for the viability of the bloodstream trypanosome", *Nature*, vol. 440, no. 7081, pp. 224-227.
- Brun, R., Blum, J., Chappuis, F., & Burri, C. 2010, "Human African trypanosomiasis", *Lancet*, vol. 375, no. 9709, pp. 148-159.
- Buttner, S., Eisenberg, T., Herker, E., Carmona-Gutierrez, D., Kraemer, G., & Madeo, F. 2006, "Why yeast cells can undergo apoptosis: death in times of peace, love, and war", *Journal of Cell Biology*, vol. 175, no. 4, pp. 521-525.
- Carmona-Gutierrez, D., Frohlich, K. U., Kroemer, G., & Madeo, F. 2010, "Metacaspases are caspases. Doubt no more", *Cell Death Differ*, vol. 17, no. 3, pp. 377-378.
- Checchi, F., Filipe, J., Haydon, D., Chandramohan, D., & Chappuis, F. 2008, "Estimates of the duration of the early and late stage of gambiense sleeping sickness", *BMC Infectious Diseases*, vol. 8, no. 1, p. 16.
- Chen, J. H., Rauch, C. A., White, J. H., Englund, P. T., & Cozzarelli, N. R. 1995, "The Topology of the Kinetoplast Dna Network", *Cell*, vol. 80, no. 1, pp. 61-69.
- Croall, D. E. & Ersfeld, K. 2007, "The calpains: modular designs and functional diversity", *Genome Biology*, vol. 8, no. 6.
- Cross, G. A. M. 1975, "Identification, purification and properties of clone-specific glycoprotein antigens constituting the surface coat of *Trypanosoma brucei*", *Parasitology*, vol. 71, no. 03, pp. 393-417.
- Cuervo, A. M. 2010, "Chaperone-mediated autophagy: selectivity pays off", *Trends in Endocrinology & Metabolism*, vol. 21, no. 3, pp. 142-150.

- Dacks, J. B., Walker, G., & Field, M. C. 2008, "Implications of the new eukaryotic systematics for parasitologists", *Parasitology International*, vol. 57, no. 2, pp. 97-104.
- Danial, N. N. & Korsmeyer, S. J. 2004, "Cell death: Critical control points", *Cell*, vol. 116, no. 2, pp. 205-219.
- de Duve, C. & Wattiaux, R. 1966, "Functions of Lysosomes", *Annual Review of Physiology*, vol. 28, no. 1, pp. 435-492.
- Delgado, M., Anderson, P., Garcia-Salcedo, J. A., Caro, M., & Gonzalez-Rey, E. 2008, "Neuropeptides kill African trypanosomes by targeting intracellular compartments and inducing autophagic-like cell death", *Cell Death Differ*, vol. 16, no. 3, pp. 406-416.
- Denny, P. W., Gokool, S., Russell, D. G., Field, M. C., & Smith, D. F. 2000, "Acylation-dependent Protein Export in *Leishmania*", *Journal of Biological Chemistry*, vol. 275, no. 15, pp. 11017-11025.
- Dessens, J. T. & Lomonosoff, G. P. 1991, "Mutational analysis of the putative catalytic triad of the cowpea mosaic virus 24K protease", *Virology*, vol. 184, no. 2, pp. 738-746.
- Dias da Silva, W. & Tambourgi, D. V. 2010, "IgY: A promising antibody for use in immunodiagnostic and in immunotherapy", *Veterinary Immunology and Immunopathology*, vol. 135, no. 3-4, pp. 173-180.
- Dice, J. F. 2007, "Chaperone-mediated autophagy", *Autophagy*, vol. 3, no. 4, pp. 295-299.
- Docampo, R., De Souza, W., Miranda, K., Rohloff, P., & Moreno, S. N. J. 2005, "Acidocalcisomes - Conserved from bacteria to man", *Nature Reviews Microbiology*, vol. 3, no. 3, pp. 251-261.
- Dunn, W. A., Cregg, J. M., Kiel, J. A. K. W., van der Klei, I. J., Oku, M., Sakai, Y., Sibirny, A. A., Stasyk, O. V., & Veenhuis, M. 2005, "Pexophagy - The selective autophagy of peroxisomes", *Autophagy*, vol. 1, no. 2, pp. 75-83.
- Elmore, S. 2007, "Apoptosis: A review of programmed cell death", *Toxicologic Pathology*, vol. 35, no. 4, pp. 495-516.
- Emmer, B. T., Maric, D., & Engman, D. M. 2010a, "Molecular mechanisms of protein and lipid targeting to ciliary membranes", *Journal of Cell Science*, vol. 123, no. 4, pp. 529-536.
- Emmer, B. T., Daniels, M. D., Taylor, J. M., Epting, C. L., & Engman, D. M. 2010b, "Calflagin Inhibition Prolongs Host Survival and Suppresses Parasitemia in *Trypanosoma brucei* Infection", *Eukaryotic Cell*, vol. 9, no. 6, pp. 934-942.
- Emmer, B. T., Souther, C., Toriello, K. M., Olson, C. L., Epting, C. L., & Engman, D. M. 2009, "Identification of a palmitoyl acyltransferase required for protein sorting to the flagellar membrane", *Journal of Cell Science*, vol. 122, no. 6, pp. 867-874.

- Engstler, M. & Boshart, M. 2004a, "Cold shock and regulation of surface protein trafficking convey sensitization to inducers of stage differentiation in *Trypanosoma brucei*", *Genes & Development*, vol. 18, no. 22, pp. 2798-2811.
- Engstler, M., Pfohl, T., Herminghaus, S., Boshart, M., Wiegertjes, G., Heddergott, N., & Overath, P. 2007, "Hydrodynamic Flow-Mediated Protein Sorting on the Cell Surface of Trypanosomes", *Cell*, vol. 131, no. 3, pp. 505-515.
- Engstler, M., Thilo, L., Weise, F., Grunfelder, C. G., Schwarz, H., Boshart, M., & Overath, P. 2004b, "Kinetics of endocytosis and recycling of the GPI-anchored variant surface glycoprotein in *Trypanosoma brucei*", *Journal of Cell Science*, vol. 117, no. 7, pp. 1105-1115.
- Enoksson, M. & Salvesen, G. S. 2010, "Metacaspases are not caspases - always doubt", *Cell Death Differ*, vol. 17, no. 8, p. 1221.
- Ersfeld, K., Barraclough, H., & Gull, K. 2005, "Evolutionary relationships and protein domain architecture in an expanded calpain superfamily in kinetoplastid parasites", *Journal of Molecular Evolution*, vol. 61, no. 6, pp. 742-757.
- Field, M. C., Allen, C. L., Dhir, V., Goulding, D., Hall, B. S., Morgan, G. W., Veazey, P., & Engstler, M. 2004, "New approaches to the microscopic imaging of *Trypanosoma brucei*", *Microscopy and Microanalysis*, vol. 10, no. 5, pp. 621-636.
- Field, M. C. & Carrington, M. 2009, "The trypanosome flagellar pocket", *Nat Rev Micro*, vol. 7, no. 11, pp. 775-786.
- Figarella, K., Rawer, M., Uzcategui, N. L., Kubata, B. K., Lauber, K., Madeo, F., Wesselborg, S., & Duszenko, M. 2005, "Prostaglandin D2 induces programmed cell death in *Trypanosoma brucei* bloodstream form", *Cell Death Differ*, vol. 12, no. 4, pp. 335-346.
- Fridberg, A., Buchanan, K. T., & Engman, D. M. 2007, "Flagellar membrane trafficking in kinetoplastids", *Parasitology Research*, vol. 100, no. 2, pp. 205-212.
- Frisch, S. M. 2008, "Caspase-8: Fly or die", *Cancer Research*, vol. 68, no. 12, pp. 4491-4493.
- Fuentes-Prior, P. & Salvesen, G. S. 2004, "The protein structures that shape caspase activity, specificity, activation and inhibition", *Biochemical Journal*, vol. 384, pp. 201-232.
- Geiger, A., Hirtz, C., Becue, T., Bellard, E., Centeno, D., Gargani, D., Rossignol, M., Cuny, G., & Peltier, J. B. 2010, "Exocytosis and protein secretion in *Trypanosoma*", *BMC Microbiology*, vol. 10, no. 1, p. 20.
- Geng, J. & Klionsky, D. J. 2008, "The Atg8 and Atg12 ubiquitin-like conjugation systems in macroautophagy", *EMBO Rep*, vol. 9, no. 9, pp. 859-864.

- Ginger, M. L., Portman, N., & Mckean, P. G. 2008, "Swimming with protists: perception, motility and flagellum assembly", *Nature Reviews Microbiology*, vol. 6, no. 11, pp. 838-850.
- Godsel, L. M., Olson, C. L., & Engman, D. M. 1999, "Flagellar protein localization mediated by a calcium-myristoyl/palmitoyl switch mechanism", *Biophysical Journal*, vol. 76, no. 1, p. A396.
- Goldshmidt, H., Matas, D., Kabi, A., Carmi, S., Hope, R., & Michaeli, S. 2010, "Persistent ER Stress Induces the Spliced Leader RNA Silencing Pathway (SLS), Leading to Programmed Cell Death in *Trypanosoma brucei*", *PLoS Pathog*, vol. 6, no. 1, p. e1000731.
- Gonzalez, I. J., Desponds, C., Schaff, C., Mottram, J. C., & Fasel, N. 2007, "Leishmania major metacaspase can replace yeast metacaspase in programmed cell death and has arginine-specific cysteine peptidase activity", *International Journal for Parasitology*, vol. 37, no. 2, pp. 161-172.
- Greaves, J. & Chamberlain, L. H. 2007, "Palmitoylation-dependent protein sorting", *The Journal of Cell Biology*, vol. 176, no. 3, pp. 249-254.
- Griffiths, S., Portman, N., Taylor, P. R., Gordon, S., Ginger, M. L., & Gull, K. 2007, "RNA interference mutant induction in vivo demonstrates the essential nature of trypanosome flagellar function during mammalian infection", *Eukaryotic Cell*, vol. 6, no. 7, pp. 1248-1250.
- Groves, M. R., Coulombe, R., Jenkins, J., & Cygler, M. 1998, "Structural basis for specificity of papain-like cysteine protease proregions toward their cognate enzymes", *Proteins-Structure Function and Bioinformatics*, vol. 32, no. 4, pp. 504-514.
- Grunfelder, C. G., Engstler, M., Weise, F., Schwarz, H., Stierhof, Y. D., Morgan, G. W., Field, M. C., & Overath, P. 2003, "Endocytosis of a Glycosylphosphatidylinositol-anchored Protein via Clathrin-coated Vesicles, Sorting by Default in Endosomes, and Exocytosis via RAB11-positive Carriers", *Molecular Biology of the Cell*, vol. 14, no. 5, pp. 2029-2040.
- Gull, K. 2003, "Host-parasite interactions and trypanosome morphogenesis: a flagellar pocketful of goodies", *Current Opinion in Microbiology*, vol. 6, no. 4, pp. 365-370.
- Hailey, D. W., Rambold, A. S., Satpute-Krishnan, P., Mitra, K., Sougrat, R., Kim, P. K., & Lippincott-Schwartz, J. 2010, "Mitochondria Supply Membranes for Autophagosome Biogenesis during Starvation", *Cell*, vol. 141, no. 4, pp. 656-667.
- Hammarton, T. C. 2007, "Cell cycle regulation in *Trypanosoma brucei*", *Molecular and Biochemical Parasitology*, vol. 153, no. 1, pp. 1-8.
- Hammarton, T. C., Monnerat, S., & Mottram, J. C. 2007, "Cytokinesis in trypanosomatids", *Current Opinion in Microbiology*, vol. 10, no. 6, pp. 520-527.

- Hanrahan, O., Webb, H., O'Byrne, R., Brabazon, E., Treumann, A., Sunter, J. D., Carrington, M., & Voorheis, H. P. 2009, "The Glycosylphosphatidylinositol-PLC in *Trypanosoma brucei* Forms a Linear Array on the Exterior of the Flagellar Membrane Before and After Activation", *PLoS Pathog*, vol. 5, no. 6, p. e1000468.
- Hart, S. R., Lau, K. W., Hao, Z., Broadhead, R., Portman, N., H3hmer, A., Gull, K., McKean, P. G., Hubbard, S. J., & Gaskell, S. J. 2009, "Analysis of the Trypanosome Flagellar Proteome Using a Combined Electron Transfer/Collisionally Activated Dissociation Strategy", *Journal of the American Society for Mass Spectrometry*, vol. 20, no. 2, pp. 167-175.
- He, C. Y., Ho, H. H., Malsam, J., Chalouni, C., West, C. M., Ullu, E., Toomre, D., & Warren, G. 2004, "Golgi duplication in *Trypanosoma brucei*", *The Journal of Cell Biology*, vol. 165, no. 3, pp. 313-321.
- He, H., Dang, Y. J., Dai, F. Y., Guo, Z. K., Wu, J. X., She, X. Y., Pei, Y., Chen, Y. J., Ling, W. H., Wu, C. Q., Zhao, S. Y., Liu, J. O., & Yu, L. 2003, "Post-translational modifications of three members of the human MAP1LC3 family and detection of a novel type of modification for MAP1LC3B", *Journal of Biological Chemistry*, vol. 278, no. 31, pp. 29278-29287.
- He, R., Drury, G. E., Rotari, V. I., Gordon, A., Willer, M., Farzaneh, T., Woltering, E. J., & Gallois, P. 2008, "Metacaspase-8 Modulates Programmed Cell Death Induced by Ultraviolet Light and H₂O₂ in Arabidopsis", *Journal of Biological Chemistry*, vol. 283, no. 2, pp. 774-783.
- Helms, M. J., Ambit, A., Appleton, P., Tetley, L., Coombs, G. H., & Mottram, J. C. 2006, "Bloodstream form *Trypanosoma brucei* depend upon multiple metacaspases associated with RAB11-positive endosomes", *Journal of Cell Science*, vol. 119, no. 6, pp. 1105-1117.
- Herman, M., Gillies, S., Michels, P. A., & Rigden, D. L. 2006, "Autophagy and related processes in trypanosomatids - Insights from genomic and bioinformatic analyses", *Autophagy*, vol. 2, no. 2, pp. 107-118.
- Herman, M., Perez-Mora, D., Schtickzelle, N., & Michels, P. A. M. 2008, "Turnover of glycosomes during life-cycle differentiation of *Trypanosoma brucei*", *Autophagy*, vol. 4, no. 3, pp. 294-308.
- Hershko, A. & Ciechanover, A. 1998, "THE UBIQUITIN SYSTEM", *Annual Review of Biochemistry*, vol. 67, no. 1, pp. 425-479.
- Hertz-Fowler, C., Ersfeld, K., & Gull, K. 2001, "CAP5.5, a life-cycle-regulated, cytoskeleton-associated protein is a member of a novel family of calpain-related proteins in *Trypanosoma brucei*", *Molecular and Biochemical Parasitology*, vol. 116, no. 1, pp. 25-34.
- Hodder, A. N., Drew, D. R., Epa, V. C., Delorenzi, M., Bourgon, R., Miller, S. K., Moritz, R. L., Frecklington, D. F., Simpson, R. J., Speed, T. P., Pike, R. N., & Crabb, B. S. 2003, "Enzymic, phylogenetic, and structural characterization of the unusual papain-like protease domain of *Plasmodium falciparum* SERA5", *Journal of Biological Chemistry*, vol. 278, no. 48, pp. 48169-48177.

- Hodder, A. N., Malby, R. L., Clarke, O. B., Fairlie, W. D., Colman, P. M., Crabb, B. S., & Smith, B. J. 2009, "Structural Insights into the Protease-like Antigen Plasmodium falciparum SERA5 and Its Noncanonical Active-Site Serine", *Journal of Molecular Biology*, vol. 392, no. 1, pp. 154-165.
- Ichimura, Y., Kirisako, T., Takao, T., Satomi, Y., Shimonishi, Y., Ishihara, N., Mizushima, N., Tanida, I., Kominami, E., Ohsumi, M., Noda, T., & Ohsumi, Y. 2000, "A ubiquitin-like system mediates protein lipidation", *Nature*, vol. 408, no. 6811, pp. 488-492.
- Inohara, N., Koseki, T., Hu, Y., Chen, S., & Núñez, G. 1997, "CLARP, a death effector domain-containing protein interacts with caspase-8 and regulates apoptosis", *Proceedings of the National Academy of Sciences of the United States of America*, vol. 94, no. 20, pp. 10717-10722.
- Ivanovska, I. & Hardwick, J. M. 2005, "Viruses activate a genetically conserved cell death pathway in a unicellular organism", *Journal of Cell Biology*, vol. 170, no. 3, pp. 391-399.
- Jensen, B. C., Sivam, D., Kifer, C. T., Myler, P. J., & Parsons, M. 2009, "Widespread variation in transcript abundance within and across developmental stages of *Trypanosoma brucei*", *Bmc Genomics*, vol. 10.
- Jiang, X. & Wang, X. 2004, "CYTOCHROME C-MEDIATED APOPTOSIS", *Annual Review of Biochemistry*, vol. 73, no. 1, pp. 87-106.
- Johnson, J. G. & Cross, G. A. M. 1977, "Carbohydrate-Composition of Variant-Specific Surface-Antigen Glycoproteins from *Trypanosoma-Brucei*", *Journal of Protozoology*, vol. 24, no. 4, pp. 587-591.
- Juhasz, G. & Neufeld, T. P. 2006, "Autophagy: A forty-year search for a missing membrane source", *Plos Biology*, vol. 4, no. 2, pp. 161-164.
- Kabeya, Y., Mizushima, N., Yamamoto, A., Oshitani-Okamoto, S., Ohsumi, Y., & Yoshimori, T. 2004, "LC3, GABARAP and GATE16 localize to autophagosomal membrane depending on form-II formation", *Journal of Cell Science*, vol. 117, no. 13, pp. 2805-2812.
- Kamada, Y., Funakoshi, T., Shintani, T., Nagano, K., Ohsumi, M., & Ohsumi, Y. 2000, "Tor-Mediated Induction of Autophagy via an Apg1 Protein Kinase Complex", *The Journal of Cell Biology*, vol. 150, no. 6, pp. 1507-1513.
- Kelly, S., Reed, J., Kramer, S., Ellis, L., Webb, H., Sunter, J., Salje, J., Marinsek, N., Gull, K., Wickstead, B., & Carrington, M. 2007, "Functional genomics in *Trypanosoma brucei*: A collection of vectors for the expression of tagged proteins from endogenous and ectopic gene loci", *Molecular and Biochemical Parasitology*, vol. 154, no. 1, pp. 103-109.
- Kihara, A., Noda, T., Ishihara, N., & Ohsumi, Y. 2001, "Two Distinct Vps34 Phosphatidylinositol 3-OH Kinase Complexes Function in Autophagy and Carboxypeptidase Y Sorting in *Saccharomyces cerevisiae*", *The Journal of Cell Biology*, vol. 152, no. 3, pp. 519-530.

- Kim, J., Dalton, V. M., Eggerton, K. P., Scott, S. V., & Klionsky, D. J. 1999, "Apg7p/Cvt2p Is Required for the Cytoplasm-to-Vacuole Targeting, Macroautophagy, and Peroxisome Degradation Pathways", *Molecular Biology of the Cell*, vol. 10, no. 5, pp. 1337-1351.
- Klionsky, D. J., Cregg, J. M., Dunn, W. A., Emr, S. D., Sakai, Y., Sandoval, I. V., Sibirny, A., Subramani, S., Thumm, M., Veenhuis, M., & Ohsumi, Y. 2003, "A unified nomenclature for yeast autophagy-related genes", *Developmental Cell*, vol. 5, no. 4, pp. 539-545.
- Klionsky, D. J., Cuervo, A. M., & Seglen, P. O. 2007, "Methods for monitoring autophagy from yeast to human", *Autophagy*, vol. 3, no. 3, pp. 181-206.
- Kohl, L. & Gull, K. 1998, "Molecular architecture of the trypanosome cytoskeleton", *Molecular and Biochemical Parasitology*, vol. 93, no. 1, pp. 1-9.
- Koopmann, R., Muhammad, K., Perbandt, M., Betzel, C., & Duszenko, M. 2009, "Trypanosoma brucei ATG8 Structural insights into autophagic-like mechanisms in protozoa", *Autophagy*, vol. 5, no. 8, pp. 1085-1091.
- Kosec, G., Alvarez, V. E., Ag³ero, F., S³nchez, D., Dolinar, M., Turk, B., Turk, V., & Cazzulo, J. J. 2006, "Metacaspases of Trypanosoma cruzi: Possible candidates for programmed cell death mediators", *Molecular and Biochemical Parasitology*, vol. 145, no. 1, pp. 18-28.
- Kozminski, K. G., Johnson, K. A., Forscher, P., & Rosenbaum, J. L. 1993, "A motility in the eukaryotic flagellum unrelated to flagellar beating", *Proceedings of the National Academy of Sciences of the United States of America*, vol. 90, no. 12, pp. 5519-5523.
- Kubi, C., Van den Abbeele, J., De Deken, R., Marcotty, T., Dorny, P., & Van den Bossche, P. 2006, "The effect of starvation on the susceptibility of teneral and non-teneral tsetse flies to trypanosome infection", *Medical and Veterinary Entomology*, vol. 20, no. 4, pp. 388-392.
- Kuma, A., Hatano, M., Matsui, M., Yamamoto, A., Nakaya, H., Yoshimori, T., Ohsumi, Y., Tokuhi, T., & Mizushima, N. 2004, "The role of autophagy during the early neonatal starvation period", *Nature*, vol. 432, no. 7020, pp. 1032-1036.
- Kunz, J. B., Schwarz, H., & Mayer, A. 2004, "Determination of four sequential stages during microautophagy in vitro", *Journal of Biological Chemistry*, vol. 279, no. 11, pp. 9987-9996.
- Kuranaga, E. & Miura, M. 2007, "Nonapoptotic functions of caspases: caspases as regulatory molecules for immunity and cell-fate determination", *Trends in Cell Biology*, vol. 17, no. 3, pp. 135-144.
- Kurokawa, M. & Kornbluth, S. 2009, "Caspases and Kinases in a Death Grip", *Cell*, vol. 138, no. 5, pp. 838-854.

- LaCount, D. J., Bruse, S., Hill, K. L., & Donelson, J. E. 2000, "Double-stranded RNA interference in *Trypanosoma brucei* using head-to-head promoters", *Molecular and Biochemical Parasitology*, vol. 111, no. 1, pp. 67-76.
- Landfear, S. M. & Ignatushchenko, M. 2001, "The flagellum and flagellar pocket of trypanosomatids", *Molecular and Biochemical Parasitology*, vol. 115, no. 1, pp. 1-17.
- Lanteri, C. A., Stewart, M. L., Brock, J. M., Alibu, V. P., Meshnick, S. R., Tidwell, R. R., & Barrett, M. P. 2006, "Roles for the *Trypanosoma brucei* P2 Transporter in DB75 Uptake and Resistance", *Molecular Pharmacology*, vol. 70, no. 5, pp. 1585-1592.
- Lee, N., Gannavaram, S., Selvapandiyan, A., & Debrabant, A. 2007a, "Characterization of Metacaspases with Trypsin-Like Activity and Their Putative Role in Programmed Cell Death in the Protozoan Parasite *Leishmania*", *Eukaryotic Cell*, vol. 6, no. 10, pp. 1745-1757.
- Lee, R. E. C., Puente, L. G., Kaern, M., & Megeney, L. A. 2008, "A Non-Death Role of the Yeast Metacaspase: Yca1p Alters Cell Cycle Dynamics", *Plos One*, vol. 3, no. 8.
- Lee, R. E. C., Brunette, S., Puente, L. G., & Megeney, L. A. 2010, "Metacaspase Yca1 is required for clearance of insoluble protein aggregates", *Proceedings of the National Academy of Sciences*.
- Lee, S. H., Stephens, J. L., & Englund, P. T. 2007b, "A fatty-acid synthesis mechanism specialized for parasitism", *Nat Rev Micro*, vol. 5, no. 4, pp. 287-297.
- Levine, B. & Klionsky, D. J. 2004, "Development by self-digestion: Molecular mechanisms and biological functions of autophagy", *Developmental Cell*, vol. 6, no. 4, pp. 463-477.
- Levine, B. & Kroemer, G. 2008, "Autophagy in the pathogenesis of disease", *Cell*, vol. 132, no. 1, pp. 27-42.
- Liu, W., Apagyi, K., McLeavy, L., & Ersfeld, K. 2010, "Expression and cellular localisation of calpain-like proteins in *Trypanosoma brucei*", *Molecular and Biochemical Parasitology*, vol. 169, no. 1, pp. 20-26.
- Lopez-Otin, C. & Bond, J. S. 2008, "Proteases: Multifunctional Enzymes in Life and Disease", *Journal of Biological Chemistry*, vol. 283, no. 45, pp. 30433-30437.
- Lopez-Otin, C. & Hunter, T. 2010, "The regulatory crosstalk between kinases and proteases in cancer", *Nat Rev Cancer*, vol. 10, no. 4, pp. 278-292.
- Lythgoe, K. A., Morrison, L. J., Read, A. F., & Barry, J. D. 2007, "Parasite-intrinsic factors can explain ordered progression of trypanosome antigenic variation", *Proceedings of the National Academy of Sciences*, vol. 104, no. 19, pp. 8095-8100.

- Madeo, F., Frohlich, E., & Frohlich, K. U. 1997, "A yeast mutant showing diagnostic markers of early and late apoptosis", *Journal of Cell Biology*, vol. 139, no. 3, pp. 729-734.
- Madeo, F., Herker, E., Maldener, C., Wissing, S., LΣchelt, S., Herlan, M., Fehr, M., Lauber, K., Sigrist, S. J., Wesselborg, S., & Fr÷hlich, K. U. 2002, "A Caspase-Related Protease Regulates Apoptosis in Yeast", *Molecular Cell*, vol. 9, no. 4, pp. 911-917.
- Maric, D., Epting, C. L., & Engman, D. M. 2010, "Composition and sensory function of the trypanosome flagellar membrane", *Current Opinion in Microbiology*, vol. 13, no. 4, pp. 466-472.
- Matthews, K. R. & Gull, K. 1994, "Evidence for an interplay between cell cycle progression and the initiation of differentiation between life cycle forms of African trypanosomes", *The Journal of Cell Biology*, vol. 125, no. 5, pp. 1147-1156.
- Mazzoni, C., Herker, E., Palermo, V., Jungwirth, H., Eisenberg, T., Madeo, F., & Falcone, C. 2005, "Yeast caspase 1 links messenger RNA stability to apoptosis in yeast", *Embo Reports*, vol. 6, no. 11, pp. 1076-1081.
- McDonnell, M. A., Abedin, M., Melendez, M., Platikanova, T. N., Ecklund, J. R., Ahmed, K., & Kelekar, A. 2008, "Phosphorylation of Murine Caspase-9 by the Protein Kinase Casein Kinase 2 Regulates Its Cleavage by Caspase-8", *Journal of Biological Chemistry*, vol. 283, no. 29, pp. 20149-20158.
- McKean, P. G. 2003, "Coordination of cell cycle and cytokinesis in *Trypanosoma brucei*", *Current Opinion in Microbiology*, vol. 6, no. 6, pp. 600-607.
- Meijer, W. H., van der Klei, I. J., Veenhuis, M., & Kiel, J. A. K. W. 2007, "ATG genes involved in non-selective autophagy are conserved from yeast to man, but the selective Cvt and pexophagy pathways also require organism-specific genes", *Autophagy*, vol. 3, no. 2, pp. 106-116.
- Menna-Barreto, R. F. S., Correa, J. R., Cascabulho, C. M., Fernandes, M. C., Pinto, A. V., Soares, M. J., & De Castro, S. L. 2009, "Naphthoimidazoles promote different death phenotypes in *Trypanosoma cruzi*", *Parasitology*, vol. 136, no. 5, pp. 499-510.
- Michels, P. A. M., Bringaud, F., Herman, M., & Hannaert, V. 2006, "Metabolic functions of glycosomes in trypanosomatids", *Biochimica et Biophysica Acta (BBA) - Molecular Cell Research*, vol. 1763, no. 12, pp. 1463-1477.
- Mills, E., Price, H. P., Johner, A., Emerson, J. E., & Smith, D. F. 2007, "Kinetoplastid PPEF phosphatases: dual acylated proteins expressed in the endomembrane system of *Leishmania*", *Molecular and Biochemical Parasitology*, vol. 152, no. 1, pp. 22-34.
- Mitchell, B. F., Pedersen, L. B., Feely, M., Rosenbaum, J. L., & Mitchell, D. R. 2005, "ATP Production in *Chlamydomonas reinhardtii* Flagella by Glycolytic Enzymes", *Molecular Biology of the Cell*, vol. 16, no. 10, pp. 4509-4518.

- Mizushima, N., Kuma, A., Kobayashi, Y., Yamamoto, A., Matsubae, M., Takao, T., Natsume, T., Ohsumi, Y., & Yoshimori, T. 2003, "Mouse Apg16L, a novel WD-repeat protein, targets to the autophagic isolation membrane with the Apg12-Apg5 conjugate", *Journal of Cell Science*, vol. 116, no. 9, pp. 1679-1688.
- Mizushima, N., Levine, B., Cuervo, A. M., & Klionsky, D. J. 2008, "Autophagy fights disease through cellular self-digestion", *Nature*, vol. 451, no. 7182, pp. 1069-1075.
- Mizushima, N., Noda, T., & Ohsumi, Y. 1999, "Apg16p is required for the function of the Apg12p-Apg5p conjugate in the yeast autophagy pathway", *Embo Journal*, vol. 18, no. 14, pp. 3888-3896.
- Mizushima, N., Noda, T., Yoshimori, T., Tanaka, Y., Ishii, T., George, M. D., Klionsky, D. J., Ohsumi, M., & Ohsumi, Y. 1998, "A protein conjugation system essential for autophagy", *Nature*, vol. 395, no. 6700, pp. 395-398.
- Mizushima, N., Yamamoto, A., Hatano, M., Kobayashi, Y., Kabeya, Y., Suzuki, K., Tokuhisa, T., Ohsumi, Y., & Yoshimori, T. 2001, "Dissection of autophagosome formation using Apg5-deficient mouse embryonic stem cells", *Journal of Cell Biology*, vol. 152, no. 4, pp. 657-667.
- Mizushima, N., Yamamoto, A., Matsui, M., Yoshimori, T., & Ohsumi, Y. 2004, "In vivo analysis of autophagy in response to nutrient starvation using transgenic mice expressing a fluorescent autophagosome marker", *Molecular Biology of the Cell*, vol. 15, no. 3, pp. 1101-1111.
- Mizushima, N. 2004, "Methods for monitoring autophagy", *The International Journal of Biochemistry & Cell Biology*, vol. 36, no. 12, pp. 2491-2502.
- Moreno, S. N. & Docampo, R. 2003, "Calcium regulation in protozoan parasites", *Current Opinion in Microbiology*, vol. 6, no. 4, pp. 359-364.
- Moss, C. X., Westrop, G. D., Juliano, L., Coombs, G. H., & Mottram, J. C. 2007, "Metacaspase 2 of *Trypanosoma brucei* is a calcium-dependent cysteine peptidase active without processing", *Febs Letters*, vol. 581, no. 29, pp. 5635-5639.
- Mottram, J. C., Helms, M. J., Coombs, G. H., & Sajid, M. 2003, "Clan CD cysteine peptidases of parasitic protozoa", *Trends in Parasitology*, vol. 19, no. 4, pp. 182-187.
- Nakatogawa, H., Suzuki, K., Kamada, Y., & Ohsumi, Y. 2009, "Dynamics and diversity in autophagy mechanisms: lessons from yeast", *Nature Reviews Molecular Cell Biology*, vol. 10, no. 7, pp. 458-467.
- Natesan, S. K., Peacock, L., Matthews, K., Gibson, W., & Field, M. C. 2007, "Activation of Endocytosis as an Adaptation to the Mammalian Host by Trypanosomes", *Eukaryotic Cell*, vol. 6, no. 11, pp. 2029-2037.
- Nemecek, J., Nakayashiki, T., & Wickner, R. B. 2009, "A prion of yeast metacaspase homolog (Mca1p) detected by a genetic screen", *Proceedings of the National Academy of Sciences*, vol. 106, no. 6, pp. 1892-1896.

- Nett, I. R. E., Martin, D. M. A., Miranda-Saavedra, D., Lamont, D., Barber, J. D., Mehlert, A., & Ferguson, M. A. J. 2009, "The Phosphoproteome of Bloodstream Form *Trypanosoma brucei*, Causative Agent of African Sleeping Sickness", *Molecular & Cellular Proteomics*, vol. 8, no. 7, pp. 1527-1538.
- Newton, B. A. 1968, "Biochemical Peculiarities of Trypanosomatid Flagellates", *Annual Review of Microbiology*, vol. 22, no. 1, pp. 109-130.
- Noda, T. & Ohsumi, Y. 1998, "Tor, a phosphatidylinositol kinase homologue, controls autophagy in yeast", *Journal of Biological Chemistry*, vol. 273, no. 7, pp. 3963-3966.
- Obara, K., Sekito, T., Niimi, K., & Ohsumi, Y. 2008, "The Atg18-Atg2 complex is recruited to autophagic membranes via phosphatidylinositol 3-phosphate and exerts an essential function", *Journal of Biological Chemistry*, vol. 283, no. 35, pp. 23972-23980.
- Obara, K., Sekito, T., & Ohsumi, Y. 2006, "Assortment of phosphatidylinositol 3-kinase complexes-Atg14p directs association of complex I to the pre-autophagosomal structure in *Saccharomyces cerevisiae*", *Molecular Biology of the Cell*, vol. 17, no. 4, pp. 1527-1539.
- Oberholzer, M., Marti, G., Baresic, M., Kunz, S., Hemphill, A., & Seebeck, T. 2007, "The *Trypanosoma brucei* cAMP phosphodiesterases TbrPDEB1 and TbrPDEB2: flagellar enzymes that are essential for parasite virulence", *The FASEB Journal*, vol. 21, no. 3, pp. 720-731.
- Odiit, M., Kansiime, F., & Enyaru, J. C. 1997, "Duration of symptoms and case fatality of sleeping sickness caused by *Trypanosoma brucei rhodesiense* in Tororo, Uganda", *East Afr Med J*, vol. 74, no. 12, pp. 792-795.
- Ogbadoyi, E. O., Robinson, D. R., & Gull, K. 2003, "A High-Order Trans-Membrane Structural Linkage Is Responsible for Mitochondrial Genome Positioning and Segregation by Flagellar Basal Bodies in Trypanosomes", *Molecular Biology of the Cell*, vol. 14, no. 5, pp. 1769-1779.
- Ohsumi, Y. & Mizushima, N. 2004, "Two ubiquitin-like conjugation systems essential for autophagy", *Seminars in Cell & Developmental Biology*, vol. 15, no. 2, pp. 231-236.
- Otto, G. P., Wu, M. Y., Kazgan, N., Anderson, O. R., & Kessin, R. H. 2003, "Macroautophagy Is Required for Multicellular Development of the Social Amoeba *Dictyostelium discoideum*", *Journal of Biological Chemistry*, vol. 278, no. 20, pp. 17636-17645.
- Paindavoine, P., Rolin, S., Van Assel, S., Geuskens, M., Jauniaux, J. C., Dinsart, C., Huet, G., & Pays, E. 1992, "A gene from the variant surface glycoprotein expression site encodes one of several transmembrane adenylate cyclases located on the flagellum of *Trypanosoma brucei*", *Molecular and Cellular Biology*, vol. 12, no. 3, pp. 1218-1225.
- Pal, A., Hall, B. S., Jeffries, T. R., & Field, M. C. 2003, "Rab5 and Rab11 mediate transferrin and anti-variant surface glycoprotein antibody recycling in *Trypanosoma brucei*", *Biochemical Journal*, vol. 374, pp. 443-451.

- Pal, A., Hall, B. S., Nesbeth, D. N., Field, H. I., & Field, M. C. 2002, "Differential Endocytic Functions of Trypanosoma brucei Rab5 Isoforms Reveal a Glycosylphosphatidylinositol-specific Endosomal Pathway", *Journal of Biological Chemistry*, vol. 277, no. 11, pp. 9529-9539.
- Pan, J. & Snell, W. J. 2000, "Signal transduction during fertilization in the unicellular green alga, Chlamydomonas", *Current Opinion in Microbiology*, vol. 3, no. 6, pp. 596-602.
- Petiot, A., Ogier-Denis, E., Blommaert, E. F. C., Meijer, A. J., & Codogno, P. 2000, "Distinct classes of phosphatidylinositol 3'-kinases are involved in signaling pathways that control macroautophagy in HT-29 cells", *Journal of Biological Chemistry*, vol. 275, no. 2, pp. 992-998.
- Pils, B. & Schultz, J. r. 2004, "Inactive Enzyme-homologues Find New Function in Regulatory Processes", *Journal of Molecular Biology*, vol. 340, no. 3, pp. 399-404.
- Pop, C. & Salvesen, G. S. 2009, "Human Caspases: Activation, Specificity, and Regulation", *Journal of Biological Chemistry*, vol. 284, no. 33, pp. 21777-21781.
- Portman, N. & Gull, K. 2010, "The paraflagellar rod of kinetoplastid parasites: From structure to components and function", *International Journal for Parasitology*, vol. 40, no. 2, pp. 135-148.
- Priest, J. W. & Hajduk, S. L. 1994, "Developmental regulation of mitochondrial biogenesis in <i>Trypanosoma brucei</i>", *Journal of Bioenergetics and Biomembranes*, vol. 26, no. 2, pp. 179-191.
- Pullen, T. J., Ginger, M. L., Gaskell, S. J., & Gull, K. 2004, "Protein Targeting of an Unusual, Evolutionarily Conserved Adenylate Kinase to a Eukaryotic Flagellum", *Molecular Biology of the Cell*, vol. 15, no. 7, pp. 3257-3265.
- Ralston, K. S. & Hill, K. L. 2008, "The flagellum of Trypanosoma brucei: New tricks from an old dog", *International Journal for Parasitology*, vol. 38, no. 8-9, pp. 869-884.
- Ralston, K. S. & Hill, K. L. 2006a, "Trypanin, a Component of the Flagellar Dynein Regulatory Complex, Is Essential in Bloodstream Form African Trypanosomes", *PLoS Pathog*, vol. 2, no. 9, p. e101.
- Ralston, K. S., Kabututu, Z. P., Melehani, J. H., Oberholzer, M., & Hill, K. L. 2009, "The Trypanosoma brucei Flagellum: Moving Parasites in New Directions", *Annual Review of Microbiology*, vol. 63, no. 1, pp. 335-362.
- Ralston, K. S., Lerner, A. G., Diener, D. R., & Hill, K. L. 2006b, "Flagellar Motility Contributes to Cytokinesis in Trypanosoma brucei and Is Modulated by an Evolutionarily Conserved Dynein Regulatory System", *Eukaryotic Cell*, vol. 5, no. 4, pp. 696-711.
- Ravikumar, B., Moreau, K., Jahreiss, L., Puri, C., & Rubinsztein, D. C. 2010, "Plasma membrane contributes to the formation of pre-autophagosomal structures", *Nat Cell Biol*, vol. 12, no. 8, pp. 747-757.

- Rawlings, N. D., Barrett, A. J., & Bateman, A. 2010, "MEROPS: the peptidase database", *Nucleic Acids Research*, vol. 38, p. D227-D233.
- Reggiori, F. & Klionsky, D. J. 2005a, "Autophagosomes: biogenesis from scratch?", *Current Opinion in Cell Biology*, vol. 17, no. 4, pp. 415-422.
- Reggiori, F., Shintani, T., Nair, U., & Klionsky, D. J. 2005b, "Atg9 cycles between mitochondria and the pre-autophagosomal structure in yeasts", *Autophagy*, vol. 1, no. 2, pp. 101-109.
- Ren, J., Wen, L. P., Gao, X. J., Jin, C. J., Xue, Y., & Yao, X. B. 2008, "CSS-Palm 2.0: an updated software for palmitoylation sites prediction", *Protein Engineering Design & Selection*, vol. 21, no. 11, pp. 639-644.
- Resh, M. D. 1999, "Fatty acylation of proteins: new insights into membrane targeting of myristoylated and palmitoylated proteins", *Biochimica et Biophysica Acta-Molecular Cell Research*, vol. 1451, no. 1, pp. 1-16.
- Richert, S., Luche, S., Chevallet, M., Van Dorsselaer, A., Leize-Wagner, E., & Rabilloud, T. 2004, "About the mechanism of interference of silver staining with peptide mass spectrometry", *Proteomics*, vol. 4, no. 4, pp. 909-916.
- Rigden, D. J., Michels, P. A., & Ginger, M. L. 2009, "Autophagy in protists: Examples of secondary loss, lineage-specific innovations, and the conundrum of remodeling a single mitochondrion", *Autophagy*, vol. 5, no. 6, pp. 784-794.
- Rodriguez, J. A., Lopez, M. A., Thayer, M. C., Zhao, Y., Oberholzer, M., Chang, D. D., Kisalu, N. K., Penichet, M. L., Helguera, G., Bruinsma, R., Hill, K. L., & Miao, J. 2009, "Propulsion of African trypanosomes is driven by bihelical waves with alternating chirality separated by kinks", *Proceedings of the National Academy of Sciences*, vol. 106, no. 46, pp. 19322-19327.
- Roth, A. F., Wan, J., Bailey, A. O., Sun, B., Kuchar, J. A., Green, W. N., Phinney, B. S., Yates III, J. R., & Davis, N. G. 2006, "Global Analysis of Protein Palmitoylation in Yeast", *Cell*, vol. 125, no. 5, pp. 1003-1013.
- Sarkany, Z. & Polgar, L. 2003, "The unusual catalytic triad of poliovirus protease 3C", *Biochemistry*, vol. 42, no. 2, pp. 516-522.
- Schlumpberger, M., Schaeffeler, E., Straub, M., Bredschneider, M., Wolf, D. H., & Thumm, M. 1997, "AUT1, a gene essential for autophagocytosis in the yeast *Saccharomyces cerevisiae*", *Journal of Bacteriology*, vol. 179, no. 4, pp. 1068-1076.
- Shen, S. Y., Arhin, G. K., Ullu, E., & Tschudi, C. 2001, "In vivo epitope tagging of *Trypanosoma brucei* genes using a one step PCR-based strategy", *Molecular and Biochemical Parasitology*, vol. 113, no. 1, pp. 171-173.
- Sherwin, T. & Gull, K. 1989, "The Cell Division Cycle of *Trypanosoma brucei*: Timing of Event Markers and Cytoskeletal Modulations", *Philosophical Transactions of the Royal Society of London. B, Biological Sciences*, vol. 323, no. 1218, pp. 573-588.

- Shintani, T., Mizushima, N., Ogawa, Y., Matsuura, A., Noda, T., & Ohsumi, Y. 1999, "Apg10p, a novel protein-conjugating enzyme essential for autophagy in yeast", *Embo Journal*, vol. 18, no. 19, pp. 5234-5241.
- Silva, R. D., Sotoca, R., Johansson, B., Ludovico, P., Sansonetty, F., Silva, M. T., Peinado, J. M., & Corte-Real, M. 2005, "Hyperosmotic stress induces metacaspase- and mitochondria-dependent apoptosis in *Saccharomyces cerevisiae*", *Molecular Microbiology*, vol. 58, no. 3, pp. 824-834.
- Silverman, J. M., Chan, S. K., Robinson, D. P., Dwyer, D. M., Nandan, D., Foster, L. J., & Reiner, N. E. 2008, "Proteomic analysis of the secretome of *Leishmania donovani*", *Genome Biology*, vol. 9, no. 2.
- Silverman, J. M., Clos, J., de'Oliveira, C. C., Shirvani, O., Fang, Y., Wang, C., Foster, L. J., & Reiner, N. E. 2010, "An exosome-based secretion pathway is responsible for protein export from *Leishmania* and communication with macrophages", *Journal of Cell Science*, vol. 123, no. 6, pp. 842-852.
- Stennicke, H. R. & Salvesen, G. S. 1999, "Catalytic properties of the caspases", *Cell Death and Differentiation*, vol. 6, no. 11, pp. 1054-1059.
- Stuart, K. D., Schnauffer, A., Ernst, N. L., & Panigrahi, A. K. 2005, "Complex management: RNA editing in trypanosomes", *Trends in Biochemical Sciences*, vol. 30, no. 2, pp. 97-105.
- Suarez, M. F., Filonova, L. H., Smertenko, A., Savenkov, E. I., Clapham, D. H., von Arnold, S., Zhivotovsky, B., & Bozhkov, P. V. 2004, "Metacaspase-dependent programmed cell death is essential for plant embryogenesis", *Current Biology*, vol. 14, no. 9, p. R339-R340.
- Sugawara, K., Suzuki, N. N., Fujioka, Y., Mizushima, N., Ohsumi, Y., & Inagaki, F. 2004, "The crystal structure of microtubule-associated protein light chain 3, a mammalian homologue of *Saccharomyces cerevisiae* Atg8", *Genes to Cells*, vol. 9, no. 7, pp. 611-618.
- Sundstrom, J. F., Vaculova, A., Smertenko, A. P., Savenkov, E. I., Golovko, A., Minina, E., Tiwari, B. S., Rodriguez-Nieto, S., Zamyatnin, A. A., Valineva, T., Saarikettu, J., Frilander, M. J., Suarez, M. F., Zavialov, A., Stahl, U., Hussey, P. J., Silvennoinen, O., Sundberg, E., Zhivotovsky, B., & Bozhkov, P. V. 2009, "Tudor staphylococcal nuclease is an evolutionarily conserved component of the programmed cell death degradome", *Nature Cell Biology*, vol. 11, no. 11, p. 1347-U198.
- Suzuki, K., Kirisako, T., Kamada, Y., Mizushima, N., Noda, T., & Ohsumi, Y. 2001, "The pre-autophagosomal structure organized by concerted functions of APG genes is essential for autophagosome formation", *EMBO J*, vol. 20, no. 21, pp. 5971-5981.
- Suzuki, K., Kubota, Y., Sekito, T., & Ohsumi, Y. 2007, "Hierarchy of Atg proteins in pre-autophagosomal structure organization", *Genes to Cells*, vol. 12, no. 2, pp. 209-218.
- Szallies, A., Kubata, B. K., & Duszenko, M. 2002, "A metacaspase of *Trypanosoma brucei* causes loss of respiration competence and clonal death

- in the yeast *Saccharomyces cerevisiae*", *Febs Letters*, vol. 517, no. 1-3, pp. 144-150.
- Taloczy, Z., Jiang, W. X., Virgin, H. W., Leib, D. A., Scheuner, D., Kaufman, R. J., Eskelinen, E. L., & Levine, B. 2002, "Regulation of starvation- and virus-induced autophagy by the eIF2 alpha kinase signaling pathway", *Proceedings of the National Academy of Sciences of the United States of America*, vol. 99, no. 1, pp. 190-195.
- Tanida, I., Tanida-Miyake, E., Ueno, T., & Kominami, E. 2001, "The human homolog of *Saccharomyces cerevisiae* Apg7p is a protein-activating enzyme for multiple substrates including human Apg12p, GATE-16, GABARAP, and MAP-LC3", *Journal of Biological Chemistry*, vol. 276, no. 3, pp. 1701-1706.
- Tanida, I., Ueno, T., & Kominami, E. 2004a, "Human light chain 3/MAP1LC3B is cleaved at its carboxyl-terminal Met(121) to expose Gly(120) for lipidation and targeting to autophagosomal membranes", *Journal of Biological Chemistry*, vol. 279, no. 46, pp. 47704-47710.
- Tanida, I., Ueno, T., & Kominami, E. 2004b, "LC3 conjugation system in mammalian autophagy", *International Journal of Biochemistry & Cell Biology*, vol. 36, no. 12, pp. 2503-2518.
- Teter, S. A., Eggerton, K. P., Scott, S. V., Kim, J., Fischer, A. M., & Klionsky, D. J. 2001, "Degradation of Lipid Vesicles in the Yeast Vacuole Requires Function of Cvt17, a Putative Lipase", *Journal of Biological Chemistry*, vol. 276, no. 3, pp. 2083-2087.
- Tsukada, M. & Ohsumi, Y. 1993, "Isolation and characterization of autophagy-defective mutants of *Saccharomyces cerevisiae*", *Febs Letters*, vol. 333, no. 1-2, pp. 169-174.
- Tull, D., Vince, J. E., Callaghan, J. M., Naderer, T., Spurck, T., McFadden, G. I., Currie, G., Ferguson, K., Bacic, A., & McConville, M. J. 2004, "SMP-1, a Member of a New Family of Small Myristoylated Proteins in Kinetoplastid Parasites, Is Targeted to the Flagellum Membrane in *Leishmania*", *Molecular Biology of the Cell*, vol. 15, no. 11, pp. 4775-4786.
- Tyler, K. M., Fridberg, A., Toriello, K. M., Olson, C. L., Cieslak, J. A., Hazlett, T. L., & Engman, D. M. 2009, "Flagellar membrane localization via association with lipid rafts", *Journal of Cell Science*, vol. 122, no. 6, pp. 859-866.
- Uren, A. G., O'Rourke, K., Aravind, L., Pisabarro, M. T., Seshagiri, S., Koonin, E. V., & Dixit, V. M. 2000, "Identification of Paracaspases and Metacaspases: Two Ancient Families of Caspase-like Proteins, One of which Plays a Key Role in MALT Lymphoma", *Molecular Cell*, vol. 6, no. 4, pp. 961-967.
- Uzcategui, N. L., Carmona-Gutierrez, D., Denninger, V., Schoenfeid, C., Lang, F., Figarella, K., & Duszenko, M. 2007, "Antiproliferative effect of dihydroxyacetone on *Trypanosoma brucei* bloodstream forms: Cell cycle progression, subcellular alterations, and cell death", *Antimicrobial Agents and Chemotherapy*, vol. 51, no. 11, pp. 3960-3968.

- Van den Abbeele, J., Claes, Y., van Bockstaele, D., Le Ray, D., & Coosemans, M. 1999, "Trypanosoma brucei spp. development in the tsetse fly: characterization of the post-mesocyclic stages in the foregut and proboscis", *Parasitology*, vol. 118, pp. 469-478.
- Van den Bossche, P. & Hargrove, J. W. 1999, "Seasonal variation in nutritional levels of male tsetse flies *Glossina morsitans morsitans* (Diptera : Glossinidae) caught using fly-rounds and electric screens", *Bulletin of Entomological Research*, vol. 89, no. 4, pp. 381-387.
- Vassella, E., Reuner, B., Yutzy, B., & Boshart, M. 1997, "Differentiation of African trypanosomes is controlled by a density sensing mechanism which signals cell cycle arrest via the cAMP pathway", *Journal of Cell Science*, vol. 110, no. 21, pp. 2661-2671.
- Vercammen, D., Declercq, W., Vandenabeele, P., & Van Breusegem, F. 2007, "Are metacaspases caspases?", *The Journal of Cell Biology*, vol. 179, no. 3, pp. 375-380.
- Vercammen, D., van de Cotte, B., De Jaeger, G., Eeckhout, D., Casteels, P., Vandepoele, K., Vandenberghe, I., Van Beeumen, J., Inz+®, D., & Van Breusegem, F. 2004, "Type II Metacaspases Atmc4 and Atmc9 of *Arabidopsis thaliana* Cleave Substrates after Arginine and Lysine", *Journal of Biological Chemistry*, vol. 279, no. 44, pp. 45329-45336.
- Vickerman, K. 1978, "Antigenic variation in trypanosomes", *Nature*, vol. 273, no. 5664, pp. 613-617.
- Wang, Q., Pan, J., & Snell, W. J. 2006, "Intraflagellar transport particles participate directly in cilium-generated signaling in *Chlamydomonas*", *Cell*, vol. 125, no. 3, pp. 549-562.
- Watanabe, N. & Lam, E. 2004, "Recent advance in the study of caspase-like proteases and Bax inhibitor-1 in plants: their possible roles as regulator of programmed cell death", *Molecular Plant Pathology*, vol. 5, no. 1, pp. 65-70.
- Watanabe, N. & Lam, E. 2005, "Two *Arabidopsis* Metacaspases AtMCP1b and AtMCP2b Are Arginine/Lysine-specific Cysteine Proteases and Activate Apoptosis-like Cell Death in Yeast", *Journal of Biological Chemistry*, vol. 280, no. 15, pp. 14691-14699.
- Webb, H., Carnall, N., Vanhamme, L., Rolin, S., Abbeele, J. V. D., Welburn, S., Pays, E., & Carrington, M. 1997, "The GPI-Phospholipase C of *Trypanosoma brucei* Is Nonessential But Influences Parasitemia in Mice", *The Journal of Cell Biology*, vol. 139, no. 1, pp. 103-114.
- Weidberg, H., Shvets, E., Shpilka, T., Shimron, F., Shinder, V., & Elazar, Z. 2010, "LC3 and GATE-16/GABARAP subfamilies are both essential yet act differently in autophagosome biogenesis", *Embo Journal*, vol. 29, no. 11, pp. 1792-1802.

- Williams, R. A., Tetley, L., Mottram, J. C., & Coombs, G. H. 2006, "Cysteine peptidases CPA and CPB are vital for autophagy and differentiation in *Leishmania mexicana*", *Molecular Microbiology*, vol. 61, no. 3, pp. 655-674.
- Williams, R. A. M., Woods, K. L., Juliano, L., Mottram, J. C., & Coombs, G. H. 2009, "Characterization of unusual families of ATG8-like proteins and ATG12 in the protozoan parasite *Leishmania major*", *Autophagy*, vol. 5, no. 2, pp. 159-172.
- Wirtz, E., Leal, S., Ochatt, C., & Cross, G. A. M. 1999, "A tightly regulated inducible expression system for conditional gene knock-outs and dominant-negative genetics in *Trypanosoma brucei*", *Molecular and Biochemical Parasitology*, vol. 99, no. 1, pp. 89-101.
- Wullschleger, S., Loewith, R., & Hall, M. N. 2006, "TOR Signaling in Growth and Metabolism", *Cell*, vol. 124, no. 3, pp. 471-484.
- Xie, Z. & Klionsky, D. J. 2007, "Autophagosome formation: core machinery and adaptations", *Nat Cell Biol*, vol. 9, no. 10, pp. 1102-1109.
- Yang, Z., Huang, J., Geng, J., Nair, U., & Klionsky, D. J. 2006, "Atg22 Recycles Amino Acids to Link the Degradative and Recycling Functions of Autophagy", *Molecular Biology of the Cell*, vol. 17, no. 12, pp. 5094-5104.
- Yeoh, S., O'Donnell, R. A., Koussis, K., Dluzewski, A. R., Ansell, K. H., Osborne, S. A., Hackett, F., Withers-Martinez, C., Mitchell, G. H., Bannister, L. H., Bryans, J. S., Kettleborough, C. A., & Blackman, M. J. 2007, "Subcellular discharge of a serine protease mediates release of invasive malaria parasites from host erythrocytes", *Cell*, vol. 131, no. 6, pp. 1072-1083.
- Yu, J. W. & Shi, Y. 2008, "FLIP and the death effector domain family", *Oncogene*, vol. 27, no. 48, pp. 6216-6227.
- Yu, J. W., Jeffrey, P. D., & Shi, Y. 2009, "Mechanism of procaspase-8 activation by c-FLIPL", *Proceedings of the National Academy of Sciences*, vol. 106, no. 20, pp. 8169-8174.
- Yuan, J. Y., Shaham, S., Ledoux, S., Ellis, H. M., & Horvitz, H. R. 1993, "The *C. Elegans* Cell-Death Gene *Ced-3* Encodes A Protein Similar to Mammalian Interleukin-1-Beta-Converting Enzyme", *Cell*, vol. 75, no. 4, pp. 641-652.
- Zheng, X. F., Fiorentino, D., Chen, J., Crabtree, G. R., & Schreiber, S. L. 1995, "TOR kinase domains are required for two distinct functions, only one of which is inhibited by rapamycin", *Cell*, vol. 82, no. 1, pp. 121-130.
- Ziegelbauer, K., Quinten, M., Schwarz, H., Pearson, T. W., & Overath, P. 1990, "Synchronous Differentiation of *Trypanosoma-Brucei* from Blood-Stream to Procyclic Forms *In vitro*", *European Journal of Biochemistry*, vol. 192, no. 2, pp. 373-378.